Point-of-use Drinking Water Purification: Chromium(VI) Capture and Beyond

VERA SABINE BIEBER

Point-of-Use Drinking Water Purification: Chromium(VI) Capture and Beyond

Vera Sabine Bieber

PhD Thesis

Department of Chemistry

Durham University

2022

Declaration

The experimental work contained within this thesis was carried out at the Department of Chemistry, University of Durham, between July 2017 and March 2020. It is the original work of this author (except where otherwise acknowledged) and has not been submitted by the author for a degree at this or any other higher education establishment. The funding for this thesis was provided by the Royal Society (International Collaboration Award reference IC160021).

Researcher Contributions

Chapter 4

- DMAM-calixarene was synthesized by Egemen Ozcelik, Mustafa Karaman, and Mustafa Tabakci (Konya Technical University).
- X-ray photoelectron spectroscopy measurements were conducted by Harrison J. Cox (Durham University), as was the scanning electron microscopy for this chapter.
- Inductively coupled plasma optical emission spectrometry was conducted by Vera S. Bieber under the close supervision and guidance of Christopher J. Ottley (Durham University).
- All other practical experiments, as well as all data evaluation for the DMAM-calixarene and butylimidazole chapters (Chapter 4, 5) were conducted by Vera S. Bieber.
- This chapter has previously been published in a scientific journal (see “Publication arising from this work”). Text and figures of this chapter are mostly taken from this publication, meaning that they were proof-read by all publication authors.

Chapter 5

- Inductively coupled plasma optical emission spectrometry was conducted by Vera S. Bieber under the close supervision and guidance of Christopher J. Ottley (Durham University).

- All other practical experiments, as well as all data evaluation for the DMAM-calixarene and butylimidazole chapters (Chapter 4, 5) were conducted by Vera S. Bieber.

Chapter 6

- Most MOF samples in the MOF-508 chapter (chapter 6) were prepared by Philippa K. Edge (Durham University) in consultation with Vera S. Bieber and Jas Pal S. Badyal as part of her fourth-year project, except for samples for XPS analysis, which were prepared by Vera S. Bieber.
- Infrared spectra of MOF samples were measured by Philippa K. Edge.
- X-ray photoelectron spectroscopy measurements were conducted by Harrison J. Cox
- X-ray diffractograms of MOF samples were captured by Harrison J. Cox.
- Scanning electron microscopy of MOF samples was conducted jointly by Philippa K. Edge and Vera S. Bieber at Newcastle University, with assistance from Tracey Davey.
- Photographs of MOF samples were taken by Vera S. Bieber.
- All data evaluation presented within the MOF chapter of this thesis was conducted by Vera S. Bieber based on the existing raw data. While some conclusions were inspired by Philippa K. Edge's fourth year report, all background literature research leading up to the conclusions presented in this thesis was conducted by Vera S. Bieber.

General

The entire text of this thesis was written by Vera S. Bieber. All figures, schemes, and photographs in this thesis were created by Vera S. Bieber as well, except for some figures taken from the internet for the introduction and impact chapter (Chapters 1, 2), see figure captions.

Publication arising from this work

Bieber, V.S.; Ozcelik, E.; Cox, H.J.; Ottley, C.J.; Ratan, J.K.; Karaman, M.; Tabakci, M.; Beaumont, S.K.; Badyal, J.P.S. Capture and Release Recyclable Dimethylaminomethyl-Calixarene Functional Cloths for Point-of-Use Removal of Highly Toxic Chromium Water Pollutants. *ACS Appl. Mater. Interfaces* **2020**, *12*, 52136–52145.

Statement of Copyright

Acknowledgements

Now, as I think back to these past years,
A PhD comes with sweat and tears;
But also, much joy and things to explore,
And numerous people I'm grateful for:

Prof. Jas Pal Badyal, your guiding hands
Led us through research and foreign lands.
Thanks for encouraging me in every endeavour,
The things you taught me I'll remember forever.

Dr. Simon Beaumont, my second supervisor,
Thanks for your help as expert analyser.
Your feedback was always useful to me,
Your lab one of my favourite places to be.

Thanks to all co-authors of my paper
For your contributions and your hard labour.
Dr. Ratan from Jalandhar's technology institution,
Thanks for letting me see real water pollution

Egemen, Prof. Tabakci, Prof. Karaman,
Thank you for everything you have done:
For all the calixarenes you made,
And your hospitality when in Konya we stayed.

I thank Dr. Chris Ottley for the success
Of my analyses with ICP-OES.
Aileen Congreve was an angel (save for wings)
In all IR and UV-Vis things.

Annette Passmoor from chemistry stores
Had everything I need behind her doors.
In Newcastle Tracey Davey does dwell,
She helped us to take SEM images well.

Electrical workshop, you guys were stunning:
Kelvin and Bryan helped keep my plasma running.
Thanks, mechanical workshop, especially Neil:
I sketched my Faraday cage, you made it real.

Thanks to the friends from Lab 98,
My time with you was always great.
Andrea, you were the best plasma teacher,
Thanks for helping me know each feature.

Thank you, Harry, my partner in crime,
We started our PhDs at almost the same time.
Thanks for XPS, SEM, XRD,
And for travelling to Turkey and India with me.

Pippa, thank you for being the best
Fourth year student one could request.
On MOF-508 you worked at full steam,
With SEM we made an excellent team.

George, my successor on water filtration,
Thanks for taking over this operation.
May all your experiments run well,
And may you make filters that excel.

Ustinov College, what a great place,
Provided a home I was glad to embrace.
Anna, the porters, Glenn, all the staff,
Thanks for your help and many a laugh.

GCR, through you I learned more
Than I would have ever imagined before.
Work with your volunteers was great fun and I knew
The world would be better if all were like you.

Thanks to all international friends I made,
I wish we could forever have stayed.
Though life draws us out of the Durham bubble,
When we meet again, the joy will be double.

A special shout-out to the Spindoctors team!
Ultimate Frisbee can be extreme.
I enjoyed it greatly and you were the best,
A great antidote when I felt stressed.

In Durham I moved through houses and flats;
I thank all my flatmates for all the nice chats.
Especially those during my final year:
The lockdown was bearable with you near.

Ευχαριστώ τον Χρήστο, το αγόρι μου,
Για τη νόστιμη μαγειρική του,
Και τη συναισθηματική υποστήριξη;
Πάντα διασκεδάζουμε πολύ.

Auch meiner Familie danke ich gerne
Für die Unterstützung aus der Ferne:
Anna, Nina, Papa mit Laki, dem Hunde,
Oma, Opa, Schedls, die ganze Runde

媽媽谢谢你教我的紛紛東西.
不管你跟誰在一起, 你總是讓他們開心.
你是我認識最勇敢的人, 我非常想念你,
但是我知道你永遠在我心裡.

Finally, thank YOU for reading this rhyme,
And, above all, for taking the time
To read my thesis that starts below,
I hope you'll learn things you did not yet know.

In loving memory of my mum 劉麗雲 and my grandpa Willi Jakob who passed away near the beginning and the end of my PhD.

Abstract

Millions of people around the world are at risk of exposure to polluted water. According to the United Nations, unsafe water claims more lives each year than all forms of violence put together. Particularly in developing countries, where the population has no access to centrally treated tap water, point-of-use water purification techniques are important to mitigate the risks of consuming ground- or surface waters. Many such techniques already exist and are in use today, but they mostly target bacteria and macroscopic contaminations that can be removed due to size. Dissolved ions are significantly more difficult to remove, especially because they can be harmful even at extremely low concentrations. Some of the most dangerous heavy metals polluting drinking water around the world today are chromium, arsenic, and lead. In this thesis I first highlight the impact of these pollutants before presenting filter materials I synthesized that can efficiently remove chromium(VI) oxoanions from drinking water. By attaching functional molecules such as a dimethylaminomethyl-calixarene and N-butylimidazole to non-woven cloth via a pulsed plasma polymer linker layer, I created filters that can capture chromium(VI) at neutral pH, from solutions with low starting concentrations, in the presence of competitive anions, and even from real wastewater samples. Moreover, these filters can be easily recycled many times. In the last results chapter, I present new findings regarding the epitaxial growth mechanism of the metal–organic framework MOF-508. These materials are attractive candidates for filtration applications due to their vast internal surface. The discovery that they can be grown on untreated polymer surfaces, as well as the presented method for simple MOF film transfer, can aid future developments in this field.

Abbreviations

4,4‘-bipy / BP	4,4’-Bipyridine
AA linker	Poly(1-allylimidazole) linker
ATR-FTIR	Attenuated total reflectance fourier-transform infrared spectroscopy
BDC	Benzene-1,4-dicarboxylate
DMAM-Calixarene	Dimethylaminomethyl-calixarene; full name (5,11,17,23-tetrakis[(dimethylamino)methyl]-25,26,27,28-tetrahydroxycalix[4]arene
DMAM-Phenol	(2,6-di-tert-butyl-4-(dimethylaminomethyl)phenol
DMF	Dimethylformamide
EDTA	Ethylenediaminetetraacetic acid
EPA	Environment Protection Agency (of the United States of America)
EU	European Union
EtOH	Ethanol
HDPE	High-density polyethylene
ICP-OES	Inductively coupled optical emission spectroscopy
IR spectroscopy	Infrared spectroscopy
MOF	Metal–organic framework
MOF-5	[Zn(benzene-1,4-dicarboxylate)$_{1.5}$]
MOF-508	[Zn(benzene-1,4-dicarboxylate) -(4,4’-bipyridine)$_{0.5}$]
SEM	Scanning electron microscopy
SURMOF	Surface-mounted metal–organic framework
PES	Polyether sulfone
PET	Polyethylene terephthalate
PG&E	Pacific Gas and Electric (Company)
PMMA	Poly(methyl methacrylate)
PP	Polypropylene
pp-VBC	Pulsed plasma poly(vinylbenzyl) chloride
ppb	Parts per billion = µg L^{-1}

ppm	Parts per million = mg L^{-1}
PTFE	Polytetrafluorethylene
tBu-Calixarene	5,11,17,23-tetra-tert-butyl-25,26,27,28-tetrahydroxycalix[4]arene
THF	Tetrahydrofuran
TPA	Terephthalic acid
US	United States of America
UV–Vis spectroscopy	Ultraviolet visible spectroscopy
WHO	World Health Organization
XPS	X-ray photoelectron spectroscopy
XRD	X-ray diffraction
ZnAc	Zinc acetate

Table of Contents

CHAPTER 1: INTRODUCTION

1.1 The Threat of Water Pollution

Water pollution is a major threat for human health around the world. Particularly in developing countries, large amounts of industrial wastes are still emptied into waters without any treatment, thus polluting the population's drinking water sources.[1] According to the United Nations, every year more people die from unsafe water than from all forms of violence put together, including war.[2]

1.2 Recent Examples of Inorganic Water Pollution around the World

In 2018, India was reported to be suffering from its worst ever water crisis which was predicted to only increase in the following years.[3] Almost half of the inhabitants of the world's second most populous country were facing acute water shortage leading to nearly 200,000 deaths per year.[4] In fact, up to 70% of India's water was reported to be contaminated, posing a major challenge throughout the country.[3] With only one third of its wastewater being treated, countless harmful substances are carried into surface waters from where they eventually seep into the groundwater. The difficulty of accessing clean drinking water is further exacerbated by climate change which is gradually drying out the country. Monsoon rain amounts have been below the historic average in six out of seven years between 2012–2018, and by 2019, 21 Indian cities were expected to run out of groundwater within one year.[5] Clean drinking water is thus quickly becoming a luxury that only the wealthy can afford.

Figure 1: Wastewater basin at a small factory in rural India; photo taken in February 2020. The water contains high chromium concentrations and is only treated rudimentarily before being released into the environment.

The 2019–2020 bushfire season in Australia was reported on by media around the world due to its severity and extent: the state of New South Wales for example experienced more than 240 consecutive days of fire activity.[6,7] Fires not only cost human and animal lives, but they are also suspected to have a negative long-term effect on water quality. Plant debris landing in waterways leads to an influx of nutrients which can cause algae blooms that reduce the oxygen concentration in the water, killing fish and other fauna.[8] Ash and soot from wildfires can also dramatically increase the concentrations of various heavy metals in water, making it unsafe for human consumption.[9] As climate change progresses, wildfires are becoming more frequent and intense in many parts of the world.[10] Some of the recent major fires covered extensively in the media include the ones in the Western United States during Autumn 2020 and in Greece and Russia during Summer 2021.[11,12,13] Along with them, water pollution from wildfire debris may also become a more and more global issue.

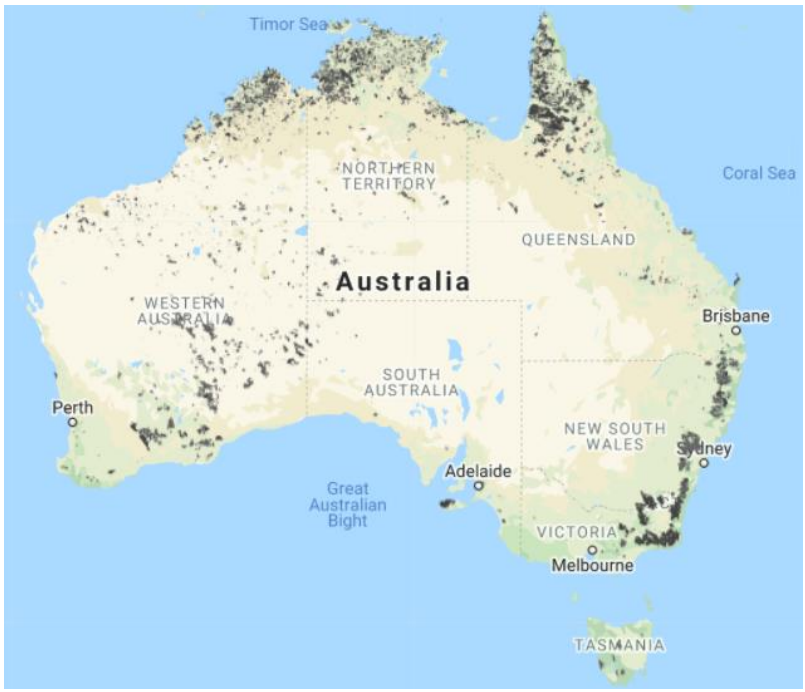

Figure 2: Map of Australia with areas burned in 2019–2020 shaded in grey. Map taken from reference 14.

In July 2021 a pollutant reservoir belonging to a diamond mine in Angola was breached and polluted water entered the Chicapa river flowing into the Democratic Republic of the Congo (where the river is known as Tshikapa) and continued from there into the Kasai river, one of the main tributaries of the Congo river.[15,16] The waters turned red, killing wildlife from fish to hippopotamuses and causing diarrhoea and other health issues in the population along the rivers.[15] While the mining company claimed that the breach was sealed through the construction of two dykes by August 9, the pollution continued to spread.[17] By early September, it had killed twelve Congolese while putting nearly one million people at risk, a number that is likely to rise as the polluted water flows downstream and approaches the capital city Kinshasa.[18,19] The chemical composition of the pollution was still unknown at this point, though heavy metals were suspected.[16]

Figure 3: Map illustrating the locations of the Tshikapa/Chicapa, Kasai, and Congo rivers in relation to each other, as well as the location of the diamond mine that caused the pollution event in 2021. Base map taken from OpenStreetMap.

These examples together with many more cases reported throughout the past decades show that drinking water pollution by heavy metals continues to be a major danger to human health around the world, particularly where water is being ingested that does not stem from a centralized treatment facility, as is the case in many developing countries.

To provide the population of developing countries with access to clean drinking water in a safe and decentralized manner, numerous point-of-use water purification systems have been developed over the past decades. The mechanisms by which they work mostly fall under the categories of heat[20], UV light[21,22], chemical treatment[23,24], and filtration through small pores[25,26], as illustrated in Figure 4.

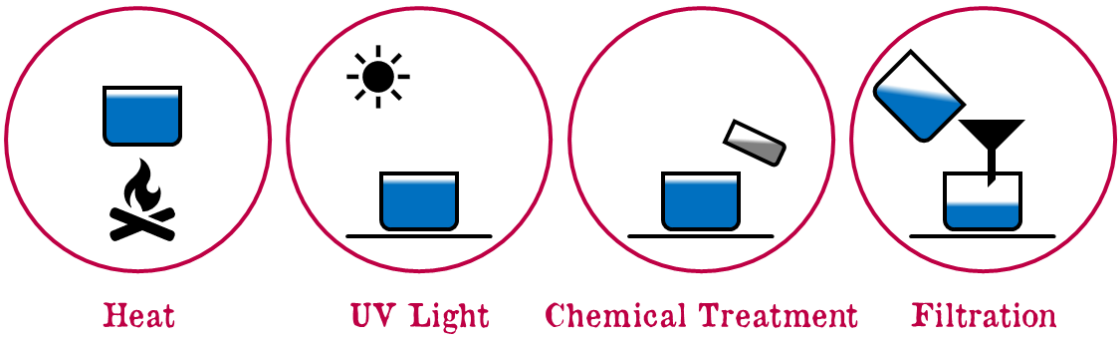

Figure 4: Existing point-of-use water purification techniques, mainly used for antibacterial treatment.

Some point-of-use water purification devices and methods have gained large media attention in the past. One example is LifeStraw, described in the New York Times in 2011, a thick straw-like device that can filter out particles down to a size of 5 µm and additionally disinfects the water passing through it by iodination.[25,27] Another filtration-based device is PAUL (short for Potable Aqua Unit for Living), which was developed at the University of Kassel in Germany and has been distributed to 85 countries worldwide between 2010 and 2020.[28] It has the appearance of a large blue dust bin and was constructed to be particularly easy to use: water is added at the top and can be tapped at the bottom after passing through a polymer membrane with 100 nm pore sizes.[26,28] A very different water purification system that gained a lot of attention in 2019 is P&G's "Purifier of Water" powder: a video by the YouTuber Mark Rober where he demonstrates this product to Bill Gates has gathered over 56 million views to this day.[29] The powder contains ferric sulfate as cationic coagulant that causes suspended particles to aggregate, making it easier to remove them from the water by simple filtration through cloth.[30,31] Additional chemicals within the powder release chlorine into the water for disinfection.[30,31]

Despite the wide range of existing point-of-use water purification techniques, most of them (including the three examples listed above) only target bacterial contamination and are entirely ineffective against contaminants dissolved in water, such as heavy metal ions.[32] Therefore, considerable effort is being put into developing methods to remove dissolved contaminants from water.[33,34,35,36]

Some of the most popular methods for the removal of heavy metal ions from water are listed in Table 1. While many of them are being used in large scale water purification facilities, due to their various disadvantages most are not suitable for point-of-use application. Thus, it remains challenging to develop robust, low-cost, and effective means of removing toxic pollutants from water, particularly for developing countries where the population uses water from wells or rivers that may be contaminated with different heavy metal ions.[32,37,38]

Table 1: Approaches for the removal of heavy metal ions from water. Descriptions based on ref. 37 and 38.

Method	**Description**	**Disadvantage**
Membrane Filtration, such as Ultrafiltration or Reverse Osmosis	Use membrane with different (but always very small) pore sizes and high pressure.	Expensive and toxic sludge is generated
Electrodialysis	Uses semi-permeable ion-selective membranes and electrical potential.	Metal hydroxides may form and clog the membrane.
Ion exchange	Ions held on exchange resin by electrostatic forces are exchanged for metal ions in solution.	Expensive and not always very efficient and selective.
Chemical precipitation	Addition of coagulants causes metals to precipitate.	Generates large amount of sludge.
Phytoremediation	Usage of live plants to clean soil and water.	Very time-consuming; plant regeneration is difficult.
Adsorption / Biosorption	Usage of the affinity of (biological) materials towards certain pollutants to remove them efficiently.	If not immobilized: difficult to separate from reaction system; poor mechanical strength.

1.3 Structure of this Thesis

Since the Covid-19 pandemic unfortunately interrupted my experimental work, my thesis includes an extended literature chapter (chapter 2) in addition to the results chapters (chapters 4, 5, 6).

Chapter 2 sheds light on the impact of heavy metal water pollution with a specific focus on chromium, arsenic, and lead, the three pollutants I was planning to prepare targeted filters for. As I was unable to complete my experiments regarding arsenic and lead, chapter 2 also outlines what my plans were for these pollutants.

Chapter 3 describes all experimental methods I used. A detailed list of contributions by other researchers is given at the beginning of this thesis.

Chapter 4 presents a calixarene-functionalized filter material I prepared and its efficient capture of Cr(VI) oxoanions from water. This chapter has previously been published under the title “Capture and Release Recyclable Dimethylaminomethyl-Calixarene Functional Cloths for Point-of-Use Removal of Highly Toxic Chromium Water Pollutants”.[39]

Chapter 5 presents a butylimidazole-functionalized filter material I prepared which is also efficient in capturing Cr(VI) oxoanions from water. These results are yet to be published.

Chapter 6 presents the linker-layer free synthesis of a metal organic framework on various polymer surfaces, as well as its transfer onto different substrates. Metal organic frameworks have a high potential as filtration material due to their vast internal surface area and an understanding of their growth mechanism as well as the possibility to transfer them from one substrate onto another could be very useful for future application in water purification.

1.4 References

(1) United Nations, The United Nations World Water Development Report 2021: Valuing Water. UNESCO, Paris.

(2) United Nations, International Decade for Action 'WATER FOR LIFE' 2005–2015: Water quality. http://www.un.org/waterforlifedecade/quality.shtml (accessed on 10 Mar 2019).

(3) NITI Aayog, Composite Water Management Index. National Institution for Transforming India June 2018.

(4) Benerji, A. India's 'worst water crisis in history' leaves millions thirsty. Reuters 5 Jul 2018 https://www.reuters.com/article/us-india-water-crisis-idUSKBN1JV01G (accessed on 18 Sep 2021).

(5) Yeung, J.; Gupta, S.; Guy, M. India has just five years to solve its water crisis, experts fear. Otherwise hundreds of millions of lives will be in Danger. CNN 4 July 2019 https://edition.cnn.com/2019/06/27/india/india-water-crisis-intl-hnk/index.html (accessed on 18 Sep 2021).

(6) Gill, V. Australia fires were far worse than any prediction. BBC 24 Feb 2020 https://www.bbc.com/news/science-environment-51590080 (accessed on 7 Sep 2021).

(7) New South Wales in Australien: Nach mehr als 240 Tagen feuerfrei. Der Spiegel 5 Mar 2020 https://www.spiegel.de/panorama/australien-new-south-wales-ist-nach-mehr-als-240-tagen-feuerfrei-a-70e01ad5-1332-4727-8aab-2d606d9bc486 (accessed on 7 Sep 2021).

(8) Pickrell, J. Australia's raging fires will create big problems for fresh drinking water. National Geographic 10 Jan 2020 https://www.nationalgeographic.com/science/article/australian-fires-threaten-to-pollute-water (accessed on 7 Sep 2021).

(9) Santín, C.; Doerr, S.H.; Otero, X.L.; Chafer, C.J. Quantity, Composition and Water Contamination Potential of Ash Produced under Different Wildfire Severities. *Environmental Research* **2015**, *142*, 297–308.

(10) Borunda, A. The science connecting wildfires to climate change. National Geographic 17 Sep 2020 https://www.nationalgeographic.com/science/article/climate-change-increases-risk-fires-western-us (accessed on 19 Sep 2021).

(11) BBC Visual and Data Journalim Team. California and Oregon 2020 wildfires in maps, graphics and images. BBC 18 Sep 2020 https://www.bbc.com/news/world-us-canada-54180049 (accessed on 19 Sep 2021).

(12) Liakos, C.; Labropoulou, E.; Woodyatt, A. Greece faces 'disaster of unprecedented proportions' as wildfires ravage the country. CNN 10 Aug 2021 https://edition.cnn.com/2021/ 08/09/europe/greece-wildfire-warning-climate-intl/index.html (accessed on 19 Sep 2021).

(13) Kammer, A. Waldbrände erreichen laut Umweltschützern historisches Ausmaß. Die Zeit 12 Sep 2021 https://www.zeit.de/gesellschaft/zeitgeschehen/2021-09/russland-walbraende-umweltschuetzer-historisches-ausmass-greenpeace-feuer (accessed on 19 Sep 2021).

(14) MyFireWatch map produced by Landgate, Western Australia's land information authority. https://myfirewatch.landgate.wa.gov.au/map.html (accessed on 07 Sep 2021).

(15) Holland, H. Angola mine leaks causes 'unprecedented' pollution in Congo rivers, researchers say. Reuters 21 Aug 2021 https://www.reuters.com/world/africa/angola-mine-leak-causes-unprecedented-pollution-congo-rivers-researchers-say-2021-08-20/ (accessed on 20 Sep 2021).

(16) Römer, J. Umweltkatastrophe im Kongo: Die Giftbrühe, die Tod und Verderben brachte. Der Spiegel 6 Sep 2021 https://www.spiegel.de/wissenschaft/weltall/kongo-leidet-unter-umweltkatastrophe-diamanten-rote-fluesse-und-tote-flusspferde-a-1d9da756-ae0c-496b-a989-e6f3e844badf (accessed on 7 Sep 2021).

(17) Reid, H.; Holland, H. Waste from Angola's Catoca diamond mine leaked into waterways last month. Reuters 23 Aug 2021 https://www.reuters.com/business/environment/waste-angolas-catoca-diamond-mine-leaked-into-waterways-last-month-2021-08-23/ (accessed on 20 Sep 2021).

(18) Holland, H.; Reid, H. Congo says Angola tailings pollution kills 12, to seek compensation. Reuters 3 Sep 2021 https://www.reuters.com/world/africa/congo-says-12-dead-4400-sick-following-angola-mine-tailings-leak-2021-09-02/ (accessed on 20 Sep 2021).

(19) Tizi, H. Kasai and Tshikapa rivers polluted by waste dumping. Afrik21 30 Aug 2021 https://www.afrik21.africa/en/kasai-and-tshikapa-rivers-polluted-by-waste-dumping/ (accessed on 20 Sep 2021).

(20) Backer, H. Water Disinfection for International and Wilderness Travelers. *Clinical Infectious Diseases* **2002**, *34*, 355–364.

(21) McGuigan, K.G.; Joyce, T.M.; Conroy, R.M. Solar disinfection: use of sunlight to decontaminate drinking water in developing countries. *J. Med. Microbiol.* **1999**, *48*, 785–787.

(22) Boyle, M.; Sichel, C.; Fernández-Ibánez, P.; Arias-Quiroz, G.B.; Iriarte-Puna, M.; Mercado, A.; Ubomba-Jaswa, E.; McGuigan, K.G. Bactericidal Effect of Solar Water Disinfection under Real Sunlight Conditions. *Applied and Environmental Microbiology* **2008**, *74* (10), 2997–3001.

(23) Tata uses nano technology for water purifier. Centre for Science and Environment 2010. https://www.cseindia.org/tata-uses-nano-technology-for-water-purifier-852 (accessed on 20 Mar 2019).

(24) Dankovich, T.A.; Gray, D.G. Bactericidal Paper Impregnated with Silver Nanoparticles for Point-of-Use Water Treatment. *Environ. Sci. Technol.* **2011**, *45* (5), 1992–1998.

(25) Elsanousi, S.; Abdelrahman, S.; Elshiekh, I.; Elhadi, M.; Mohamadani, A.; Habour, A.; ElAmin, S.E.; Elnoury, A.; Ahmed, E.A.; Hunter, P.R. A study of the use and impacts of LifeStraw in a settlement camp in southern Gezira, Sudan. *J. Water Health* **2009**, *7* (3), 478–483.

(26) Frechen, F.-B.; Exler, H.; Romaker, J.; Schier, W. Long-term behaviour of a gravity-driven dead end membrane filtration unit for potable water supply in cases of disasters. *Water Supply* **2011**, *11* (1), 39–44.

(27) Hoffman, J. LifeStraw Saves Those Without Access to Clean Drinking Water. New York Times 2011 https://www.nytimes.com/2011/09/27/health/27straw.html (accessed on 22 Feb 2022).

(28) Frechen, F.-B. WaterBackpack “Paul®“ for disasters and for permanent water supply. http://waterbackpack.org/download/F0_PAUL_distribution.pdf (accessed on 22 Feb 2022).

(29) Rober, M. Drinking Nasty Swamp Water (to save the world). YouTube 15 Feb 2019 https://www.youtube.com/watch?v=6qZWMNW7GmE (accessed on 22 Feb 2022).

(30) WHO International Scheme to Evaluate Household Water Treatment Technologies: P&G Purifier of Water Product evaluation report. World Health Organization 2015.

(31) Household Water Treatment and Safe Storage Fact Sheet: P&G Purifier of Water. Centre for Affordable Water and Sanitation Technology March 2018.

(32) Shannon, M.A.; Bohn, P.W.; Elimelech, M.; Georgiadis, J.G.; Marinas, B.J.; Mayes, A.M. Science and technology for water purification in the coming decades. *Nature* **2008**, *452*, 301–310.

(33) Babel, S.; Kurniawan, T.A. Low-cost adsorbents for heavy metals uptake from contaminated water: a review. *Journal of Hazardous Materials* **2003**, *97* (1–3), 219–243.

(34) Demirbas, A. Heavy metal adsorption onto agro-based waste materials: A review. *Journal of Hazardous Materials* **2008**, *157* (2–3), 220–229.

(35) Fu, F.; Wang, Q. Removal of heavy metal ions from wastewaters: A review. *Journal of Environmental Management* **2011**, *92* (3), 407–418.

(36) Hua, M.; Zhang, S.; Pan, B.; Zhang, W.; Lv, L.; Zhang, Q. Heavy metal removal from water/wastewater by nanosized metal oxides: A review. *Journal of Hazardous Materials* **2012**, *211–212*, 317–331.

(37) Ahalya, N.; Ramachandra, T.V.; Kanamadi, R.D. Biosorption of Heavy Metals. *Research Journal of Chemistry and Environment* **2003**, *7* (4), 71–79.

(38) Michalak, I.; Chojnacka, K.; Witek-Krowiak, A. State of the Art for the Biosorption Process—a Review. *Appl. Biochem. Biotechnol.* **2013**, *170* (6), 1389–1416.

(39) Bieber, V.S.; Ozcelik, E.; Cox, H.J.; Ottley, C.J.; Ratan, J.K.; Karaman, M.; Tabakci, M.; Beaumont, S.K.; Badyal, J.P.S. Capture and Release Recyclable Dimethylaminomethyl-

Calixarene Functional Cloths for Point-of-Use Removal of Highly Toxic Chromium Water Pollutants. *ACS Appl. Mater. Interfaces* **2020**, *12*, 52136–52145.

Chapter 2: Impact of Heavy Metal Water Pollution

2.1 Mercury and other Water Pollutants

When I started working on the removal of toxic heavy metal ions from drinking water, inorganic mercury (Hg(II)) was chosen fairly arbitrarily as a starting point. However, my experiments soon revealed that the mercury nitrate I was using is very difficult to dissolve in water to begin with. Research into the literature further unveiled that while the consumption of inorganic mercury salts can lead to acute poisoning, it is mostly accumulated in the liver and kidney and from there excreted in bile and urine, respectively, instead of remaining within the body.[40] Inorganic mercury furthermore does not cross the blood brain barrier, unlike organic mercury compounds such as methylmercury, which by crossing said barrier can lead to serious neurological ailments. Since organic mercury bioaccumulates in the marine food chain—unlike inorganic mercury—, one can inadvertently consume large quantities of it through fish and shellfish.[41,42] The danger of organic mercury became widely recognized following a great tragedy that took place in Japan in the 1950s and 1960s.

In the Japanese coastal city of Minamata, a mysterious illness was first observed in families of fishermen in the 1940s and over the following years became more and more prevalent in the local population, turning into an epidemic by 1956.[43,44] Symptoms in mild cases included headaches and insomnia—in more severe cases, ataxia, numbness in the extremities, as well as visual and auditory impairments were observed.[45] By 1956, 17 people had died from the illness; by 1961 the number of deaths had increased to 35, with many more patients suffering from its symptoms.[43,45] Autopsy showed disturbances within the brains of victims and even disintegration of brain cells, but few changes in other organs apart from the nervous system.[43] However, high concentrations of mercury were found within the bodies of affected humans as well as animals.[43] Elevated mercury concentrations were also found in fish and shellfish from the local bay, leading researchers from a local university to conclude that the illness, named “Minamata disease”, was caused by the consumption of large quantities of polluted marine life.[43,45] A local chemical factory was suspected to be the source of the pollution since they used mercury salts as catalysts in their large

scale acetaldehyde synthesis.[43,45,46] The debate continued for years as the company initially refused to take responsibility, instead taking steps such as draining their wastewater into the river mouth instead of straight into the bay in 1958 and installing a wastewater treatment facility in 1959.[45] While the change in wastewater dumping location was thought to lead to a better dilution of harmful chemicals due to stronger currents, it instead led to an increase of the area in which people became affected by the disease.[45] Meanwhile, the new treatment facility in fact only removed insoluble material from the water, but not dissolved chemicals.[45] The company furthermore claimed that its waste could not have caused the disease as the factory had been in operation since the 1930s.[45] However, umbilical cord analyses showed a small peak of mercury concentrations already occurring in the 1930s and 1940s, before a larger peak was detected in the 1950s and 1960s, likely caused by an increase in production from the factory and a process change that took place in 1951 and increased the amount of organic mercury byproduct created.[44,45] Cases of Minamata disease only subsided after the factory stopped production in 1967.[44]

While this case underlines the great dangers of organic mercury compared to inorganic mercury, it also hints at the difficulty of removing dissolved contaminants from water. Organic mercury is not taken up by drinking, but rather through consumption of marine animals, in particularly of fish high up in the food chain due to bioaccumulation, as illustrated in Figure 5.

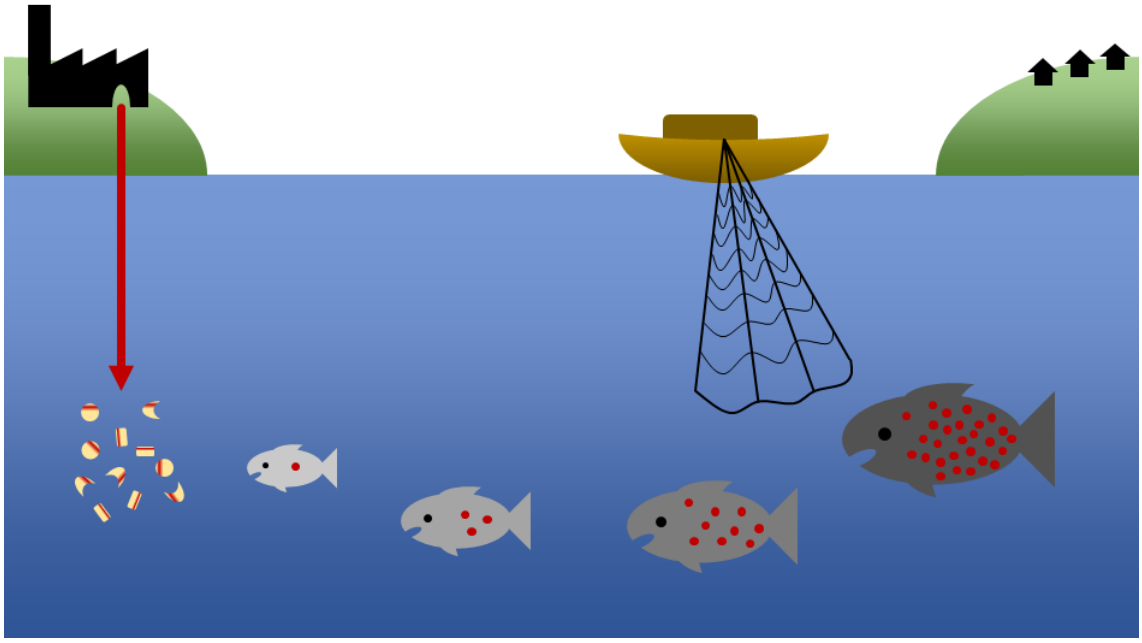

Figure 5: Bioaccumulation of organic mercury in the marine food chain from phyto- and zooplankton to increasingly large fish. Red dots (organic mercury) are shown to triple with each step up in the food chain in this illustration; in reality the factor by which organic mercury concentration increases with every step can be significantly higher.[47,48]

While point-of-use water purification would not have helped in this case, a more efficient wastewater treatment system would have saved many lives. In October 2013, the United Nations adopted the Minamata Convention on Mercury. It requires countries to restrict the use of mercury compounds and control and reduce mercury emissions as much as possible.[49] To this day, over 150 countries and the European Union have joined this treaty, which gives hope that large scale mercury poisonings will no longer occur in the future.[50] But the tale of the Minamata disaster serves as a stark reminder that even seemingly low concentrations of toxic pollutants can have a strong effect on human health. And while organic mercury poisoning is now well known and controlled, there are still other heavy metals that cause severe health issues to this day.

Which heavy metal pollutants are of particular concern to drinking water? Both the World Health Organization (WHO) and the non-for-profit Water Quality Association (WQA) have in the past published lists of chemicals of major public health concern. The most notable heavy metal pollutants on these lists which are primarily consumed through water are arsenic, chromium, copper, lead, and uranium.[51,52]

Arsenic is not only released into water through industrial activities but mainly from natural deposits.[53] While acute poisoning occurs when ingesting as little as 100 mg arsenic, even significantly lower amounts can lead to chronic health effects and death when ingested over an extended period of time.[53] Naturally high arsenic concentrations occur in the groundwaters of many Asian and American countries.[54] Bangladesh is most infamous for suffering from high Arsenic levels, with an estimated annual death toll of over 40,000.[55]

Chromium occurs in nature as trivalent ion but hexavalent chromium from industrial wastewaters is the form that is more dangerous to human health.[56] Since chromium oxide (Cr_2O_3) forms an anticorrosive passivation layer, hexavalent chromium compounds are popular for chrome plating, as additive to steel, and in cooling water, to name a few examples. During these industrial processes, Cr(VI) is reduced to Cr(III). When dissolved in water and ingested, even low concentrations of hexavalent chromium can lead to serious health effects and death over time.[56] Recognizing these dangers, the European Union only recently halved its legal limit for chromium in drinking water.[57,58]

Copper is essential to human health and surveys indicate that three quarters of the US population in fact consume less than the recommended minimum amount. However, ingesting too much copper can lead to acute copper poisoning with symptoms ranging from vomiting to kidney failure, depending on the severity. While elevated copper concentrations in water can be the result of industrial discharge, in most cases they seem to be caused by plumbing issues since many water pipes are made of copper.[59]

Lead in drinking water mostly originates from corrosion of lead containing water pipes and fittings.[60] As lead has been used by humans since ancient times, lead poisoning has a long history, starting from inadvertent slow poisonings in ancient Rome when lead acetate was used as sweetener.[61] Children are particularly vulnerable to even low concentrations of lead in drinking water. Since their bodies absorb a significantly higher fraction of the lead they ingest, compared to adults, low lead levels that are harmless for adults can still seriously damage a child's nervous system and cause irreversible harm such as reduced intelligence and stunted growth.[60]

Uranium, like arsenic, mostly occurs in drinking water due to leaching from natural deposits. Consumption of it can damage the kidneys and if uranium

decays into other radioactive elements within the body, it can cause cancer over time.[62] However, elevated uranium concentrations in water do not seem to be as widely spread as elevated arsenic concentrations.[63]

Out of these pollutants, I identified arsenic, chromium, and lead as particularly concerning and therefore planned to develop filtration materials targeting each of them. I chose chromium as the first target pollutant because chromium salts are intensely coloured and their concentration in water can therefore be easily measured using UV–Vis spectroscopy. Due to the Covid-19 pandemic, I was unfortunately unable to complete the laboratory work I had planned. While I had already successfully prepared and tested different chromium filtration materials before, the lockdown began just as I was starting my arsenic and lead experiments, thus cutting them short before I was able to gain any results. In the following I am presenting more information on these three pollutants, as well as noting my plans for arsenic and lead capture, before my chromium capture experiments and results are presented in the subsequent chapters.

2.4 Chromium | Cr(VI)

2.4.1 Chromium – History and Importance

Chromium was discovered by the French chemist Louis Nicolas Vauquelin at the end of the 18th Century when analysing the constituents of the red mineral crocoite ($PbCrO_4$).[64,65] The element was named after the Ancient Greek word for "colour" – χρῶμα (chroma) – due to the many colours of its compounds.[66,67] Chromium exists predominantly in the oxidation states 0, 3, and 6, though compounds with intermediate oxidation states are known.[68] While metallic chromium is silvery-grey, its coordination compounds can take on all the colours of the rainbow. A few examples can be seen in Figure 6.

Figure 6: Colourful chromium compounds. Top row: trivalent chromium compounds chromium chloride $CrCl_3$ (turns from purple to green when hydrated) and chromium sulfate $Cr_2(SO_4)_3$. [69, 70] Bottom row: hexavalent chromium compounds potassium chromate K_2CrO_4 and potassium dichromate $K_2Cr_2O_7$.[71,72]

In the 19th Century, chromium compounds became increasingly popular for industrial applications. They were used as mordants, pigments, for leather tanning, metallurgy, chromium-plating, and other applications.[67,73] However, the toxic properties, particularly of hexavalent chromium compounds, were also soon discovered. Already in the first third of the 19th Century, dyers who spent a lot of time with their arms immersed in concentrated potassium dichromate solutions were reported to have sores on their hands and arms. [74, 75] Animal tests furthermore showed that the injection of potassium chromate into the veins and under the skins of dogs led to adverse health effects and often death.[74] Even though these dangers were known, hexavalent chromium compounds were still widely used, and workers not protected very well for many more decades. In the early 20th Century for example, chromium plating workers, who inhaled chromic acid fumes during their work, were reported to develop ulcerations and sometimes perforation of nasal septums.[76]

2.4.2 Chromium – Danger to Human Health

While the adverse health effects of hexavalent chromium were clear to see on workers, who were in direct contact with the substances, the effect of pollution from industries using such compounds on the public remained uncertain for a long time. In 1987, the first study was published that indicated the cancerogenic effect of hexavalent chromium in drinking water on humans.[77] In Jinzhou, Liaoning Province, China, an iron alloy plant had begun trial smelting of metallic chromium in 1959 and established mass production in 1965, resulting in large amounts of wastewater that contained hexavalent chromium compounds. Some of the wastewater was drained directly into the environment, some stored in containers from which it slowly leached into the ground. Soon, the groundwater of the surrounding area was contaminated, to the point where the water from certain nearby wells turned yellow.[77] A study performed by two Chinese scientists, who documented symptoms reported by inhabitants of the villages in the contaminated area for ten years following the first reports of discoloured water, showed an increased number of gastrointestinal disorders, as well as an increased cancer mortality rate.[77]

In the same year as the Chinese study was published, in 1987, the US-American Pacific Gas and Electric Company (PG&E) notified the California Regional Water Quality Control Board of increased hexavalent chromium levels in the groundwater at their gas compressor station near the small town of Hinkley, San Bernadino County, California, USA.[78,79] The company had used hexavalent chromium compounds as corrosion inhibitors in their cooling water. Chromium-polluted water had been discharged into unlined pools since 1951, from where it seeped into the ground. In fact, PG&E had been aware of the environmental pollution by 1965.[78,80] The ensuing court case between the company and the Hinkley residents who had been suffering from increased cancer rates and other health effects due to the pollution of their drinking water is well known through the 2000 film ‘Erin Brockovich’. But even though PG&E decided to settle the lawsuit by paying $333 million to the Hinkley residents in 1996,[81] the question of how dangerous hexavalent chromium in drinking water really is remained controversial for years.

In vitro studies showed that hexavalent chromium is without doubt harmful on a cellular level. Within a cell, hexavalent chromium can be reduced by ascorbate, cysteine, and glutathione.[82] During the reduction towards the stable trivalent chromium, oxygen radicals and intermediate oxidation states are formed that can react with and damage different parts of the cell, for example by causing DNA strand breaks.[83] The resulting trivalent chromium can form complexes with amino acids and the phosphate group of DNA.[84] These complexes are very stable and difficult to break up and can therefore impair numerous cellular functions, leading to cancer and other health issues.[85] Trivalent chromium in the environment is relatively harmless because it cannot easily permeate cell membranes. Hexavalent chromium however is structurally similar to phosphates and sulfates and is therefore easily transported into cells that actively take up phosphates and sulfates as nutrients.[85,86] If hexavalent chromium is therefore delivered to any cell in the body, it can be taken up and damage the cell. Given these observations, the only factor determining the danger of hexavalent chromium in drinking water remains the questions of whether it survives the gastrointestinal tract or whether it is already completely reduced in the acidic environment of the stomach.[86]

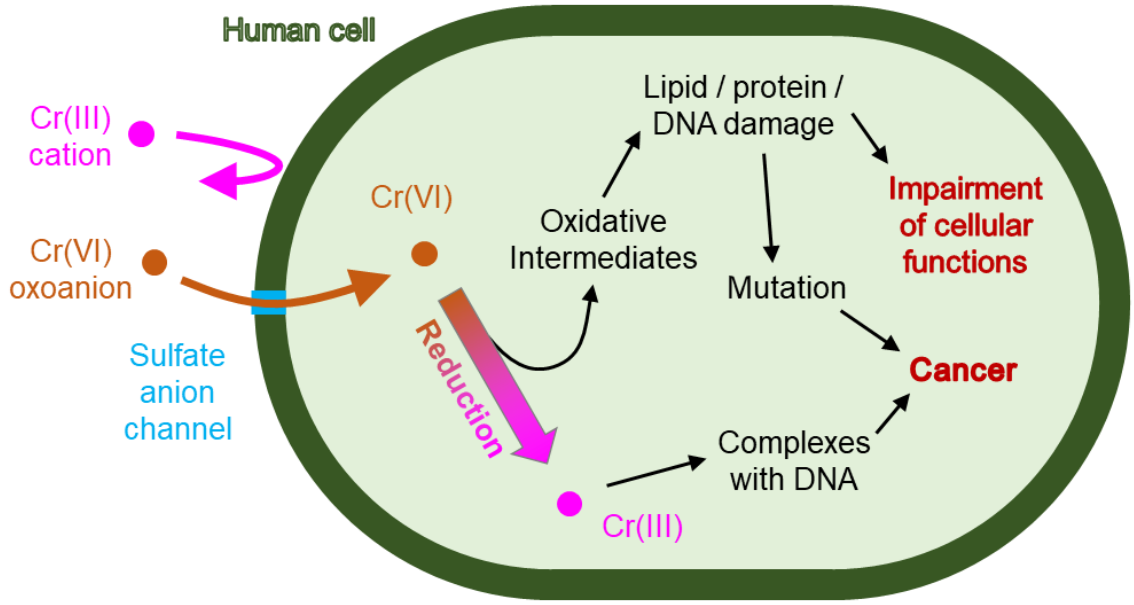

Figure 7: Schematic processes within a human cell when exposed to trivalent and hexavalent chromium.

The first and for many decades the only lifetime drinking study of hexavalent chromium on mice was published by German scientists in 1968,[87] just one year

after the Chinese study that addressed the increased cancer mortality in the hexavalent chromium polluted region in Jinzhou. The authors suspected a cancerogenic effect of the compound but were not able to fully prove it, also because many of their laboratory mice died from an infectious epidemic during the experiment.[87] Towards the end of the 20th century, more experiments showed the dangerous health effects of hexavalent chromium in drinking water on rats, and theories on the toxic mechanism of hexavalent chromium in the human body were published.[85,88,89] And yet, some scientists continued to insist that ingested hexavalent chromium is completely reduced to its less dangerous trivalent version in the gastrointestinal tract, thus arguing that it cannot cause adverse health effects.[90,91] It is interesting to note that the authors of the referenced publications doubting the harm of chromium in drinking water were all employed by ChemRisk, Exponent, or Merck at the time: ChemRisk was paid directly by PG&E, the company that had caused the chromium pollution in Hinkley, California.[78] Exponent was paid by two other companies entangled in chromium cleanup cases (General Electric Co. and Lockheed Martin Corp.), and Merck was also involved in a chromium cleanup case.[78,92,93,94]

Only in 2009 a second long-term study of the effect of hexavalent chromium in drinking water on rats and mice was published. In this study, the hexavalent chromium was clearly found to be carcinogenic.[95,96] Following this study, conducted by the U.S. National Toxicology Program, the U.S. Environmental Protection Agency (EPA) began to consider lowering the legal limit for chromium in drinking water that is currently set at 100 µg L^{-1} (total chromium content). But under the pressure of the industry, the decision was once again delayed.[78] The current legal situation is summarized in section 2.4.4.

2.4.3 Chromium – Pollution Occurrence

Pollution of aqueous systems with hexavalent chromium is not an issue that is restricted to a few places like Jinzhou and Hinkley. It is not even restricted to the last century, as many reports of Cr(VI) polluted drinking water all over the world can be found in the literature of the current decade, such as in Greece[97,98], Czech Republic[99], India[100], China[101], Italy[102], and Taiwan[103], just to name a few examples. Table 2 provides an overview of hexavalent chromium pollution found

all over the world in the past decade. The locations listed in Table 2 are furthermore marked with red dots in Figure 8. Green dots stand for Jinzhou in China and Hinkley in the USA, the locations of the cases discussed in the previous section.

Figure 8: World map showing some locations of hexavalent chromium pollution in the groundwater. Green dots (from left to right): Hinkley, CA, USA and Jinzhou, China, the locations mentioned in section 2.4.2. Red dots (from left to right): Aosta Valley (Italy), Czech Republic/Poland border region, OInofita Region and Sarigkiol Basin in Greece, Sukinda (India), Wuhan (China), and Taichung City (Taiwan), the locations from Table 2.

While it may appear from the map in Figure 8 that hexavalent chromium pollution mainly occurs in Central Europe and East Asia, there are numerous examples of chromium pollution in Middle America[104], South America[105,106], Africa[107,108], and Central Asia[109] to be found in the literature, showing that it is indeed a global issue.

Table 2: Examples of hexavalent chromium pollution from publications of the current decade.

Location	**Time**	**Cr(VI) content**	**Cr(VI) source**	**Note**	**Ref.**
Asopos river, Oinofita region, Greece	2007-2009	Maximum levels 41-156 µg L^{-1}	Industrial waste	Elevated cancer mortality observed	97

10 sites in Czech Republic, 1 in Poland	Nov 2011 – Sep 2013	2.6-3600 mg L^{-1}	Electroplating, tanning, and chemical industry. Low amounts from geogenic sources.	Industrial and natural sites	99
Sukinda Chromite Mine, India	Oct 2013	21-115 µg L^{-1} (and 27-1350 µg L^{-1} Cr(III))	Chromite mining	Calculated high cancer risk	100
Wuhan, China	2012-2014	(Only tested in urine, not in drinking water)	Industrial waste	Risk of premature rupture of membranes in pregnant women correlates with urine Cr(VI) concentrations	101
Sarigkiol Basin, Northern Greece	2014-2015	Up to 120 µg L^{-1}	Ophiolitic rock and leaching from fly ash deposits from lignite burning power plant.	Hexavalent chromium in groundwater partially of natural origin.	98
Aosta Valley, Italy	2007-2015	Up to 62-262 µg L^{-1}	Accumulation from a previously active industrial site.	Risk assessment: water needs to be treated before drinking	102
Wu river watershed near Taichung City, Taiwan	2004-2015	Average up to 5 µg L^{-1} (and polluted soil and rice)	Industrial waste from electroplating, textiles, metal surface treatment, and other industries.	Increased rate of gastric cancer, increased medical costs	103

2.4.4 Chromium – Legal Situation

Table 3 lists the current legal limits for chromium in drinking water. In most cases these values refer to total chromium content, only the Californian Environmental Protection Agency uses a separate value for hexavalent chromium.

Table 3: Legal limits for chromium in drinking water.

Organization	**Chromium limit for drinking water**	**Ref.**
WHO (World Health Organization)	50 µg L^{-1}	110
European Commission	25 µg L^{-1} since January 2021 (prior to that 50 µg L^{-1})	57, 58
US EPA (Environmental Protection Agency)	100 µg L^{-1}	111
California EPA	50 µg L^{-1}; previously 10 µg L^{-1} for Cr(VI) (no longer active)	112, 113

In the European Union, the legal limit for chromium in drinking water originally followed WHO recommendations but was recently reduced. While the European Commission's initial Drinking Water Directive from 1998 set a limit of 50 µg L^{-1},[57] the revised Directive that entered in force in January 2021 halved it to 25 µg L^{-1}.[58] This recent amendment shows that the dangers of chromium in drinking water are more and more politically recognized nowadays.

The limit set by the United States Environmental Protection Agency (US EPA) is the highest on the list. In fact, the US used to have a federal chromium maximum contaminant level of 50 µg L^{-1} but raised it to 100 µg L^{-1} in 1991.[113] Since 2010, the US EPA has been in the progress of reassessing the danger of hexavalent chromium. However, to this date, only some preliminary assessment materials have been released in 2014 and 2019, covering the first two of seven steps.[114,115]

In California, the regulation of hexavalent chromium in drinking water meanwhile suffered a severe setback less than a year ago. After the National Toxicology Program's lifetime study on mice and rats was published in 2009,

things were looking good for supporters of stricter hexavalent chromium limits in the state where the Hinkley case took place decades prior. In 2011, the Office of Environmental Health Hazard Assessment (OEHHA) belonging to the California Environmental Protection Agency (EPA) recommended a public health goal (PHG) of 0.2 µg L^{-1} hexavalent chromium in drinking water as a concentration where the contaminant does not pose a significant risk to human health.[116] The state's Department of Public Health then proceeded to create a maximum contaminant level (MCL) for hexavalent chromium that is as close to the PHG as possible, since US federal legislation only defines a MCL for total chromium in drinking water. In July 2014, the hexavalent chromium MCL of 10 µg L^{-1} became effective.[112] Only one and a half years later however, the California Manufacturers and Technology Association and Solano County Taxpayers Association filed a petition with the Superior Court of California, demanding the MCL to be withdrawn. In May 2017, the court ruled to make the MCL invalid, supporting the petitioners' argument that the California Department of Public Health had "failed to properly consider the economic feasibility of complying with the MCL"[117]. The California Water Board, while disagreeing with the court's decision, decided not to appeal it and instead to focus on adopting a new MCL.

2.4.5 Chromium – Removal from Water

A large variety of materials has in the past been employed to capture chromium oxoanions from water, made from natural or synthetic media with many utilizing amine functional groups to target the pollutants. However, most of these materials only work efficiently under low pH conditions which are unfit for human consumption.[118,119,120,121,122]

During the first year of my PhD, I investigated the hexavalent chromium sorption efficiency of non-woven cloth functionalized with chitosan, derived from chitin. Chitin is the second-most abundant natural polymer and found in the exoskeletons of crabs, shrimps, and other arthropods.[123,124] As waste product of the crab meat canning industry, it is available in large quantities at very low cost. Chitosan is generated from chitin by partial deacetylation under alkaline conditions. Chitin is insoluble in all usual solvents. Once the degree of deacetylation reaches about 50%, the resulting chitosan becomes soluble in

acidic aqueous solutions. In the acidic environment, the amine groups become protonated, thus turning the polysaccharide into a polyelectrolyte.[124] The large number of hydroxyl and primary amine groups make chitosan highly adsorbent for heavy metals.[123] This adsorption is thought to happen via an ion exchange mechanism. It is hypothesized in the literature that the negatively charged chromate anions are attracted to the NH_3^+ groups of the chitosan via electrostatic interactions, though the mechanism has not been proven.[125,126]

While my results were initially promising, the method for immobilizing chitosan onto the cloth turned out not to be very reliable and further difficulties were brought on by variations in the chitosan properties between different batches, due to it being a natural material. Therefore, I changed my strategy and functionalized filters with different capture molecules which will be discussed in more detail in chapters 4 & 5.

2.3 Arsenic | As(III) & As(V)

2.3.1 Arsenic – History and Importance

The etymology of the word “arsenic” is less clear than that of “chromium”, tracing back to Latin, Ancient Green, Aramaic, and Persian.[127] Arsenic has been used by humans since ancient times, for a multitude of applications from medicine to murder.[128,129] The ancient Romans used arsenic containing eye shadow, it was a popular pesticide prior to the invention of synthetic organic pesticides, and traditional Chinese and Indian herbal medicine can contain high arsenic concentrations.[128] In Europe, the 19th century has been called the “age of arsenic” because of the element’s widespread popularity at the time.[130] Green arsenic containing dyes and pigment were used in wallpapers, clothing, accessories, and much more (see Figure 9) and only towards the end of the century the understanding grew that many mysterious illnesses had likely been caused by exposure to arsenic through all these sources, leading to a turn from arsenophilia to arsenophobia.[130]

Figure 9: Illustration in the London Times newspaper from 1862. The title "The Arsenic Waltz" refers to the health danger from the ubiquitous use of arsenic during the 19th century, including as part of dyes for clothing and accessories, such as the headdress of the skeleton lady in the illustration.[131]

While awareness for the danger of chronic exposure to arsenic only began to spread in the past 150 years or so, the effect of acute arsenic poisoning has been known for centuries. Starting from the Middle Ages, the popularity of arsenic as poison grew because it was easy to obtain (due to its use as rat poison), tasteless, and symptoms of acute arsenic poisonings were easy to confuse with other common illnesses since they typically included nausea, vomiting, abdominal pain, and diarrhoea.[129] For these reasons it became known as “King of Poisons” but also as “Poison of Kings” due to rumours about its involvement in the murders of multiple members of the ruling class, including Napoleon.[128,129] The element’s popularity as poison only began to decline after the Marsh Test was developed in 1836 that allowed reliable detection of arsenic.[129] Nevertheless arsenic compounds such as lead arsenate continued to be widely used, for example as pesticides, until concerns about health effects of arsenic residues on food crop finally led to bans, in the US as late as 1988.[129] In medicine arsenic is used to this day, particularly in cancer chemotherapy. The origins of this

application go back to the late 18th century when a 1% potassium arsenite solution known as Fowler's solution was used to treat numerous diseases from asthma to malaria.[129] In the late 19th century, Fowler's solution was found to be effective in treating leukaemia patients.[129] While potassium arsenite is no longer consumed today due to its known toxicity, arsenic trioxide is used to this day for the treatment of a certain type of acute leukaemia and its effects on other cancers are under investigation.[129,132,133]

2.3.2 Arsenic – Danger to Human Health

While the consumption of high concentrations of arsenic has been known to be toxic since ancient times, the effects of chronic exposure to low concentrations of arsenic have only been studied since the second half of the twentieth century. Studies focusing on the inhabitants of areas in Taiwan with naturally elevated arsenic concentrations in the groundwater have been particularly insightful. With the help of Prof. Lin (林安邦) of the National Taiwan Normal University (國立臺灣師範大學) I was able to obtain the two earliest publications that studied Blackfoot disease, an illness endemic to an area in southwest Taiwan. Published in 1961, they describe in great detail this affliction whose cause was not yet understood at the time. Blackfoot disease had been occurring among the inhabitants of a region located on the southwest coast of Taiwan (called Chianan plain in later publications; see Figure 11 for map) since the 1920s, but since there were initially only very few cases each year, it was not until the 1950s that the local authorities took notice of it.[134,135] During a study period between 1958 and 1960, 327 cases of Blackfoot disease were diagnosed, in both adults and children as young as seven years.[134] The first symptoms of the illness are a numb and cold feeling in the affected extremity (in most cases one foot), followed by agonizing pain.[134] Gangrenes develop in the affected area between one week and two years after the appearance of first symptoms, leading to the black discoloration that gives the disease its name.[134] Afterwards, spontaneous amputation of the affected digit or extremity occurs within six months in 80% of cases.[134] The disease sometimes affected just the tip of a finger but some patients lost both feet to it and there were even cases reported in which all four extremities were affected or where the illness led to death.[134] Due to the horrifying effects of Blackfoot disease, scientists

in Taiwan conducted thorough studies to find out its causes. While diet, financial situation, smoking habits, and familial relationship to other patients appeared to have no effect on the incidence of the illness, drinking water was soon suspected to play a major part.[135] The inhabitants of the endemic area originally consumed surface water (from ponds, streams, and rainwater) until artesian wells with depths of about 100–280 m were introduced in the 1910s and 1920s.[136] Researchers soon realized that all patients suffering from Blackfoot disease had been consuming water from these deep wells, while no cases were found in villages within the same region where shallower wells were used.[134,135] While there was no difference in the bacteria and fungi found in waters from different well types, it was already suspected in 1961 that a chemical found within the water from the deeper wells was the likely cause for Blackfoot disease.[134] Even though pipes were built beginning in 1956 that supplied the region with fresh water from the country interior, many remote communities continued relying on artesian wells and the main peak of Blackfoot disease case numbers only took place in 1957–1958, indicating a delayed effect.[135]

In 1968 a major epidemiologic study investigated for the first time the connection between arsenic content of drinking water and illnesses such as Blackfoot disease and skin cancer within the population of the Chianan plain.[136] While skin cancer caused by UV rays from the sun is usually developed on exposed skin, in three quarters of cases observed within this region it was found on unexposed surfaces, indicating a different cause.[136] Surveying artesian wells and over 40,000 inhabitants of the area, a clear correlation was found between the arsenic concentration (400–600 ppb in most cases, but some as high as 1820 ppb) of well water and prevalence of both Blackfoot disease and skin cancer among the individuals using the wells, across all age groups and genders. Water from shallow wells on the other hand was found to contain no more than 17 ppb arsenic and individuals consuming water from them were not affected by these illnesses.[136] Later studies also showed that prevalence rates of other types of cancer (including bladder, kidney, lung, and liver) were increased within the Blackfoot disease endemic area compared to the rest of the country.[137,138] Even though arsenic-free tap water was made available to all inhabitants of the Chianan plain in 1966, long term studies undertaken in the following decades

continued to show a clear relationship between the cumulative exposure to arsenic and cancer incidence.[136,139]

On the opposite side of the island, arsenic was also found in well waters within a smaller area (Lanyang plain, see Figure 11 for map) and with concentrations overall lower than found in the Chianan plain, at an average of 27 ppb, with less than 10% above 300 ppb though some as high as 3590 ppb.[140] A long-term study conducted in the area showed that in the twenty years after the local population stopped using drinking water from these wells, those with a higher cumulative arsenic exposure (concentration in well multiplied by the number of years an individual drank from it) had a significantly increased risk of bladder cancer compared to those subjected to a lower arsenic exposure.[140] These reports show the slow-acting effect of arsenic on the body, meaning that health issues caused by the substance can appear years after a person is no longer exposed to arsenic and impact lives for decades.

Over the past 100 and more years, the effects of arsenic on humans and animals have been closely studied. It is now understood that after ingestion of inorganic arsenic, it is quickly absorbed into the blood.[141] The metabolism of arsenic within the human body is schematically depicted in Figure 10. As(V) is reduced to As(III) on its way through the blood and liver.[141] As(III) is then easily taken up by cells through simple diffusion where it is methylated in multiple steps with the help of the enzyme arsenite methyltransferase.[141] While the precise mechanism of arsenic toxicity is not yet known, formation of reactive oxygen and nitrogen species during arsenic reduction and methylation is suspected to play an important role.[141,142] Reactions of these species with cellular components can lead to numerous adverse effects, such as the inhibition of DNA repair.[142] By the time ingested arsenic leaves the body, only 10–20% is still in its inorganic form, while the rest has been methylated, mostly to pentavalent dimethylarsenic (DMA^V, see Figure 10).[141,142] Other organisms such as certain fungi and even rats are able to further metabolize arsenic to create trimethylarsenic. In contrast to the metabolism of inorganic arsenic, organic arsenic, upon ingestion, is excreted mostly unchanged because it is not taken up as easily by body cells.[141]

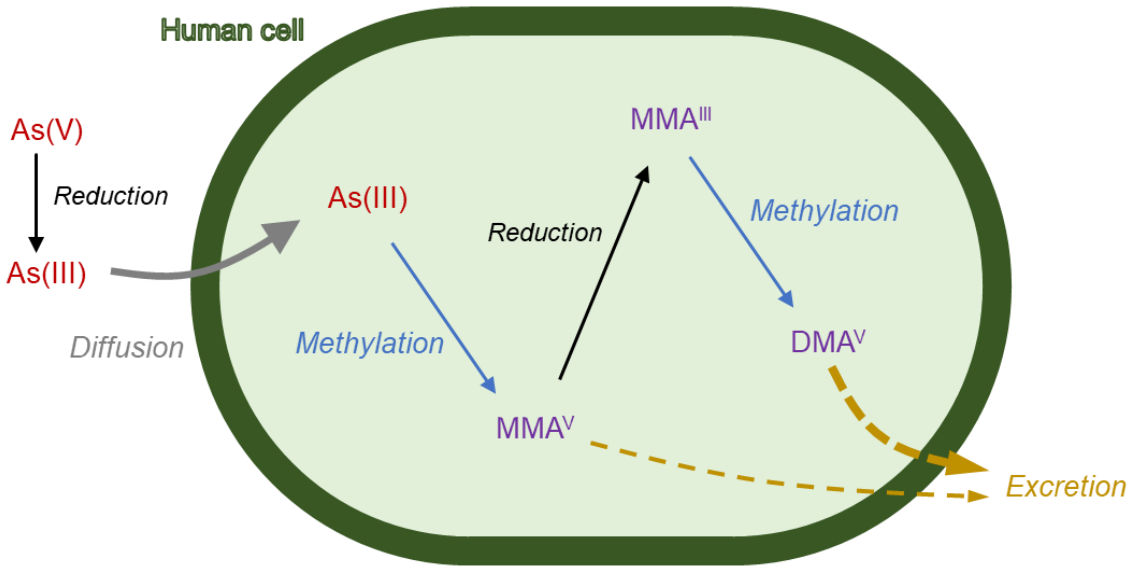

Figure 10: Metabolism scheme for arsenic within the human body. As(V) and As(III) stand for inorganic pentavalent and trivalent arsenic ions, such as arsenate and arsenite. MMA^{V} means monomethylarsonic acid (contains As(V)), MMA^{III} means monomethylarsonous acid (contains As(III)), and DMA^{V} means dimethylarsinic acid (contains As(V)). Scheme drawn using information from references 141 and 142.

2.3.3 Arsenic – Pollution Occurrence

In the past two decades, naturally occurring elevated arsenic concentrations within Taiwan have been extensively studied. Besides the Chianan plain[143,144,145], further locations included the Choushui river alluvial fan[144, 146], the Beitou–Guandu area[147] and more specifically the Guandu wetland within it[148,149], as well as the Lanyang plain[150]; see Figure 11 for a map. In all these locations, arsenic ions were found to be naturally contained within iron oxyhydroxides and released into the water when the latter are dissolved under reducing conditions, but also adsorbed back onto iron oxide minerals under oxidating conditions.[143–150] Slow groundwater flow due to impermeable clay layers and leachate from landfills can lead to an increased arsenic concentration in groundwater.[143,145,149,150] On the other hand, the formation of FeS_2 by sulfate reducing bacteria can help to immobilize arsenic, as can mangrove roots.[148,149]

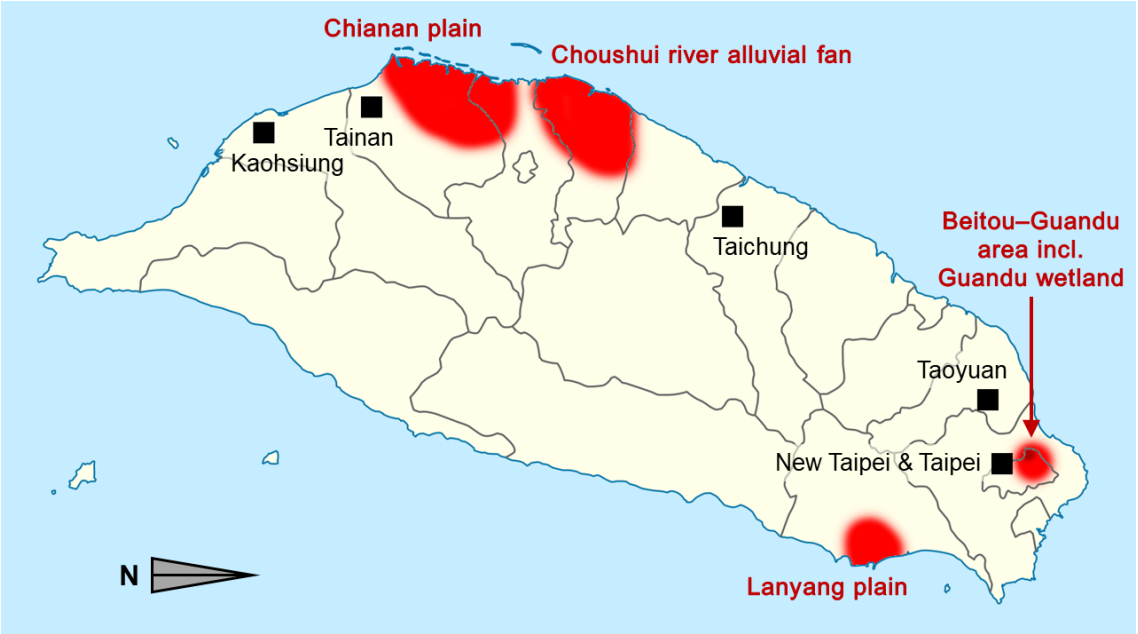

Figure 11: Map of Taiwan (main island) showing areas where naturally occurring elevated arsenic concentrations have been studied (red) and cities with populations over 1 million for reference (black squares). Base map taken from 151; arsenic occurrence areas drawn in based on studies focusing on the Chianan plain[143,144,145], Choushui river alluvial fan[144,146], Beitou–Guandu area[147], Guandu wetland (dark red spot within Beitou–Guandu area)[148,149], and Lanyang plain[150].

Since elevated arsenic concentrations in groundwater are caused by the presence of natural mineral deposits, they can occur all over the world. Arsenic has been found in waters of over 25 countries in Asia, Europe, Africa, North and South America.[129,152,153] With today's knowledge about the danger of chronic arsenic ingestion, developed countries like Taiwan can protect their population by building the necessary infrastructure to provide clean tap water to all homes. The inhabitants of developing countries are not as lucky: according to some estimates, approximately 100 million people worldwide are at risk from elevated arsenic concentrations in their drinking water, with most of them living in developing countries.[154] The country containing the largest share of people at risk from arsenic containing groundwater is Bangladesh.[154] Between 25–36 million of the country's population are at risk of chronic arsenic poisoning, according to different estimates.[154,155,156] Elevated arsenic concentrations (above 10 ppb) have been found in the groundwaters of over half of Bangladesh's districts, which is alarming because most of the population uses wells to draw groundwater for all their everyday needs due to mismanagement of surface waters.[154,155,156] In many locations the arsenic concentration is even higher than 1000 ppb.[154,155]

According to model calculations, nearly 43,000 deaths in Bangladesh can be attributed to chronic arsenic consumption every year.[157] Many more people live with skin lesions caused by arsenic, ranging from discoloration to skin cancer and amputation.[155]

These staggering numbers show that arsenic in drinking water remains a real threat around the world to this day. While the usage of alternative water sources is the most commonly suggested measure, it can be difficult to achieve in developing countries lacking the necessary infrastructure and water management.[154,155] Therefore, efficient point-of-use filters that are able to remove arsenic from drinking water could help to save countless lives.

2.3.4 Arsenic – Legal Situation

Since the danger of chronic exposure to even low concentrations of arsenic is well understood nowadays, most countries have very strict legal limits for arsenic in drinking water. Unlike with chromium, the European Union and the USA are in agreement with the World Health Organization about this pollutant, having set a limit of 10 ppb decades ago, Table 4.

Table 4: Legal limits for arsenic in drinking water.

Organization	**Arsenic limit for drinking water**	**Ref.**
WHO (World Health Organization)	10 µg L^{-1}	54
European Commission	10 µg L^{-1}	57, 58
US EPA (Environmental Protection Agency)	10 µg L^{-1}	158

2.3.5 Arsenic – Removal from Water

Numerous techniques for removing As(III) and As(V) from water have been studied in the literature. A combination of coagulation and flocculation works well

for high arsenic concentrations but the need to correctly dose coagulation and flocculation agents and the production of large amounts of arsenic-rich sludge make this method unsuitable for point-of-use.[159,160] Membrane filtration is similarly unsuitable for individuals due to its high cost and complex setup; a combination of coagulation and membrane filtration can however be efficient for large scale water purification.[159,160] Some of the most widely used techniques for arsenic removal are based on adsorption and ion exchange.[159,160] Since these are usually easy to handle, they can be well suited for point-of-use applications.[160]

A general challenge with the removal of arsenic from water are the different characteristics of arsenite As(III) and arsenate As(V). While arsenate is negatively charged across a wide pH range, which is ideal for the electrostatic interactions many removal techniques are based on, arsenite is uncharged at pH under 9.2 and thus significantly more difficult to capture through coagulation, ion exchange, and even reverse osmosis.[160] No method exists that allows the efficient removal of both As(III) and As(V) from water simultaneously.[161] A popular workaround is the oxidation of arsenite in a treatment step prior to the actual capture.[160,162] Since aerial oxidation of As(III) is slow, this step requires chemical treatment, which once again makes it difficult for point-of-use applications.[160,162]

In terms of arsenic adsorption, numerous materials have been reported in the literature, ranging from biological waste including coconut or rice husk, human hair, chicken feathers, chitosan, egg shell, and plum seeds to inorganic substances such as zeolites, titanium dioxide, and iron oxides/hydroxides.[159,160,161,163] Another interesting class of adsorbents are metal organic frameworks whose large surface area and tuneable pore sizes and functional groups make them well suited for filtration, although water stability remains a challenge.[160]

Finally, selectivity can be an important factor in choosing the best capture method. The presence of sulfate and phosphate in particular can affect arsenic removal efficiencies due to their structural similarity.[159,161,164] Clearly, there are a lot of factors to consider when developing filters for the capture of As(III) and As(V).

As part of my own plan to develop drinking water filters targeting arsenic, our cooperation partners in Turkey synthesized two calixarenes for my

experiments: 5,11,15,23-tetrakis-(N-piperidinomethyl)-25,26,27,28-tetrahydroxycalix[4]arene (short: piperidino-calixarene) and 5,11,15,23-tetrakis-(N-morpholinomethyl)-25,26,27,28-tetrahydroxycalix[4]arene (short: morpholino-calixarene). The structures of both are shown in Figure 12.

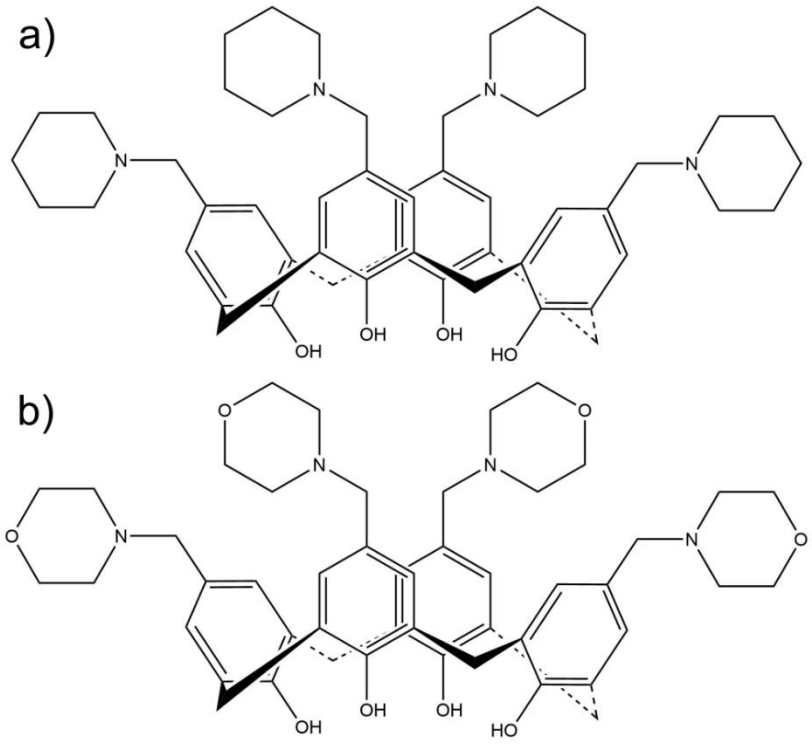

Figure 12: Structures of calixarenes meant for arsenic capture: a) piperidino-calixarene and b) morpholino-calixarene.

I chose these molecules because both piperidino- and morpholino-calixarene have previously been covalently attached to Merrifield resin, which was subsequently used to remove arsenic from water, by running the polluted water through a glass column filled with the resin with sintered glass and filter paper at the bottom to separate the microscopic resin beads from the liquid.[165] At a starting concentration of 30 µg L^{-1} and in a pH 5 to pH 7 range, the piperidino-calixarene-modified resin was able to capture over 90% of As(V), the morpholino-calixarene-modified resin over 80% of As(III) from solution.[165] Therefore, these calixarenes were promising candidates for the attachment to cloth in order to create robust and efficient filter materials. However, initial tests using cloth functionalized with either of the calixarenes and 50 µg L^{-1} As(III) and As(V) solutions only lead to uptake efficiencies below 15%. The investigation was cut short by the pandemic and further experiments will be needed to create effective arsenic filters.

2.2 Lead | Pb(II)

2.2.1 Lead – History and Importance

Lead has been used by humans for more than five thousand years.[166,167] Prehistoric cave paintings were created using pigments rich in lead and many ancient cultures made figurines from lead, be it the ancient Egyptians or Greeks.[166,168] Further east, the Assyrians used lead as one of their currencies in the second millennium BC and lead was also used in building the Hanging Gardens of Babylon.[166] During the reign of the Roman empire, lead consumption soared to new heights.[166,167] *Plumbum*, the Latin name for lead, is the origin of the English word “plumbing” and hints at its use in building pipes and containers for the transport and storage of water, wine, and other foodstuffs.[167] The Romans mined and processed so much lead, that lead deposits dating back to 500 BC–AD 300 have been found in polar ice, carried there through wind and snow.[167] Annual lead production during the peak of the Roman empire in the first two centuries AD corresponded to about two thirds of US lead consumption in the 1980s, illustrating the importance of the element at the time.[169] Besides its use in water pipes and aqueducts, lead in Roman time was very popular as interior coating for bronze and copper vessels because it prevented the leaching of copper into the food which would add an unpleasant flavour.[166,167] Lead lined vessels were also used in the preparation of a grape syrup called *sapa* or *defrutum* (depending on the concentration), the most important sweetener at the time because sugar was not yet known and honey quite expensive.[167] Through the preparation process of boiling grape juice in lead lined vessels, some lead was dissolved, leading to lead acetate concentrations up to 1000 ppm in such grape syrups.[167] *Sapa* and *defrutum* were used not only to sweeten food and wine, but also to make them last longer. The syrup was an excellent preservative because the lead in it inhibited enzyme activity, thus slowing down souring and fermenting processes.[166] But unbeknownst to the Romans, their extensive use of lead utensils and consumption of lead acetate meant that they were slowly poisoning themselves.

While awareness for the danger of inhaling fumes produced during processing of lead already existed at the time, the Romans never suspected the toxicity of their grape syrup.[166] Analyses have shown that the bones of Roman

aristocrats contained significantly higher amounts of lead than those of the lower-class population, which can be explained by the significantly higher wine (sweetened with lead acetate containing grape syrup) consumption within richer families.[167,168] Some researchers have argued that chronic lead poisoning lowered the birth rates of the Roman upper class and damaged their surviving children from a young age, leading ultimately to the downfall of the Roman empire.[170] This statement has however been debated highly controversially in the literature, with some citing other illnesses as causes for decreased fertility,[169] and others calculating that the average amounts of lead that Romans were exposed to was less than half of 21st century Europeans, meaning that lead poisoning could not have been a major cause of the fall of the Roman empire.[167]

Regardless of its impact, lead acetate, also known as “sugar of lead”, remained a popular sweetener in the centuries that followed.[171] Particularly during the Middle Ages and Renaissance, its use caused countless outbreaks of illnesses known under names such as *colica Pictonum*, saturnine colic, paralytic colic and many more; all these can simply be summarized as lead poisoning or lead colic, Figure 13.[172]

500 BC–AD 300	Ancient Roman aristocrats
1st century	Lead colic epidemics observed by Avicenna
15th–18th century	Lead colic epidemics common in Europe
1564	Death of Michelangelo who likely suffered from lead poisoning
1698	First identification of lead acetate as cause of colic epidemic by German physician Eberhard Gockel
18th century	Devonshire colic in England
18th century	Lead colic epidemic in Amsterdam
1845	Death of John Franklin’s Northwest Passage expedition

Figure 13: Examples of lead poisoning by ingestion through the ages.[167,168,171,172]

Between the 15th and 18th century, lead colics frequently occurred throughout Europe, most commonly in autumns that followed cold summers. Wines produced in such years were particularly sour due to the short grape

growing season and therefore sweetened with lead acetate to improve their taste.[172] Other sources of lead exposure at the time included ammunition manufacture, household utensils, and paints: numerous artists are suspected of having suffered from lead poisoning, including Michelangelo who not only used lead containing paints but also consumed large quantities of wine stored in lead containers while working on his art.[168] One of the first to identify lead as the cause of a colic epidemic was the German physician Eberhard Gockel who in 1698 experienced an outbreak of the illness in a monastery and observed that only the monks who had consumed wine fell ill.[172, 173] Not all lead poisonings were connected to wine: Lead was also accidentally consumed through cider prepared with presses containing lead fittings (18th century Devonshire colic in England) or through rain water collected from lead roofs where decay of leaves had caused acidic conditions (18th century lead colic epidemic in Amsterdam).[172] In 1845 John Franklin's whole expedition perished that had set out to search for the Northwest Passage. One cause for their failure is thought to be a contamination of their food from the lead used to seal the storage casks; the ensuing lead poisoning is theorized to have caused illness and madness among the crew.[168]

After knowledge about the toxic effects of lead ingestion had been established, the main sources of lead exposure in the 20th century became house paint to which lead had been added to inhibit mould formation, as well as tetraethyllead which was added to petrol from the 1920s to improve engine performance.[171,173,174] Given this extensive history of lead poisonings, the effects of the metal on the body have been thoroughly studied and will be explained in the following section.

2.2.2 Lead – Danger to Human Health

Lead when ingested is usually in the form of the divalent cation Pb^{2+}, such as in lead acetate.[172,173] Adults absorb only around 8% of ingested lead into their bloodstream, whereas in children that fraction can be as large as 50%.[167] The blood carries the lead to the liver and kidneys through which most is excreted.[167] Some is however carried into other body organs and the central nervous system.[167,173] Lead cations bind strongly to the SH groups of proteins.[172,173] Such interactions can lead to misfolding and inhibition of enzymes which can slow

down or impair the function of the affected organ.[167] As lead cations are structurally similar to calcium cations, it can furthermore affect the signalling of neurons and inhibit calcium entry into cells.[173] Eventually, more than 90% of the lead not excreted from the body is incorporated into the bone tissue.[167] There it is not toxic but accumulates over a person's lifespan. However, when an age is reached where bone resorption begins, this accumulated lead can return to the bloodstream.[167,173] Tests have shown that former lead workers' cognitive abilities declined faster at an old age compared to a control group, which may be an effect caused by lead exposure more than a decade prior to the study.[175]

Lead poisoning mostly occurs as chronic poisoning; acute poisonings are rare.[167] Acute lead poisoning is caused by very high doses. Symptoms include nausea, vomiting, abdominal pain and diarrhoea, but can go as far as kidney failure and death.[167] Chronic poisoning can follow acute poisoning because the body needs time to excrete the lead or it can be caused by an exposure to lower doses over an extended period of time.[167] Symptoms of chronic lead poisoning can include loss of appetite, constipation, and disturbances of the central nervous system, for example a loss of control of one's extremities, deafness, blindness, paralysis, insanity, and even death.[167,172] However, chronic lead poisoning can also occur without any obvious symptoms, particularly in children who are much more susceptible to low concentrations of lead than adults.[173] Not only do children absorb a higher percentage of lead ingested, particularly young children also engage in a lot of hand-to-mouth activity, increasing the risk of accidental lead ingestion, for example from house paint or from lead contained in traffic fumes that has settled onto surfaces.[173] Asymptomatic lead effects on children have only been studied since the 1970s. By measuring the lead concentration in primary school age children's deciduous teeth, a direct correlation was found between the amount of lead and cognitive impairments in terms of IQ, language processing, and attention span.[176] An 11-year follow-up study on some of the same children when they were on the cusp of adulthood revealed a persistent direct correlation between the lead amounts in the teeth they shed at a young age and negative developmental effects such as an increased risk of dropping out of school, reading disabilities, poorer hand–eye coordination and slower reaction times.[177] These studies show the devastating effect of lead poisoning, particularly in children. While poisonings with other heavy metals usually "only" have physical

consequences, the effect of lead on the developing central nervous system of children can impair their brain functions in ways that affect them for the rest of their lives.[173]

2.2.3 Lead – Pollution Occurrence

Since the toxicity of lead is very well understood nowadays, strict laws are in place to prevent exposure. For example, while almost all petrol used around the world contained lead in the 1970s, bans had been imposed in most high-income countries by the 1980s and the use of leaded petrol finally ended globally in July 2021, following a successful campaign by the United Nations Environment Programme.[173,174] Nowadays, accidental lead ingestion occurs most frequently due to old plumbing that still contains lead.[178] For example, in the EU an estimated 25% of domestic dwellings are connected to lead pipes and a recent survey concluded that between 9.7–12.8 million lead pipes are still in use in the United States to this day.[179,180]

In January 2016, the United States President Barack Obama declared a state of emergency in Flint, Michigan.[181] The city had changed its water source from pre-treated water from Lake Huron to the Flint River as a cost saving measure almost two years prior, without realizing the increased corrosiveness of the river water.[182,183,184] Most of the city's plumbing network was built in the early 20th century and therefore contained numerous lead pipes, solder, and fittings.[185] As the city's own water treatment facility was underequipped and understaffed, no corrosion inhibitor (orthophosphate) was added, which would help to create a passivation layer on lead surfaces, see Figure 14.[184,186] Due to the corrosiveness of the river water itself and additional ferric chloride, iron water pipes started to corrode and the passivation layer within lead pipes and fittings was dissolved, causing lead to leach into the water.[184,186,187]

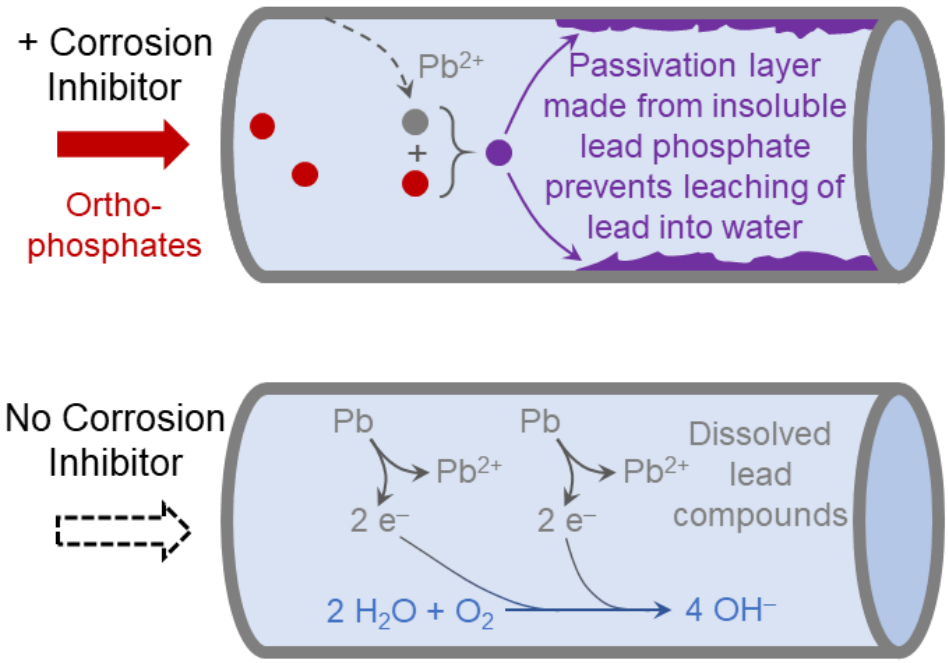

Figure 14: Schematic illustration of the effect of corrosion inhibitors in lead pipes: Addition of corrosion inhibitors (such as orthophosphates) leads to the formation of a passivation layer since lead phosphate is insoluble in water.[187] If this passivation layer is removed, elemental lead is readily oxidized to Pb^{2+}, for example through oxygen dissolved in the water.[186] Many Pb(II) salts are soluble in water, leading to increased lead ingestion.[188]

Maps illustrating the lead concentrations measured in tap water throughout the city between November 2015 and March 2016 show the wide spread of elevated lead levels, with concentrations more than ten times above the EPA federal action level in multiple locations.[189] Besides dissolving lead, the corrosive water also disrupted the biofilm within the pipes and released bacteria into the water.[184] The elevated amounts of rust in the water from corroding iron pipes provided an ideal food supply to these bacteria, leading ultimately to two deadly outbreaks of Legionnaires' disease in the city during the summers of 2014 and 2015.[184] Attempts to eradicate the bacteria caused an overchlorination and the chlorine reacted with organic matter to form carcinogenic trihalomethanes.[184] All complaints by residents were downplayed by officials who insisted that while the colour, smell, and taste of the water had been compromised, its safety remained intact. However, in September 2015 a local paediatrician found that the fraction of young children with elevated blood lead levels had doubled ever since the water source was switched in April 2014, finally forcing the administration to face

the severity of the situation.[184] In October 2015, the water supply was switched back to pre-treated Lake Huron water and flushing with orthophosphates returned lead concentrations to below the critical action level by the end of 2016.[184] At the same time, lead pipes throughout the city were stepwise replaced in the years following the crisis.[184]

While the residents of Flint, Michigan, now have access to safe drinking water, the long-term effects of their consumption of elevated lead levels still remains to be seen. First studies suggest that fertility rates within the city have decreased significantly and that all school-age children living in Flint have suffered from psychosocial effects of the crisis, causing an increase in special needs status regardless of whether the homes they live in were exposed to lead or not.[190,191] However, the age group of very young children who are typically the most affected by lead exposure had not yet reached the age of the children studied so far.[191] Therefore, only continued monitoring will reveal the true impact of the Flint drinking water crisis.

Globally, lead pollution of waters is not as widespread as for example arsenic because elevated concentrations do not occur naturally, and the health hazard is well understood nowadays. In drinking water, the most important source of lead is now lead plumbing in old systems.[178] However, some cases of elevated lead concentrations in surface waters have been reported, for example as a result of industrial pollution in Iran[192] and from lead ammunition used at outdoor shooting ranges in Canada[193]. Lead from the atmosphere can also be washed into surface waters, the impact of which has even been measured in a forest stream in northern Sweden.[194]

Furthermore, in early 2018, our cooperation partners from Selçuk University (now Konya Technical University) in Turkey analysed heavy metal pollutant concentrations in two Turkish rivers affected by industrial pollution: the Ergene in the European part of the country and the Orontes near the border to Syria. In both sampling locations of the Ergene river and seven out of nine samples taken from three locations along the Orontes river lead levels were above 5 ppb.

2.2.4 Lead – Legal Situation

Limits for lead in drinking water vary somewhat between the WHO, EU, and US, Table 5.

Table 5: Legal limits for lead in drinking water.

Organization	Lead limit for drinking water	Ref.
WHO (World Health Organization)	10 µg L^{-1}	178
European Commission	5 µg L^{-1} since January 2021 (prior to that 10 µg L^{-1})	57, 58
US EPA (Environmental Protection Agency)	Goal: 0 µg L^{-1}; action taken if over 15 µg L^{-1}	195, 196

While the World Health Organization has recommended 10 ppb as guideline value for lead concentration in drinking water since 1993, re-evaluations starting from 2010 have shown that lead can have harmful effects on children even at such low concentrations. However, because water is just one of many exposure sources to lead and because concentrations below 10 ppb can be difficult to achieve, this guideline value has been provisionally maintained. The WHO nevertheless recommends that lead concentrations should be as low as possible, even below this value.[178]

Within the EU, a maximum limit of 10 ppb lead in drinking water was set in 1998.[57] This limit was reduced to 5 ppb in January 2021 during the revision of the drinking water directive, as part of which the legal limit for chromium in drinking water was also halved.[58]

The US environmental protection agency has no legal limit for lead in drinking water and instead a maximum contaminant level goal of zero because there is no safe level of lead exposure.[195] Instead of setting a legal limit for lead in drinking water, the agency has established the so-called Lead and Copper Rule which states that action needs to be taken if more than 10% of tap water samples within a system contain a lead concentration above 15 ppb.[196]

2.2.5 Lead – Removal from Water

Unlike chromium and arsenic, lead is dissolved in water in the form of cations. Nevertheless, removal methods employed are in principle very similar, such as coagulation/flocculation, membrane filtration (such as reverse osmosis), ion exchange, and adsorption.[197,198,199] For industrial wastewaters, treatment with chemicals to cause coagulation, flocculation, and precipitation is the most common technique, but this method has many drawbacks due to the amount of reagents needed, the precision required to correctly dose them, and the generated toxic sludge.[198,199] As for other pollutants, adsorption is an intensely studied capture method for lead due to its ease of use. Promising adsorbents include biological waste products such as banana peels, onion skins, and powdered leaves, as well as the typical material classes employed to capture a variety of pollutants, such as activated carbon and zeolites.[199,200] Some attention has been given to functional nanoparticles consisting of metal oxides, polymers, or composites whose large surfaces can help to achieve higher capture efficiencies than bulk adsorbents.[201] The efficiency of metal oxide nanoparticles has been further enhanced by functionalization with molecules such as ethylenediamine-tetraacetic acid (EDTA).[202] EDTA forms stable complexes with lead cations and has therefore been employed to treat acute cases of lead poisoning (alongside other chelating agents) and to extract lead from contaminated soil in the past.[203,204]

For my own preparation of a filter material targeting lead, I had considered two options in terms of functional molecules: 5,11,17,23-tetra-tert-butyl-25,27-bis(cyanomethoxy)-26,28-dihydroxycalix[4]arene (short: cyanomethoxy-calixarene), as well as EDTA, due to its chelating properties, as mentioned above. Both are depicted in Figure 15.

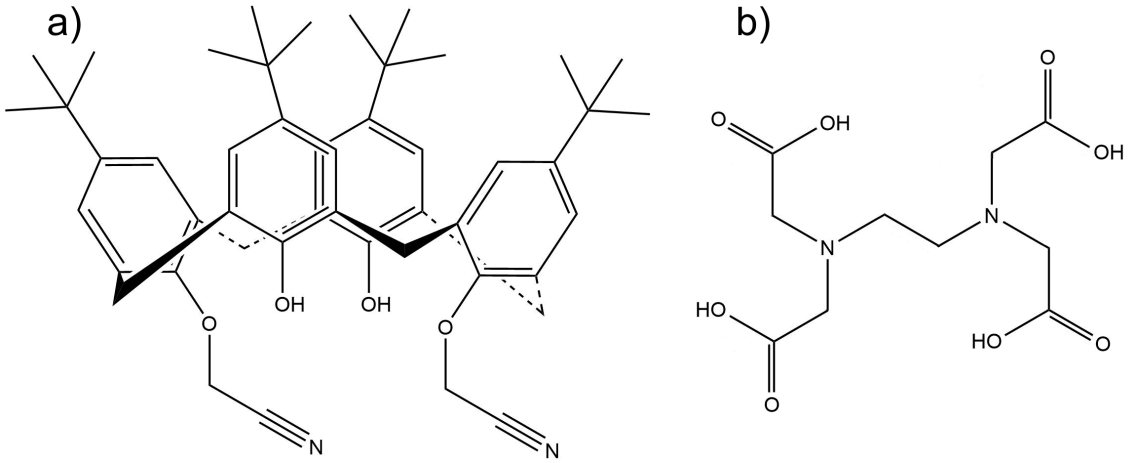

Figure 15: Structures of functional molecules meant for the preparation of lead capturing filters: a) cyanomethoxy-calixarene and b) ethylenediaminetetraacetic acid (EDTA).

Cynanomethoxy-calixarene was considered a promising capture molecule by me because it has previously shown promising lead sorption abilities when used by itself in liquid–liquid extraction studies or when attached to a polymer and suspended within heavy metal solutions.[205,206]

I had already received the calixarene from my cooperation partners in Turkey and purchased EDTA and lead acetate, when unfortunately the Covid-19 lockdown began, and I was unable to return to the laboratory. Hopefully, my successor will be able to continue this work.

2.3 Outlook on Heavy Metal Water Pollution

This chapter illustrates the dangers of the consumption of even low amounts of heavy metals over an extended period of time. It also shows that while awareness for these dangers has been increasing over the past decades, millions of people around the world are still at risk from chronic heavy metal pollution to this day. Due to the costs associated with industrial water purification processes, simple and efficient filters are urgently needed to save lives, particularly in developing countries. This thesis serves to contribute one small piece to the bigger puzzle. In the following chapters I am presenting functional filters that can efficiently remove Cr(VI) from water under realistic conditions. If my work is

continued and a series of filters targeting different pollutants is created, these could form an excellent base for the construction of custom filter systems, depending on the ions that need to be removed at a certain location. Incorporation of metal–organic frameworks, which are the subject of the final results chapter, could furthermore increase the uptake capacity of filtration materials.

2.4 References

(40) Lanford, N.J.; Ferner, R.E. Toxicity of Mercury. *Journal of Human Hypertension* **1999**, *13*, 651–656.

(41) Mason, R.P.; Reinfelder, J.R.; Morel, F.M.M. Bioaccumulation of Mercury and Methylmercury. *Water, Air, and Soil Pollution* **1995**, *80*, 915–921.

(42) Morel, F.M.M.; Kraepiel, A.M.L.; Amyot, M. The Chemical Cycle and Bioaccumulation of Mercury. *Annual Review of Ecology and Systematics* **1998**, *29*, 543–566.

(43) Takeuchi, T.; Morikawa, N.; Matsumoto, H.; Shiraishi, Y. A Pathological Study of Minamata Disease in Japan. *Acta Neuropathologica* **1962**, *2*, 40–57.

(44) Nishigaki, S.; Harada, M. Methylmercury and Selenium in Umbilical Cords of Inhabitants of the Minamata Area. *Nature* **1975**, *258*, 324–325.

(45) Hachiya, N. The History and the Present of Minamata Disease. *JMAJ* **2006**, *49* (3), 112–118.

(46) James, A.K.; Nehzati, S.; Dolgova, N.V.; Sokaras, D.; Kroll, T.; Eto, K.; O'Donoghue, J.L.; Watson, G.E.; Myers, G.J.; Krone, P.H.; Pickering, I.J. Rethinking the Minamata Tragedy: What Mercury Species Was Really Responsible? *Environ. Sci. Technol.* **2020**, *54*, 2726–2733.

(47) Mason, R.P.; Reinfelder, J.R.; Morel, F.M.M. Bioaccumulation of Mercury and Methylmercury. *Water, Air, and Soil Pollution* **1995**, *80*, 915–921.

(48) Morel, F.M.M.; Kraepiel, A.M.L.; Amyot, M. The Chemical Cycle and Bioaccumulation of Mercury. *Annual Review of Ecology and Systematics* **1998**, *29*, 543–566.

(49) Minamata Convention on Mercury booklet. United Nations Environment Programme, September 2019. www.mercuryconvention.org (accessed on 10 Feb 2022).

(50) Minamata Convention on Mercury Parties and Signatories https://www.mercuryconvention.org/en/parties (accessed on 10/02/2022).

(51) WHO 10 chemicals of public health concern, Wold Health Organization 1 Jun 2020 https://www.who.int/news-room/photo-story/photo-story-detail/10-chemicals-of-public-health-concern (accessed on 10 Feb 2022).

(52) WQA Common Waterborne Contaminants https://wqa.org/learn-about-water/common-contaminants (accessed on 10 Feb 2022).

(53) WQA Technical Fact Sheet: Arsenic. Water Quality Association 2013.

(54) WHO Fact Sheet: Arsenic. World Health Organization 2018 https://www.who.int/news-room/fact-sheets/detail/arsenic (accessed on 10 Feb 2022).

(55) Flanagan, S.V.; Johnston, R.B.; Zheng, Y. Arsenic in Tube Well Water in Bangladesh: Health and Economic Impacts and Implications for Arsenic Mitigation. *Bulletin of the World Health Organization* **2012**, *90*, 839–846.

(56) WQA Technical Fact Sheet: Chromium. Water Quality Association 2013.

(57) European Commission Council Directive 98/83/EC, Official Journal of the European Communities 1998 (http://ec.europa.eu/environment/water/water-drink/legislation_en.html) (accessed on 12 Mar 2018).

(58) Directive (EU) 2020/2184 of the European Parliament and of the Council, Official Journal of the European Union 2020 (https://eur-lex.europa.eu/eli/dir/2020/2184/oj) (accessed on 28 Dec 2021).

(59) WQA Technical Fact Sheet: Copper. Water Quality Association 2013.

(60) WQA Technical Fact Sheet: Lead. Water Quality Association 2013.

(61) Lessler, M.A. Lead and Lead Poisoning from Antiquity to Modern Times. *Ohio J. Science* **1988**, *88* (3), 78–84.

(62) WQA Technical Fact Sheet: Uranium. Water Quality Association 2013.

(63) Uranium in Drinking-water. Background document for development of WHO Guidelines for Drinking-water Quality. World Health Organization 2005.

(64) Vauquelin, L.N. Memoir on a New Metallic Acid Which Exists in the Red Lead of Siberia. *Journal of Natural Philosophy, Chemistry, and the Art* **1798**, *2*, 145–146.

(65) Vauquelin, L.N. On the Use of the New Metal Called Chrome, the Oxyd of Chrome, and the Chromic Acid. *The Philosophical Magazine* **1798**, *2* (5), 75–77.

(66) Vauquelin, L.N. Memoir on the Best Method of Decomposing the Chromate of Iron, Obtaining Oxide of Chrome, Preparing Chromic Acid, and on some Combinations of the Latter. *The Philosophical Magazine* **1810**, *35* (141), 20–31.

(67) Weeks, M.E. The Discovery of the Elements. V. Chromium, Molybdenum, Tungsten, and Uranium. *Journal of Chemical Education* **1932**, *9* (3), 459–473.

(68) Lennartson, A. The Colours of Chromium. *Nature Chemistry* **2014**, *6*, 942.

(69) Photograph of a Sample of Anhydrous Chromium(III) Chloride, $CrCl_3$. Wikipedia 20 Feb 2009 https://en.wikipedia.org/wiki/Chromium(III)_chloride#/media/File:Chromium(III)-chloride-purple-anhydrous-sunlight.jpg (accessed on 09 Mar 2018).

(70) Chromium(III)sulfate. Wikipedia 29 May 2009 https://en.wikipedia.org/wiki/Chromium(III)_sulfate#/media/File:Chromium(III)_sulfate.jpg (accessed on 09 Mar 2018).

(71) Potassium chromate sample. Wikipedia 16 May 2007 https://en.wikipedia.org/wiki/Potassium_chromate#/media/File:Potassium-chromate-sample.jpg (accessed on 09 Mar 2018).

(72) Potassium dichromate. Wikipedia 16 May 2007 https://en.wikipedia.org/wiki/Potassium_dichromate#/media/File:Potassium-dichromate-sample.jpg (accessed on 09 Mar 2018).

(73) Baruthio, F. Toxic Effects of Chromium and Its Compounds. *Biological Trace Element Research* **1992**, *32* (1–3), 145–153.

(74) Gmelin, C.G. Experiments on the Effects of Baryta, Strontia, Chrome, Molybdenum, Tungstene, Tellurium, Titanium, Osmium, Platinum, Iridium, Rhodium, Palladium, Nickel, Cobalt, Uranium, Cerium, Iron and Manganese, on the Animal Systems. *Edinburgh Medical and Surgical Journal* **1826**, *26*, 131–133.

(75) Cumin, W. Remarks on the Medicinal Properties of Madar, and on the Effects of Bichromate of Potass on the Human Body. *Edinburgh Medical and Surgical Journal* **1827**, *93*, 295–302.

(76) Bloomfield, J.J.; Blum, W. Health Hazards in Chromium Plating. *Public Health Reports* **1928**, *43* (36), 2330–2351.

(77) Zhang, J.; Li, X. Investigation and Study of Chromium Pollution in Jinzhou. *Chinese Journal of Preventive Medicine* **1987**, *21* (5).

(78) Heath, D. How Industry Scientists Stalled Action on Carcinogen. Center for Public Integrity 13 Mar 2013 https://www.publicintegrity.org/2013/03/13/12290/how-industry-scientists-stalled-action-carcinogen (accessed on 12 Dec 2017). New URL: https://publicintegrity.org/environment/how-industry-scientists-stalled-action-on-carcinogen/ (accessed on 26 Feb 2022).

(79) California Regional Water Quality Control Board: Cleanup and Abatement Order No. 6-87-160. Lahontan Region, 29 Dec 1987.

(80) Jacobs, R.P. PG&E Intra-Company Memorandum. Hinkley, 22 Dec1965.

(81) Welkos, R.W. Digging for the Truth. Los Angeles Times 12 Mar 2000 http://articles.latimes.com/2000/mar/12/entertainment/ca-7856 (accessed on 14 Mar 2018). New URL: https://www.latimes.com/archives/la-xpm-2000-mar-12-ca-7856-story.html (accessed on 26 Feb 2022).

(82) Connett, P.H.; Wetterhahn, K.E. *In Vitro* Reaction of the Carcinogen Chromate with Cellular Thiols and Carboxylic Acids. *J. Am. Chem. Soc.* **1985**, *107* (14), 4282–4288.

(83) Kortenkamp, A.; O'Brien, P. The Generation of DNA Single-Strand Breaks During the Reduction of Chromate by Ascorbic Acid and/or Gluthathione *In Vitro*. *Environ. Health Perspect.* **1994**, *102*, 237–241.

(84) Zhitkovich, A.; Voitkun, V.; Costa, M. Formation of the Amino Acid–DNA Complexes by Hexavalent and Trivalent Chromium *in Vitro*: Importance of Trivalent Chromium and the Phosphate Group. *Biochemistry* **1996**, *35*, 7275–7282.

(85) Costa, M. Toxicity and Carcinogenicity of Cr(VI) in Animal Models and Humans. *Critical Reviews in Toxicology* **1997**, *27* (5), 431–442.

(86) Costa, M. Potential Hazard of Hexavalent Chromate in our Drinking Water. *Toxicology and Applied Pharmacology* **2003**, *188*, 1–5.

(87) Borneff, J.; Engelhardt, K.; Griem, W.; Kunte, H.; Reichert, J. Kanzerogene Substanzen in Wasser und Boden. XXII. Mäusetränkversuch mit 3.4-Benzpyren und Kaliumchromat. *Archiv für Hygiene und Bakteriologie* **1968**, *152* (1), 45–53.

(88) Katz, S.A.; Salem, H. The Toxicology of Chromium with Respect to its Chemical Speciation: a Review. *Journal of Applied Toxicology* **1993**, *13* (3), 217–224.

(89) Sutherland, J.E.; Zhitkovich, A.; Kluz, T.; Costa, M. Rats Retain Chromium in Tissues Following Chronic Ingestion of Drinking Water Containing Hexavalent Chromium. *Biological Trace Element Research* **2000**, *74*, 41–53.

(90) Finley, B.L.; Kerger, B.D.; Katona, M.W.; Gargas, M.L.; Corbett, G.C.; Paustenbach, D.J. Human Ingestion of Chromium (VI) in Drinking Water: Pharmacokinetics Following Repeated Exposure. *Toxicology and Applied Pharmacology* **1997**, *142*, 151–159.

(91) Proctor, D.M.; Otani, J.M.; Finley, B.L.; Paustenbach, D.J.; Bland, J.A.; Speizer, N.; Sargent, E.V. Is Hexavalent Chromium Carcinogenic via Ingestion? A Weight-of-Evidence Review. *Journal of Toxicology and Environmental Health, Part A* **2002**, *65* (10), 701–746.

(92) Documentation of Environmental Indicator Determination. Environmental Protection Agency 2004 https://www3.epa.gov/region02/waste/geriv725.pdf (accessed on 14 Mar 2018).

(93) Environmental Studies and Cleanup Fact Sheet. Lockheed Martin 2015 https://www.lockheedmartin.com/content/dam/lockheed/data/corporate/documents/remediation/msa/fact-sheet-april2015.pdf (accessed on 14 Mar 2018). New URL: https://www.lockheedmartin.com/content/dam/lockheed-martin/eo/documents/remediation/msa/fact-sheet-april2015.pdf (accessed on 26 Feb 2022).

(94) Order No. R5-2011-0006 Soil Remediation, Waste Discharge Requirements for Track Four Inc. (A Wholly Owned Subsidiary of Amsted Industries Inc.), and Merck & Co., Inc., Former Baltimore Aircoil Company Facility. California Regional Water Quality Control Board. https://www.waterboards.ca.gov/rwqcb5/board_decisions/adopted_orders/merced/r5-2011-0006.pdf (accessed on 14 Mar 2018).

(95) National Toxicology Program Technical Report 2008 (NTP TR 546, NIH Publication No. 08-5887).

(96) Stout, M.D.; Herbert, R.A.; Kissling, G.E.; Collins, B.J.; Travlos, G.S.; Witt, K.L.; Melnick, R.L.; Abdo, K.M.; Malarkey, D.E.; Hooth, M.J. Hexavalent Chromium Is Carcinogenic to F344/N Rats and B6C3F1 Mice after Chronic Oral Exposure. *Environmental Health Perspectives* **2009**, *117* (5), 716–722.

(97) Linos, A.; Petralias, A.; Christophi, C.A.; Christoforidou, E.; Kouroutou, P.; Stoltidis, M.; Veloudaki, A.; Tzala, E.; Makris, K.C.; Karagas, M.R. Oral Ingestion of Hexavalent Chromium through Drinking Water and Cancer Mortality in an Industrial Area of Greece – An Ecological Study. *Environmental Health* **2011**, *10*, 50.

(98) Kazakis, N.; Kantiranis, N.; Kalaitzidou, K.; Kaprara, E.; Mitrakas, M.; Frei, R.; Vargemezis, G.; Tsourlos, P.; Zouboulis, A.; Filippidis, A. Origin of Hexavalent Chromium in Groundwater: The Example of Sarigkiol Basin, Northern Greece. *Science of the Total Environment* **2017**, *593–594*, 552–566.

(99) Novak, M.; Chrastny, V.; Cadkova, E.; Farkas, J.; Bullen, T.D.; Tylcer, J.; Szurmanova, Z.; Cron, M.; Prechova, E.; Curik, J.; Stepanova, M.; Pasava, J.; Erbanova, L.; Houskova, M.; Puncochar, K.; Hellerich, L.A. Common Occurrence of a Positive $\delta^{53}Cr$ Shift in Central European Waters Contaminated by Geogenic/Industrial Chromium Relative to Source Values. *Environ. Sci. Technol.* **2014**, *48*, 6089–6096.

(100) Naz, A.; Mishra, B.K.; Gupta, S.K. Human Health Risk Assessment of Chromium in Drinking Water: A Case Study of Sukinda Chromite Mine, Odisha, India. *Exposure and Health* **2016**, *8* (2), 253–264.

(101) Huang, S.; Xia, W.; Li, Y.; Zhang, B.; Zhou, A.; Zheng, T.; Qian, Z.; Huang, Z.; Lu, S.; Chen, Z.; Wang, Y.; Pan, X.; Huo, W.; Jin, S.; Jiang, Y.; Xu, S. Association Between Maternal Urinary Chromium and Premature Rupture of Membranes in the Healthy Baby Cohort Study in China. *Environmental Pollution* **2017**, *230*, 53–60.

(102) Tiwari, A.K.; De Maio, M. Assessment of Risk to Human Health due to Intake of Chromium in the Groundwater of the Aosta Valley Region, Italy. *Human and Ecological Risk Assessment: An International Journal* **2017**, *23* (5), 1153–1163.

(103) Tseng, C.-H.; Lei, C.; Chen, Y.-C. Evaluating the Health Cost of Oral Hexavalent Chromium Exposure from Water Pollution: A Case Study in Taiwan. *Journal of Cleaner Production* **2018**, *172*, 819–826.

(104) Armienta-Hernández, M.A.; Rodríguez-Castillo, R. Environmental Exposure to Chromium Compounds in the Valley of León, México. *Environmental Health Perspectives* **1995**, *103*, 47–51.

(105) Jordao, C.P.; Pereira, J.L.; Jham, G.N. Chromium Contamination in Sediment, Vegetation and Fish Caused by Tanneries in the State of Minas Gerais, Brazil. *Science of the Total Environment* **1997**, *207* (1), 1–11.

(106) Villegas, L.B.; Fernández, P.M.; Amoroso, M.J.; de Figueroa, L.I.C. Chromate Removal by Yeasts Isolated from Sediments of a Tanning Factory and a Mine Site in Argentina. *BioMetals* **2008**, *21*, 591.

(107) Leghouchi, E.; Laub, E.; Guerbet, M. Evaluation of Chromium Contamination in Water, Sediment and Vegetation Caused by the Tannery of Jijel (Algeria): a Case Study. *Environmental Monitoring and Assessment* **2009**, *153*, 111.

(108) Coetzee, L.; Du Preez, H.H. ; Van Vuren, J.H.J. Metal Concentrations in *Clarias gariepinus* and *Labeo umbratus* from the Olifants and Klein Olifants River, Mpumalanga, South Africa: Zinc, Copper, Manganese, Lead, Chromium, Nickel, Aluminium and Iron. *Water SA* **2002**, *28* (3), 433–448.

(109) Leslie, H.A.; Pavluk, T.I.; bij de Vaate, A. ; Kraak, M.H.S. Triad Assessment of the Impact of Chromium Contamination on Benthic Macroinvertebrates in the Chusovaya River (Urals, Russia). *Archives of Environmental Contamination and Toxicology* **1999**, *37* (2), 182–189.

(110) Chromium in Drinking-water, Guidelines for drinking-water quality. World Health Organization, Geneva 1996 (http://www.who.int/water_sanitation_health/dwq/chemicals/chromium.pdf) (accessed on 12 Mar 2018).

(111) United States Environmental Protection Agency: Chromium in Drinking Water https://www.epa.gov/dwstandardsregulations/chromium-drinking-water (accessed on 12 Mar 2018).

(112) Fact Sheet: Frequently Asked Questions about Hexavalent Chromium in Drinking Water. California Water Boards, September 2015. (https://www.waterboards.ca.gov/drinking_water/certlic/drinkingwater/documents/chromium6/chromium_ffac_sheet_2015_final.pdf) (accessed on 12 Mar 2018).

(113) Announcement: Chromium-6 Drinking Water MCL. California Water Boards. Last updated on 23/02/2018 (https://www.waterboards.ca.gov/drinking_water/certlic/drinkingwater/Chromium6.html) (accessed on 12 Mar 2018).

(114) U.S. EPA. IRIS Toxicological Review of Hexavalent Chromium Part 2: Human, Toxicokinetic, and Mechanistic Studies (Preliminary Assessment Materials). U.S. Environmental Protection Agency, Washington, DC, EPA/635/R-14/218, 2014. (https://cfpub.epa.gov/ncea/iris_drafts/recordisplay.cfm?deid=298830#tab-3) (accessed on 12 Mar 2018).

(115) U.S. EPA Chromium(VI) Review Step 2 https://cfpub.epa.gov/ncea/iris_drafts/recordisplay.cfm?deid=343950 (accessed on 28 Dec 2021).

(116) Public Health Goal for Hexavalent Chromium in Drinking Water. Office of Environmental Health Hazard Assessment, California Environmental Protection Agency, July 2011. https://oehha.ca.gov/media/downloads/water/chemicals/phg/cr6phg072911.pdf (accessed on 12 Mar 2018).

(117) Judgement of the Superior Court of California, Country of Sacramento on May 31, 2017. Case No. 34-2014-80001850. https://www.waterboards.ca.gov/drinking_water/certlic/drinkingwater/documents/chromium6/cmtajud.pdf (accessed on 12 Mar 2018).

(118) Unnithan, M. R.; Vinod, V. P.; Anirudhan, T. S. Synthesis, Characterization, and Application as a Chromium(VI) Adsorbent of Amine-Modified Polyacrylamide-Grafted Coconut Coir Pith. *Ind. Eng. Chem. Res.* **2004**, *43*, 2247−2255.

(119) Memon, S.; Tabakci, M.; Roundhill, D. M.; Yilmaz, M. Synthesis and Evaluation of the Cr(VI) Extraction Ability of Amino/ Nitrile Calix[4]arenes Immobilized onto a Polymeric Backbone. *React. Funct. Polym.* **2006**, *66*, 1342−1349.

(120) Pehlivan, E.; Cetin, S. Sorption of Cr(VI) Ions on Two Lewatit-Anion Exchange Resins and their Quantitative Determination using UV−Visible Spectrophotometer. *J. Hazard. Mater.* **2009**, *163*, 448−453.

(121) Xu, X.; Gao, B.-Y.; Tan, X.; Yue, Q.-Y.; Zhong, Q.-Q.; Li, Q. Characteristics of Amine-Crosslinked Wheat Straw and its Adsorption Mechanisms for Phosphate and Chromium(VI) Removal from Aqueous Solution. *Carbohydr. Polym.* **2011**, *84*, 1054−1060.

(122) des Ligneris, E.; Dumée, L. F.; Kong, L. Nanofibers for heavy metal ion adsorption: Correlating Surface Properties to Adsorption Performance, and Strategies for Ion Selectivity and Recovery. *Environ. Nanotechnol., Monit. Manag.* **2020**, *13*, 100297.

(123) Owlad, M.; Aroua, M.K.; Daud, W.A.W.; Baroutian, S. Removal of Hexavalent Chromium-Contaminated Water and Wastewater: A Review. Water, Air, and Soil Pollution **2009**, *200* (1–4), 59–77.

(124) Rinaudo, M. Chitin and Chitosan: Properties and Applications. *Progress in Polymer Science* **2006**, *31*, 603–632.

(125) Dambies, L.; Guimon, C.; Yiacoumi, S.; Guibal, E. Characterization of Metal Ion Interactions with Chitosan by X-ray Photoelectron Spectroscopy. *Colloids and Surfaces A: Physicochemical and Engineering Aspects* **2001**, *177*, 203–214.

(126) Boddu, V.M.; Abburi, K.; Talbott, J.L.; Smith, E.D. Removal of Hexavalent Chromium from Wastewater Using a New Composite Chitosan Biosorbent. *Environ. Sci. Technol.* **2003**, *37*, 4449–4456.

(127) Merriam Webster: arsenic [noun] https://www.merriam-webster.com/dictionary/arsenic (accessed on 04 Feb 2022).

(128) Vahidnia, A.; van der Voet, G.B.; de Wolff, F.A. Arsenic Neurotoxicity – A Review. *Human & Experimental Toxicology* **2007**, *26*, 823–832.

(129) Hughes M.F.; Beck, B.D.; Chen, Y.; Lewis, A.S.; Thomas, D.J. Arsenic Exposure and Toxicology: A Historical Perspective. *Toxicol. Sci.* **2011**, *123* (2), 305–332.

(130) Cullen, W.R. The Toxicity of Trimethylarsine: an Urban Myth. *J. Environ. Monit.* **2005**, *7*, 11–15.

(131) A skeleton gentleman at a ball asks a skeleton lady to dance; representing the effect of arsenical dyes and pigments in clothing and accessories. Wood engraving, 1862. https://wellcomecollection.org/works/awbr7whm (accessed on 17 Feb 2022).

(132) Baj, G.; Arnulfo, A.; Deaglio, S.; Mallone, R.; Vigone, A.; De Cesaris, M.G.; Surico, N.; Malavasi, F.; Ferrero, E. Arsenic Trioxide and Breast Cancer: Analysis of the Apoptotic, Differentiative and Immunomodulatory Effects. *Breast Cancer Research and Treatment* **2002**, *73*, 61–73.

(133) Huang, W.; Zeng, Y.C. A Candidate for Lung Cancer Treatment: Arsenic Trioxide. *Clinical and Translational Oncology* **2019**, *21*, 1115–1126.

(134) Tseng, W.P.; Chen, W.Y.; Sung, J.L.; Chen, J.S. A Clinical Study of Blackfoot Disease in Taiwan, an Endemic Peripheral Vascular Disease. *國立臺灣大學醫學院研究報告 Memoirs of the College of Medicine of the National Taiwan University* **1961**, *7* (1), 1–18.

(135) Wu, H.Y.; Chen, K.P.; Tseng, W.P.; Hsu, C.L. Epidemiologic Studies on Blackfoot Disease. 1. Prevalence and Incidence of the Disease by Age, Sex, Year, Population and Geographic Distribution. *國立臺灣大學醫學院研究報告 Memoirs of the College of Medicine of the National Taiwan University* **1961**, *7* (1), 33–50.

(136) Tseng, W.P.; Chu, H.M.; How, S.W.; Fong, J.M.; Lin, C.S.; Yeh, S. Prevalence of Skin Cancer in an Endemic Area of Chronic Arsenicism in Taiwan. *J. Natl. Cancer Inst.* **1968**, *40*, 453–463.

(137) Chen, C.-J.; Chuang, Y.-C.; Lin, T.-M.; Wu, H.Y. Malignant Neoplasms Among Residents of a Blackfoot Disease-Endemic Area in Taiwan: High-Arsenic Artesian Well Water and Cancers. *Cancer Research* **1985**, *45*, 5895–5899.

(138) Chen, C.-J.; Wu, M.-M.; Lee, S.-S.; Wang, J.-D.; Cheng, S.-H.; Wu, H.-Y. Atherogenicity and Carcinogenicity of High-Arsenic Artesian Well Water. Multiple Risk Factors and Related Malignant Neoplasms of Blackfoot Disease. *Arteriosclerosis* **1988**, *8* (5), 452–460.

(139) Chiou, H.-Y.; Hsueh, Y.-M.; Liaw, K.-F.; Horng, S.-F.; Chiang, M.-H.; Pu, Y.-S.; Lin, J.S.-N.; Huang, C.-H.; Chen, C.-J. Incidence of Internal Cancers and Ingested Inorganic Arsenic: A Seven-Year Follow-up Study in Taiwan. *Cancer Research* **1995**, *55*, 1296–1300.

(140) Tsai, T.-L.; Kuo, C.-C.; Hsu, L.-I.; Tsai, S.-F.; Chiou, H.-Y.; Chen, C.-J. ; Hsu, K.-H.; Wang, S-L. Association Between Arsenic Exposure, DNA Damage, and Urological Cancers Incidence: A Long-Term Follow-up Study of Residents in an Arseniasis Endemic Area of Northeastern Taiwan. *Chemosphere* **2021**, *266*, 129094.

(141) Cohen, S.M.; Arnold, L.L. Methylated Arsenicals: The Implications of Metabolism and Carcinogenicity Studies in Rodents to Human Risk Assessment. *Critical Reviews in Toxicology* **2006**, *36*, 99–133.

(142) Hughes, M.F.; Beck, B.D.; Chen, Y.; Lewis, A.S.; Thomas, D.J. Arsenic Exposure and Toxicology: A Historical Perspective. *Toxicological Sciences* **2011**, *123* (2), 305–332.

(143) Lin, Y.-B.; Lin, Y.-P.; Liu, C.-W.; Tan, Y.-C. Mapping of Spatial Multi-Scale Sources of Arsenic Variation in Groundwater on ChiaNan Floodplain of Taiwan. *Science of the Total Environment* **2006**, *370*, 168–181.

(144) Wang, S.-W.; Liu, C.-W.; Jang, C.-S. Factors Responsible for High Arsenic Concentrations in Two Groundwater Catchments in Taiwan. *Applied Geochemistry* **2007**, *22*, 460–476.

(145) Sengupta, S.; Sracek, O.; Jean, J.-S. ; Lu, H.-Y. ; Wang, C.-H. ; Palcsu, L. ; Liu, C.-C. ; Jen, C.-H.; Bhattacharya, P. Spatial Variation of Groundwater Arsenic Distribution in the Chianan Plain, SW Taiwan: Role of Local Hydrogeological Factors and Geothermal sources. *Journal of Hydrology* **2014**, *518*, 393–409.

(146) Liu, C.-W.; Wang, S.-W.; Jang, C.-S.; Lin, K.-H. Occurrence of Arsenic in Ground Water in the Choushui River Alluvial Fan, Taiwan. *J. Environ. Qual.* **2006**, *35*, 68–75.

(147) Liu, C.-W.; Wang, C.-J.; Kao, Y.-H. Assessing and Simulating the Major Pathway and Hydrogeochemical Transport of Arsenic in the Beitou–Guandu Area, Taiwan. Environ. Geochem. Health 2016, 38, 219–231.

(148) Kao, Y.-H.; Wang, S.-W.; Maji, S.K.; Liu, C.-W.; Wang, P.-L.; Chang, F.-J.; Liao, C.-M. Hydrochemical, Mineralogical and Isotopic Investigation of Arsenic Distribution and Mobilization in the Guandu Wetland of Taiwan. *Journal of Hydrology* **2013**, *498*, 274–286.

(149) Liu, C.-W.; Chen, Y.-Y.; Kao, Y.-H. Bioaccumulation and Translocation of Arsenic in the Ecosystem of the Guandu Wetland, Taiwan. *Wetlands* **2014**, *34*, 129–140.

(150) Liu, C.-W.; Wu, M.-Z. Geochemical, Mineralogical and Statistical Characteristics of Arsenic in Groundwater of the Lanyang Plain, Taiwan, *Journal of Hydrology* **2019**, *577*, 123975.

(151) Taiwan location map. Wikipedia 27 Aug 2008 https://de.m.wikipedia.org/wiki/Datei:Taiwan_location_map.svg (accessed on 14 Feb 2022).

(152) Nordstrom, D.K. Worldwide Occurrences of Arsenic in Ground Water. *Science* **2002**, *296*, 2143–2144.

(153) Bundschuh, J.; Litter, M.I.; Parvez, F.; Román-Ross, G. ; Nicolli, H.B. ; Jean, J.-S. ; Liu, C.-W. ; López, D. ; Armienta, M.A. ; Guilherme, L.R.G. ; Cuevas, A.G. ; Cornejo, L. ; Cumbal, L. ; Toujaguez, R. One Century of Arsenic Exposure in Latin America : A Review of History and Occurrence from 14 Countries. *Science of the Total Environment* **2012**, *429*, 2–35.

(154) Huq, M.E.; Fahad, S.; Shao, Z.; Sarven, M.S.; Khan, I.A.; Alam, M.; Saeed, M.; Ullah, H.; Adnan, M.; Saud, S.; Cheng, Q.; Ali, S.; Wahid, F.; Zamin, M.; Raza, M.A.; Saeed, B.; Riaz, M.; Khan, W.U. Arsenic in a Groundwater Environment in Bangladesh: Occurrence and Mobilization. *Journal of Environmental Management* **2020**, *262*, 110318.

(155) Dhar, R.K.; Biswas, B.K.; Samanta, G.; Mandal, B.K.; Chakraborti, D.; Roy, S.; Jafar, A.; Islam, A.; Ara, G.; Kabir, S.; Khan, A.W.; Ahmed, S.A.; Hadi, S.A. Groundwater Arsenic Calamity in Bangladesh. *Current Science* **1997**, *73* (1) 48–59.

(156) Hossain, M.F. Arsenic Contamination in Bangladesh—An Overview. *Agriculture, Ecosystems and Environment* **2006**, *113*, 1–16.

(157) Flanagan, S.V.; Johnston, R.B.; Zheng, Y. Arsenic in Tube Well Water in Bangladesh: Health and Economic Impacts and Implications for Arsenic Mitigation. *Bull. World Health Organ.* **2012**, *90*, 839–846.

(158) Drinking Water Standard for Arsenic. United States Environmental Protection Agency Jan 2001 https://nepis.epa.gov/Exe/ZyPdf.cgi?Dockey=20001XXC.txt (accessed on 14 Feb 2022).

(159) Choong, T.S.Y.; Chuah, T.G.; Robiah, Y.; Koay, F.L.G.; Azni, I. Arsenic Toxicity, Health Hazards and Removal Techniques from Water: An Overview. *Desalination* **2007**, *217*, 139–166.

(160) Nicomel, N.R.; Leus, K.; Folens, K.; Van Der Voort, P.; Du Laing, G. Technologies for Arsenic Removal from Water: Current Status and Future Perspectives. *Int. J. Environ. Res. Public Health* **2016**, *13*, 62.

(161) Weerasundara, L.; Ok, Y.-S.; Bundschuh, J. Selective Removal of Arsenic in Water: A Critical Review. *Environmental Pollution* **2021**, *268*, 115668.

(162) Bissen, M.; Frimmel, F.H. Arsenic – a Review. Part II: Oxidation of Arsenic and its Removal in Water Treatment. *Acta hydrochim. hydrobiol.* **2003**, *2*, 97–107.

(163) Shakoor, M.B.; Niazi, N.K.; Bibi, I.; Shahid, M.; Saqib, Z.A.; Nawaz, M.F.; Shaheen, S.M.; Wang, H.; Tsang, D.C.W.; Bundschuh, H.; Ok, Y.S.; Rinklebe, J. Exploring the Arsenic Removal Potential of Various Biosorbents from Water. *Environment International* **2019**, *123*, 567–579.

(164) Hering, J.G.; Chen, P.-Y.; Wilkie, J.A.; Elimelech, M. Arsenic Removal from Drinking Water during Coagulation. *J. Environ. Eng.* **1997**, *123* (8), 800–807.

(165) Qureshi, I.; Qazi, M.A.; Bhatti, A.A.; Memon, S.; Sirajuddin, Yilmaz, M. An efficient calix[4]arene appended resin for the removal of arsenic. *Desalination* **2011**, *278*, 98–104.

(166) Waldron, H.A. Lead Poisoning in the Ancient World. *Medical History* **1973**, *17* (4), 391–399.

(167) Retief, F.P.; Cilliers, L. Lead Poisoning in Ancient Rome. *Acta Theologica* **2006**, 26 (2), 147–164.

(168) Montes-Santiago, J. The Lead-Poisoned Genius: Saturnism in Famous Artists Across Five Centuries. In *Progress in Brain Research Vol. 203: The Fine Arts, Neurology, and Neuroscience*; Finger, S.; Zaidel, D.W.; Boller, F.; Bogousslavsky, J.; Elsevier: Amsterdam, NL, 2013; 223–240.

(169) Needleman, L.; Needleman, D. Lead Poisoning and the Decline of the Roman Aristocracy. *Echos du monde Classique: Classical views* **1985**, *24* (1), 63–94.

(170) Gilfillan, S.C. Lead Poisoning and the Fall of Rome. *Journal of Occupational Medicine* **1965**, *7* (2), 53–60.

(171) Reddy, A.; Braun, C.L. Lead and the Romans. *Journal of Chemical Education* **2010**, *87* (10), 1052–1055.

(172) Eisinger, J. Lead and Wine: Eberhard Gockel and the *Colica Pictonum*. *Medical History* **1982**, *26*, 279–302.

(173) Needleman, H. Lead Poisoning. *Annu. Rev. Med.* **2004**, *55*, 209–222.

(174) Era of Leaded Petrol Over, Eliminating a Major Thread to Human and Planetary Health. United Nations Environment Programme 30 Aug 2021 https://www.unep.org/news-and-stories/press-release/era-leaded-petrol-over-eliminating-major-threat-human-and-planetary#:~:text=By%20the%201970s%2C%20almost%20all,environmental%20threats%20to%20human%20health. (accessed on 19 Feb 2022).

(175) Schwartz, B.S.; Stewart, W.F.; Bolla, K.I.; Simon, D.; Bandeen-Roche, K.; Gordon, B.; Links, J.M.; Todd, A.C. Past Adult Lead Exposure is Associated with Longitudinal Decline in Cognitive Function. *Neurology* **2000**, *55* (8), 1144–1150.

(176) Needleman, H.L.; Gunnoe, C.; Leviton, A.; Reed, R.; Peresie, H.; Maher, C.; Barrett, P. Deficits in Psychologic and Classroom Performance of Children with Elevated Dentine Lead Levels. *The New England Journal of Medicine* **1979**, *300* (13), 689–695.

(177) Needleman, H.L.; Schell, A.; Bellinger, D.; Leviton, A.; Allred, E.N. The Long-Term Effects of Exposure to Low Doses of Lead in Childhood: An 11-Year Follow-up Report. *The New England Journal of Medicine* **1990**, *322* (2), 83–88.

(178) Lead in Drinking-water. Background document for development of WHO Guidelines for Drinking-water Quality. World Health Organization 2016.

(179) Hayes, C.R.; Skubala, N.D. Is there still a Problem with Lead in Drinking Water in the European Union? *J. Water Health* **2009**, *7* (4), 569–580.

(180) Lead Pipes are Widespread and Used in Every State. Natural Resources Defense Council 2021 https://www.nrdc.org/lead-pipes-widespread-used-every-state (accessed on 20 Feb 2022).

(181) Domonoske, C. Obama Declares State Of Emergency Over Flint's Contaminated Water. NPR 16 Jan 2016 https://www.npr.org/sections/thetwo-way/2016/01/16/463319454/obama-declares-state-of-emergency-over-flints-contaminated-water (accessed on 20 Feb 2022).

(182) Flint Water Crisis Fast Facts. CNN 14 Jan 2021 https://edition.cnn.com/2016/03/04/us/flint-water-crisis-fast-facts/ (accessed on 20 Feb 2022).

(183) Gostin, L.O. Politics and Public Health: The Flint Drinking Water Crisis. *Hastings Center Report* **2016**, *46* (4), 5–6.

(184) Pauli, B.J. The Flint Water Crisis. *WIREs Water* **2020**, *7*, e1420.

(185) Larsen, K.R. The Science Behind It: Corrosion Caused Lead-Tainted Water in Flint, Michigan. Materials Performance 4 May 2020 https://www.materialsperformance.com/articles/material-selection-design/2016/06/the-science-behind-it-corrosion-caused-lead-tainted-water-in-flint-michigan (accessed on 20 Feb 2022).

(186) Santucci Jr, R.J.; Scully, J.R. The Pervasive Thread of Lead (Pb) in Drinking Water: Unmasking and Pursuing Scientific Factors that Govern Lead Release. *PNAS* **2020**, *117* (38) 23211–23218.

(187) Torrice, M. How Lead Ended Up In Flint's Tap Water. Chemical & Engineering News 11 Feb 2016 https://cen.acs.org/articles/94/i7/Lead-Ended-Flints-Tap-Water.html (accessed on 22 Feb 2022).

(188) Clever, H.L.; Johnston, F.J. The Solubility of Some Sparingly Soluble Lead Salts: An Evaluation of the Solubility in Water and Aqueous Electrolyte Solution. *J. Phys. Chem. Ref. Data* **1980**, *9* (3), 751–784.

(189) Brush, M. MAP: Month to Month Lead Testing Results in Flint. Michigan Radio 01 Apr 2016 https://www.michiganradio.org/post/map-month-month-lead-testing-results-flint (accessed on 22 Feb 2022).

(190) Grossman, D.S.; Slusky, D.J.G. The Impact of the Flint Water Crisis on Fertility. *Demography* **2019**, *56*, 2005–2031.

(191) Trejo, S.; Yeomans-Maldonado, G.; Jacob, B. The Psychosocial Effects of the Flint Water Crisis on School-Age Children. NBER Working Paper No. 29341. Oct 2021.

(192) Karrari, P.; Mehrpour, O.; Abdollahi, M. A Systematic Review on Status of Lead Pollution and Toxicity in Iran; Guidance for Preventive Measures. *DARU Journal of Pharmaceutical Sciences* **2012**, *20*, 2.

(193) Darling, C.T.R.; Thomas, V.G. The Distribution of Outdoor Shooting Ranges in Ontario and the Potential for Lead Pollution of Soil and Water. *The Science of the Total Environment* **2003**, *313*, 235–243.

(194) Klaminder, J.; Bindler, R.; Laudon, H.; Bishop, K.; Emteryd, O.; Renberg, I. Flux Rates of Atmospheric Lead Pollution within Soils of a Small Catchment in Northern Sweden and Their Implications for Future Stream Water Quality. *Environ. Sci. Technol.* **2006**, *40*, 4639–4645.

195 EPA information on lead in drinking water (https://www.epa.gov/ground-water-and-drinking-water/basic-information-about-lead-drinking-water#regs)

196 EPA „Lead and Copper Rule" (https://www.epa.gov/dwreginfo/lead-and-copper-rule)

(197) Zahra, N. Lead Removal from Water by Low Cost Adsorbents: A Review. *Pak. J. Anal. Environ. Chem.* **2012**, *13* (1), 1–8.

(198) Arbabi, M.; Hemati, S.; Amiri, M. Removal of Lead Ions from Industrial Wastewater: A Review of Removal Methods. *International Journal of Epidemiologic Research* **2015**, *2* (2), 105–109.

(199) Kumar, V.; Dwivedi, S.K.; Oh, S. A Critical Review on Lead Removal from Industrial Wastewater: Recent Advances and Future Outlook. *Journal of Water Process Engineering* **2022**, *45*, 102518.

(200) Saka, C.; Sahin, Ö.; Kücük, M.M. Applications on Agricultural and Forest Waste Adsorbents for the Removal of Lead (II) from Contaminated Waters. *Int. J. Environ. Sci. Technol.* **2012**, *9*, 379–394.

(201) Bhatia, M.; Babu, R.S.; Sonawane, S.H.; Gogate, P.R.; Girdhar, A.; Reddy, E.R.; Pola, M. Application of Nanoadsorbents for Removal of Lead from Water. *Int. J. Environ. Sci. Technol.* **2017**, *14*, 1135–1154.

(202) Huang, Y.; Keller, A.A. EDTA Functionalized Magnetic Nanoparticle Sorbents for Cadmium and Lead Contaminated Water Treatment. *Water Research* **2015**, *80*, 159–168.

(203) Porru, S.; Alessio, L. The Use of Chelating Agents in Occupational Lead Poisoning. *Occup. Med.* **1996**, *46* (1), 41–48.

(204) Kim, C.; Lee, Y.; Ong, S.K. Factors Affecting EDTA Extraction of Lead from Lead-Contaminated Soils. *Chemosphere* **2003**, *51*, 845–853.

(205) Tabakci, M.; Ersoz, M.; Yilmaz, M. A Calix[4]arene-Containing Polysiloxane Resin for Removal of Heavy Metals and Dichromate Anion. *Journal of Macromolecular Science, Part A: Pure and Applied Chemistry* **2006**, *43* (1), 57–69.

(206) Tabakci, M.; Yilmaz, M. Synthesis of a Chitosan-Linked Calix[4]arene Chelating Polymer and its Sorption Ability Toward Heavy Metals and Dichromate Anions. *Bioresource Technology* **2008**, *99*, 6642–6645.

CHAPTER 3: EXPERIMENTAL METHODS

3.1 Preparation of Functionalized Cloths

3.1.1 Plasma Polymerisation

Functionalized cloth was prepared using non-woven polypropylene cloth (taken from the middle layer of disposable surgical masks, 80 µm thickness, 5.0 ± 1.5 µm fibre diameter, SD Medical Ltd.). The cloth was rinsed with ethanol and thoroughly dried in air prior to surface functionalization.

Pulsed plasma deposition using vinylbenzyl chloride precursor (97% mixture of 3- and 4-isomers, Sigma Aldrich Ltd.) was conducted in a cylindrical glass chamber (5 cm diameter, 470 cm^3 volume, base pressure less than 3 x 10^{-3} mbar, and a leak rate better than 2 x 10^{-9} mol s^{-1}) enclosed in a Faraday cage.[207,208] The chamber was connected to a 30 L min^{-1} two-stage rotary pump (E2M2, Edwards Vacuum Ltd.) via a liquid nitrogen cold trap. An inductor−capacitor impedance matching network was used to minimize the standing-wave ratio for power transmission from a 13.56 MHz radio frequency (RF) power generator to a copper coil (10 turns, spanning 8 cm) externally wound around the glass chamber. For pulsed plasma deposition, a signal generator (model TH503, Thurlby Thandar Instruments Ltd.) was used to trigger the RF power supply, and the corresponding pulse shape was monitored with an oscilloscope (model V-252, Hitachi Ltd.). The setup is shown in Figure 16.

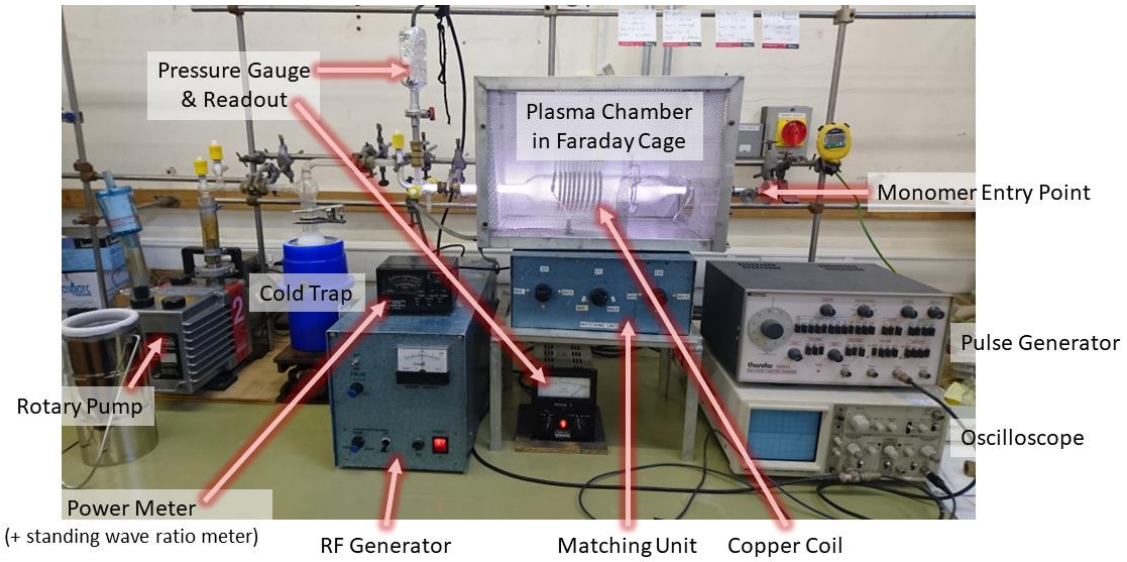

Figure 16: Pulsed plasma deposition setup. Photo taken during air plasma cleaning.

Prior to each plasma deposition, the reactor was scrubbed with detergent, rinsed with acetone, and oven dried at 200 °C. Next, a continuous wave air plasma was run at 0.2 mbar pressure and 50 W for a total of at least 30 min to remove any remaining contaminants from the chamber walls. Non-woven polypropylene cloth sheets (12 cm x 15 cm) were rolled against the interior chamber walls avoiding any overlap. Following evacuation to the system base pressure, vinylbenzyl chloride monomer (purified using at least five freeze−pump−thaw cycles) vapour was admitted into the chamber at 0.15 mbar pressure for 15 min. Next, the electrical discharge was ignited with a pulse duty cycle on-period of 100 µs and off-period of 4 ms, in conjunction with 30 W peak power for a duration of 20 min. Upon extinction of the plasma, the chamber was purged with monomer vapour for an additional 15 min. Finally, the system was evacuated to base pressure, and vented to the atmosphere. Following coating of one side of the non-woven polypropylene cloth, it was removed from the chamber, flipped over, placed into a clean chamber, and the process repeated for uniform coating of the other side. Subsequently, the pulsed plasma poly(vinylbenzyl chloride) functionalized cloth was cut into four pieces each measuring about 6 cm x 7 cm.

3.1.2 Calixarene Functionalization

Each cloth piece was placed into a separate glass vial (28 mL volume) containing 15.2 mg potassium carbonate (Sigma Aldrich Ltd.). Subsequently, 27.5 mL of a 8 mmol L^{-1} sodium iodide acetone solution (Fisher Scientific UK Ltd.) and either 0.4 mmol L^{-1} of the desired calixarene or 1.6 mmol L^{-1} 2,6-di-*tert*-butyl-4-(dimethylaminomethyl)phenol (DMAM-phenol; Tokyo Chemical Industry UK Ltd.) were added into each vial. The calixarenes used were either 5,11,17,23-tetrakis[(dimethylamino)methyl]-25,26,27,28-tetrahydroxycalix[4]arene (DMAM-calixarene; synthesized according to earlier literature[209,210]) or 5,11,17,23-tetra-*tert*-butyl-25,26,27,28-tetrahydroxycalix[4]arene (tBu-calixarene; 99%, Acros Organics B.V.B.A). The vials were sealed and rotated at 40 rpm for about 70 h. Subsequently the functionalized cloth pieces were removed from the vials, rinsed with acetone, then water, and finally air dried.

3.1.3 Butylimidazole Functionalization

The butylimidazole functionalization was adapted based on a previously reported method.[211] Each 6 cm x 7 cm cloth piece was placed into a glass vial (28 mL or 7 mL volume) together with a mixture of 1-butylimidazole (98%, Sigma Aldrich Ltd.) and dimethylformamide (DMF; Fisher Scientific UK Ltd.). The vials were sealed and left to rotate at room temperature with a speed of 40 rpm for five days. Subsequently the cloth pieces were rinsed with DMF, acetone, and ultra-high purity water, and finally dried in air.

3.2 Characterisation of Filtration Cloths

3.2.1 pp-VBC Thickness

The thickness of pulsed plasma poly(vinylbenzyl chloride) coatings deposited onto silicon wafers placed at each end of the cloth was measured using a spectrophotometer (NKD-6000, Aquila Instruments Ltd.). Transmittance−reflectance curves (350−1000 nm wavelength) were acquired using a parallel p-polarised light source at 30° incident angle to the substrate. These curves were fitted to a Cauchy model for dielectric materials[212] using a modified Levenberg−Marquardt algorithm (version 2.2 Pro-Optix software, Aquila Instruments Ltd.).[213]

3.2.2 Infrared Spectroscopy

Infrared spectra of the functionalized cloth were recorded using a FT-IR spectrometer (model Frontier IR, Perkin Elmer Inc.) equipped with a universal attenuated total reflectance (ATR) accessory (DiComp™ crystal with diamond surface (refractive index 2.4) in direct contact with a zinc selenide focusing element, Perkin Elmer Inc.) providing a penetration depth in the range of a few µm.[214] Samples were pressed against the ATR accessory crystal with a force of 110 N using the instrument software. Acquired spectra were averaged over 20 scans at 2 cm^{-1} resolution across the 380–4000 cm^{-1} wavenumber range.

3.2.3 X-Ray Photoelectron Spectroscopy

X-ray photoelectron spectroscopy (XPS) was carried out using an electron spectrometer (ESCALAB II, VG Scientific Ltd.) fitted with an unmonochromatised Mg Kα X-ray source (1253.6 eV) and a concentric hemispherical analyser. Photoemitted electrons were collected at a take-off angle of 20° from the substrate normal with electron detection in the constant analyser energy mode (CAE mode pass energy = 20 eV). Experimentally determined instrument sensitivity (multiplication) factors were C(1s):O(1s):N(1s):Cl(2p) equalling 1.00:0.35:0.70 respectively. A linear background was subtracted from core level spectra and then fitted using Gaussian peak shapes with a constant full-width-half-maximum (FWHM).[215]

3.3 Chromium Concentration Determination

3.3.1 UV-Vis

Cr(VI) oxoanion solution concentrations and changes thereof were measured using a UV–Vis–NIR spectrophotometer (Cary 5000, Agilent Technologies Inc.) and a quartz cell (10 mm light path length, SUPRASIL® high precision quartz 300, Hellma Analytics GmbH & Co. KG).[216] The previously reported isosbestic point for the light absorbance of Cr(VI) oxoanion solutions at 339 nm was verified by acquiring UV–Vis spectra of fixed concentration potassium dichromate solutions at six different pH values ranging between pH 2.25–10.11. Subsequently, a calibration curve was created by measuring the absorbance at 339 nm for ten different potassium dichromate solutions spanning a hexavalent chromium concentration range of three orders of magnitude from 70 µg L^{-1} (70 ppb) to 70 mg L^{-1} (70 ppm). For each solution, division of the measured absorbance at 339 nm by the respective Cr(VI) concentration and light path length (Beer−Lambert Law[217]) yielded the mean molar extinction coefficient value ($\varepsilon = (1.47 \pm 0.04) \times 10^3\ M^{-1}\ cm^{-1}$)—which is in agreement with the literature.[216] Unknown concentrations of Cr(VI) oxoanion solutions collected following filtration experiments were subsequently calculated by measuring their

absorbance at 339 nm in conjunction with the aforementioned experimentally determined molar extinction coefficient (ε).

3.3.2 ICP-OES

The total chromium content of real-world industrial wastewater samples, as well as the total chromium and arsenic contents of mixed solutions were measured using Inductively Coupled Plasma Optical Emission Spectrometry (iCAP 6500, Thermo Fisher Scientific Inc.). Calibration standards were prepared by serial dilution of a 1000 mg L^{-1} Cr(III) (as $Cr(NO_3)_3$) reference solution (Romil Ltd.) and a 1000 mg L^{-1} As(III) (as As_2O_3) reference solution (Romil Ltd.). The optical emission at thirteen characteristic chromium wavelengths and seven characteristic arsenic wavelengths was measured three times for each sample.

3.4 Cr(VI) Oxoanion Capture Experiments

Cr(VI) oxoanion solutions were prepared by dissolving potassium dichromate (>99.0%, Sigma Aldrich Ltd.) in ultra-high purity water (18.2 MΩcm, SELECT Neptune Analytical water polishing unit, Purite Ltd.) and subsequent dilution to the desired concentrations for water purification testing.

3.4.1 Static Capture

In order to determine the static Cr(VI) uptake capacity of DMAM-calixarene functionalized cloth, four 30 mm x 35 mm pieces of functionalized cloth (quarters of the initial 6 cm x 7 cm pieces) from different batches were each immersed into 13 mL of potassium dichromate solution containing 20 mg L^{-1} Cr(VI) concentration. The sealed vials were rotated at 40 rpm for 4 h. Subsequently, the Cr(VI) concentration in the initial and the final set of four purified solutions were measured.

3.4.2 Dynamic Filtration

Flow-through water filtration testing entailed inserting 30 mm x 35 mm pieces of functionalized non-woven polypropylene cloth into glass Pasteur pipettes (Fisherbrand, 15 cm length, inner diameter 5.6 mm, Fisher Scientific UK Ltd.). Potassium dichromate solutions and real-world water samples were passed through the cloth loaded Pasteur pipette in the absence of any externally applied pressure (this filtration typically took about 8–15 min for 10 mL volumes of liquid). By measuring the Cr(VI) concentration in each of the filtrates, the amount of chromium captured in the cloth following each filtration step could be calculated. All measurements were repeated at least twice, and standard deviation values are reported. The filtration setup is depicted in Figure 17.

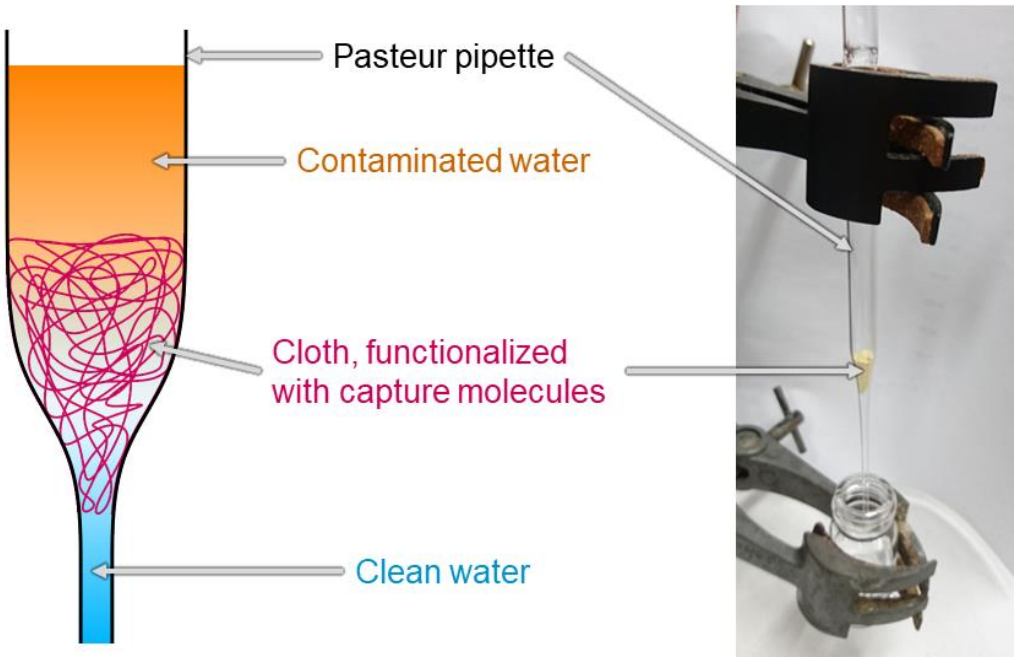

Figure 17: Setup for dynamic filtration. Left: schematic sketch. Right: photograph of the setup prior to filtration.

3.4.3 Competitive Anion and Real Water

Model solutions used to test the selectivity of functionalized cloth for chromium(VI) oxoanion capture in the presence of competitive anions were prepared using sodium chloride (>99.5%, Sigma Aldrich Ltd.), monosodium phosphate (Sigma Aldrich Ltd.), sodium sulfate (>99% anhydrous, Fisher Scientific UK Ltd.), sodium nitrate (99%, Acros Organics B.V.B.A.), and arsenic

acid (arsenic standard solution, 1000 mg L^{-1} As as H_3AsO_4 in 0.5 mol L^{-1} HNO_3, Merck Chemicals Ltd.).

Water from a vegetated rainwater pond (Durham University, UK) was used to simulate real-world water containing a natural mixture of ions. The water was collected directly from the pond and filtered using a membrane filter (Whatman Polydisc GW In-Line polyamide filter with 0.45 µm pore size, GE Healthcare Inc.) to remove particulate matter (as stipulated for dissolved chromium analysis by the United States Environmental Protection Agency[218]). Following removal of particulate matter, the pond water was spiked with potassium dichromate solution at known concentrations. All filtration experiments with pond water were conducted within 3 hours of collection. Untreated pond water samples were analysed to determine the concentration of anions competing with chromate, namely chloride, phosphate, sulfate, and nitrate (ALS Environmental Ltd.).

Real-world industrial wastewater samples were collected in polypropylene bottles (Azlon 30 mL round wide neck bottles, SciLab Ltd.) in 2 different locations (A and B) from an industrial zone near Jalandhar, India. Filtration experiments and analyses were performed within days of water sample collection. Particulate matter was removed using a membrane filter (Whatman Polydisc GW In-Line polyamide filter with 0.45 µm pore size, GE Healthcare Inc.) as stipulated for dissolved chromium analysis by the United States Environmental Protection Agency[218].

3.4.4 Regeneration and Recycling

The release of Cr(VI) oxoanions captured by DMAM-calixarene cloths back into solution through deprotonation of the calixarene amine groups was done by adding base.[219] Regeneration solutions were prepared using sodium hydroxide (analytic reagent grade pellets, Fisher Scientific UK Ltd.), sodium bicarbonate (99+%, extra pure, Acros Organics B.V.B.A.), and sodium chloride (>99.5%, Sigma Aldrich Ltd.). For regeneration experiments, first 10 mL of a 6 mg L^{-1} Cr(VI) oxoanion solution was filtered through the DMAM-calixarene functionalized cloth, then 5 mL deionized water was filtered through to rinse out any chromium(VI) solution trapped by capillary forces, followed by passing 5 mL of one of the prepared regeneration solutions through the hexavalent chromium oxoanion

loaded cloth. By measuring the Cr(VI) concentration in each of the filtrates via UV–Vis spectroscopy, the amount of Cr(VI) retained in the cloth could be calculated. The amount of chromium(VI) released by each regeneration solution was divided by the initial filtrate chromium(VI) uptake in the cloth to determine the release efficiency (percentage).

3.5 MOF-508 Preparation

3.5.1 Epitaxial Synthesis

Epitaxial synthesis of MOF-508 was performed on the following substrates: high density polyethylene sheet (HDPE; about 1 mm thick), polypropylene film (PP), polypropylene cloth (middle layer of disposable surgical masks, 80 µm thickness, SD Medical Ltd.), polyethylene terephthalate film (PET), polyethersulfone film (PES; Westlake Plastics Company Inc.), paper (80 g m^{-2}, Office Depot Inc.), cotton cloth, glass (Academy microscope slides), and polytetrafluoroethylene tape (PTFE; 0.075 mm thickness, Everbuild Building Products Ltd.). Selected substrates were coated with a poly(1-allylimidazole) linker layer created from 1-allylimidazole (97%, Acros Organics B.V.B.A.) via pulsed plasma deposition as described previously.[220]

MOF-508 synthesis was conducted using a 1.0 mM solution of zinc acetate (99.99%, Sigma Aldrich Co.) and a second solution consisting of 0.2 mM terephthalic acid (98%, Sigma Aldrich Co.) and 0.2 mM 4,4’-bipyridine (98%, Sigma Aldrich Co.), all in tetrahydrofuran (≥99.5%, Fisher Scientific UK Ltd.). A volume of 50 mL of each of the solutions and slightly above 50 mL tetrahydrofuran (as wash solution) were filled into three 120 mL glass jars positioned on a dipping robot. In selected cases (for PET and PES substrates and wherever specified), ethanol (≥99.8%, Fisher Scientific UK Ltd.) was used as solvent instead of tetrahydrofuran. Up to four approximately square substrates (lengths 10–15 mm) were attached to the robot with small metal clips. Each dipping cycle consisted of a 5 min immersion in the zinc acetate solution, a 5 s rinse in THF, a 30 s air drying period, a 5 min immersion in the linker solution, another 5 s rinse in THF, and a final 30 s air drying period. Dipping cycles were

repeated automatically until a desired number of layers was reached, and all solutions were changed after every ten cycles. The process is illustrated in Figure 18.

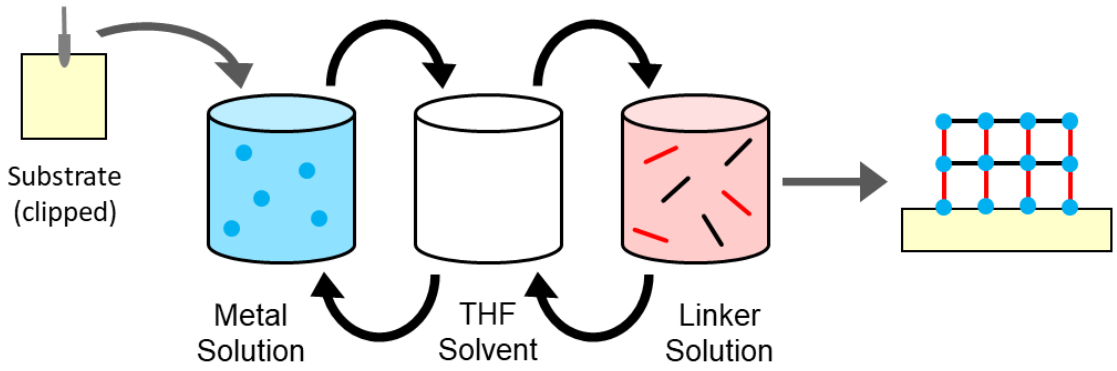

Figure 18: Schematic illustration of the epitaxial synthesis of MOF-508. The substrate is repeatedly dipped into metal and linker solutions with intermittent wash steps, resulting in a gradual growth of the MOF film.

3.5.2 Tape Transfer

To test the possibility of MOF-508 lift-off from HDPE following epitaxial synthesis, the MOF was transferred onto commercial adhesive tape (Scotch Magic™ tape, 3M Co.). For this purpose, the tape was placed on the SURMOF while applying gentle pressure for a few seconds before removal.

In order to transfer a MOF-508 thin film from HDPE onto glass (two transfer steps), a thermal release sheet (90 °C REVALPHA, Nitto Denko Co.) was used instead of regular tape. As before, the sheet was placed on the SURMOF while applying gentle pressure and then removed. Subsequently, the sheet carrying the MOF was placed on a clean glass slide and pressure was applied again. Finally, the glass (with the sheet attached to it) was placed on a 90 °C hot plate where the sheet lost its adhesion and curled up, making it easy to remove. Any residual tape adhesive was dissolved by dropping a small amount of acetone onto the glass.

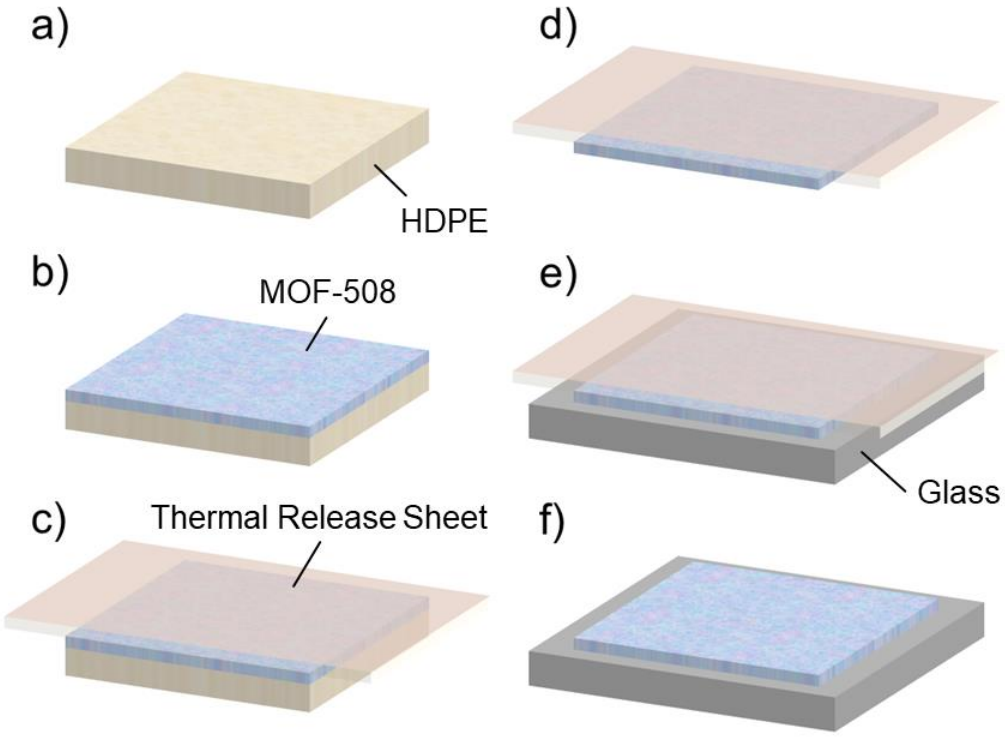

Figure 19: Transfer of thin MOF-508 films from HDPE to glass using thermal release sheet; schematic steps. HDPE (a) is coated with MOF-508 via layer-by-layer synthesis (b). Thermal release sheet is pressed onto MOF (c) and used to lift off the MOF from the HDPE substrate (d). Sheet and MOF are then pressed onto a clean glass substrate (e). Through heat, the sheet is released, leaving the thin MOF film behind (f).

3.6 MOF-508 Characterisation

3.6.1 Infrared (IR) Spectroscopy

Infrared (IR) spectra were recorded using an FT-IR spectrometer (Frontier IR, PerkinElmer Inc.) equipped with a universal attenuated total reflectance (ATR) accessory (DiComp crystal with the diamond surface (refractive index 2.4) in direct contact with a zinc selenide focusing element, PerkinElmer Inc.), providing a penetration depth in the range of a few micrometers.[214] Samples were pressed against the ATR accessory crystal with a force of 110 N using the instrument software. Acquired spectra were averaged over 20 scans at 0.5 cm^{-1} step width across the 380–4000 cm^{-1} wavenumber range.

3.6.2 X-Ray Diffraction (XRD)

X-ray diffractograms (XRD) were acquired with a powder diffractometer (d8, Bruker Corp.) across the 5–60° 2θ range using a 0.02° step size. The copper anode X-ray source (Cu Kα 1.5418 Å wavelength radiation) was operated at 40 kV and 40 mA.

3.6.3 Scanning Electron Microscopy (SEM)

For scanning electron microscopy (SEM), the samples were mounted onto carbon disks supported on aluminium stubs and then coated with a thin gold layer (5–10 nm, Polaron SEM Coating Unit, Quorum Technologies Ltd.) Surface topography images were acquired using a scanning electron microscope (VEGA3 LMU, Tescan Orsay Holdings a.s.) operating in secondary electron detection mode, in conjunction with an accelerating voltage of 8–20 kV and a working distance of 7–16 nm.

3.6.4 Photography

Photographs of samples were taken using a Fujifilm X-M1 mirrorless digital camera with an aperture of F/5.6 and exposure times of 0.08–0.10 seconds.

3.6.5 X-Ray Pholoelectron Spectroscopy (XPS)

X-ray photoelectron spectroscopy (XPS) was carried out using an electron spectrometer (ESCALAB II, VG Scientific Ltd.) fitted with an unmonochromatized Mg Kα X-ray source (1253.6 eV) and a concentric hemispherical analyzer. Photoemitted electrons were collected at a take-off angle of 20° from the substrate normal with electron detection in the constant analyzer energy mode (CAE mode pass energy = 20 eV). Experimentally determined instrument sensitivity (multiplication) factors were C(1s) : F(1s) : N(1s) : O(1s) : Zn(2p) = 1 : 0.25 : 0.7 : 0.35 : 0.056, respectively. A linear background was subtracted from core-level spectra and then fitted using Gaussian peak shapes with a constant full width at half-maximum.[221]

3.8 References

(207) Ehrlich, C. D.; Basford, J. A. Recommended Practices for the Calibration and Use of Leaks. *J. Vac. Sci. Technol. A* **1992**, *10*, 1–17.

(208) Wilson, M.; Kore, R.; Ritchie, A. W.; Fraser, R. C.; Beaumont, S. K.; Srivastava, R.; Badyal, J. P. S. Palladium-Poly(Ionic Liquid) Membranes for Permselective Sonochemical Flow Catalysis. *Colloids Surf., A* **2018**, *545*, 78−85.

(209) Memon, S.; Tabakci, M.; Roundhill, D. M.; Yilmaz, M. Synthesis and Evaluation of the Cr(VI) Extraction Ability of Amino/Nitrile Calix[4]arenes Immobilized onto a Polymeric Backbone. *Reactive & Functional Polymers* **2006**, *66*, 1342−1349.

(210) Gutsche, C. D.; Nam, K. C. Calixarenes. 22. Synthesis, Properties, and Metal Complexation of Aminocalixarenes. *J. Am. Chem. Soc.* **1988**, *110*, 6153−6162.

(211) Wilson, M. Kore, R.; Ritchie, A.W.; Fraser, R.C.; Beaumont, S.K.; Srivastava, R.; Badyal, J.P.S. Palladium–poly(ionic liquid) membranes for permselective sonochemical flow catalysis. *Colloids and Surfaces A* **2018**, *545*, 78–85.

(212) Dieblod, A. C.; Chism, W. W. Characterisation and Metrology of Medium Dielectric Constant Gate Dielectric Films. In *High Dielectric Constant Materials*: *VSLI MOSFET Applications*; Huff, H. R., Gilmer, D. C., Eds.; Springer-Verlag: Berlin, 2005; p 486.

(213) Lovering, D. NKD-6000 Technical Manual; Aquila Instruments: Cambridge, 1999.

(214) Technical Note: FT-IR Spectroscopy ATR accessories. Perkin Elmer 2004. https://shop.perkinelmer.com/Content/technicalinfo/tch_atraccessories.pdf (accessed on Mar 31, 2019).

(215) Evans, J. F.; Gibson, J. H.; Moulder, J. F.; Hammond, J. S.; Goretzki, H. Angle Resolved ESCA Analysis of Plasma Modified Polystyrene. *Fresenius' Z. Anal. Chem.* **1984**, *319*, 841–844.

(216) Xia, L.; Akiyama, E.; Frankel, G.; McCreery, R. Storage and Release of Soluble Hexavalent Chromium from Chromate Conversion Coatings Equilibrium Aspects of CrVI Concentration. *J. Electrochem. Soc.* **2000**, *147*, 2256−2562.

(217) Beer, A. Bestimmung der Absorption des Rothen Lichts in Farbigen Flüssigkeiten. *Ann. Phys. Chem.* **1852**, *86*, 78−88.

(218) Laboratory Operations and Quality Assurance Manual1; U.S. Environmental Protection Agency, Analytical Services Branch, April 24, 2018. https://www.epa.gov/sites/production/files/2018-05/documents/asb_loqam_042418.pdf (accessed on Jun 12, 2019).

(219) Georgiev, E. M.; Wolf, N.; Roundhill, D. M. Lower Rim Alkylammonium-Substituted Calix[4]arenes as "Proton-Switchable" Extractants for Chromate and Dichromate Anions. *Polyhedron* **1997**, *16*, 1581−1584.

(220) Wilson, M.; Barrientos-Palomo, S.N.; Stevens, P.C.; Mitchell, N.L.; Oswald, G.; Nagaraja, C.M.; Badyal, J.P.S. Substrate-Independent Epitaxial Growth of the Metal–Organic Framework MOF-508a. *ACS Appl. Mater. Interfaces* **2018**, *10*, 4057–4065.

(221) Evans, J. F.; Gibson, J. H.; Moulder, J. F.; Hammond, J. S.; Goretzki, H. Angle Resolved ESCA Analysis of Plasma Modified Polystyrene. *Fresenius' Z. Anal. Chem.* **1984**, *319*, 841–844.

Chapter 4: Dimethylaminomethyl-Calixarene Functional Cloths for Selective Capture of Toxic Chromium Water Pollutants

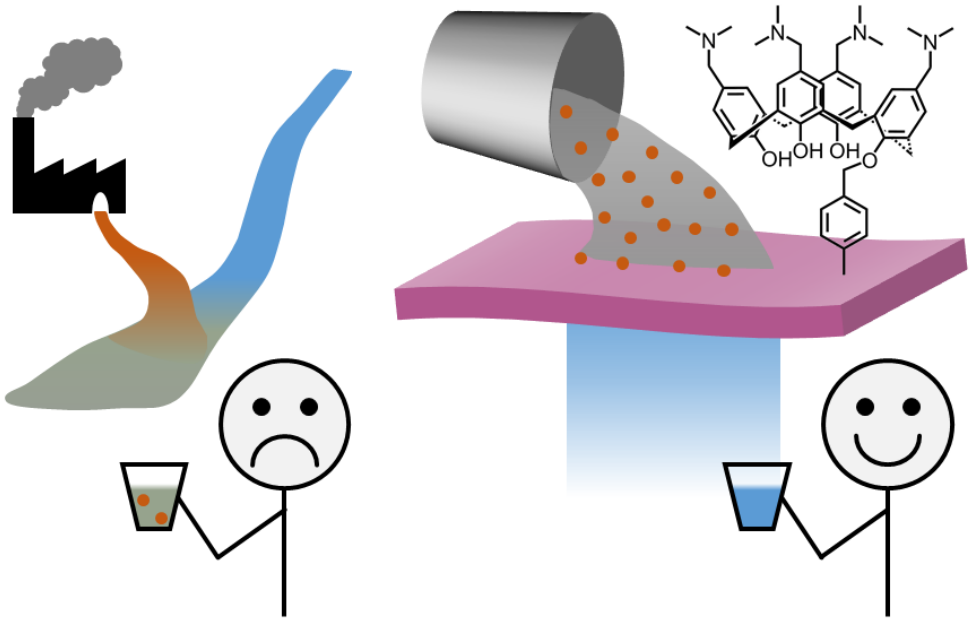

Figure 20: Graphic chapter summary: Filter functionalized with dimethylaminomethyl-calixarene purifies Cr(VI)-polluted water, making it safe to drink.

4.1 Introduction

Water pollution is a major threat to human health around the world and is considered to be a major global sustainable development challenge. Particularly in some developing countries, large amounts of industrial wastes are sometimes emptied into rivers without adequate remediation, leading to contaminated human drinking supplies.[222] According to the United Nations, each year more people die from unsafe water than from all forms of violence put together (including war). [223] In contrast, for example in the European Union, strict regulations are enforced.[224,225,226]

Conventional large-scale removal of toxic heavy metal ion pollutants from drinking water relies on methods such as reverse osmosis, electrodialysis, or ultrafiltration; these techniques can be expensive or require a constant energy supply and are therefore not readily accessible in many low-income countries.[227] Point-of-use water purification systems offer a safer alternative for poorly

regulated scenarios. Despite there being a wide range of techniques available employing mechanisms such as heat[228], UV light[229,230], antibacterial agents[231,232], and filtration through small pores[233,234], most of them only target bacterial contamination and are entirely ineffective against dissolved contaminants (such as heavy metal ions).[235] Hence there exists a need for the development of point-of-use methods targeting the removal of dissolved contaminants from water supplies.[236,237,238,239]

A common class of toxic heavy metal water pollutants are aqueous hexavalent chromium compounds based on Cr(VI) oxoanions (chromate (CrO_4^{2-}), hydrogen chromate ($HCrO_4^-$), and dichromate ($Cr_2O_7^{2-}$)). These chemicals have been widely utilized by industry since the 19th Century for pigments, leather tanning, metallurgy, chrome-plating, corrosion inhibitors, and numerous other applications.[240,241,242] However, there are significant dangers associated with their usage towards human health—skin contact leads to sores,[243] inhalation causes perforation of the nasal septum,[244] whilst animal testing has shown that injection and ingestion give rise to cancer.[245,246,247] Such high levels of toxicity associated with Cr(VI) oxoanions (such as chromate) are attributed to structural similarities with phosphate and sulphate anions—which are known to be easily transported into biological cells acting as nutrients (whereas chromate leads to cell damage).[248,85] *In vitro* studies have shown that within a biological cell, hexavalent chromium can be reduced to stable trivalent chromium compounds by ascorbate and different thiol-containing molecules (such as glutathione and the amino acid cysteine).[249] During this reduction of Cr(VI) oxoanions, oxygen radicals and intermediate chromium oxidation states are formed which are able to react with and damage different parts of the biological cell—for example cleavage of DNA strands.[250] The resultant trivalent chromium ions are able to form complexes with amino acids and the phosphate group of DNA present within the cell.[251] These stable Cr(III) complexes are difficult to break up and therefore impair the functions of the cell, leading to cancer and other health issues.[252] In contrast, trivalent chromium species found in the environment are relatively harmless because they are unable to easily permeate biological cell walls.[86] Given the aforementioned toxicity of hexavalent chromium (even when ingested at very low concentrations over an extended period of time), strict legal limits

have been set by government regulatory bodies for the maximum permitted chromium concentration in drinking water (for the European Union, the current legal limit of 50 μg L^{-1}, will shortly be lowered to 25 μg L^{-1} (accepted by the European Commission in December 2019).[224,225,226] However, elevated concentrations of Cr(VI) oxoanions are often detected in ground and drinking water supplies across many parts of the world.[253,254,255]

Point-of-use water purification systems for chromium oxoanion containing effluents potentially offer a cheaper and more targeted approach compared to larger scale upstream installations which are susceptible to mismanagement due to lack of legal enforcement of safe pollutant drinking levels within some developing countries. In this chapter, pieces of high surface area cloth are functionalized with tertiary amine terminated calixarene (5,11,17,23-tetrakis[(dimethylamino)methyl]-25,26,27,28-tetrahydroxycalix[4]arene, DMAM-calixarene) and then used to capture Cr(VI) oxoanions from polluted industrial wastewater, Scheme 1. This encompasses pulsed plasma deposition of poly(vinylbenzyl chloride) onto the cloth substrate to provide benzylchloride groups for reaction with the calixarene lower rim hydroxyl groups via a nucleophilic substitution mechanism.[256,257] Non-woven polypropylene cloth is employed because it is less prone to fungal growth compared to natural materials such as cotton,[258] whilst being flexible enough to be easily inserted into cartridges of any size and geometry without leaving any gaps through which the water flow could circumvent the filtration media. Cr(VI) oxoanions are removed from water by simply filtering the pollutant solution through the functionalized cloth. It is shown that DMAM-calixarene functionalized cloth completely removes hexavalent chromium oxoanions from water at pollutant levels comparable to real-world scenarios (up to 100−260 μg L^{-1} [254,271,272]). Furthermore, high selectivity towards Cr(VI) oxoanion capture is measured for real-world polluted wastewater, and multiple-use recyclability is demonstrated.

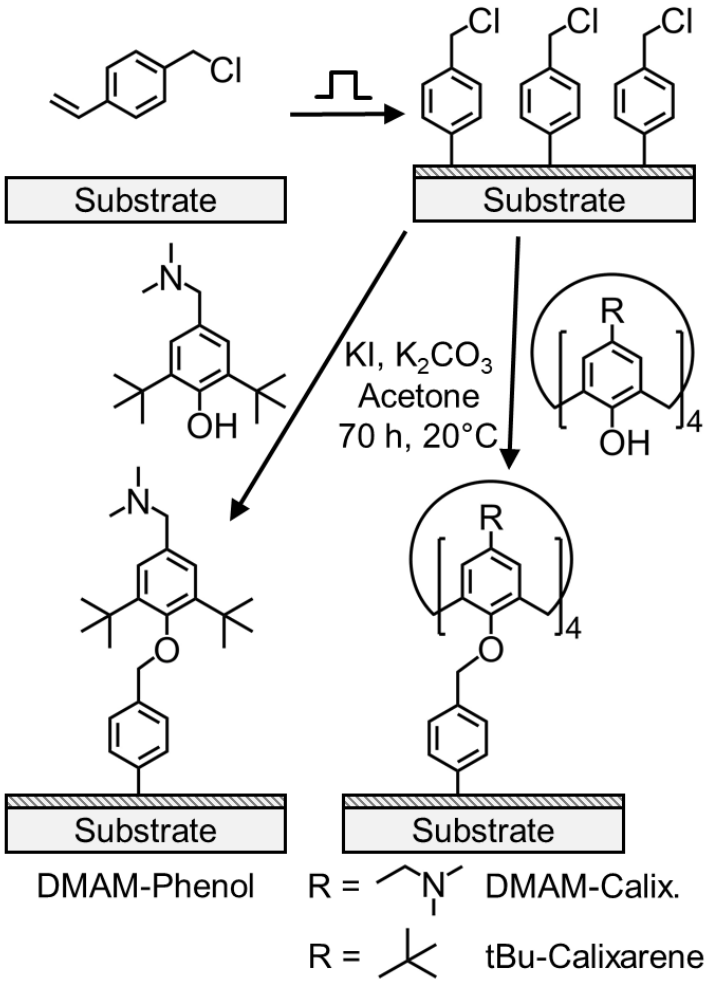

Scheme 1: Pulsed plasma poly(vinylbenzyl chloride) deposition onto a cloth substrate, followed by tethering of calixarenes containing either tertiary amine groups (5,11,17,23-tetrakis[(dimethylamino)methyl]-25,26,27,28-tetrahydroxycalix[4]arene, DMAM-calixarene) or tert-butyl groups (5,11,17,23-tetra-tert-butyl-25,26,27,28-tetrahydroxycalix[4]arene, t-Bu-calixarene) on the upper rim, or alternatively with a phenol derivative containing a tertiary amine group (2,6-di-tert-butyl-4-(dimethylaminomethyl)phenol, DMAM-phenol).

4.2 Results

4.2.1 DMAM-Calixarene-Functionalized Cloths

The deposition rate for pulsed plasma poly(vinylbenzyl chloride) films coated onto silicon wafers was measured to be 43.6 ± 3.6 nm min^{-1}. All of the non-woven cloth filters were uniformly coated.[259]

Functionalized cloths were characterized using ATR-infrared spectroscopy. Given the thin nature of the plasma deposited coatings, features from the

underlying non-woven polypropylene cloth were also visible with the ATR-FTIR sampling depth (few μm)[260], Figure 21.

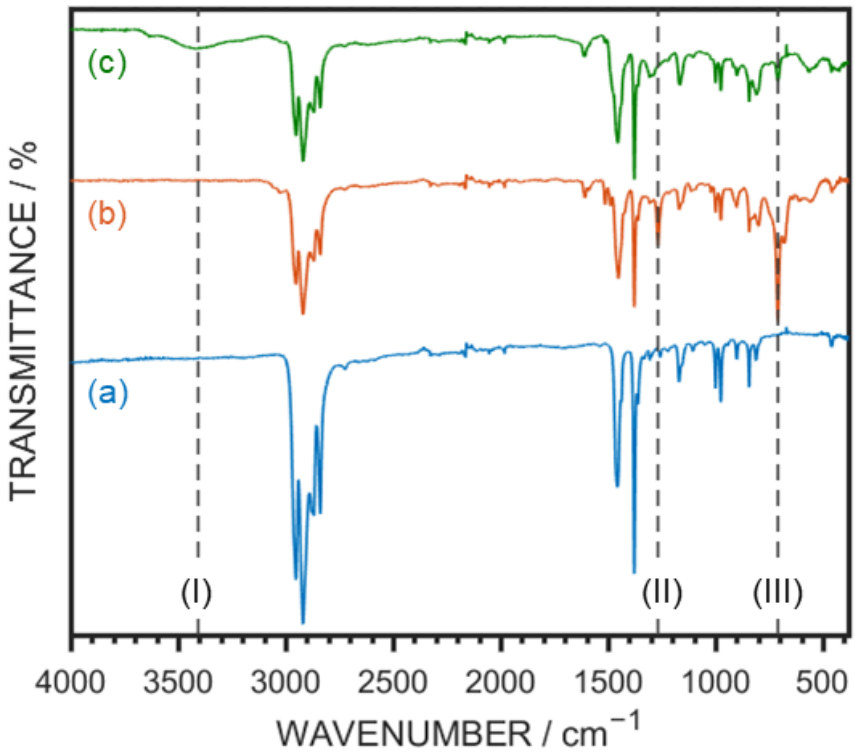

Figure 21: ATR-infrared spectra of: (a) untreated non-woven polypropylene cloth, (b) pulsed plasma poly(vinylbenzyl chloride) coated cloth, and (c) following functionalization of (b) with DMAM-calixarene. Dashed lines indicate characteristic vibrations: (I) O−H stretch, (II) C−H wag of the −CH_2Cl group, and (III) C−Cl stretch.

The infrared spectrum of the untreated non-woven polypropylene cloth shows features characteristic for polypropylene, such as broad and intense C-H stretch vibration absorbances in the 2830−2970 cm^{-1} region and two intense bands at 1454 cm^{-1} and 1377 cm^{-1} corresponding to the methylene CH_2 and methyl CH_3 bending vibrations respectively.[261,262] Fingerprint peaks of the pulsed plasma poly(vinylbenzyl chloride) layer on the cloth include a characteristic C−Cl stretch absorbance at 708 cm^{-1} (III) and a −CH_2Cl group C−H wag absorbance at 1263 cm^{-1} (II).[257,259, 262 , 263] These features became attenuated following reaction with DMAM-calixarene. The absorbance peak associated with the calixarene tertiary amine group C−N stretch (1020−1250 cm^{-1}) is difficult to assign unambiguously due to overlap with the underlying polypropylene cloth spectral features.[214,262] However, a broad O−H stretch band at 3406 cm^{-1} (I)

associated with the unreacted hydroxyl groups on the lower rim of the calixarene molecules is clearly visible.[262]

XPS analysis gave surface elemental compositions in good agreement with expected theoretical values for pulsed plasma poly(vinylbenzyl chloride) functionalized cloth, Table 6.[259,263,264,265] A small amount of aerial oxidation was evident due to the reaction of trapped free radicals within the deposited plasma polymer film.[266,267,268]

Table 6: XPS compositions for: vinylbenzyl chloride (VBC, theoretical); pulsed plasma deposited poly(vinylbenzyl chloride) (pp-VBC); one unit of vinylbenzyl chloride reacted with one DMAM-calixarene molecule (theoretical see Scheme 1); and pulsed plasma deposited poly(vinylbenzyl chloride) subsequently functionalized with DMAM-calixarene.

	Composition / atom %			
	C	**O**	**N**	**Cl**
VBC (Theory)	90.0	0.0	0.0	10.0
pp-VBC	89.4 ± 1.6	1.0 ± 1.1	0.0 ± 0.0	9.5 ± 0.4
VBC + DMAM-Calix (Theory)	86.0	7.0	7.0	0.0
pp-VBC + DMAM-Calix	85.7 ± 1.0	8.3 ± 1.0	3.5 ± 0.4	2.4 ± 0.3

The XPS surface elemental composition following DMAM-Calixarene functionalisation is consistent with predicted theoretical values. The detection of 2.4 at.% chloride following DMAM-calixarene reaction is either due to not all surface chloride groups of the pulsed plasma poly(vinylbenzyl chloride) undergoing reaction or the presence of unreacted sub-surface chloride groups within the XPS technique sampling depth (0.2−5 nm)[269,270]. This also explains why the measured nitrogen content of the DMAM-calixarene functionalized cloth is lower than theoretically expected for the model reaction mechanism where each vinylbenzyl chloride repeat unit reacts with one DMAM-calixarene molecule, Scheme 1.

SEM images showed that the pores within the non-woven polypropylene cloth remained free after coating with poly(vinylbenzyl chloride). Additionally,

there was no significant swelling of the pulsed plasma poly(vinylbenzyl chloride) films following DMAM-calixarene functionalization, Figure 22.

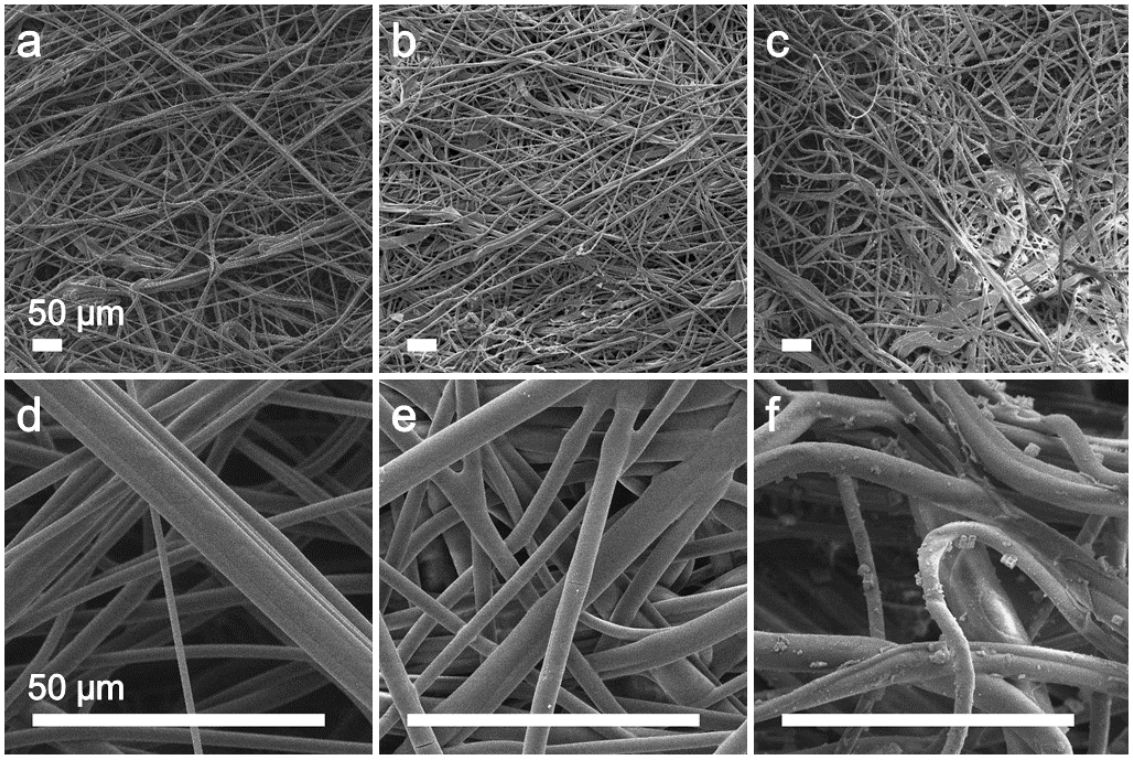

Figure 22: SEM micrographs of uncoated non-woven polypropylene cloth (a, d); pulsed plasma poly(vinylbenzyl chloride) functionalized non-woven polypropylene cloth (b, e); and following subsequent reaction with DMAM-calixarene (c, f). Scale bar represents 50 µm in all images.

4.2.2 Cr(VI) Oxoanion Static Capture

Static immersion of 30 mm x 35 mm DMAM-calixarene functionalized cloth pieces into 13 mL of 2 mg L^{-1} Cr(VI) solution (approximately ten times greater concentration compared to typical real-world pollution levels[254,271,272]) for 4 h removed at least 99% of chromium(VI) oxoanions from solution (concentration dropped to below the UV−Vis instrument detection limit of 20 µg L^{-1})—the residual pollutant level met the forthcoming lower European Union drinking water standards (< 25 µg L^{-1}).[224] For an even higher starting chromium(VI) concentration of 20 mg L^{-1}, 70 ± 4% of the chromium(VI) oxoanions (6.6 ± 0.4 $mg_{Cr(VI)}$ g_{Cloth}^{-1}) could be captured by the DMAM-calixarene cloth following an immersion time of 4 h, thereby demonstrating the high overall pollutant capture capacity.

As each 30 mm x 35 mm piece of DMAM-calixarene functionalized cloth weighing an average of 28.5 ± 2.5 mg captured an average of 6.6 ± 0.4 $mg_{Cr(VI)}\ g_{Cloth}^{-1}$ or 188 ± 11 µg Cr(VI) per cloth piece, this means that every piece captured about 3.6 µmol Cr(VI).

When preparing the cloth, 31.3 mg or 47.9 µmol of DMAM-calixarene (M = 652.9 g mol^{-1}) was dissolved in 120 ml of acetone. In total, 110 ml of this solution was used to functionalize the cloth, split up into four vials containing 27.5 ml solution and one quarter (60 mm x 70 mm) of the full cloth each. Therefore, the maximum amount of calixarene that could have been attached to the cloth is:

$$n_{Calix\ in\ 110\ ml} = 47.9\ \mu mol\ \times\ 110/120 = 43.9\ \mu mol$$

Each full cloth (120 mm x 140 mm) was cut into 16 pieces (30 mm x 35 mm each) with which the uptake and filtration experiments were performed. Assuming that all calixarene became attached to the cloth during functionalization in an evenly distributed manner, each of the sixteen cloth pieces contains:

$$n_{Calix\ on\ cloth} = 43.9\ \mu mol/16 = 2.7\ \mu mol$$

As it was experimentally determined that each 30 mm x 35 mm piece of cloth captured an average of 3.6 µmol Cr(VI), this leads to an average capture of 1.3 Cr(VI) atoms per calixarene molecule:

$$3.6\ \mu mol\ Cr(VI)/2.7\ \mu mol\ Calix = 1.3\ Cr(VI)/Calix$$

This ratio can be viewed as a minimum because it would be even higher if the calixarene molecules in solution are not completely attached to the cloths. While it may at first seem surprising that each calixarene can capture more than one chromium atom, one needs to bear in mind that the chromium exists in an equilibrium of chromate and dichromate in solution and that the calixarene has four positive charges (four amine groups) at neutral pH. Both of these factors contribute to the chromium to calixarene ratio being larger than one.

4.2.3 Cr(VI) Oxoanion Dynamic Capture

Dynamic flow-through filtration testing of DMAM-calixarene functionalized cloths utilised a range of different concentrations of aqueous potassium dichromate solutions, Figure 23. Virtually all chromium(VI) oxoanion content was removed for starting Cr(VI) concentrations below 1 mg L^{-1} (i.e. applicable real-world scenario pollution concentrations which are reported to be up to 100−260 µg L^{-1} [254,271,272]). Even for significantly higher Cr(VI) concentrations (20 mg L^{-1}), 78 ± 9% of the aqueous chromium(VI) oxoanion species could be captured in a single pass (corresponds to 2.7 ± 0.4 $mg_{Cr(VI)}$ g_{Cloth}^{-1}).

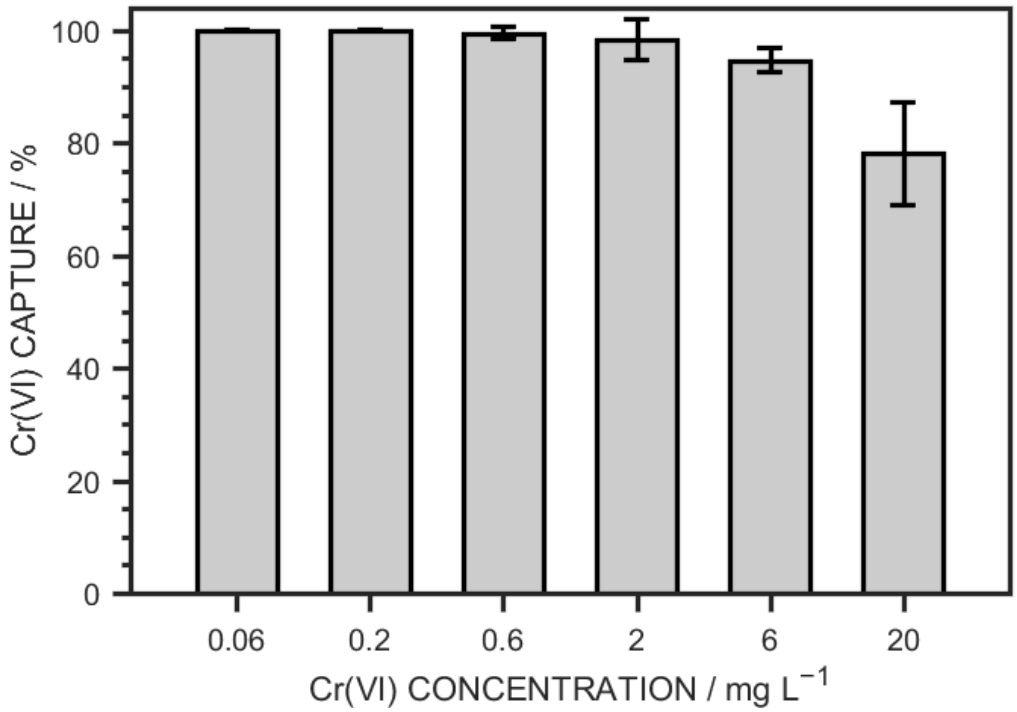

Figure 23: Flow-through Cr(VI) oxoanion capture using DMAM-calixarene functionalized non-woven polypropylene cloth as a function of starting pollutant concentration. Volumes of 5 mL of potassium dichromate solution were used for each filtration and repeated 5 times using fresh pieces of cloth. Three different batches of DMAM-calixarene functionalized cloths were tested. Typical real-world pollution levels correspond to about 0.2 mg L^{-1}.[254,271,272]

Control Cr(VI) oxoanion filtration experiments were conducted using pulsed plasma poly(vinylbenzyl chloride) coated non-woven polypropylene cloth, as well as following functionalisation with either a calixarene containing *tert*-butyl groups instead of dimethylaminomethyl groups (tBu-calixarene) or 2,6-di-*tert*-butyl-4-(dimethylaminomethyl)phenol (DMAM-phenol—equivalent to the repeat building

block for DMAM-calixarene), Scheme 1 and Figure 24. Virtually no chromium(VI) oxoanion capture was measured for *t*-Bu-calixarene cloth, whereas DMAM-phenol cloth showed similar levels of removal efficiency as found for DMAM-calixarene cloth—thereby confirming the role of dimethylaminomethyl groups for Cr(VI) oxoanion capture. Notable advantages of DMAM-calixarene compared to DMAM-phenol functionalized cloths were found with respect to better Cr(VI) oxoanion capture selectivity in the presence of other pollutants (as described later in Section 4.2.4).

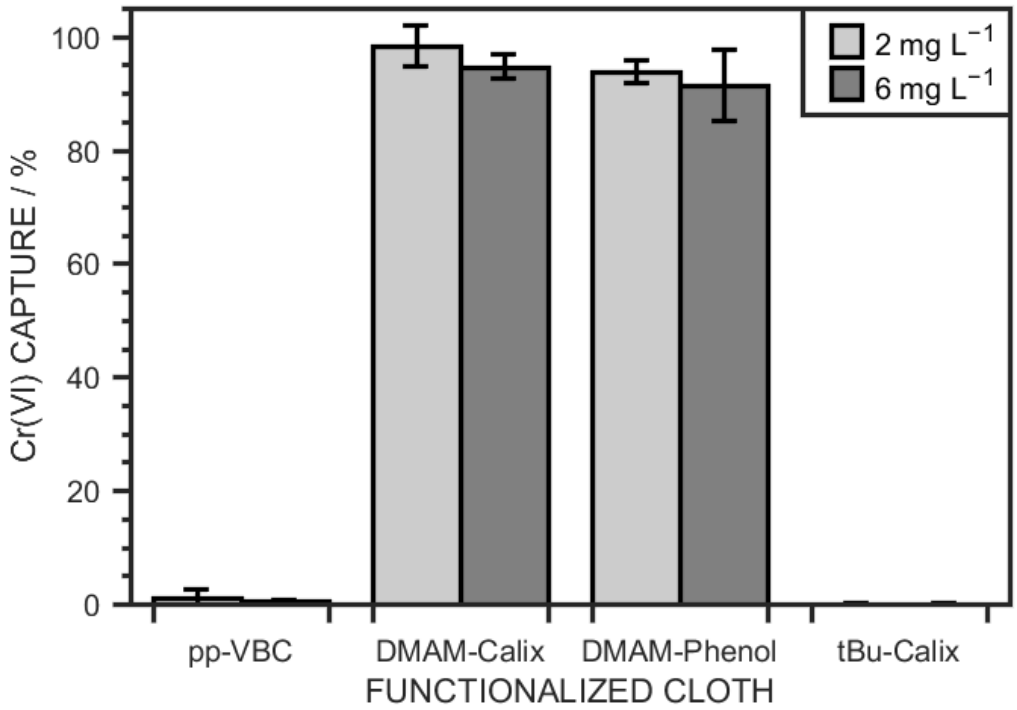

Figure 24: Flow-through Cr(VI) oxoanion capture efficiencies for pulsed plasma poly(vinylbenzyl chloride) functionalized non-woven polypropylene cloth pieces (pp-VBC) and following subsequent reaction with dimethylaminomethyl (DMAM) calixarene, DMAM-phenol, or *tert*-butyl (*t*-Bu) calixarene, Scheme 1. 5 mL potassium dichromate solutions were used with starting Cr(VI) concentrations of 2 mg L^{-1} and 6 mg L^{-1}.

4.2.4 Cr(VI) Oxoanion Filtration Selectivity

Flow-through filtration tests were conducted with solutions containing commonly occurring competitive anions in order to compare the selectivities between the DMAM-calixarene versus DMAM-phenol functionalized cloths for chromium(VI) oxoanion removal, Scheme 1. The real-world competitive anions chosen were chloride (due to its ubiquitous presence in water), phosphate, sulfate,

and nitrate (the last three because of their structural similarity to chromate CrO_4^{2-}). In order to allow a direct comparison to be made against earlier reported studies[256], solutions were prepared with similar molar chromium(VI) oxoanion to competitive anion ratios as those employed previously (1:10 and 1:100), Figure 25. The presence of chloride, phosphate, or sulfate ions did not have any significant impact on the chromium(VI) oxoanion removal efficiency for the DMAM-calixarene and DMAM-phenol functionalized cloths. However, the chromium(VI) pollutant removal efficiency in the presence of nitrate anions was reduced significantly more for the case of DMAM-phenol compared to DMAM-calixarene functionalised cloths. The Cr(VI) oxoanion pollutant capture efficiency of DMAM-calixarene cloth remains high (88% ± 5%) at Cr(VI):Nitrate ratio of 1:10 (containing about 24 mg L^{-1} nitrate—which is similar to 18−20 mg L^{-1} nitrate concentration commonly found in real world scenarios [273]). Hence, the multidentate calixarene macrocycle is key for Cr(VI) oxoanion capture in the presence of other water-borne anions.

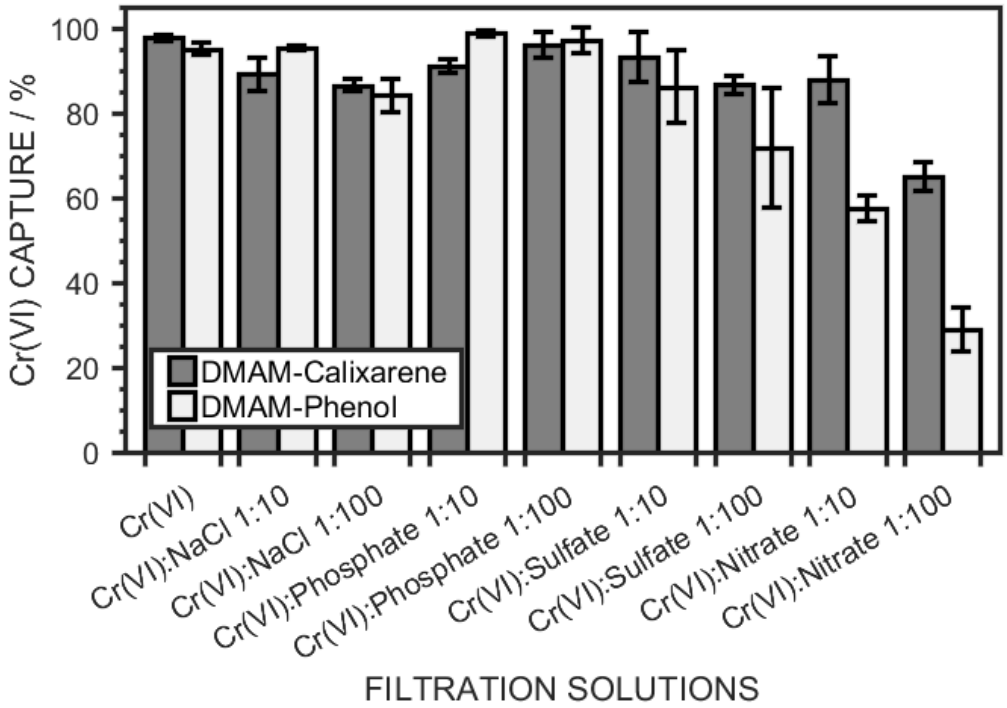

Figure 25: Flow-through Cr(VI) oxoanion capture efficiencies for pulsed plasma poly(vinylbenzyl chloride) coated non-woven polypropylene cloth functionalized with DMAM-calixarene or DMAM-phenol. 10 mL solutions were used, each containing 2 mg L^{-1} Cr(VI) and either a 1:10 or 1:100 molar ratio of competitive anions, as indicated (compounds used are sodium chloride, monosodium phosphate, sodium sulfate, and sodium nitrate).

4.2.5 Model Real-World Contaminated Wastewater

To further model chromium(VI) oxoanion removal for real-world applications, a water sample was collected from a vegetated rainwater pond. The slightly opaque and greenish pond water was filtered through a 0.45 µm membrane filter to remove particulate matter. Chemical analysis conducted by ALS Environmental Ltd. gave the anion concentrations listed in Table 7.

Table 7: Anion concentrations in pond water samples analysed by ALS Environmental Ltd. The company is UKAS / ISO17025 accredited for all listed analyses.

Analyte	Concentration / mg L^{-1}	Technique
Chloride as Cl	4.0 ± 0.1	Spectrophotometry
Phosphate as P	<0.120	ICP-OES
Sulfate as SO_4^{2-}	<4.4	Spectrophotometry
Nitrate as N	<0.7	Spectrophotometry

The pond water was subsequently spiked with potassium dichromate to give a Cr(VI) concentration of 2 mg L^{-1}, Figure 26. Compared to the earlier filtration experiments performed with ultra-high purity (UHP) water, both DMAM-calixarene and DMAM-phenol functionalized cloths captured slightly less Cr(VI) oxoanions from the spiked pond water. However, both functionalised cloth types still managed to remove more than 80% of the chromium(VI) oxoanions from pond water—highlighting the selectivity of the tertiary amine groups in real-world scenarios. The much lower measured real-world nitrate concentration (< 0.7 mg L^{-1} N) compared to the earlier modelling studies (Section 4.2.4) means that the DMAM-phenol functionalised cloths also display good Cr(VI) oxoanion capture efficiency, Figure 25 and Figure 26.

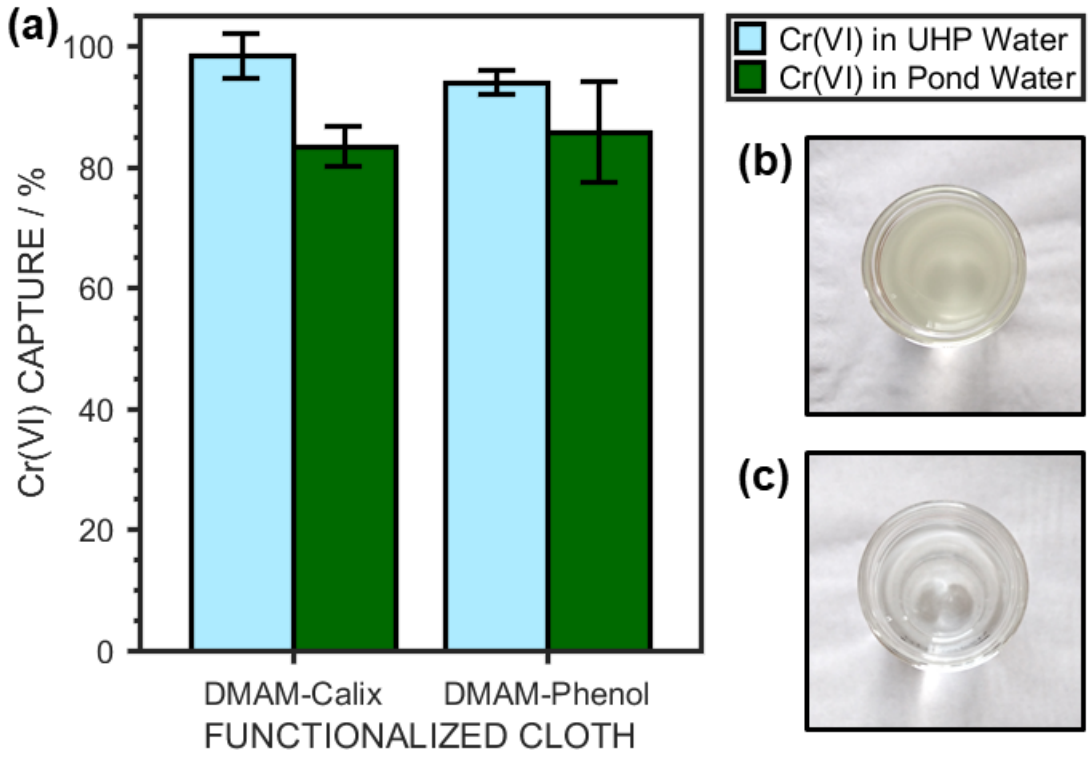

Figure 26: DMAM-calixarene and DMAM-phenol functionalized cloths flow-through filtration of 2 mg L^{-1} Cr(VI) solution. Cr(VI) oxoanion solutions were prepared using either ultra-high purity (UHP) water or filtered pond water: (a) filtration efficiency; (b) untreated pond water appearing slightly coloured and opaque; and (c) after filtration of particulate matter through 0.45 µm membrane filter showing clarity (prior to spiking with Cr(VI) oxoanion solution).

4.2.6 Real-World Polluted Industrial Wastewater

Chromium pollutant containing drainage wastewater from an industrial zone in India was collected. After removal of sludge by filtration through 0.45 µm membrane filters, the water was passed through DMAM-calixarene functionalized cloth and analysed for total chromium content via inductively coupled plasma optical emission spectroscopy. Compared to Cr(VI) solutions prepared in the laboratory, the real-world wastewater samples had a fairly low chromium concentration, Figure 27. The chromium concentration for location A was, however, well above the WHO recommended limit of 50 µg L^{-1} and the concentration for location B was higher than the forthcoming EU limit of 25 µg L^{-1} (provisionally approved by the European Commission[225]). This indicates that water from both sources can be harmful for the population living nearby if they are exposed to it for a long time. Following passage through the DMAM-

calixarene cloth, the chromium concentration in both elutes was lower than 20 µg L^{-1}, confirming that sufficient chromium was successfully removed to make the water safe for human consumption (in compliance with EU regulations).

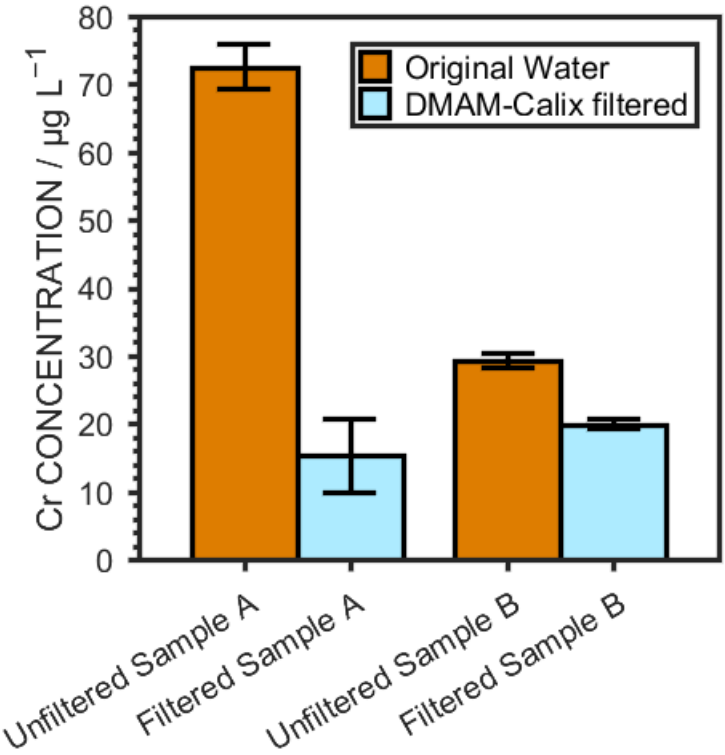

Figure 27: Chromium concentration of real water samples from industrial zone locations A and B in India before and after filtration through DMAM-calixarene cloth. 10 mL of wastewater was used for each filtration.

4.2.7 Cloth Recycling

Cloth regeneration using different permutations of aqueous solutions ($NaCl_{(aq)}$, a weak base ($NaHCO_{3(aq)}$), and a strong base ($NaOH_{(aq)}$)) showed that combined salt and base mixtures are the most efficient, Figure 28. Almost 80% Cr(VI) oxoanion release from DMAM-calixarene cloths could be achieved for an aqueous regeneration solution comprising a mixture of 2 M NaCl and 0.5 M NaOH.

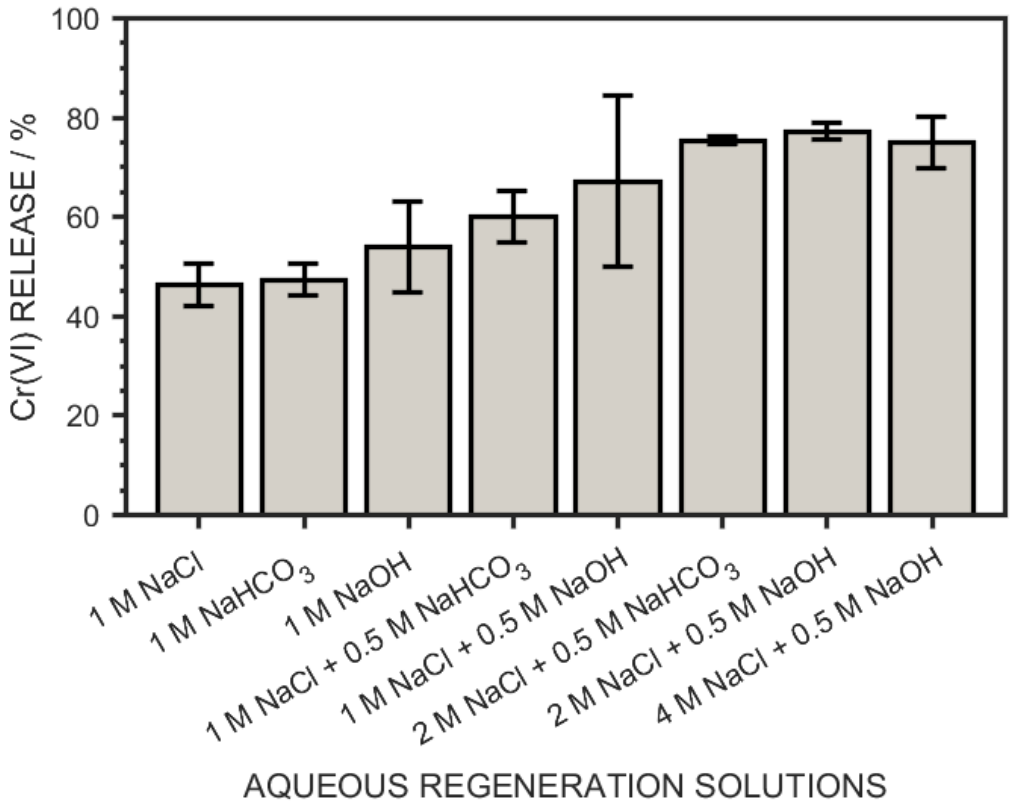

Figure 28: Cr(VI) release into solution (filtrate) from Cr(VI) oxoanion-loaded DMAM-calixarene cloth using different aqueous regeneration solutions. The cloths were pre-loaded using 10 mL of a 6 mg L^{-1} Cr(VI) solution followed by rinsing with 5 mL of ultra-high purity water (to give an average cloth loading of 1.8 $mg_{Cr(VI)}$ g_{Cloth}^{-1}).

To demonstrate the scope for repeat usage (recycling) of DMAM-calixarene cloth, the 2 M NaCl and 0.5 M NaOH mixture regeneration solution was used following consecutive Cr(VI) oxoanion capture cycles, Figure 29. Multiple recycling of the functionalized cloth did not lead to any deterioration in Cr(VI) oxoanion capture capacity. In fact, the recycled cloth showed a slightly improved hexavalent chromium oxoanion uptake during the second and third cycles compared to the first cycle.

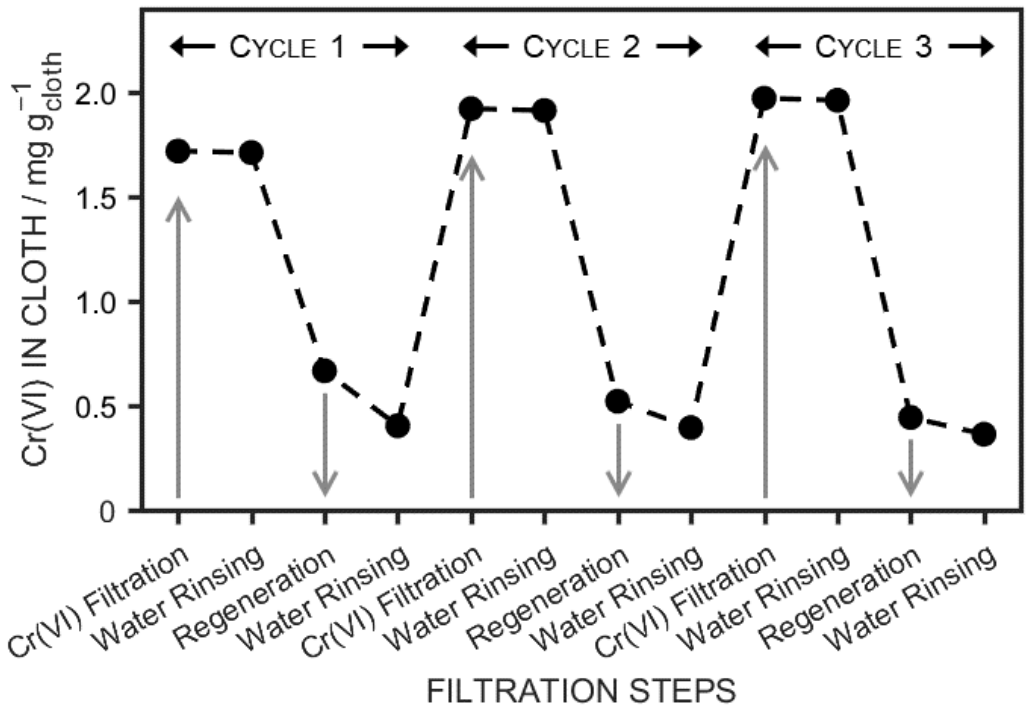

Figure 29: Recycling of DMAM-calixarene functionalized cloth for Cr(VI) oxoanion capture by alternate passage of 10 mL of 6 mg L^{-1} Cr(VI) solution and 5 mL of 0.5 M NaOH + 2 M NaCl regeneration solution through the cloth, interjected with 5 mL water rinsing steps.

4.3 Discussion

In real world scenarios, point-of-use filtration is a straightforward water purification technique. Cloths functionalized with DMAM-calixarene have been shown to effectively capture chromium(VI) oxoanion species from polluted water. Previously reported chromium pollutant capture studies using amine functionalized materials were predominantly performed at extremely low pH values—conditions that are unrealistic in terms of real-world water purification applications as well as being unfit for human consumption.[247,256] Effectively, such low pH values promote the capture of Cr(VI) oxoanions through protonated (positively charged) amine groups.[274,275,276] Literature pKa values for tertiary amine groups indicate that they remain charged even at neutral pH (conditions employed in the present investigation) because the amine group acts as a Lewis base and its nitrogen atom electron lone pair is protonated leading to a net positive charge.[277,278] The efficient capture of chromium(VI) oxoanions by both

DMAM-calixarene and DMAM-phenol functionalized cloths indicates that there is sufficient positive charge on the amine groups to facilitate the removal of pollutant Cr(VI) oxoanions by filtration without requiring any alteration to the water pH (through usage of chemical additives), Figure 23. In the literature, chromate and dichromate anions are thought to bind to positively charged amine groups of calixarenes through electrostatic interactions. The functional groups on the upper rim of the cup-shaped molecules are typically drawn to coordinate to the ions in the fashion of a multidentate ligand, holding them slightly above the cup itself.[279,280,281]

At the employed neutral pH, a very high capture efficiency is attained with up to 100% chromium removal. For a Cr(VI) concentration of 200 μg L^{-1} (a value comparable to real-world chromium pollution levels[254,271,272]), the DMAM-calixarene cloth removes all of the chromium from solution (UV−Vis instrument detection limit for quantification is about 20 μg L^{-1}), thus rendering the water safe to drink (European Union limit for chromium in drinking water is 50 μg L^{-1}, to be lowered to 25 μg L^{-1} soon[224,225,226]).

To determine overall capture capacities of the DMAM-calixarene functionalized cloth, static immersion of DMAM-calixarene functionalized pieces of cloth into 13 mL of much higher concentration Cr(VI) solutions (20 mg L^{-1}) for 4 h gave rise to 70% ± 4% removal of chromium(VI) oxoanion species (6.6 ± 0.4 $mg_{Cr(VI)}$ g_{Cloth}^{-1}). For most conservative estimation purposes, if one assumes that all of the DMAM-calixarene molecules present in solution during cloth functionalisation become tethered to the pulsed plasma poly(vinylbenzyl chloride) coating, then the experimentally measured maximum Cr(VI) uptake value correlates to each calixarene molecule capturing 1.3 ± 0.1 chromium atoms belonging to Cr(VI) oxoanions (see calculation in 4.2.2). Given that there exists a concentration- and pH-dependent equilibrium between $Cr_2O_7^{2-}$, $HCrO_4^-$, and CrO_4^{2-} oxoanion species in solution, it is feasible to envisage the surface tethered calixarene macrocycles capturing a combination of chromate and dichromate anions—thus accounting for the estimated chromium to calixarene ratio exceeding 1:1. On this premise, the use of higher surface area support cloths and larger densities of tethered calixarene could provide even greater Cr(VI) oxoanion removal capacities.

Whilst a variety of molecules containing amine groups are capable of capturing Cr(VI) oxoanions, the comparison between DMAM-calixarene and DMAM-phenol functionalized cloths illustrates that the macrocycle cavity shape of calixarenes underpins the higher chromium(VI) oxoanion capture selectivity in the presence of other water pollutants (particularly high concentrations of nitrate), Figure 25. In the European Union, the legal limit for nitrate in drinking water is 50 mg L^{-1}.[224] Groundwaters in the European Union contained an average of about 18−20 mg L^{-1} of nitrate in the years 1992–2012.[273] The Cr(VI) : Nitrate 1:10 solution used in the present study corresponds to a nitrate concentration of about 24 mg L^{-1}. At these nitrate concentrations, DMAM-calixarene functionalized cloth readily captures 88% of Cr(VI) from solution in a single filtration pass (whereas the chromium capture efficiency for DMAM-phenol cloth is much lower at about 57%). This greater capture efficiency of DMAM-calixarene compared to DMAM-phenol can be explained by the concerted orientation of coordinating tertiary amine groups associated with each calixarene cup. The calixarene cavity shape enhances the chelating effect between the tertiary amine groups and the Cr(VI) oxoanions.[282] Experiments with spiked pond water and polluted industrial wastewater samples from India have shown that DMAM-calixarene cloth is capable of reducing the chromium concentration in real-world water matrices to levels safe for human consumption (meeting the forthcoming lower European Union drinking water standards < 25 µg L^{-1}).[224]

Recyclability for multiple usage is a crucial factor for real-world applications. DMAM-calixarene cloths can be used multiple times by rinsing with an aqueous solution containing salt (NaCl) and base (NaOH), Figure 29. In earlier studies, the regeneration of amine groups employed for the capture of Cr(VI) oxoanions was often performed using pure base solutions (following the logic that higher pH values eliminate the protonation of the amine groups).[283,284] In the present investigation, the regeneration efficiency has been further improved by sodium chloride addition to the base solution. As well as the base-assisted deprotonation of the surface tethered DMAM-calixarene amine groups, the chloride anions displace Cr(VI) oxoanions being held by the positively charged amine coordination sites in the aqueous phase.[285] Such a displacement is realistic given

the significantly higher concentration of chloride anions present in solution compared to chromium(VI) oxoanions.

4.4 Conclusion

5,11,17,23-Tetrakis[(dimethylamino)methyl]-25,26,27,28-tetrahydroxy-calix[4]arene (DMAM-calixarene) macrocycles can be tethered to pulsed plasma poly(vinylbenzyl chloride) functionalized non-woven polypropylene cloths. These cloths are able to remove pollutant chromium(VI) oxoanions from water with high efficiencies (up to 100% at typical real-world pollutant levels). Unlike most other Cr(VI) oxoanion filtration materials, there is complete Cr(VI) oxoanion removal from water (even at low pollutant concentrations) without the need to decrease the pH. Selectivity remains high in the presence of other commonly present anions in water, including chloride, and those that are structurally similar to chromates (phosphate, sulfate, and nitrate). Furthermore, the captured chromium(VI) oxoanion species can be easily released by rinsing the cloth with a small amount of a NaCl and NaOH mixture solution—thereby providing multiple time re-use of the DMAM-calixarene functionalized cloths. Removal of toxic chromium pollutant species from real-world industrial wastewaters to meet safe drinking water standards has been demonstrated.

4.5 References

(222) Nunez, C. Water Pollution is a Rising Global Crisis. Here's What You Need to Know. National Geographic 2010. https://www.nationalgeographic.com/environment/freshwater/pollution/ (accessed Dec 3, 2018).

(223) United Nations International Decade for Action 'Water for Life' Website. http://www.un.org/waterforlifedecade/quality.shtml (accessed Dec 3, 2018).

(224) Council Directive 98/83/EC. *Official Journal of the European Commission* **1998** http://ec.europa.eu/environment/water/water-drink/legislation_en.html (accessed Mar 12, 2018).

(225) European Commission. *Proposal for a Directive of the European Parliament and of the Council on the Quality of Water Intended for Human Consumption*. COM(2017) 753 final. Brussels, 2018. http://ec.europa.eu/environment/water/water-drink/review_en.html (accessed Mar 12, 2018).

(226) European Commission Press Release. *Commission Welcomes Provisional Agreement to Improve the Quality of Drinking Water and the Access to it.* Brussels, 2019. https://ec.europa.eu/commission/presscorner/detail/en/ip_19_6830 (accessed Mar 3, 2020).

(227) Ahalya, N.; Ramachandra, T. V.; Kanamadi, R. D. Biosorption of Heavy Metals. *Res. J. Chem. Environ.* **2003**, *7* (4), 71−79.

(228) Backer, H. Water Disinfection for International and Wilderness Travelers. *Clin. Infect. Dis.* **2002**, *34*, 355−364.

(229) McGuigan, K. G.; Joyce, T. M.; Conroy, R. M. *Solar Disinfection: Use of Sunlight to Decontaminate Drinking Water in Developing Countries*. *J. Med. Microbiol.* **1999**, *48*, 785−787.

(230) Boyle, M.; Sichel, C.; Fernández-Ibánez, P.; Arias-Quiroz, G. B.; Iriarte-Puna, M.; Mercado, A.; Ubomba-Jaswa, E.; McGuigan, K. G. Bactericidal Effect of Solar Water Disinfection under Real Sunlight Conditions. *Appl. Environ. Microbiol.* **2008**, *74* (10), 2997−3001.

(231) Tata Uses Nano Technology for Water Purifier. Centre for Science and Environment. https://www.cseindia.org/tata-uses-nano-technology-for-water-purifier-852 (accessed on Mar 20, 2019).

(232) Dankovich, T. A.; Gray, D. G. Bactericidal Paper Impregnated with Silver Nanoparticles for Point-of-Use Water Treatment. *Environ. Sci. Technol.* **2011**, *45* (5), 1992−1998.

(233) Elsanousi, S.; Abdelrahman, S.; Elshiekh, I.; Elhadi, M.; Mohamadani, A.; Habour, A.; ElAmin, S. E.; Elnoury, A.; Ahmed, E. A.; Hunter, P. R. A Study of the Use and Impacts of LifeStraw in a Settlement Camp in Southern Gezira, Sudan. *J. Water Health* **2009**, *7* (3), 478−483.

(234) Frechen, F.-B.; Exler, H.; Romaker, J.; Schier, W. Long-term Behaviour of a Gravity-Driven Dead End Membrane Filtration Unit for Potable Water Supply in Cases of Disasters. *Water Sci. Technol.: Water Supply* **2011**, *11* (1), 39−44.

(235) Shannon, M.A.; Bohn, P.W.; Elimelech, M.; Georgiadis, J.G.; Marinas, B.J.; Mayes, A.M. Science and Technology for Water Purification in the Coming Decades. *Nature* **2008**, *452*, 301−310.

(236) Babel, S.; Kurniawan, T.A. Low-Cost Adsorbents for Heavy Metals Uptake from Contaminated Water: a review. *J. Hazard. Mater.* **2003**, *97* (1−3), 219−243.

(237) Demirbas, A. Heavy Metal Adsorption onto Agro-Based Waste Materials: A Review. *J. Hazard. Mater.* **2008**, *157* (2−3), 220−229.

(238) Fu, F.; Wang, Q. Removal of Heavy Metal Ions from Wastewaters: A Review. *J. Environ. Manage.* **2011**, *92* (3), 407−418.

(239) Hua, M.; Zhang, S.; Pan, B.; Zhang, W.; Lv, L.; Zhang, Q. Heavy Metal Removal from Water/Wastewater by Nanosized Metal Oxides: A review. *J. Hazard. Mater.* **2012**, 211−212, 317−331.

(240) Cruywagen, J. J.; Heyns, J. B. B.; Rohwer, E. A. New Spectrophotometric Evidence for the Existence of $HCrO_4^-$. *Polyhedron* **1998**, *17*, 1741–1746.

(241) Baruthio, F. Toxic Effects of Chromium and Its Compounds. *Biol. Trace Elem. Res*. **1992**, *32*, 145–153.

(242) Banks, S. The Erin Brockovich Effect: How Media Shapes Toxics Policy. *Environs: Envtl. L. Pol'y J*. **2003**, *26*, 219–251.

(243) Cumin, W. Remarks on the Medicinal Properties of Madar, and on the Effects of Bichromate of Potass on the Human Body. *Edinb. Med. Surg. J*. **1827**, *28*, 295–302.

(244) Bloomfield, J. J.; Blum, W. Health Hazards in Chromium Plating. *Public Health Rep.* **1928**, *43*, 2330–2351.

(245) Gmelin, C.G. Experiments on the Effects of Baryta, Strontia, Chrome, Molybdenum, Tungsten, Tellurium, Titanium, Osmium, Platinum, Iridium, Rhodium, Palladium, Nickel, Cobalt, Uranium, Cerium, Iron and Manganese, on the Animal System. *Edinb. Med. Surg. J*. **1826**, *26*, 131–139.

(246) Borneff, J.; Engelhardt, K.; Griem, W.; Kunte, H.; Reichert, J. Carcinogens in Water and Soil. XXII. Experiment with 3,4-Benzopyrene and Potassium Chromate in Mice Drink. *Arch. Hyg. Bakteriol*. **1968**, *152*, 45–53.

(247) Stout, M. D.; Herbert, R. A.; Kissling, G. E.; Collins, B. J.; Travlos, G. S.; Witt, K. L.; Melnick, R. L.; Abdo, K. M.; Malarkey, D. E.; Hooth, M. J. Hexavalent Chromium is Cancerogenic to F344/N Rats and B6C3F1 Mice after Chronic Oral Exposure. *Environ. Health Perspect*. **2009**, *117*, 716–722.

(248) Costa, M. Potential Hazards of Hexavalent Chromate in our Drinking Water. *Toxicol. Appl. Pharmacol*. **2003**, *188*, 1–5.

(249) Connett, P.H.; Wetterhahn, K.E. In Vitro Reaction of the Carcinogen Chromate with Cellular Thiols and Carboxylic Acids. *J. Am. Chem. Soc*. **1985**, *107*, 4282–4288.

(250) Kortenkamp, A.; O'Brien, P. The Generation of DNA Single-Strand Breaks During the Reduction of Chromate by Ascorbic Acid and/or Glutathione *In Vitro*. *Environ. Health Perspect*. **1994**, *102*, 237–241.

(251) Zhitkovich, A.; Voitkun, V.; Costa, M. Formation of the Amino Acid-DNA Complexes by Hexavalent and Trivalent Chromium *In Vitro*: Importance of Trivalent Chromium and the Phosphate Group. *Biochemistry* **1996**, *35*, 7275–7282.

(252) Costa, M. Toxicity and Carcinogenicity of Cr(VI) in Animal Models and Humans. *Crit. Rev. Toxicol*. **1997**, *27*, 431–442.

(253) Linos, A.; Petralias, A.; Christophi, C. A.; Christoforidou, E.; Kouroutou, P.; Stoltidis, M.; Veloudaki, A.; Tzala, E.; Makris, K. C.; Karagas, M. R. Oral Ingestion of Hexavalent Chromium Through Drinking Water and Cancer Mortality in an Industrial Area of Greece – An Ecological Study. *Environ. Health* **2011**, 10, 50.

(254) Naz, A.; Mishra, B.K.; Gupta, S.K. Human Health Risk Assessment of Chromium in Drinking Water: A Case Study of Sukinda Chromite Mine, Odisha, India. *Exposure Health* **2016**, *8*, 253–264.

(255) Tseng, C.-H.; Lei, C.; Chen, Y.-C. Evaluating the Health Costs of Oral Hexavalent Chromium Exposure from Water Pollution: A Case Study in Taiwan. *J. Cleaner Prod*. **2018**, *172*, 819–826.

(256) Memon, S.; Tabakci, M.; Roundhill, D. M.; Yilmaz, M. Synthesis and Evaluation of the Cr(VI) Extraction Ability of Amino/Nitrile Calix[4]arenes Immobilized onto a Polymeric Backbone. *Reactive & Functional Polymers* **2006**, *66*, 1342−1349.

(257) Schofield, W. C. E.; Badyal, J. P. S. Controlled Fragrant Molecule Release from Surface-Tethered Cyclodextrin Host-Guest Inclusion Complexes. *ACS Appl. Mater. Interfaces* **2011**, *3*, 2051−2056.

(258) Kirk, T. K.; Ibach, R.; Mozuch, M. D.; Conner, A.H.; Highley, L. Characteristics of Cotton Cellulose Depolymerized by a Brown-Rot Fungus, by Acid, or by Chemical Oxidants. *Holzforschung* **1991**, *45*, 239−244.

(259) Morsch, S.; Wood, T. J.; Schofield, W. C. E.; Badyal, J. P. S.; A Combined Plasmachemical and Emulsion Templating Approach for Actuated Macroporous Scaffolds. *Adv. Func. Mater.* **2012**, *22*, 313−322.

(260) Technical Note: FT-IR Spectroscopy ATR accessories. Perkin Elmer 2004. https://shop.perkinelmer.com/Content/technicalinfo/tch_atraccessories.pdf (accessed on Mar 31, 2019).

(261) Rjeb, A.; Tajounte, L.; Chafik El Idrissi, M.; Letarte, S.; Adnot, A.; Roy, D.; Claire, Y.; Périchaud, A.; Kaloustian, J. IR Spectroscopy Study of Polypropylene Natural Aging. *J. Appl. Polym. Sci.* **2000**, *77*, 1742−1748.

(262) D. Lin-Vien, N.B. Colthup, W.G. Fateley, J.G. Grasselli, The Handbook of Infrared and Raman Characteristic Frequencies of Organic Molecules, Academic Press, Inc., San Diego, 1991.

(263) Schofield, W. C. E.; Bain, C. D.; Badyal, J. P. S. Cyclodextrin-Functionalized Hierarchical Porous Architectures for High-Throughput Capture and Release of Organic Pollutants from Wastewater. *Chem. Mat.* **2012**, *24*, 1645−1653.

(264) Wilson, M.; Kore, R.; Ritchie, A. W.; Fraser, R. C.; Beaumont, S. K.; Srivastava, R.; Badyal, J. P. S. Palladium-Poly(Ionic Liquid) Membranes for Permselective Sonochemical Flow Catalysis. *Colloids Surf., A* **2018**, *545*, 78−85.

(265) Brown, P. S.; Wood, T. J.; Badyal, J. P. S. Combining Plasmachemical Emulsion-Templating with ATRP to Create Macroporous Lipophilic Surfaces. *J. Colloid Interface Sci.* **2014**, *421*, 44−48.

(266) Sharma, A. K.; Yasuda, H. Polymerization of Methane. *J. Appl. Polym. Sci.* **1989**, *38*, 741−754.

(267) Ryan, M. E.; Fonseca, J. L. C.; Tasker, S.; Badyal, J. P. S. Plasma Polymerization of Sputtered Poly(tetrafluoroethylene). *J. Phys. Chem.* **1995**, *99*, 7060−7064.

(268) Teare, D. O. H.; Schofield, W. C. E.; Garrod, R. P.; Badyal, J. P. S. Rapid Polymer Brush Growth by TEMPO-Mediated Controlled Free-Radical Polymerization from Swollen Plasma Deposited Poly(maleic anhydride) Initiator Surfaces. *Langmuir* **2005**, *21*, 10818−10824.

(269) Thomas, H. R.; O'Malley, J. J. Surface Studies on Multicomponent Polymer Systems by X-ray Photoelectron Spectroscopy. Polystyrene/Poly(Ethylene Oxide) Diblock Copolymers. *Macromolecules* **1979**, *12*, 323–329.

(270) Briggs, D. Surface Analysis of Polymers by XPS and Static SIMS; Cambridge University Press: Cambridge, 1998; pp 34–39.

(271) Kazakis, N.; Kantiranis, N.; Kalaitzidou, K.; Kaprara, E.; Mitrakas, M.; Frei, R.; Vargemezis, G.; Tsourlos, P.; Zouboulis, A.; Filippidis, A. Origin of Hexavalent Chromium in Groundwater: The Example of Sarigkiol Basin, Northern Greece. *Sci. Total Environ.* **2017**, *593−594*, 552−566.

(272) Tiwari, A. K.; De Maio, M. Assessment of Risk to Human Health due to Intake of Chromium in the Groundwater of the Aosta Valley Region, Italy. *Hum. Ecol. Risk Assess.* **2017**, *23* (5), 1153−1163.

(273) Nitrate in Groundwater in Europe; European Environment Agency, 2019. https://www.eea.europa.eu/data-and-maps/daviz/groundwater-nitrate-3 (accessed Mar 09, 2020).

(274) Unnithan, M. R.; Vinod, V. P.; Anirudhan, T. S. Synthesis, Characterization, and Application as a Chromium(VI) Adsorbent of Amine-Modified Polyacrylamide-Grafted Coconut Coir Pith. *Ind. Eng. Chem. Res.* **2004**, *43*, 2247−2255.

(275) Anirudhan, T. S.; Jalajamony, S.; Suchithra, P. S. Improved Performance of a Cellulose-Based Anion Exchanger with Tertiary Amine Functionality for the Adsorption of Chromium(VI) from Aqueous Solutions. *Colloids Surf., A* **2009**, *335*, 107−113.

(276) Xu, X.; Bao, B.-Y.; Tan, X.; Yue, Q.-Y.; Zhong, Q.-Q.; Li, Q. Characteristics of Amine-Crosslinked Wheat Straw and its Adsorption Mechanisms for Phosphate and Chromium(VI) Removal from Aqueous Solution. *Carbohydr. Polym.* **2011**, *84*, 1054−1060.

(277) Rayer, A. V.; Sumon, K. Z.; Jaffari, L.; Henni, A. Dissociation Constants (pKa) of Tertiary and Cyclic Amines: Structural and Temperature Dependences. *J. Chem. Eng. Data* **2014**, *59*, 3805−3813.

(278) Muller, P. Glossary of Terms Used in Physical Organic Chemistry (IUPAC Recommendations 1994). *Pure & Appl. Chem.* **1994**, 66, p 1135.

(279) Bayrakci, M.; Ertul, S.; Yilmaz, M. Synthesis of Di-substituted Calix[4]arene-based Receptors for Extraction of Chromate and Arsenate Anions. *Tetrahedron* **2009**, *65*, 7963–7968.

(280) Akoz, E.; Erdemir, S.; Yilmaz, M. Immobilization of Novel the Semicarbazone Derivatives of Calix[4]arene onto Magnetite Nanoparticles for Removal of Cr(VI) Ion. *J. Incl. Phenom. Macrocycl. Chem.* **2012**, *73*, 449–458.

(281) Tabakci, M.; Tabakci, B.; Beduk, A.D. Synthesis and Application of an Efficient Calix[4]arene-based Anion Receptor Bearing Imidazole Groups for Cr(VI) Anionic Species. *Tetrahedron* **2012**, *68*, 4182–4186.

(282) Gutsche, C. D.; Nam, K. C. Calixarenes. 22. Synthesis, Properties, and Metal Complexation of Aminocalixarenes. *J. Am. Chem. Soc.* **1988**, *110*, 6153−6162

(283) Georgiev, E. M.; Wolf, N.; Roundhill, D. M. Lower Rim Alkylammonium-Substituted Calix[4]arenes as “Proton-Switchable” Extractants for Chromate and Dichromate Anions. *Polyhedron* **1997**, *16*, 1581−1584.

(284) Roundhill, D. M.; Koch, H. F. Methods and Techniques for the Selective Extraction and Recovery of Oxoanions. *Chem. Soc. Rev.* **2002**, *31*, 60−67.

(285) Elwakeel, K. Z. Removal of Cr(VI) from Alkaline Aqueous Solutions using Chemically Modified Magnetic Chitosan Resins. *Desalination* **2010**, *250*, 105−112.

Chapter 5: Recyclable Ionic Liquid Functionalized Cloths for Selective Extraction of Toxic Chromium Water Pollutants

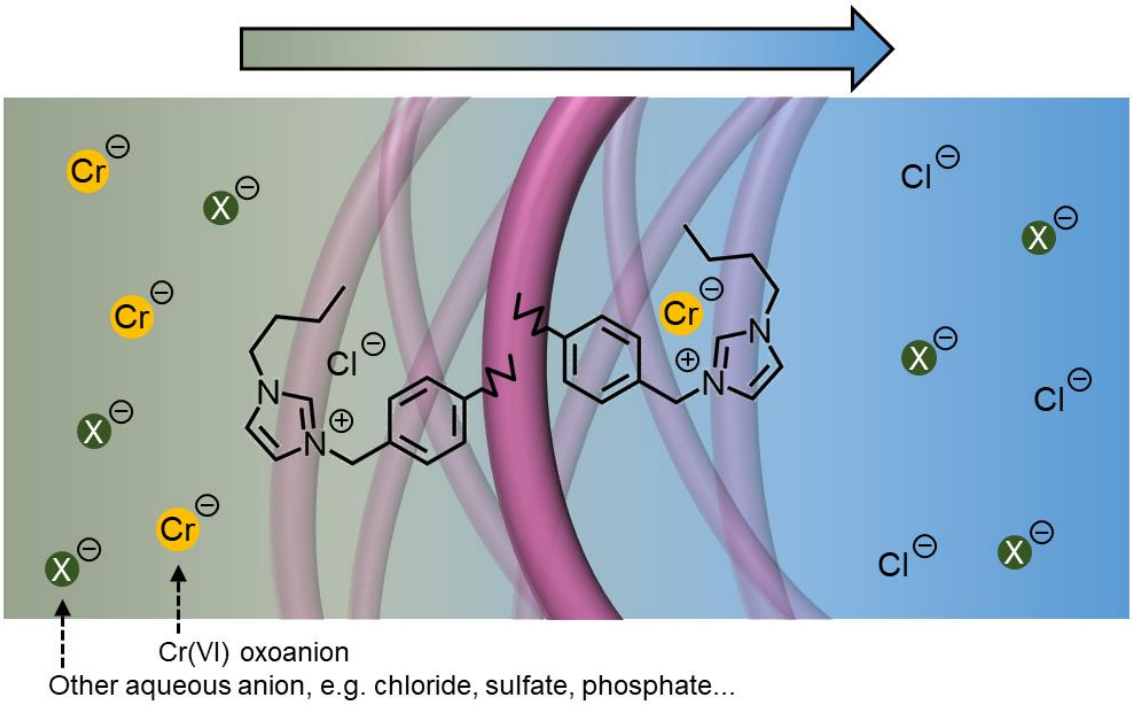

Figure 30: Graphic chapter summary: Filter functionalized with N-butylimidazole purifies polluted water by selectively capturing Cr(VI) oxoanions (orange) through ion exchange.

5.1 Introduction

While ionic liquids were invented in the early 20th century, they only became an intensely studied field of research around thirty years ago.[286] One popular class of ionic liquids are salts based on dialkylimidazolium, organic cations with particularly low reduction potentials.[287] Many applications for ionic liquids have been developed over the years, for example as solvents[288], in catalysis[289], and for extraction of various substances from solution. Ionic liquid-modified solids have become a popular tool for solid phase extraction of organic molecules and metal ions alike. These modified materials are most frequently silica or polymers, with the latter typically being lower in price and possessing a higher coverage of functional groups and better pH stability.[290]

In this work we used butylimidazole to functionalize cloth via an intermittent poly(vinylbenzyl chloride) attachment layer based on a method reported in the

literature[291], to create a capture material for Cr(VI) oxoanions. Butylimidazolium-based ionic liquids are widely reported in the literature, be it as solvent for cellulose[292,293], for CO_2 capture[294], as antibacterial agents[295], in catalysis[291], or for liquid phase extraction of various substances including organic molecules[296], sulfur[297], and heavy metal ions[298]. In fact, the reaction of an alkylimidazole with poly(vinylbenzyl chloride) to form a surface tethered ionic liquid goes back to the very first supported ionic liquid.[299]

Hexavalent chromium oxoanions (chromate (CrO_4^{2-}), hydrogenchromate ($HCrO_4^-$), and dichromate ($Cr_2O_7^{2-}$)) are a class of water pollutants whose ingestion can lead to cancer and death even at low concentration when ingested over an extended period of time.[300,301,302] The maximum concentration of chromium in water is therefore strictly regulated (e.g. European Union legal limit was recently reduced from 50 µg L^{-1} to 25 µg L^{-1}).[303,304,305,306] However, industrial pollution can result in waters containing increased Cr(VI) concentrations, up to 100−260 µg L^{-1}.[307,308,309] Various imidazolium based ionic liquids have been used to capture hexavalent chromium over the years. Table 8 presents an overview of their employed experimental conditions. Notably, the used Cr(VI) concentrations are mostly either extremely low (in studies aimed at concentrating trace amounts of Cr(VI) for analysis) or extremely high and far beyond real Cr(VI) pollution levels reported in the literature. Furthermore, while the selectivity of the capture material in the presence of competing anions was studied in some cases, none used real polluted water.

Table 8: Supported ionic liquids used to capture Cr(VI) found in the literature.

Ionic Liquid	**Support**	**Cr(VI) Conc. Range**	**Cr(VI) Uptake**	**Refer-ence**
Methyl-imidazolium chloride	PVC particles	0.5−5 µg L^{-1} (capture experiments); 10−300 mg L^{-1} (capacity determination)	23.2 mg g^{-1} (maximum retention capacity)	310

3-Ethyl-1-vinyl-imidazolium with bis(trifluoro-methane-sulfonyl) imide counterion	Polymerized vinyl groups	30 mg L^{-1} (capture experiment); 5−30 mg L^{-1} (capacity determination)	17.9 mg g^{-1} (maximum adsorption capacity)	311
Imidazolium chloride	Silica	100 mg L^{-1} (capture experiments)	41.8 mg g^{-1} (adsorption capacity)	312
1-Allyl-3-methyl-imidazolium chloride	Hydrogel formed by copolymerisation of allyl group with three other monomers	100 mg L^{-1} (capture experiments); 20−120 mg L^{-1} (capacity determination)	74.5 mg g^{-1} (maximum adsorption capacity at 50°C)	313
1-butyl-3-methyl-imidazolium tetracloro-aluminate	Metal organic framework impregnated with the ionic liquid	100 mg L^{-1} (capture experiments); 20-200 mg L^{-1} (capacity determination)	285.7 mg g^{-1} (maximum sorption capacity)	314
1,3-substituted imidazolium bromide	Hypercrosslinked poly ionic liquid made from imidazolium containing monomers	50−500 mg L^{-1} (capture experiments & capacity determination)	236.8 mg g^{-1} (maximum sorption capacity)	315
N,N’-methylene-bis(1-(3-vinyl-imidazolium)) chloride	Polymerized dicationic monomer	50 mg L^{-1} (capture experiments); 50−450 mg L^{-1} (capacity determination)	328.2 mg g^{-1} (maximum sorption capacity)	316

Another similarity among the Cr(VI) capture materials listed in Table 8 is that they are all powders. While powders have a large surface area, they can be challenging to handle, particularly for a layperson. When a batch adsorption method is employed by stirring a suspension of the capture material in a chromium(VI) oxoanion solution, a subsequent centrifugation[311,313,314] or filtration[315,316] step is typically required to separate the powder from the purified water. Alternatively, when used in a flow-through setup, another layer (e.g. glass wool[310] or silica sand[316]) needs to be placed underneath the capture material to hold it back.

In this work, non-woven polypropylene cloth was functionalized with poly(vinylbenzyl chloride) as attachment layer via pulsed plasma deposition and subsequently with butylimidazole to create a supported ionic liquid with butylimidazolium chloride functional groups, Scheme 2.[291] The material was used to remove Cr(VI) from solutions prepared in the laboratory and from real polluted water. The advantage of non-woven cloth over capture material in powder form is its ease of use. As the functional groups that capture Cr(VI) are covalently bound to the cloth, no centrifugation or additional filtration is required to remove the Cr(VI) loaded capture material from the purified water. At the same time, the used non-woven polypropylene cloth is flexible enough to be easily inserted into cartridges of any size and geometry without leaving any gaps through which the water flow could circumvent the filtration media. It is shown that the butylimidazolium functionalized cloth efficiently removes hexavalent chromium oxoanions from water while demonstrating high selectivity in the presence of competitive anions and even in real industrial wastewater. Finally, successful regeneration of the cloth is demonstrated, allowing it to be recycled for multiple use.

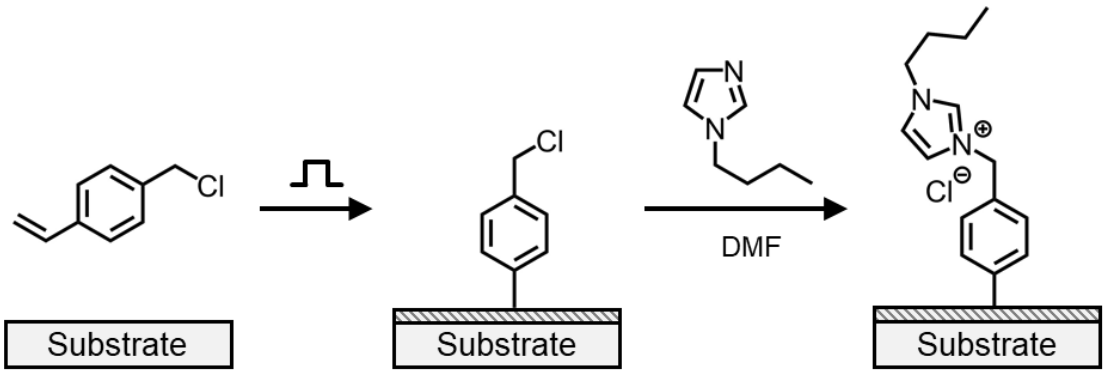

Scheme 2: Pulsed plasma poly(vinylbenzyl chloride) deposition onto a cloth substrate and subsequent functionalisation with butylimidazole, leading to the formation of butylimidazolium chloride tethered to the polymer. This method to tether butylimidazole to a surface was first reported in reference 291.

5.2 Results

5.2.1 Butylimidazolium-Functionalized Cloths

Cloth Preparation

The measured deposition rate for pulsed plasma poly(vinylbenzyl chloride) films coated onto silicon wafers was 48.5 ± 4.9 nm min^{-1}. All non-woven cloth filters were uniformly coated.[317]

Functionalized and unfunctionalized cloths were characterized via ATR-infrared spectroscopy. As the plasma deposited coatings are very thin, features from the underlying non-woven polypropylene cloth were also visible with the ATR-FTIR sampling depth (few µm), Figure 31. The infrared spectrum of the untreated non-woven polypropylene cloth shows features characteristic for polypropylene, such as broad and intense C-H stretches in the 2830−2970 cm^{-1} region and two intense bands at 1454 cm^{-1} and 1377 cm^{-1} corresponding to the methylene CH_2 and methyl CH_3 bending vibrations respectively.[318,319] Fingerprint peaks of the pulsed plasma poly(vinylbenzyl chloride) layer on the cloth include a characteristic C−Cl stretch absorbance at 709 cm^{-1} (III) and a $-CH_2Cl$ group C−H wag absorbance at 1266 cm^{-1} (II).[317,319, 320 , 321] Both features became attenuated following the subsequent functionalization with butylimidazole. However, an increased absorbance in the 1110−1170 cm^{-1} region is found, which can be attributed to spectral features of the underlying polypropylene cloth being

superimposed with an absorbance from the C-N stretch.[319] Furthermore, a broad absorbance at 3369 cm^{-1} (I) is clearly visible in the spectrum of the butylimidazolium functionalized cloth, owing to hydrogen bond interactions between small amounts of adsorbed water and the charged quaternized imidazolium groups and their Cl^- counterions.[322] No spectral features from the charged imidazolium ring itself (absorbances expected at 1350 cm^{-1} and 1180 cm^{-1}) were detected, indicating the formation of a very thin imidazolium surface layer whose contribution is small compared to the underlying polymer, within the infrared sampling depth.[291,323]

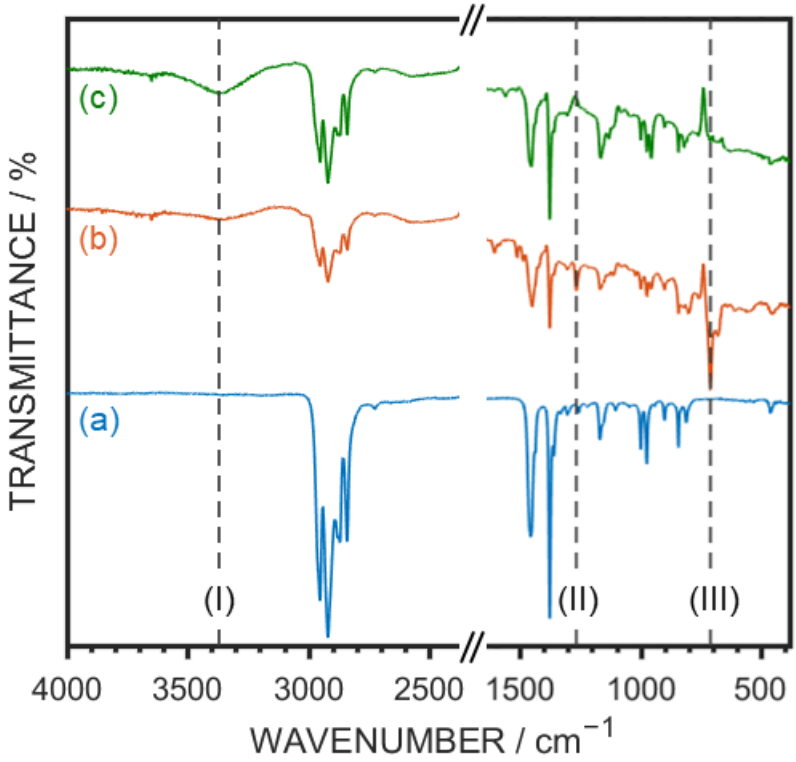

Figure 31: Infrared spectra of: (a) untreated non-woven polypropylene cloth, (b) pulsed plasma poly(vinylbenzyl chloride) coated cloth, and (c) following functionalization of (b) with butylimidazole. Dashed lines indicate characteristic vibrations: (I) hydrogen bond interactions, (II) C−H wag of the $-CH_2Cl$ group, and (III) C−Cl stretch.

Cloth Functionalization Optimization

To determine the ideal functionalization conditions to maximize the Cr(VI) oxoanion capture of butylimidazolium cloth, pulsed plasma poly(vinylbenzyl chloride) coated cloth was treated with butylimidazole solutions of varying

concentrations in varying container volumes. As initial proof of concept for the functionalization (including the infrared spectra shown in Figure 31), the procedure was derived from those previously reported in the literature: the butylimidazole to dimethyl formamide (DMF) solvent ratio (1 : 6 by volume), temperature (room temperature), and duration of the treatment (5 days) were taken from a publication detailing the attachment of butylimidazole to a pp-VBC-coated PTFE membrane.[291] As the solution volume was not specified in said publication, each 60 x 70 mm² pp-VBC-coated non-woven PP cloth was inserted into a 28 mL vial together with 27.5 mL of the functionalization solution and the vials were rotated during the treatment period, same as executed for the attachment of calixarenes to pp-VBC-coated non-woven PP cloth, see chapter 3.1.3 and Ref. [324]. While the treatment was successful, as shown from IR spectra (Figure 31) and successful Cr(VI) capture from solution, the employed conditions meant that a large butylimidazole volume was used for each cloth. To optimize the procedure, multiple 60 x 70 mm² cloth samples were prepared using a series of different conditions involving treatment volumes between 3.5–28 mL per cloth quarter and butylimidazole to DMF ratios ranging from 1 : 1000 up to 1 : 2 by volume. The Cr(VI) capture efficiencies of 30 x 35 mm² pieces of these cloths are shown in Figure 32, plotted against the volume of butylimidazole used for the preparation of each cloth quarter. Note that the coverage and surface area were not determined, though it can be assumed that a plateau in coverage is reached at high butylimidazole volumes because a plateau in Cr(VI) capture efficiency is observed.

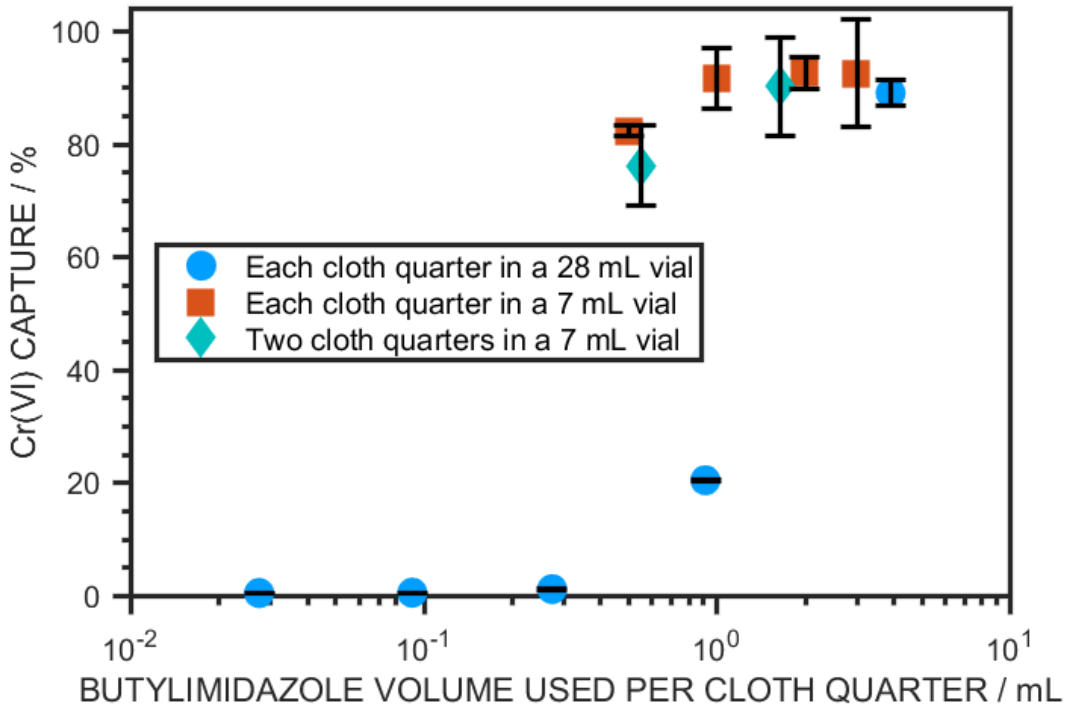

Figure 32: Optimization of butylimidazole functionalization conditions. 5 mL of 20 mg L^{-1} Cr(VI) solutions were filtered through each 30 mm x 35 mm cloth piece. The Cr(VI) capture efficiency is plotted against the volume of butylimidazole used to treat one 'cloth quarter', meaning a 60 mm x 70 mm piece.

The results show that in general at least 1 ml of butylimidazole per cloth quarter (60 mm x 70 mm) is required to yield a Cr(VI) capture efficiency above 90%. It is also apparent that the usage of 7 mL vials is beneficial for the functionalization process compared to 28 mL vials. However, placing two pieces of cloth in one vial (diamond shaped turquoise markers) added no benefit when similar volumes of butylimidazole per cloth quarter were used, while also leading to a larger deviation in cloth performance, possibly due to the mixing being less effective. From the results of this comparison, it was decided to continue functionalizing each 60 mm x 70 mm cloth quarter in a separate 7 ml vial containing 2 mL butylimidazole and 4 mL DMF. All filters used to produce the subsequently presented results were prepared under these conditions.

Film Thickness Dependency

Pulsed plasma treatment duration times ranging from 10 minutes to 30 minutes were furthermore assessed to explore whether the thickness of the deposited poly(vinylbenzyl chloride) layer influences the Cr(VI) capture efficiency after subsequent butylimidazole functionalization, Figure 33. No discernible trend was found within the samples used whose plasma polymer layers ranged in thickness from a few hundred nm to almost 2 µm. One can therefore deduce that while the butylimidazole functionalization conditions have an influence on the cloth performance, the thickness of the underlying poly(vinylbenzyl chloride) layer does not, provided that a uniform layer is present.

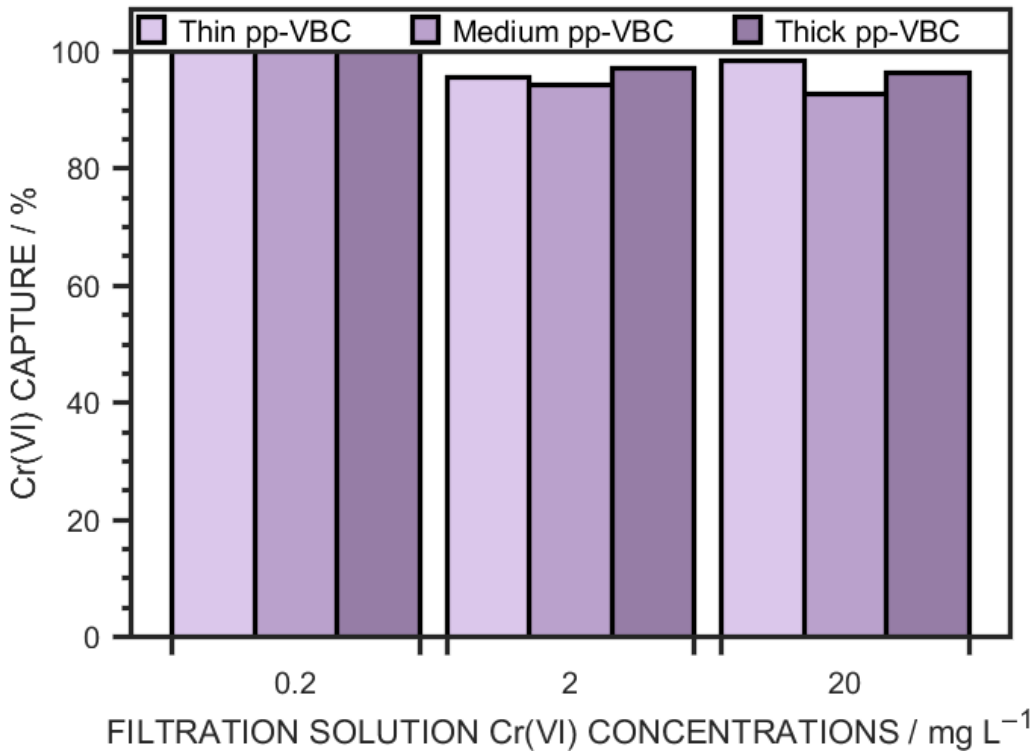

Figure 33: Cr(VI) oxoanion capture efficiency of butylimidazole-functionalized cloths with varying pulsed plasma poly-(vinylbenzyl chloride) layer thicknesses while using filtration solutions of different Cr(VI) concentrations. No correlation between polymer layer thickness and capture efficiency could be found and a high amount of Cr(VI) was captured for each concentration.

5.2.2 Cr(VI) Oxoanion Static Capture

Static immersion of butylimidazolium functionalized cloth pieces in 13 mL of 20 mg L^{-1} Cr(VI) solution (approximately 100 times greater concentration compared to typical real-world pollution levels[307,308,309]) for two hours led to a capture of 6.2 ± 0.6 $mg_{Cr(VI)}$ g_{Cloth}^{-1}. Based on this capacity, one gram of functionalized cloth would be able to clean about 31 litres of water containing the typical concentration of real-world Cr(VI) pollution (200 µg L^{-1}).

5.2.3 Cr(VI) Oxoanion Filtration Selectivity

Flow-through filtration tests were conducted with solutions containing competitive anions to study the selectivity of butylimidazolium functionalized cloths for chromium(VI) oxoanion removal. The chosen competitive anions were the ubiquitously occurring chloride and several oxoanions that are structurally similar to chromate anions, namely nitrate, sulfate, phosphate, and arsenate. While the first three oxoanions were chosen due to their prevalence in natural water sources, arsenate was included since arsenic is one of the most notable water pollutants among the World Health Organization's list of ten chemicals of major public health concern; a capture affinity of the functional cloth towards arsenic compounds (in addition to hexavalent chromium) could therefore be advantageous.[325] For the filtration experiments solutions containing 2 mg L^{-1} Cr(VI) were prepared. Chloride, nitrate, sulfate, and phosphate were added in a molar ratio of 1:100 to simulate a large excess whereas arsenate was added in a molar ratio of 1:1 and 1:10 as it is highly carcinogenic and regulated even more strictly than chromium, Figure 34. When comparing to a 2 mg L^{-1} Cr(VI) solution with no added anions, the presence of chloride and phosphate ions did not have any significant impact on the chromium(VI) oxoanion capture efficiency of the butylimidazolium cloth. On the other hand, the presence of high concentrations of nitrate and sulfate anions reduced the chromium(VI) oxoanion uptake of the butylimidazolium cloth significantly. Given that the uptake capacity of the cloth was determined as 6.2 ± 0.6 $mg_{Cr(VI)}$ g_{Cloth}^{-1}, no chromium would be captured under these conditions if the butylimidazolium cloth had a higher affinity to the 100 times higher concentrated nitrate and sulfate. Therefore, while the presence

of these anions impacts the chromium(VI) oxoanion capture of butylimidazolium cloth, it does not make the capture impossible.

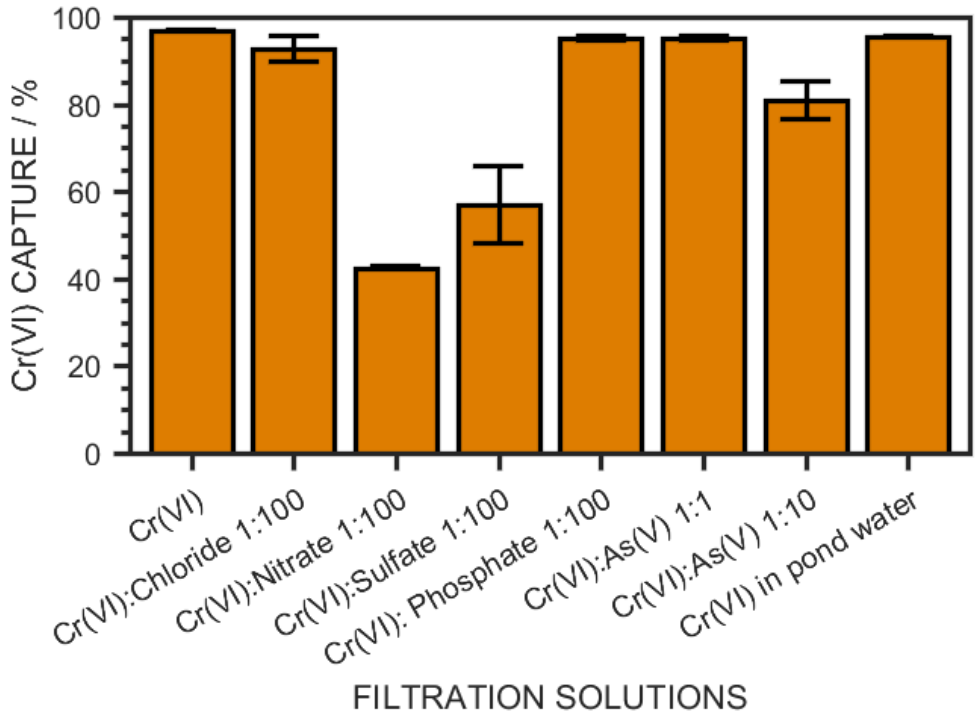

Figure 34: Flow-through Cr(VI) oxoanion capture efficiencies for pulsed plasma poly(vinylbenzyl chloride) coated non-woven polypropylene cloth functionalized with butylimidazolium. 10 mL solutions were used, each containing 2 mg L^{-1} Cr(VI) and different molar ratios of competitive anions, as indicated (compounds used are sodium chloride, sodium nitrate, sodium sulfate, monosodium phosphate, and arsenic acid). Furthermore, a filtered pond water sample was spiked with potassium dichromate to also reach a concentration of 2 mg L^{-1} Cr(VI).

The addition of arsenate in an equimolar ratio to the chromate solution showed no impact on the Cr(VI) capture of the butylimidazolium cloth, however the capture was slightly reduced when the arsenate concentration was increased by a factor of ten.

In addition to the solutions with known ion concentrations, a water sample from a vegetated rainwater pond was spiked with 2 mg L^{-1} Cr(VI) following removal of particulate matter. Filtration of this model real-world contaminated wastewater sample through butylimidazolium cloth showed that the unknown ion composition of the water did not affect the Cr(VI) capture efficiency. Chemical analysis of the pond water for anions used in the above selectivity tests gave the following concentrations: chloride = 4.0 mg L^{-1}, N (nitrate) < 0.7 mg L^{-1}, sulfate

< 4.4 mg L^{-1}, P (phosphate) < 0.120 mg L^{-1} (see Table 7, Chapter 4.2.5). In terms of molar ratios, the chloride concentration in the Cr(VI) spiked pond water was therefore three times higher than the chromate concentration, the nitrate and sulfate concentrations less than 1.3 times the chromate concentration, and the phosphate concentration less than a tenth of the chromate concentration. These results show that while a large surplus of nitrate and sulfate anions will negatively impact the chromium(VI) oxoanion capture efficiency of butylimidazolium cloth, low concentrations of these ions have no effect.

5.2.4 Real-World Polluted Industrial Wastewater

Chromium pollutant containing drainage wastewater was collected from an industrial zone in India. After removal of sludge by filtration through 0.45 µm membrane filters, the water was passed through butylimidazolium functionalized cloth and analysed for total chromium content via inductively coupled plasma optical emission spectroscopy. Compared to Cr(VI) solutions prepared in the laboratory, the real-world wastewater samples had a very low chromium concentration, Figure 35. The chromium concentration at both locations was however higher than the EU limit of 25 µg L^{-1} and the concentration at location A was even above the WHO recommended limit of 50 µg L^{-1} that has been in place for decades.[306, 326] As such, water from both sources can be harmful to the communities living nearby when consuming it over an extended period of time. Following passage through the butylimidazolium cloth, the chromium concentration in both elutes was lower than 20 µg L^{-1} (easily meeting the safe water regulations). The remaining chromium in the filtered sample B is likely to be in the form of much less toxic cationic Cr(III) species which can also be present in industrial wastewaters.

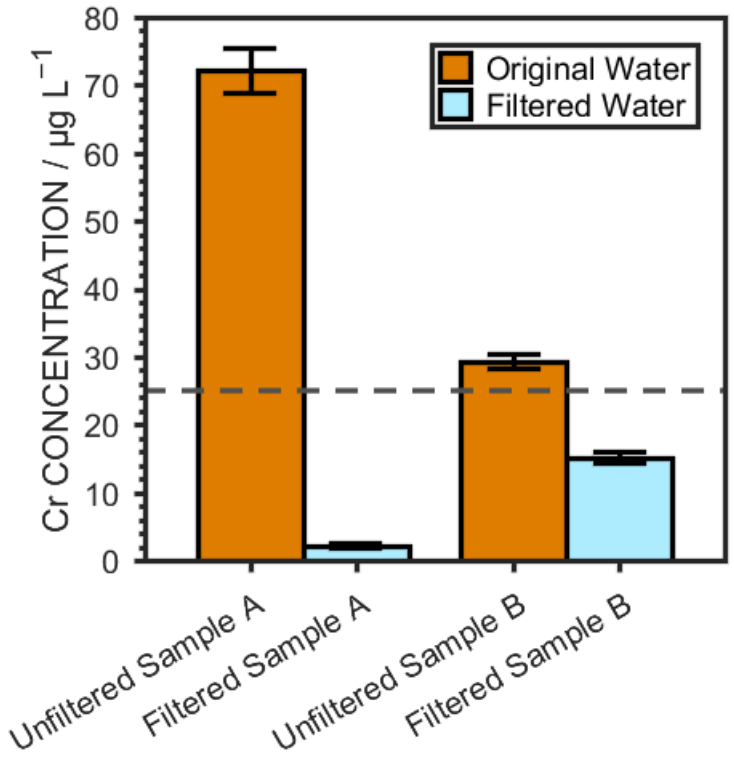

Figure 35: Chromium concentration of real water samples from industrial zone locations A and B in India before and after filtration through butylimidazolium cloth. 10 mL of wastewater was used for each filtration. Dashed line indicates the EU limit of 25 µg L^{-1}.[306]

5.2.5 Cloth Recycling

Previously it has been reported that hexavalent chromium oxoanions adsorbed to imidazolium compounds can be desorbed by rinsing with 1−2 mol L^{-1} NaCl solutions.[312] On the other hand, NaOH solutions (in conjunction with NaCl) are frequently used to regenerate chromium sorption materials.[327,328,329] For the present butylimidazolium functionalized cloth the desorption efficiency was therefore tested for a 2 M NaCl solution, a 0.5 M NaOH solution, and a solution that contains both 2 M NaCl and 0.5 M NaOH. While flushing with a 2 M NaCl solution resulted in a desorption of about 80% of the adsorbed Cr(VI), the functionalized cloth could be regenerated to an even higher degree when using NaOH. A full desorption of the adsorbed Cr(VI) was achieved with a 2 M NaCl and 0.5 M NaOH solution.

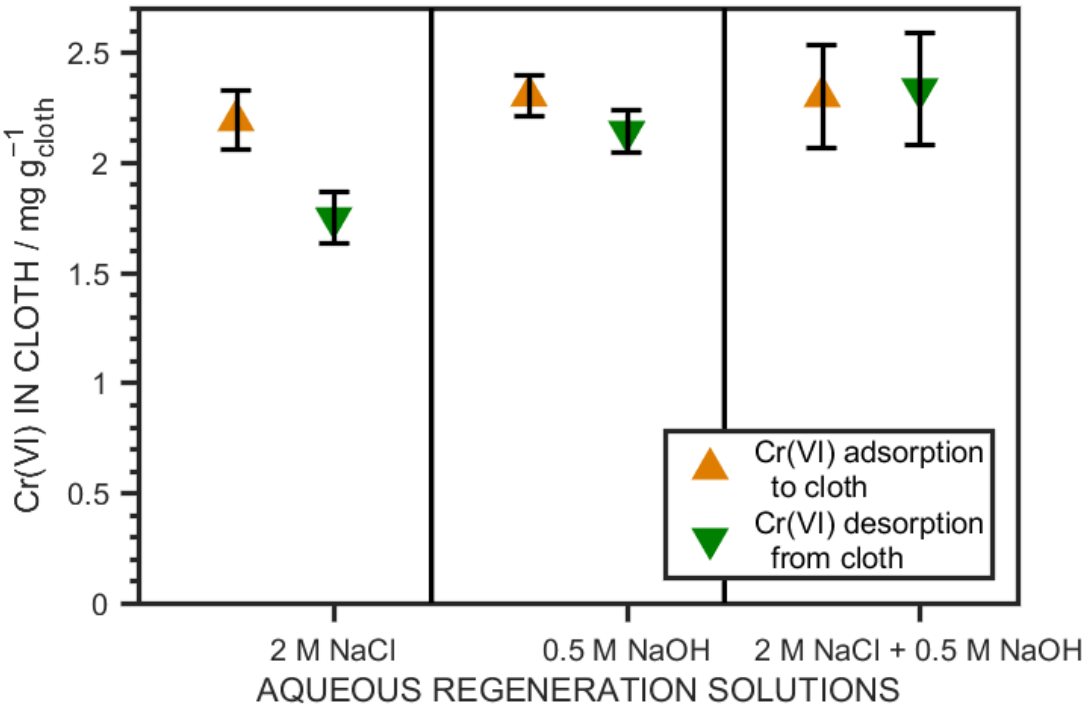

Figure 36: Cr(VI) adsorption to butylimidazolium cloth through filtration of 10 mL 6 mg L^{-1} Cr(VI) solutions and subsequent desorption using 5 mL of different aqueous regeneration solutions. Cloths were rinsed with 5 mL of ultra-high purity water after loading with Cr(VI) and before desorption.

To demonstrate the scope for repeated usage of butylimidazolium cloth, Cr(VI) adsorption and desorption was performed five times on the same piece of cloth, Figure 37. Each cycle consisted of passing five 10 mL portions of 2 mg L^{-1} Cr(VI) solution through the filter, followed by rinsing with 5 mL UHP water, desorption using 5 mL regeneration solution consisting of 2 M NaCl and 0.5 NaOH, and another 5 mL UHP water rinsing. The Cr(VI) oxoanion uptake was 3.6 mg g^{-1} in the first cycle, 3.1 mg g^{-1} in the second cycle, 3.2 mg g^{-1} in the third cycle, 3.1 mg g^{-1} in the fourth cycle, and 3.0 mg g^{-1} in the fifth cycle. While a 13% decrease in uptake capacity was registered after the first regeneration, it only changed slightly in the following cycles, showing a high potential for repeated Cr(VI) capture and release.

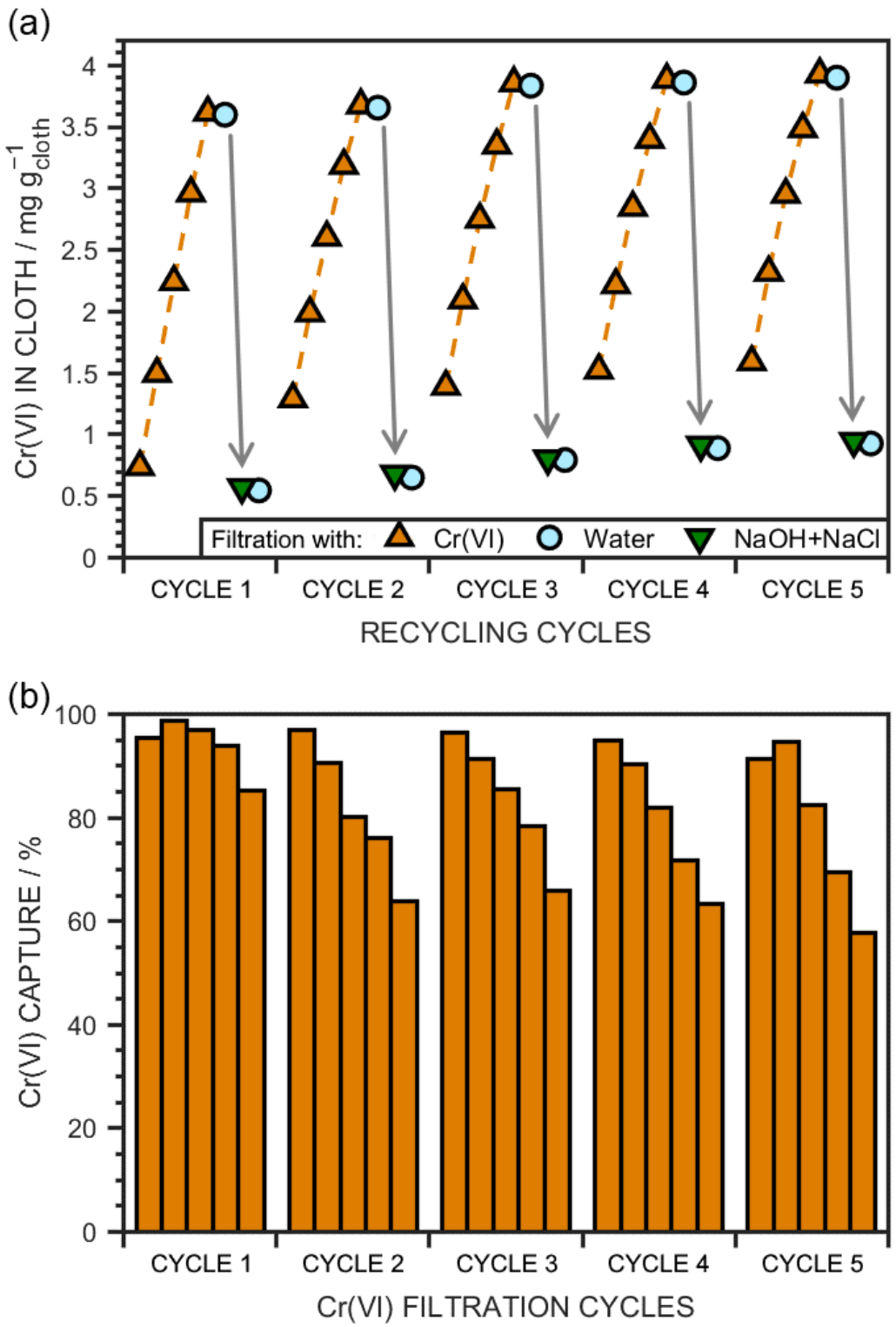

Figure 37: (a) Recycling of butylimidazolium functionalized cloth for Cr(VI) oxoanion capture by passage through the cloth of five times 10 mL of 2 mg L^{-1} Cr(VI) solution and then 5 mL of 0.5 M NaOH + 2 M NaCl regeneration solution, interjected with 5 mL water rinsing steps. (b) Cr(VI) oxoanion capture efficiencies of the butylimidazolium cloth used for recycling shown for each filtration step of 10 mL 2 mg L^{-1} Cr(VI) solution.

When examining the Cr(VI) capture for each of the 10 mL filtration steps, one can see that the capture efficiency gradually decreases throughout each cycle as the chromium(VI) oxoanions are accumulated in the functionalized cloth, Figure 37. After each regeneration, the capture efficiency returns to a high level, indicating a successful regeneration of the cloth.

5.3. Discussion

Cloths functionalized with butylimidazolium chloride have been shown to effectively capture chromium(VI) oxoanions from polluted water. The capture most likely occurs through an anion exchange mechanism whereby chloride ions that are electrostatically bound to positively charged butylimidazolium are exchanged for chromium(VI) oxoanions. The Cr(VI) uptake from a 20 mg L^{-1} solution was found to be 6.2 ± 0.6 $mg_{Cr(VI)}$ g_{Cloth}^{-1} with 61% ± 1% of the Cr(VI) in solution captured by the cloth. This uptake appears low, compared to values reported for solid phase extraction of Cr(VI) from aqueous solution by imidazolium functionalized materials which vary between 17.9−328.2 mg g^{-1}.[310−316] However, given that the used non-woven polypropylene cloth possesses an average fibre diameter of 5.0 ± 1.5 µm and the thickness of the poly(vinylbenzyl) layer is 985 ± 99 nm, the underlying cloth contributes significantly to the overall mass of the butylimidazolium functionalized material. The uptake relative to the mass of the capture material is therefore not a suitable parameter to compare a functionalized cloth to powders.

The Cr(VI) filtration selectivity of butylimidazolium cloth was initially tested by adding five different anions to 2 mg L^{-1} Cr(VI) solutions: chloride, nitrate, sulfate, phosphate, and arsenate. The first four were used in a 1:100 molar ratio to Cr(VI). While the Cr(VI) capture efficiency decreased by less than 5% in the presence of chloride and phosphate, the presence of sulfate led to a 41% decrease in Cr(VI) capture efficiency, the presence of nitrate even to a 56% decrease. In the literature, the concentrations chosen for selectivity experiments vary greatly. In reference 312 the capture of 100 mg L Cr(VI) decreased by almost 20% in the presence of a 100 times surplus of chloride. Nitrate and phosphate concentrations 42 and 27 times higher than the Cr(VI) concentration did not affect the Cr(VI) uptake efficiency, while a 27 times sulfate concentration

decreased the Cr(VI) uptake by 18.4%. Butylimidazolium cloth showed a higher selectivity in the presence of chloride compared to the imidazolium functionalized silica used in 312. The other three anions were significantly more concentrated in the present work, so a larger decrease in Cr(VI) uptake can be expected. In reference 315 the same four anions were used in concentrations up to 12 times of the Cr(VI) molar concentration in a 50 mg L^{-1} Cr(VI) solution. Their presence was found to affect the Cr(VI) uptake efficiency in the order $Cl^- < NO_3^- < H_2PO_4^- < SO_4^{2-}$, with the presence of a 12-fold concentration of sulfate decreasing the Cr(VI) capture efficiency by 18.9%. In conclusion, the interference of sulfate with the Cr(VI) capture of butylimidazolium cloth is expected from reports in the literature while the strong interference of nitrate is somewhat surprising. Nevertheless, in all cases the functional cloth was still able to capture more than 40% of Cr(VI) from the 2 mg L^{-1} solution, even in the presence of a 100 times excess of competitive anions. Even a 10 times excess concentration of arsenate, a pollutant whose capture is often attempted together with chromate,[330,331,332] only decreased the Cr(VI) capture efficiency by 17%. When considering real world applications, the concentrations of these competitive anions in fresh water vary significantly around the world. For the application of butylimidazolium cloth for point-of-use drinking water purification, it would therefore be important to test the Cr(VI) capture efficiency using real water instead of solutions prepared in the laboratory. As a model, water from a rainwater pond was spiked with 2 mg L Cr(VI) and filtration through butylimidazolium cloth showed that the capture efficiency was only 2% lower than from a pure Cr(VI) solution in UHP water. Analysis of the pond water showed that nitrate and sulfate were at most 1.5 times higher concentrated than Cr(VI), proving the high selectivity of butylimidazolium cloth at moderate concentrations of competitive anions. When examining the thermochemical and solution radii of the used anions, chromate anions appear to have a larger radius than chloride, nitrate, sulfate, dihydrogenphosphate, and dihydrogenarsenate anions according to most sources.[333,334,335,336,337] This makes chromate a slightly softer anion than the other anions used.[338] While the double negative charge of chromate adds to its chemical hardness, a lot of it exists in the form of hydrogen chromate at neutral pH and low concentrations[339,340,341], which in turn reduces its hardness again. As imidazoles

are fairly soft cations,[342] the size and softness of Cr(VI) oxoanions may explain their favourable adsorption to butylimidazolium cloth.

Filtration of industrial water samples from India through butylimidazolium cloth showed that the material is capable of successfully reducing the chromium concentration of real polluted water to concentrations that are harmless to human health. The initial chromium concentration in these samples was lower than in solutions prepared in the laboratory and they were analysed using ICP-OES instead of UV–Vis spectroscopy for higher accuracy. These successful filtrations show that butylimidazolium cloth is capable of capturing Cr(VI) from solution even when its concentration is already below the 50 µg L^{-1} limit recommended by the World Health Organization to make water even safer to drink.

Besides its high selectivity for Cr(VI) oxoanions, butylimidazolium cloth was also successfully regenerated, meaning that it can be used multiple times. When recycling for five times, only 5 mL of 2 M NaCl + 0.5 M NaOH regeneration solution was used each time to successfully desorb most of the chromium adsorbed to the cloth from filtration of 50 mL 2 mg L^{-1} Cr(VI) solution, meaning that significantly less water is required to regenerate the filtration material than can be purified by it. However, the Cr(VI) uptake percentage slowly decreased with each passage within a filtration cycle even though the total Cr(VI) uptake at the end of the cycle remained below 65% of the Cr(VI) uptake reached when using a 20 mg L^{-1} Cr(VI) solution. This decrease in uptake is likely caused by the decreasing number of available chromium capture sites as the material is increasingly loaded with chromium(VI) oxoanions following each solution passage. The fact that the absolute Cr(VI) uptake when filtering 2 mg L^{-1} Cr(VI) solutions does not reach the same level as when using a 20 mg L^{-1} Cr(VI) solution shows that the uptake capacity of a capture material measured at high pollutant concentrations only has very little significance when the pollutant is captured from a solution with a lower concentration. When purifying real water which typically has even lower Cr(VI) concentrations than the one used in this recycling experiment[307,308,309], it would therefore be important to determine experimentally in each case the volume of polluted water that can be purified instead of relying on the uptake capacity of a material.

Compared to other immobilized ionic liquid based materials for capture of Cr(VI) found in the literature, the main difference of this material is that it is a

continuous cloth and not in the form of powder or microbeads.[311,312,314,315,316] While functionalized powder may be convenient for industrial processes, functional cloth is more suitable for point-of-use application: it is easier to use for untrained laypersons as no additional filtration or centrifugation is required to separate the filtration material from the cleaned water and safer to use in simple setups and around children as the filtration material cannot be accidentally ingested as easily as a powder.

While in the literature, the successful capture of Cr(VI) from solution prepared in the laboratory (with and without competitive anions) using immobilized ionic liquid based materials has been shown on multiple occasions, this work is the first using real polluted water from small scale industrial sites in India to show the effective Cr(VI) capture by imidazolium functionalized cloth under real world conditions. The ability of the cloth to decrease the chromium concentration in the polluted water from one that is already low (compared to other concentrations used in the literature) but still dangerous to human health to a concentration that is considered safe even under the recently lowered legal chromium levels in the EU is very promising for future applications as point-of-use filtration material.

5.4 Conclusion

N-butylimidazole was reacted at room temperature with pulsed plasma poly(vinylbenzyl chloride) functionalized non-woven polypropylene cloths, forming supported butylimidazolium chloride functional groups. This surface tethered ionic liquid was shown to efficiently remove chromium(VI) oxoanions from water at starting concentrations ranging from 30 µg L^{-1} to 20 mg L^{-1} and using solutions prepared in the laboratory, spiked pond water, and real industrial polluted water. Selectivity remains high even when the solutions contain a large surplus of competitive structurally similar anions, likely due to chemical softness. Finally, the Cr(VI) oxoanions captured by the butylimidazolium cloth could be easily desorbed by rinsing with a small volume of NaCl and NaOH solution, thereby providing multiple time re-use of the filtration material.

5.5 References

(286) Welton, T. Ionic Liquids: A Brief History. *Biophysical Reviews* **2018**, *10*, 691–706.

(287) Wilkes, J.S.; Levisky, J.A.; Wilson, R.A.; Hussey, C.L. Dialkylimidazolium Chloroaluminate Melts: A New Class of Room-Temperature Ionic Liquids for Electrochemistry, Spectroscopy, and Synthesis. *Inorg. Chem.* **1982**, *21*, 1263–1264.

(288) Fidale, L.C.; Possidonio, S. ; El Seoud, O.A. Application of 1-Allyl-3-(1-butyl)imidazolium Chloride in the Synthesis of Cellulose Esters: Properties of the Ionic Liquid, and Comparison with Other Solvents. *Macromol. Biosci.* **2009**, *9*, 813–821.

(289) Li, H.; Bhadury, P.S.; Song, B.; Yang, S. Immobilized Functional Ionic Liquids: Efficient, Green, and Reusable Catalysts. *RSC Advances* **2012**, *2*, 12525–12551.

(290) Vidal, L.; Riekkola, M.-L.; Canals, A. Ionic Liquid-Modified Materials for Solid-Phase Extraction and Separation: A Review. *Analytica Chimica Acta* **2012**, *715*, 19–41.

(291) Wilson, M.; Kore, R.; Ritchie, A.W.; Fraser, R.C.; Beaumont, S.K.; Srivastava, R.; Badyal, J.P.S. Palladium-poly(ionic liquid) membranes for permselective sonochemical flow catalysis. *Colloids and Surfaces A* **2018**, *545*, 78–85.

(292) Swatloski, R.P.; Spear, S.K.; Holbrey, J.D.; Rogers, R.D. Dissolution of Cellose with Ionic Liquid. *J. Am. Chem. Soc.* **2002**, *124*, 4974–4975.

(293) Köhler, S.; Heinze, T. Efficient Synthesis of Cellulose Furoates in 1-N-butyl-3-methylimidazolium Chloride. *Cellulose* **2007**, *14*, 489–495.

(294) Bates, E.D.; Mayton, R.D.; Ntai, I.; Davis, J.H. CO2 Capture by a Task-Specific Ionic Liquid. *J. Am. Chem. Soc.* **2002**, *124*, 926–927.

(295) Ranjan, P.; Kitawat, B.S.; Singh, M. 1-Butylimidazole-Derived Ionic Liquids: Synthesis, Characterisation and Evaluation of their Antibacterial, Antifungal and Anticancer Activities. *RSC Adv.* **2014**, *4*, 53634–53644.

(296) Usuki, T.; Onda, S.; Yoshizawa-Fujita, M.; Rikukawa, M. Use of [C4mim]Cl for Efficient Extraction of Caffeoylquinic Acids from Sweet Potato Leaves. *Scientific Reports* **2017**, *7*, 6890.

(297) Dharaskar, S.A.; Wasewar, K.L. Varma, M.N.; Shende, D.Z.; Yoo, C.K. Deep Removal of Sulfur from Model Liquid Fuels using 1-Butyl-3-Methylimidazolium Chloride. *Procedia Engineering* **2013**, *51*, 416–422.

(298) Visser, A.E.; Swatloski, R.P.; Reichert, W.M.; Mayton, R.; Sheff, S.; Wierzbicki, A.; Davis, J.H.; Rogers, R.D. Task-Specific Ionic Liquids Incorporating Novel Cations for the Coordination and Extraction of Hg2+ and Cd2+: Synthesis, Characterization, and Extraction Studies. *Environ. Sci. Technol.* **2002**, *36*, 2523–2529.

(299) Fontanals, N.; Ronka, S.; Borrull, F.; Trochimczuk, A.W.; Marcé, R.M. Supported Imidazolium Ionic Liquid Phases: A New Material for Solid-Phase Extraction. *Talanta* **2009**, *80*, 250–256.

(300) Costa, M. Toxicity and Carcinogenicity of Cr(VI) in Animal Models and Humans. *Crit. Rev. Toxicol.* **1997**, *27*, 431–442.

(301) Costa, M. Potential Hazards of Hexavalent Chromate in our Drinking Water. *Toxicol. Appl. Pharmacol.* **2003**, *188*, 1–5.

(302) Stout, M. D.; Herbert, R. A.; Kissling, G. E.; Collins, B. J.; Travlos, G. S.; Witt, K. L.; Melnick, R. L.; Abdo, K. M.; Malarkey, D. E.; Hooth, M. J. Hexavalent Chromium is Cancerogenic to F344/N Rats and B6C3F1 Mice after Chronic Oral Exposure. *Environ. Health Perspect.* **2009**, *117*, 716–722.

(303) Council Directive 98/83/EC. Official Journal of the European Commission 1998 http://ec.europa.eu/environment/water/water-drink/legislation_en.html (accessed Mar 12, 2018).

(304) European Commission. Proposal for a Directive of the European Parliament and of the Council on the Quality of Water Intended for Human Consumption. COM(2017) 753 final. Brussels, 2018. http://ec.europa.eu/environment/water/waterdrink/review_en.html (accessed Mar 12, 2018).

(305) European Commission Press Release. Commission Welcomes Provisional Agreement to Improve the Quality of Drinking Water and the Access to it. Brussels, 2019.

https://ec.europa.eu/commission/presscorner/detail/en/ip_19_6830 (accessed Mar 3, 2020).

(306) Directive (EU) 2010/2184 of the European Parliament and of the Council of 16 December 2010 on the quality of water intended for human consumption. Official Journal of the European Union 2020. https://eur-lex.europa.eu/legal-content/EN/TXT/PDF/?uri=CELEX:32020L2184&from=EN (accessed on Apr 30, 2021).

(307) Naz, A.; Mishra, B.K.; Gupta, S.K. Human Health Risk Assessment of Chromium in Drinking Water: A Case Study of Sukinda Chromite Mine, Odisha, India. *Exposure Health* **2016**, *8*, 253–264.

(308) Kazakis, N.; Kantiranis, N.; Kalaitzidou, K.; Kaprara, E.; Mitrakas, M.; Frei, R.; Vargemezis, G.; Tsourlos, P.; Zouboulis, A.; Filippidis, A. Origin of Hexavalent Chromium in Groundwater: The Example of Sarigkiol Basin, Northern Greece. *Sci. Total Environ.* **2017**, *593−594*, 552−566.

(309) Tiwari, A. K.; De Maio, M. Assessment of Risk to Human Health due to Intake of Chromium in the Groundwater of the Aosta Valley Region, Italy. *Hum. Ecol. Risk Assess.* **2017**, *23*, 1153−1163.

(310) Chen, M.-L.; Zhao, Y.-N.; Zhang, D.-W.; Tian, Y.; Wang, J.-J. The Immobilization of Hydrophilic Ionic Liquid for Cr(VI) Retention and Chromium Speciation. *J. Anal. At. Spectrom.* **2010**, *25*, 1688–1694.

(311) Mi, H.; Jiang, Z.; Kong, J. Hydrophobic Poly(ionic liquid) for Highly Effective Separation of Methyl Blue and Chromium Ions from Water. *Polymers* **2013**, *5* (4), 1203–1214.

(312) Wang, Z.; Ye, C.; Wang, X.; Li, J. Adsorption and Desorption Characteristics of Imidazole-Modified Silica for Chromium(VI). *Applied Surface Science* **2013**, *287*, 232–241.

(313) Jiang, Y.; Li, F.; Ding, G.; Chen, Y.; Liu, Y.; Hong, Y.; Liu, P.; Qi, X.; Ni, L. Synthesis of a novel ionic liquid modified copolymer hydrogel and its rapid removal of Cr (VI) from aqueous solution. *Journal of Colloid and Interface Science* **2015**, *455*, 125–133.

(314) Nasrollahpour, A.; Moradi, S.E. Hexavalent Chromium Removal from Water by Ionic Liquid Modified Metal-Organic Frameworks Adsorbent. *Microporous and Mesoporous Materials* **2017**, *243*, 47–55.

(315) Xie, Y.; Lin, J.; Liang, J. ; Li, M. ; Fu, Y.; Wang, H.; Tu, S.; Li, J. Hypercrosslinked Mesoporous Poly(Ionic Liquid)s with High Density of Ion Pairs: Efficient Adsorbents for Cr(VI) Removal via Ion-Exchange. *Chemical Engineering Journal* **2019**, *378*, 122107.

(316) Xie, Y.; Lin, J.; Lin, H.; Jiang, Y. ; Liang, J.; Wang, H.; Tu, S.; Li, J. Removal of Anionic Hexavalent Chromium and Methyl Orange Pollutants by Using Imidazolium-Based Mesoporous Poly(Ionic Liquid)s as Efficient Adsorbents in Column. *Journal of Hazardous Materials* **2020**, *392*, 122496.

(317) Morsch, S.; Wood, T. J.; Schofield, W. C. E.; Badyal, J. P. S.; A Combined Plasmachemical and Emulsion Templating Approach for Actuated Macroporous Scaffolds. *Adv. Func. Mater.* **2012**, *22*, 313−322.

(318) Rjeb, A.; Tajounte, L.; Chafik El Idrissi, M.; Letarte, S.; Adnot, A.; Roy, D.; Claire, Y.; Périchaud, A.; Kaloustian, J. IR Spectroscopy Study of Polypropylene Natural Aging. *J. Appl. Polym. Sci.* **2000**, *77*, 1742−1748.

(319) D. Lin-Vien, N.B. Colthup, W.G. Fateley, J.G. Grasselli, The Handbook of Infrared and Raman Characteristic Frequencies of Organic Molecules, Academic Press, Inc., San Diego, 1991.

(320) Schofield, W. C. E.; Badyal, J. P. S. Controlled Fragrant Molecule Release from Surface-Tethered Cyclodextrin Host-Guest Inclusion Complexes. *ACS Appl. Mater. Interfaces* **2011**, *3*, 2051−2056.

(321) Schofield, W. C. E.; Bain, C. D.; Badyal, J. P. S. Cyclodextrin-Functionalized Hierarchical Porous Architectures for High-Throughput Capture and Release of Organic Pollutants from Wastewater. *Chem. Mat.* **2012**, *24*, 1645−1653.

(322) Yamada, T.; Tominari, Y.; Tanaka, S.; Mizuno, M. Infrared Spectroscopy of Ionic Liquids Consisting of Imidazolium Cations with Different Alkyl Chain Lengths and Various Halogen or Molecular Anions with and without a Small Amount of Water. *J. Phys. Chem. B* **2017**, *121* (14), 3121–3129.

(323) K. Noack, P.S. Schulz, N. Paape, J. Kiefer, P. Wasserscheid, A. Leipertz, The role of the C2 position in interionic interactions of imidazolium based ionic liquids: a vibrational and NMR spectroscopic study. *Phys. Chem. Chem. Phys* **2010**, *12*, 14153–14161.

(324) Bieber, V.S.; Ozcelik, E.; Cox, H.J.; Ottley, C.J.; Ratan, J.K.; Karaman, M.; Tabakci, M.; Beaumont, S.K.; Badyal, J.P.S. Capture and Release Recyclable Dimethylaminomethyl-Calixarene Functional Cloths for Point-of-Use Removal of Highly Toxic Chromium Water Pollutants. *ACS Appl. Mater. Interfaces* **2020**, *12*, 52136–52145.

(325) Ten chemicals of major public health concern. World Health Organization, Geneva, 2010. https://www.who.int/ipcs/assessment/public_health/chemicals_phc/en/ (accessed on Sep 27, 2017).

(326) Guidelines for drinking-water quality, 2nd ed. Vol. 2. Health criteria and other supporting information. World Health Organization, Geneva, 1996.

(327) Atia, A.A. Synthesis of a Quaternary Amine Anion Exchange Resin and Study its Adsorption Behaviour for Chromate Oxyanions. *Journal of Hazardous Materials* **2006**, *137*, 1049–1055.

(328) Rafati, L.; Mahvi, A.H.; Asgari, A.R.; Hosseini, S.S. Removal of Chromium (VI) from Aqueous Solutions using Lewatit FO36 Nano Ion Exchange Resin. *Int. J. Environ. Sci. Tech.* **2010**, *7*, 147–156.

(329) Fontanals, N.; Borrull, F.; Marcé, R.M. Ionic Liquids in Solid-Phase Extraction. *Trends in Analytical Chemistry* **2012**, *41*, 15–26.

(330) Badruddoza, A.Z.M.; Shawon, Z.B.Z.; Rahman, M.T.; Hao, K.W.; Hidajat, K.; Uddin, M.S. Ionically Modified Magnetic Nanomaterials for Arsenic and Chromium Removal from Water. *Chemical Engineering Journal* **2013**, *225*, 607–615.

(331) Agrafioti, E.; Kalderis, D.; Diamadopoulos, E. Arsenic and Chromium Removal from Water Using Biochars Derived from Rice Husk, Organic Solid Wastes and Sewage Sludge. *Journal of Environmental Management* **2014**, *133*, 309–314.

(332) Su, X.; Kushima, A.; Halliday, C.; Zhou, J.; Li, J.; Hatton, A. Electrochemically-Mediated Selective Capture of Heavy Metal Chromium and Arsenic Oxyanions from Water. *Nature Communications* **2018**, *9*, 4701.

(333) Kapustinskii, A.F. Lattice Energy of Ionic Crystals. *Quarterly Reviews, Chemical Society* **1956**, *10* (3), 283–294.

(334) Jenkins, H.D.B.; Thakur, K.P. Reappraisal of Thermochemical Radii for Complex Ions. *Journal of Chemical Education* **1979**, *56* (9), 576–577.

(335) Marcus, Y. A Simple Empirical Model Describing the Thermodynamics of Hydration of Ions of Widely Varying Charges, Sizes, and Shapes. *Biophysical Chemistry* **1994**, *51*, 111–127.

(336) Roobottom, H.K.; Jenkins, H.D.B. Thermochemical Radii of Complex Ions. *Journal of Chemical Education* **1999**, *78* (11), 1570–1573.

(337) Simoes, M.C.; Hughes, K.J.; Ingham, D.B.; Ma, L.; Pourkashanian, M. Estimation of the Thermochemical Radii and Ionic Volumes of Complex Ions. *Inorg. Chem.* **2017**, *56*, 7566–7573.

(338) Parr, R.G.; Pearson, R.G. Absolute Hardness: Companion Parameter to Absolute Electronegativity. *J. Am. Chem. Soc.* **1983**, *105*, 7512–7516.

(339) Perrin, D.D. Dissociation Constants of Inorganic Acids and Bases in Aqueous Solution. *Pure and Applied Chemistry* **1969**, *20* (2), 133–236.

(340) Cruywagen, J. J.; Heyns, J. B. B.; Rohwer, E. A. New Spectrophotometric Evidence for the Existence of HCrO4–. *Polyhedron* **1998**, *17*, 1741–1746.

(341) Heyns, J.B.B.; Cruywagen, J.J.; Carron, K.T. Raman Spectroscopic Investigation of Chromium(VI) Equilibria—Another Look. *J. Raman Spectrosc.* **1999**, *30*, 335–338.

(342) Hu, X.; Jia, X.; Su, K. ; Gu, X. Electronic Structural Properties of Amino/Hydroxyl Functionalized Imidazolium-Based Bromide Ionic Liquids. *Open Chemistry* **2020**, *18*, 576–583.

Chapter 6: Stranski–Krastanov Growth of MOF-508 on Uncoated Polymers and SURMOF Double Transfer

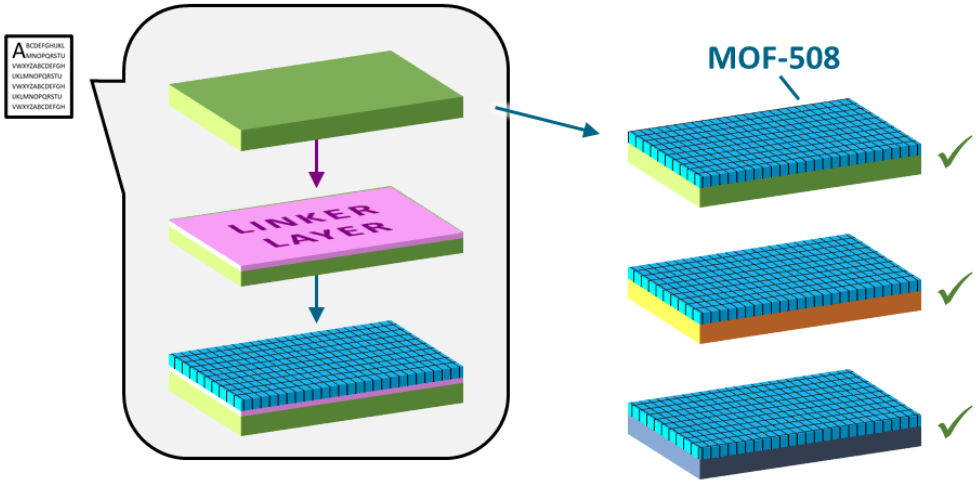

Figure 38: Graphic chapter summary: While in the literature it has been reported that a linker layer is required to grow MOF-508 on a surface, here it was epitaxially grown on different uncoated substrates.

6.1 Introduction

Metal–organic frameworks or MOFs are coordination networks consisting of metal centres that are connected by organic linkers, forming a porous structure.[343,344] They contain up to 90 % free volume and vast internal surface areas that exceed other porous materials such as zeolites, mesoporous silica, or activated carbon.[344,345] The term “metal–organic framework” was first coined by Omar Yaghi in 1995.[346] Potential applications for these materials soon became apparent when MOFs capable of ion exchange and gas sorption were described in 1996 and 1997.[347,348] Interest in the field rapidly accelerated once permanent porosity upon removal of solvent molecules was reported in two MOFs in 1999.[349,350] Ever since, there has been almost unparalleled growth of interest in this topic, evidenced by thousands of MOF-related publications and the continuously expanding scope of research they cover.[345]

Due to their porosity which allows the reversible adsorption and desorption of guest molecules, MOFs have been considered for many applications.[344] These include catalysis[351], chemical sensing[352], separation of hydrocarbons[353], gas storage[354], and removal of organic and inorganic pollutants from water[355,356]. As of 2020, over 90,000 different MOFs had been synthesized and over 500,000 predicted.[357] These MOFs can be characterized mainly by four traits: metal chemistry, linker chemistry, functional groups, and pore geometry.[357] Metal chemistry describes the nature of the metal centres, as well as the way linkers are coordinated to them. Linker chemistry describes the nature and size of the linker molecules. Functional groups can be incorporated that branch off linkers, for example to instigate the adsorption of selected molecules. Pore geometry describes the size and shape of pores formed by the 3D structure.

MOFs could be an interesting platform for the synthesis of filters for the capture of heavy metal pollutants, analogous to the ones described in the previous chapters. Their porous structure could lead to far higher capture efficiencies than functional molecules directly attached to polymer surfaces, due to the greatly increased surface area of the material. The work in this chapter is aimed at illuminating the growth mechanism of a well-documented MOF (MOF-508), which can form a basis for the preparation of inorganic pollutant capturing MOFs in the future.

The metal organic framework synthesized in this work is known as MOF-508, with the structure [Zn(benzene-1,4-dicarboxylate) -(4,4'-bipyridine)$_{0.5}$], which can be shortened to [Zn(bdc)(4,4'-bipy)$_{0.5}$]. It possesses a layered-pillar structure, meaning that the metal clusters are bridged by terephthalic acid ligands to form a distorted 2D square grid, with 4,4'-bipyridine molecules acting as pillars linking the 2D grids to give a 3D elongated primitive cubic lattice, Figure 39.[358]

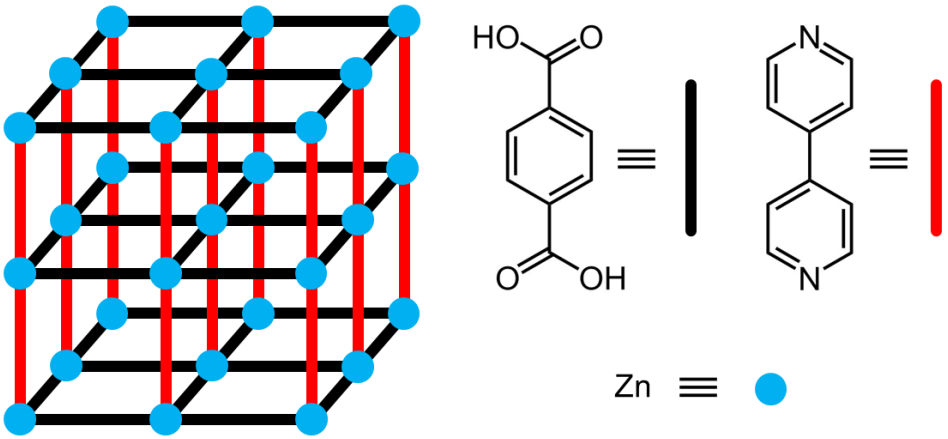

Figure 39: Schematic structure of MOF-508, consisting of Zn metal clusters (blue dots) bridged by “layer” linkers, terephthalic acid (black bars), and “pillar” linkers, 4,4'-bipyridine (red bars).

MOF-508 displays high capabilities for CO_2 capture and separation of linear alkanes. First synthesised in 2006, it was the first MOF to be selective in the gas chromatographic separation of alkanes.[358] The bulk form can be synthesized solvothermally by heating a DMF/ethanol solution of the reagents at 90°C for 24 h and forms colourless block-shaped crystals.[358358] Solvothermal synthesis produces MOF-508a, which is guest-filled with the formula $[Zn(BDC)(4,4'\text{-}Bipy)_{0.5}\cdot(DMF)(H_2O)_{0.5}]$.[358] Heating the compound leads to a release of the solvent molecules from the pores, resulting in the guest-free phase MOF-508b, $[Zn(BDC)(4,4'\text{-}Bipy)_{0.5}]$, which is thermally stable up to 360°C.[358]

When synthesized in solution, both forms, while drawn as simple lattices, in fact consist of two identical interpenetrated networks, Figure 40.[358,359] Thus, the resulting pores consist of 1D channels with a cross section of about 4.0 x 4.0 Å, significantly smaller than the unit cell of the simple lattice.[358]

.

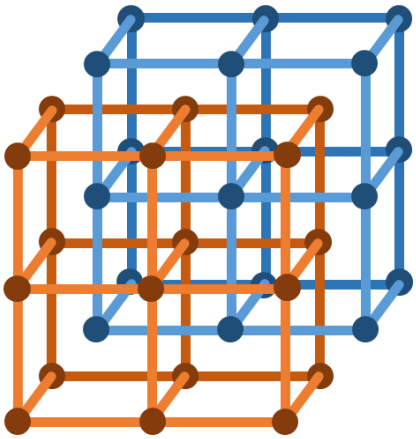

Figure 40: When synthesized solvothermally, MOF-508 consists of two identical interpenetrated networks which are depicted here as a blue and an orange grid, leading to pore sizes that are significantly smaller than the unit cell of a simple lattice. Drawing inspired by reference 359.

For many applications, such as membranes and sensors, it is beneficial or even necessary for MOFs to be processed as homogenous films of defined thickness.[344, 360] MOF thin films typically fall into one of two categories: Polycrystalline MOF films can be prepared in a variety of ways (including insertion of a substrate into a MOF growth solution, electrochemical methods, and assembly of pre-synthesized MOF nanocrystals) and consist of unoriented crystallites, leading to a rough surface.[344] SURMOFs (surface-mounted metal–organic frameworks) on the other hand are smooth MOF multilayers oriented in the direction of growth whose thickness can usually be precisely controlled.[344,360]

There are typically two ways to synthesize SURMOFs.[344] The first is through the Langmuir–Blodgett method and can only be used for 2D structured MOFs.[360] These 2D arrays are prepared on the surface of an aqueous solution within a Langmuir trough and subsequently placed onto a substrate by dip coating.[361] Additional layers can be created by repeated dipping, however no covalent bonds exist between the layers, only weak π-π interactions.[360,361] The second, and more common strategy to synthesize SURMOFs is via liquid-phase epitaxy. Here, a substrate is immersed in an alternating fashion in a metal precursor solution and a ligand solution with rinsing steps in between.[362] In most cases the substrate used is functionalized with a self-assembled monolayer carrying functional groups that coordinate to the metal centres, thus binding them to the surface and allowing a stepwise growth of the MOF.[360] Ideally, each cycle of metal and linker

solution dipping adds one unit cell layer to the SURMOF thin film, thus allowing for very precise thickness control.[360]

The first SURMOF preparation of MOF-508 via liquid-phase epitaxy was conducted using substrates coated with a pyridine-terminated self-assembled monolayer mimicking the functional end groups of 4,4'-bipyridine which forms the "pillars" of the MOF structure.[359] This structured substrate facilitated the synthesis of the first non-interpenetrated version of MOF-508.[359] However, interpenetrated MOF-508 has also been synthesized as SURMOF via liquid-phase epitaxy, namely on substrates coated with pulsed plasma poly(1-allylimidazole).[363] This shows that while it is possible to suppress interpenetration with the use of a very flat and well-structured surface, it can still occur in surface-grown MOF-508 when it is synthesized on a more "forgiving" (e.g. less well-defined) substrate. In fact, the interpenetrated version is superior for applications such as CO_2 capture because the increased interaction between guest molecules and MOF channel walls leads to an improved adsorption.[363]

Usually, substrates used for layer-by-layer MOF synthesis are coated with functional groups that provide anchor points for the reagents.[344,360] Very little research has been conducted into the growth of MOFs via liquid-phase epitaxy onto unfunctionalized surfaces. While gold substrates are usually coated with self-assembled monolayers,[344,360] various coatings have been reported for polymer substrates, such as poly(1-allylimidazole), Al_2O_3, single-layer graphene, and a gold coating treated with piranha solution to carry –OH groups.[363,364,365,366] There is one publication that reported MOF growth on $–CH_3$ terminated self-assembled monolayers [367], a case described as "unusual because $–CH_3$ terminated [self-assembled monolayers] typically are chemically inactive" in a review article[368]. However, in this setup the MOF was grown from a crystallization solution in which the MOF components had already been heated for 8 days, thus the deposition of MOF on the $–CH_3$ terminated surface was explained with the formation of crystallites in solution whose organic crystal faces then adhered to the surface via dispersive forces, leading to an unoriented MOF layer.[367,368]

When it comes to transferring a thin MOF film from the substrate it was synthesized on to another, a few strategies have been described in the literature.

2D MOFs synthesized via the Langmuir–Blodgett method can be transferred from the liquid–air interface where they are grown onto any solid substrate.[361,369] MOF thin films grown on the interface of two immiscible liquids (one containing the linkers, the other a metal precursor) can be transferred in a similar fashion.[370371] Such free-standing MOF thin films can also be synthesized by first preparing MOF particles in solution followed by dispersion on a water surface and dip-coating of a substrate.[372] A very different approach is the usage of a solid metal oxide/hydroxide precursor as substrate that is completely corroded during MOF growth, leaving only a MOF film behind.[373,374]

If, however, the goal is to synthesize a well oriented, homogenous 3D MOF film and transfer it from one substrate to another, none of the methods mentioned above are applicable. For this case two methods involving the use of poly(methyl methacrylate) (PMMA) have been reported. The first method starts with regular liquid phase epitaxy of MOF onto a substrate coated with a functional self-assembled monolayer.[375] PMMA resin is then coated on top of the SURMOF and both are physically shaved off from the substrate together.[375] Subsequent dissolution of the PMMA in acetone leaves free-standing MOF that can be transferred onto other substrates.[375] The second method is similar but simpler: MOF is synthesized via liquid-phase epitaxy straight onto a substrate coated with PMMA that was previously acidified to carry carboxylic acid groups.[376] By dissolving the PMMA layer, the MOF could then be removed from the substrate.[376]

In this work we examined the growth of MOF-508 on different unfunctionalized surfaces, finding that a SURMOF can be synthesised through liquid-phase epitaxy on untreated polymer surfaces including polypropylene non-woven (PP) and high-density poly ethylene (HDPE). The surface-attached MOF-508 was successfully delaminated using tape and transferred onto glass slides using a thermal release sheet, thus providing a simple method to move an ultra-thin and well-oriented MOF layer from the substrate it was synthesized on to another.

6.2 Results

6.2.1 Characterization of MOF-508 grown on Linker Layer Free Surfaces

Infrared Spectra

ATR-FTIR spectra were captured of high-density polyethylene (HDPE) sheets after 0, 10, 20 and 200 MOF-508 deposition cycles via liquid phase epitaxy, Figure 41.

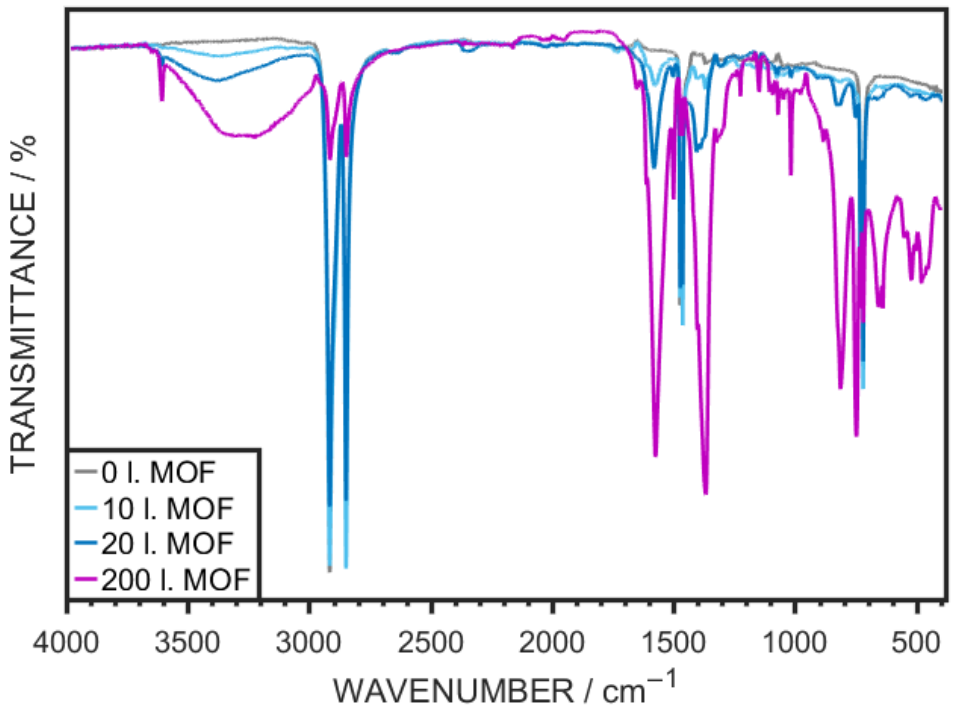

Figure 41: ATR–infrared spectra of HDPE after 0 (grey), 10 (light blue), 20 (blue) and 200 (purple) deposition cycles. Data was captured by PKE and plotted / evaluated by VSB.

The epitaxial deposition of MOF-508 on HDPE led to the appearance of new infrared absorbance peaks in addition to the HDPE absorbances at 2916 cm^{-1} (CH_2 antisymmetric stretch), 2848 cm^{-1} (CH_2 symmetric stretch), 1473–1463 cm^{-1} (CH_2 scissoring), and 730–719 cm^{-1} ($–(CH_2)_n–$ in-phase rock for long-chain CH_2 in crystalline solid state), Figure 41. The intensities of the additional absorbance peaks gradually increased with an increasing number of depositions, indicating a gradual growth on the surface. In order to verify that these peaks are caused by MOF-508, the spectra were compared to ones of the MOF building blocks zinc

acetate, terephthalic acid, and 4,4'-bipyridine, Figure 42. The most notable absorbance peaks of the spectra are assigned in Table 9.

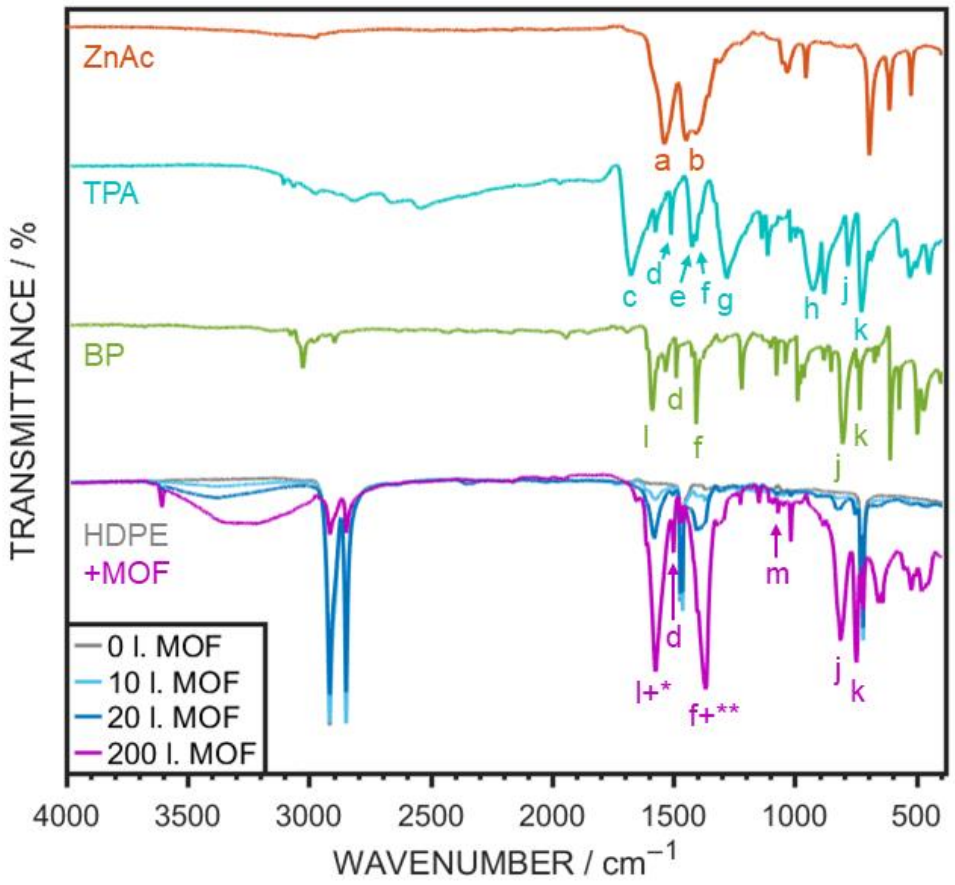

Figure 42: ATR–infrared spectra of zinc acetate, terephthalic acid, and 4,4-bipyridine (the three components of MOF-508), as well as HDPE with an increasing number of MOF-508 layers. Notable absorbance peaks are labelled a–m and assigned in Table 9. Data was captured by PKE and plotted / evaluated by VSB.

Table 9: Assignment of notable peaks in the FTIR spectra of zinc acetate, terephthalic acid, 4,4'-bipyridine, and 200-layer MOF-508 grown on HDPE, as depicted in Figure 42. Data was captured by PKE and evaluated by VSB.

		Absorbance / cm^{-1}				
Peak	**Assignment**	**Literature[377]**	**Zinc Acetate**	**Tereph-thalic Acid**	**4,4'-Bipyridine**	**200-layer MOF-508**
a	COO^- antisym. stretch	1650–1540	1536	–	–	–
b	COO^- sym. stretch	1450–1360	1449–1405	–	–	–
c	C=O stretch of aromatic	1710–1660	–	1673	–	–

	carboxylic acid					
d	Para substituted benzene / 4-substituted pyridine ring semicircle stretch 1	1525–1480	–	1510	1489	1500
e	COH in-plane bending	1440–1395	–	1424	–	–
f	Para substituted benzene / 4-substituted pyridine ring semicircle stretch 2	1420–1400	–	1407	1407	1367**
g	C–O stretch band cluster for COOH in condensed state	1315–1200	–	1281	–	–
h	In-phase, out-of-plane OH…O wag of COOH dimers	960–875	–	926.5	–	–
j	Aryl C–H wag for rings with two adjacent H	880–795	–	781	804	813
k	Sextant out-of-plane bend	735–665	–	726	733	747
l	4-substituted pyridine ring quadrant stretch	1605–1565	–	–	1587	1574*
m	COC antisym. stretch	1150–1060	–	–	–	1070

The zinc acetate infrared spectrum displays two characteristic peaks caused by the antisymmetric and symmetric stretch of the COO^- group (a, b). These cannot be found in MOF-508 as the acetate remains in solution while the Zinc is incorporated in the framework.

The spectrum of terephthalic acid contains absorbance peaks caused by the carboxylic acid groups and the para-substituted benzene ring. The carboxylic

acid peaks at 1673 cm^{-1} (C=O stretch of aromatic carboxylic acid, c), 1424 cm^{-1} (COH in-plane bending, e), 1281 cm^{-1} (C-O stretch band cluster for COOH in condensed state, g), and 926.5 cm^{-1} (in-phase, out-of-plane OH…O wag of COOH dimers, h) do not translate directly into the MOF-508 spectrum since the terephthalic acid is deprotonated during incorporation into the framework. Instead, the resulting COO^- groups contribute antisymmetric and symmetric stretch absorbances similar to those found in the zinc acetate spectrum, albeit shifted due to metal coordination. The MOF-508 absorbance peaks that these COO^- groups contribute to are marked with * and ** in Figure 42 and Table 9.

The peaks in the terephthalic acid spectrum that are associated with the benzene ring can also be found in the 4,4'-bipyridine spectrum due to the similar vibrations of para-substituted benzene and 4-substituted pyridine. These include two semicircle stretch absorbances (d, f), and a sextant out-of-plane bend (k) of the rings, as well as an absorbance peak caused by the aryl C–H wags of two adjacent H on the aromatic rings (j). However, the 4,4'-bipyridine spectrum also contains a peak at 1587 cm^{-1} that can be attributed to a quadrant stretch of the 4-substituted pyridine ring (l), a vibration that is not IR-active in terephthalic acid due to the symmetry of the substituents.

The appearance of all expected component peaks on the coated HDPE spectrum as well as its similarity to MOF-508 spectra reported in the literature and spectra of MOF-508 grown on poly(1-allylimidazole) linker coated substrates (Figure 43) support the assumption that MOF-508 was successfully synthesized on the unfunctionalized polymer. More precisely, the absorbance peak at 1070 cm^{-1} (m) in the MOF-508 spectrum indicates the incorporation of tetrahydrofuran solvent, showing that the solvent-inclusive MOF-508a polymorph was synthesized.

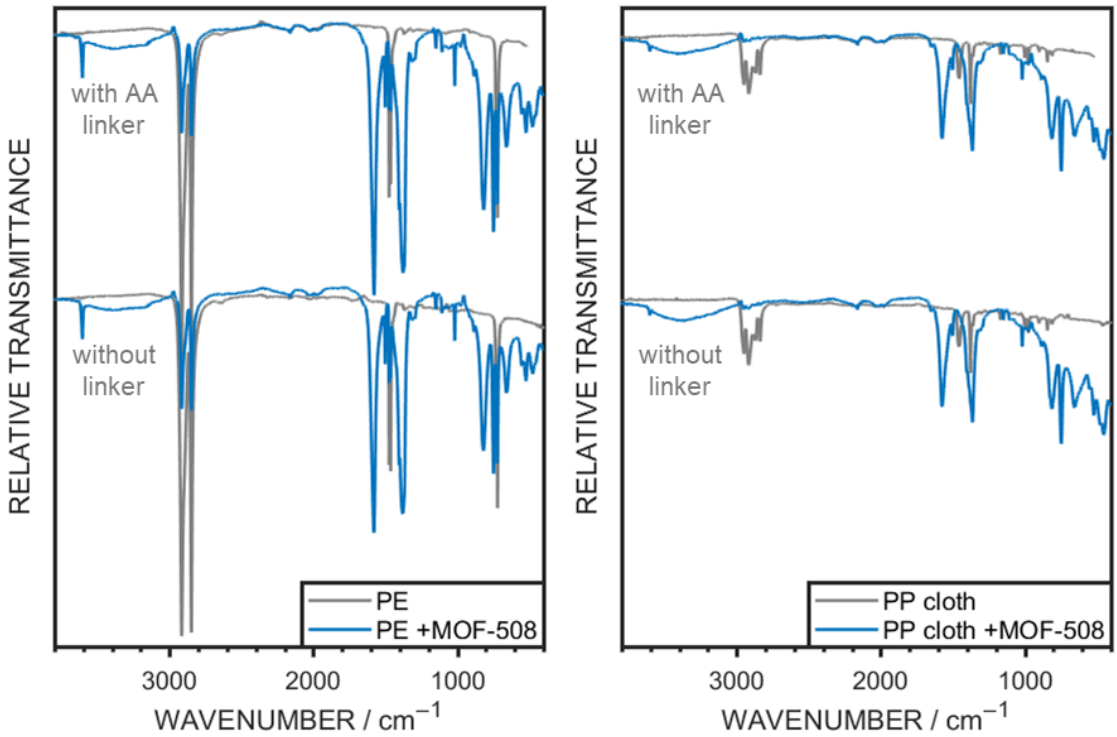

Figure 43: Infrared spectra comparison between HDPE and PP cloth with and without poly(1-allylimidazole) (AA) linker and with and without 170 layers MOF-508. For both substrates the MOF-508 spectra with and without underlying linker layers look nearly identical, showing successful SURMOF growth on unfunctionalized HDPE and PP cloth.

X-Ray Diffractograms

Powder X-ray diffractograms of 180-layer MOF-508 grown on HDPE sheets and PP cloth with and without a pulsed plasma poly(1-allylimidazole) linker layer show three prominent peaks at low detector angles that do not appear on diffractograms of the underlying HDPE and PP, indicating the presence of an oriented large lattice constant material, Figure 44. From the crystal data for MOF-508 found in the literature one can calculate the theoretical (100), (010), and (001) peaks for the solvent-inclusive MOF-508a to appear at 2θ detector angles of 8.12°, 8.09°, and 6.38°, respectively.[358,378] The peaks around 6.2–6.5° found in all four spectra can therefore be identified as (001) peaks of MOF-508a, while the (100) and (010) peaks are missing, showing a high degree of orientation of the MOF where the (001) planes run parallel to the substrate surface. A weaker (002) peak was observed in most spectra near the expected angle of 12.77°, showing that an interpenetrated network of MOF-508a was synthesized.[359] The peaks

between them in the region of 8.9–9.1° as well as the appearance of the (002) MOF-508a peak at slightly lower angles than expected can be attributed to small amounts of nonoriented solvent-free MOF-508b whose theoretical (100), (010), and (001) peaks are expected to appear at 12.49°, 9.52°, and 8.49°, respectively.[358,378]

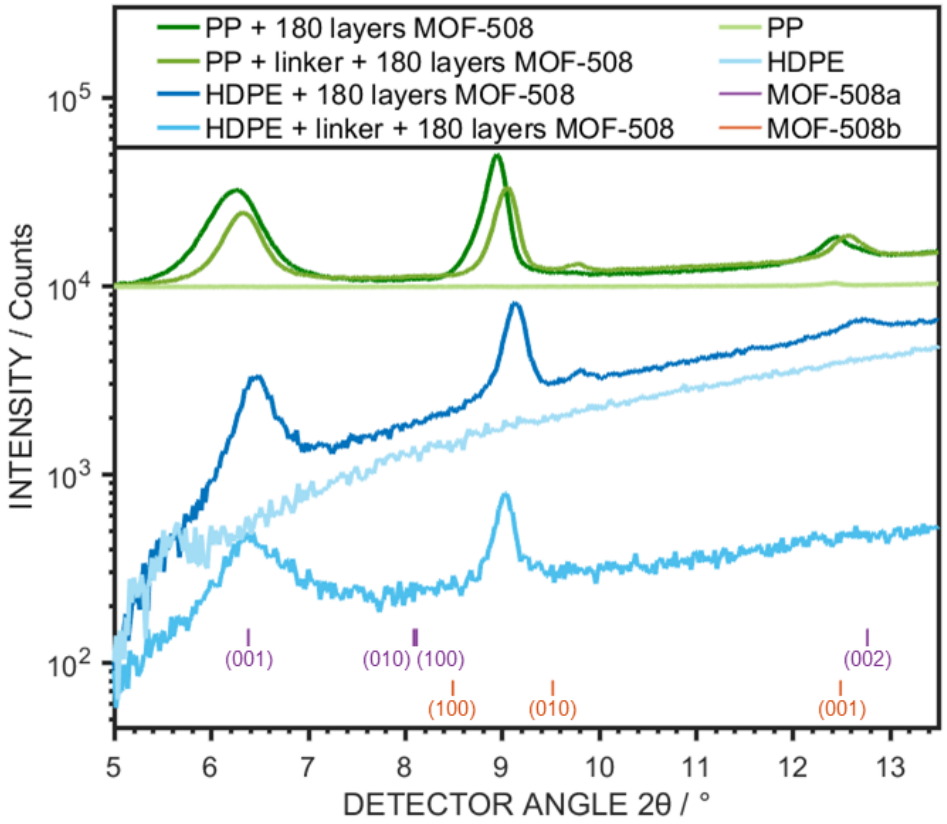

Figure 44: Powder XRD spectra of 180-layer MOF-508 grown on PP cloth and HDPE sheets with and without a pulsed plasma poly(1-allylimidazole) linker layer, as well as spectra of pure PP cloth and HDPE sheet. Spectra are displayed grouped on a logarithmic axis for better comparison. The theoretical peak positions of solvent-inclusive MOF-508a ((001), (010), (100), (002)) and solvent-free MOF-508b ((100), (010), (001)) are included for reference. Based on them, the three main peaks of the synthesized MOF-508 can be assigned to highly oriented MOF-508a ((001), (002)) and a small amount of nonoriented MOF-508b. Data was captured by HJC and plotted / evaluated by VSB.

Very little difference between MOF-508 grown on pure HDPE/PP and linker functionalized substrates can be seen, showing that the poly(1-allylimidazole) linker layer is not necessary for synthesis of MOF-508 on these polymer surfaces. The only slight difference are minimally higher peaks (indicating more MOF growth) and slightly higher intensities of the peaks near 9° assigned to

nonoriented MOF-508b, however the absence of MOF-508a (100) and (010) peaks still indicates a high orientation.

Scanning Electron Micrographs

Scanning electron micrographs of 180 layers MOF-508 grown on HDPE sheets reveal the formation of a continuous SURMOF layer both on pure HDPE and HDPE functionalized with a linker layer, as can be seen from cracks within the crystalline framework, Figure 45 c, d. These cracks were likely formed when cutting the substrates for SEM imaging. The images further reveal that the HDPE surface is not perfectly smooth but instead has many scratches and grooves, Figure 45 a. These disappear when coated with the linker layer which instead introduces small bumps, Figure 45 b. When comparing the MOF-508 grown on these surfaces, both lead to a complete coverage with small crystallites atop the continuous layer, although the surface of the SURMOF on the linker layer coated HDPE appears smoother (Figure 45 d) while the MOF-508 grown on pure HDPE contains more disordered crystallites (Figure 45 c).

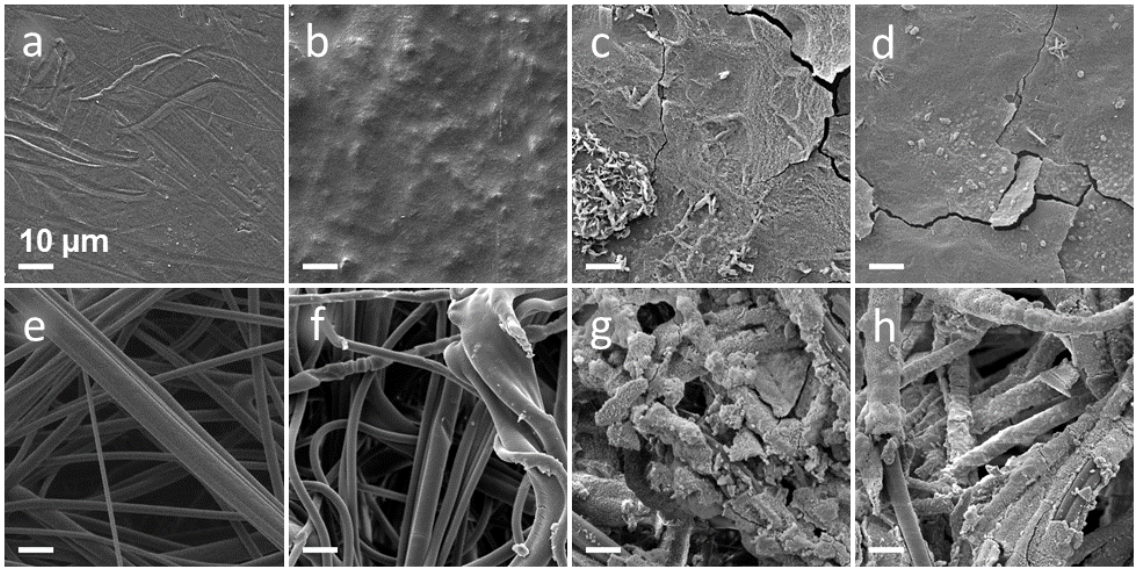

Figure 45: SEM images of HDPE and PP cloth substrates with and without 180 layers MOF-508; a: plain HDPE, b: HDPE + linker, c: HDPE + MOF-508, d: HDPE + linker + MOF-508, e: plain PP cloth, f: PP + linker, g: PP + MOF-508, h: PP + linker + MOF-508. Scale bars represent 10 µm in all images. Images were captured jointly by PKE & VSB and cropped / evaluated by VSB.

On non-woven PP cloth, a similarly complete MOF-508 coverage could be seen in the SEM micrographs, Figure 45 g, h. No major difference between the

fibre surfaces of uncoated and 1-allyl functionalized PP cloth is visible (Figure 45 e, f). However, like SURMOFs on HDPE, the MOF-508 grown on PP with linker layer appears smoother (Figure 45 h) while the topography of MOF-508 grown on plain PP cloth is somewhat bumpy (Figure 45 g). In both cases the pore structure of the cloth is mostly maintained even though some neighbouring fibres became bridged by the MOF coating.

Thickness determination

The thickness of MOF-508 coating on HDPE was approximately determined by cutting through a HDPE sheet coated with 200 layers MOF-508 with scissors and examining the cross-section by scanning electron microscopy. Through the mechanical stress from cutting, the SURMOF near the cross-section lifted from the surface in flakes, as shown in Figure 46.

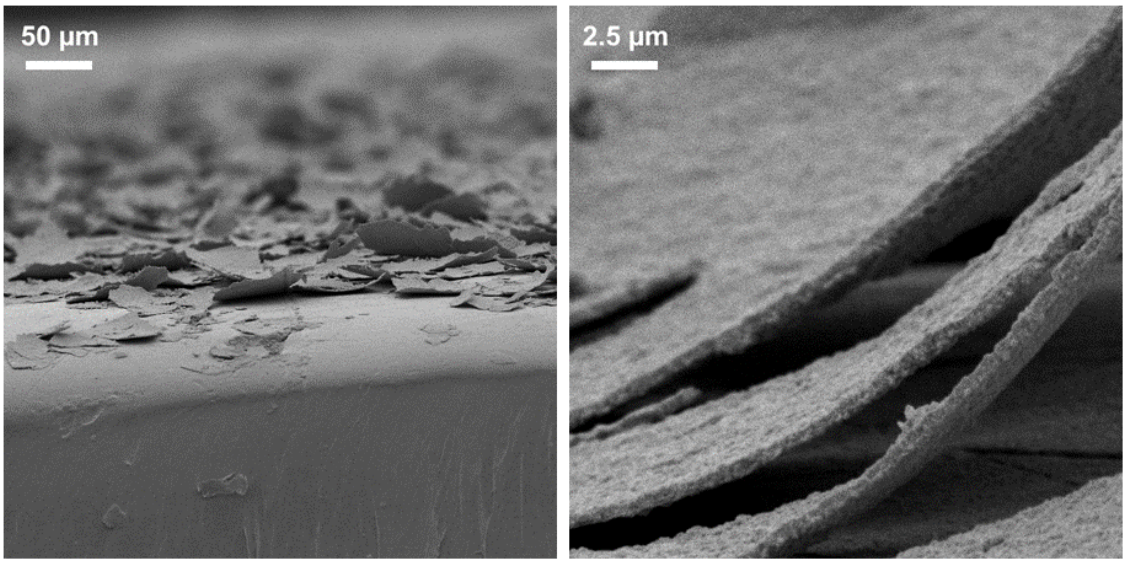

Figure 46: SEM micrographs of MOF-508 flakes on HDPE near the cutting edge. At low magnification (left) flakes of different orientations can be seen, while at high magnification (right) it is possible to measure the thickness of flakes. Images were captured jointly by PKE & VSB and cropped / evaluated by VSB.

By measuring the cross-sectional thickness of these MOF flakes in fifty places within seven SEM micrographs at a magnification of 10,000x, an average thickness of 544 ± 41 nm was determined. The histogram in Figure 47 shows the distribution of measured thicknesses.

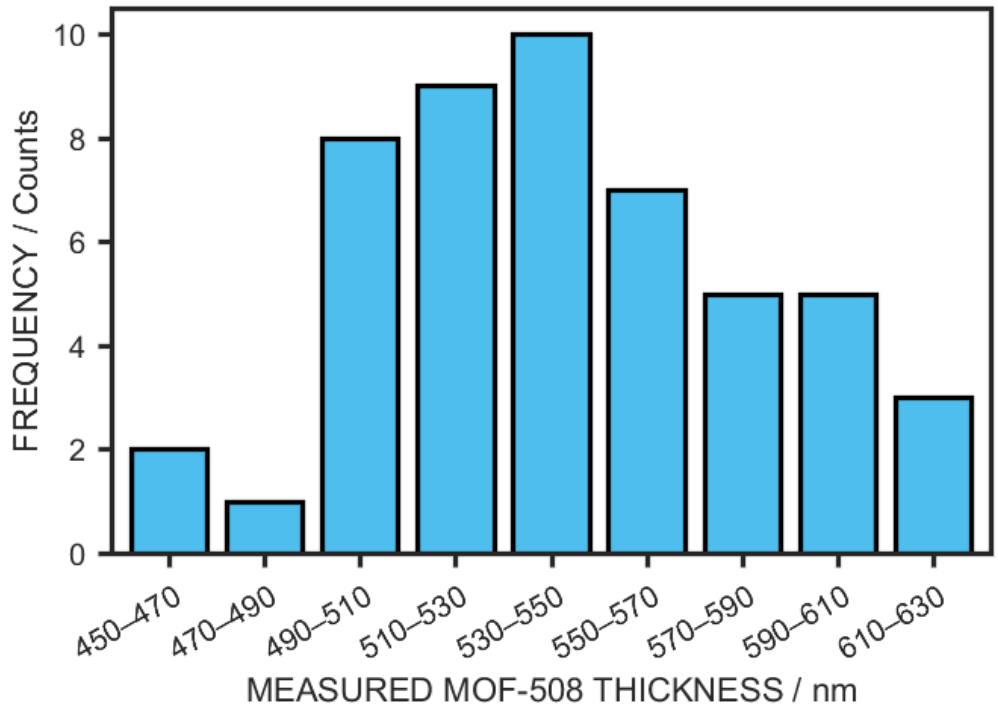

Figure 47: Histogram of MOF-508 thicknesses measured from seven SEM images at 10,000x magnification. Thicknesses were measured in fifty places on the edges of MOF flakes lifting up from the surface, as shown in Figure 46. Data measured & plotted by VSB based on SEM images captured jointly by PKE & VSB.

6.2.2 Investigating the MOF Growth Mechanism

Substrate Variation

Layer-by-layer growth of MOF-508 was tested on nine unfunctionalized substrates of different chemistry and morphology: high density polyethylene (HDPE), polypropylene (PP) film, non-woven polypropylene (PP) cloth, polyethylene terephthalate (PET), polyether sulfone (PES), paper, cotton cloth (woven), glass, and polytetrafluorethylene (PTFE). When comparing the infrared spectra of the substrates after MOF-508 growth to the spectra of pure substrates, the appearance of peaks around 1580 cm^{-1} and 1372 cm^{-1} indicated successful MOF growth on the surfaces, since these were the two most prominent MOF-508 absorbance peaks found previously (see Figure 42). The IR spectra of substrates where these peaks already appeared after 10 MOF growth cycles are displayed in Figure 48.

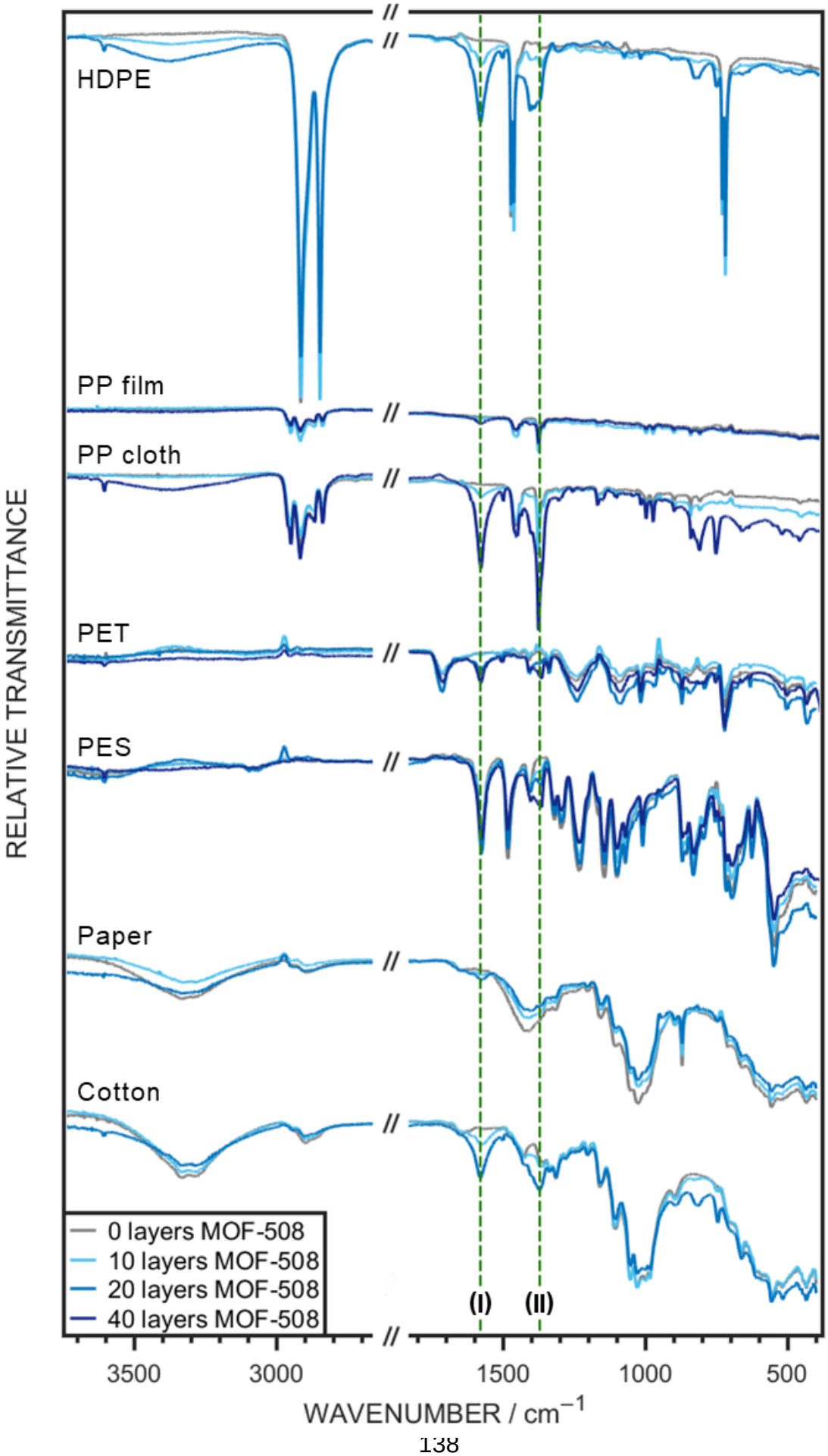
HDPE
PP film
PP cloth
PET
PES
Paper
Cotton
RELATIVE TRANSMITTANCE
0 layers MOF-508
10 layers MOF-508
20 layers MOF-508
40 layers MOF-508
(I)
(II)
3500
3000
1500
1000
500
WAVENUMBER / cm^{-1}

Figure 48 (previous page): Infrared spectra of MOF-508 grown on seven different untreated substrates: HDPE, PP film, non-woven PP cloth, PET, PES, paper, and cotton cloth. Each set of IR spectra includes one of the pure substrate (grey) and at least two spectra taken after growing different numbers of MOF-508 layers atop the substrates, as shown in the legend. Dashed lines at 1580 cm^{-1} (I) and 1372 cm^{-1} (II) indicate the characteristic MOF-508 peaks appearing on all substrates, showing successful MOF growth. Data was captured by PKE and plotted / evaluated by VSB.

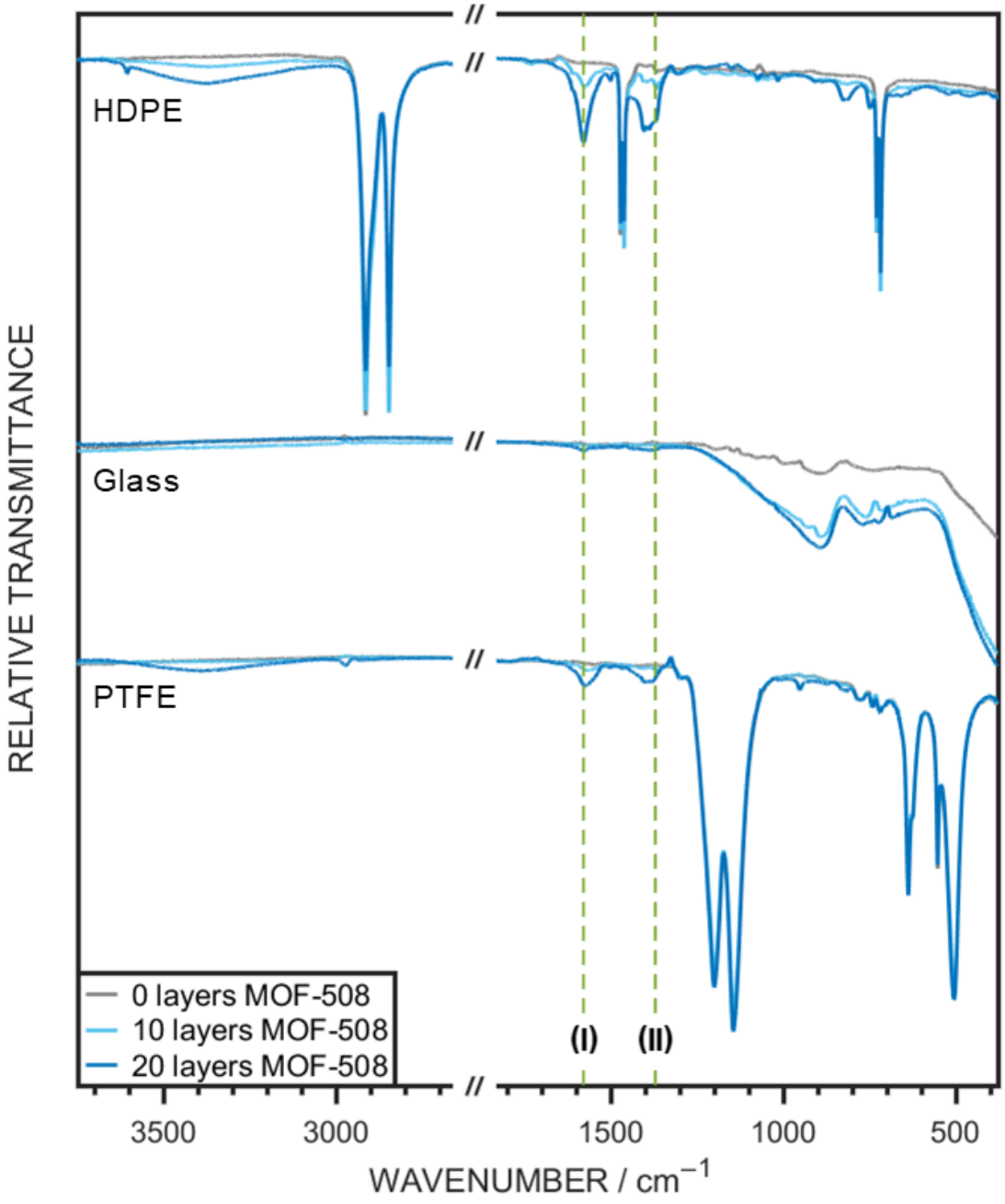

Figure 49: Infrared spectra of MOF-508 grown on three different untreated substrates: high density polyethylene sheet (same spectra as in Figure 48, included for comparison), glass, and PTFE. Each set of IR spectra includes one of the pure substrate (grey) and two spectra taken after growing 10 and 20 MOF-508 layers atop the substrates, as shown in the legend. Dashed lines at 1580 cm^{-1} (I) and 1372 cm^{-1} (II) indicate the characteristic MOF-508 peaks appearing on substrates with successful MOF growth. Data was captured by PKE and plotted / evaluated by VSB.

On all substrates apart from glass and PTFE, characteristic MOF peaks were already visible after 10 deposition cycles and their intensity increased with additional deposition. The peaks are easier to spot on some substrates than on others (for example, uncoated PES already possesses an absorbance peak at a similar wavelength range as MOF-508 peak I, Figure 48), but at least one of the two main MOF peaks is visible for all substrates in Figure 48 without interference from the spectrum of the underlying material.

For glass and PTFE, the MOF-508 absorbance peaks are not clearly visible after ten deposition cycles, yet after twenty cycles they begin to form, on PTFE more clearly than on glass. The smaller intensity of these peaks on these two substrates compared to all other used substrates indicates that MOF-508 grows more easily on some unfunctionalized surfaces than on others.

In addition to infrared spectroscopy, MOF-508 grown on a variety of substrates was also examined via scanning electron microscopy. Images of 20-layer SURMOF on eight different linker layer free substrates are compiled in Figure 50. Two different magnifications are displayed for each substrate, with one image giving an overview and the other showing a more detailed view of the MOF topography.

As discussed previously, flat HDPE and non-woven PP fibres are evenly coated with a MOF-508 layer. The SURMOF on HDPE is less clear to see than in Figure 45 and Figure 46 since the layer grown here is thinner and therefore less prone to cracking. However, compared to the scanning electron micrograph of plain HDPE (Figure 45) it is nevertheless clear that twenty deposition cycles led to a complete SURMOF coverage.

The MOF-508 grown on PET and PES sheets carries more separate crystallites on the surface than on HDPE. They appear similar to the crystallites atop 180-layer MOF-508 (Figure 45) but are more evenly spread.

Paper mainly consists of cellulose fibres but commercial office paper like the printing paper used here additionally contains calcium carbonate as filler for improved whiteness.[379,380] These agglomerates are clearly visible in SEM, even at low magnifications, Figure 50. At higher magnifications, the smaller MOF-508 crystallites become visible that coat both the fibres and the agglomerates.

On woven cotton cloth the SURMOF coating is easy to see due to small cracks caused by mechanical bending of the underlying material. The fibres are evenly coated with MOF-508 and the SURMOF appears topographically more similar to the one grown on 1-allylamine functionalized PP than on bare PP.

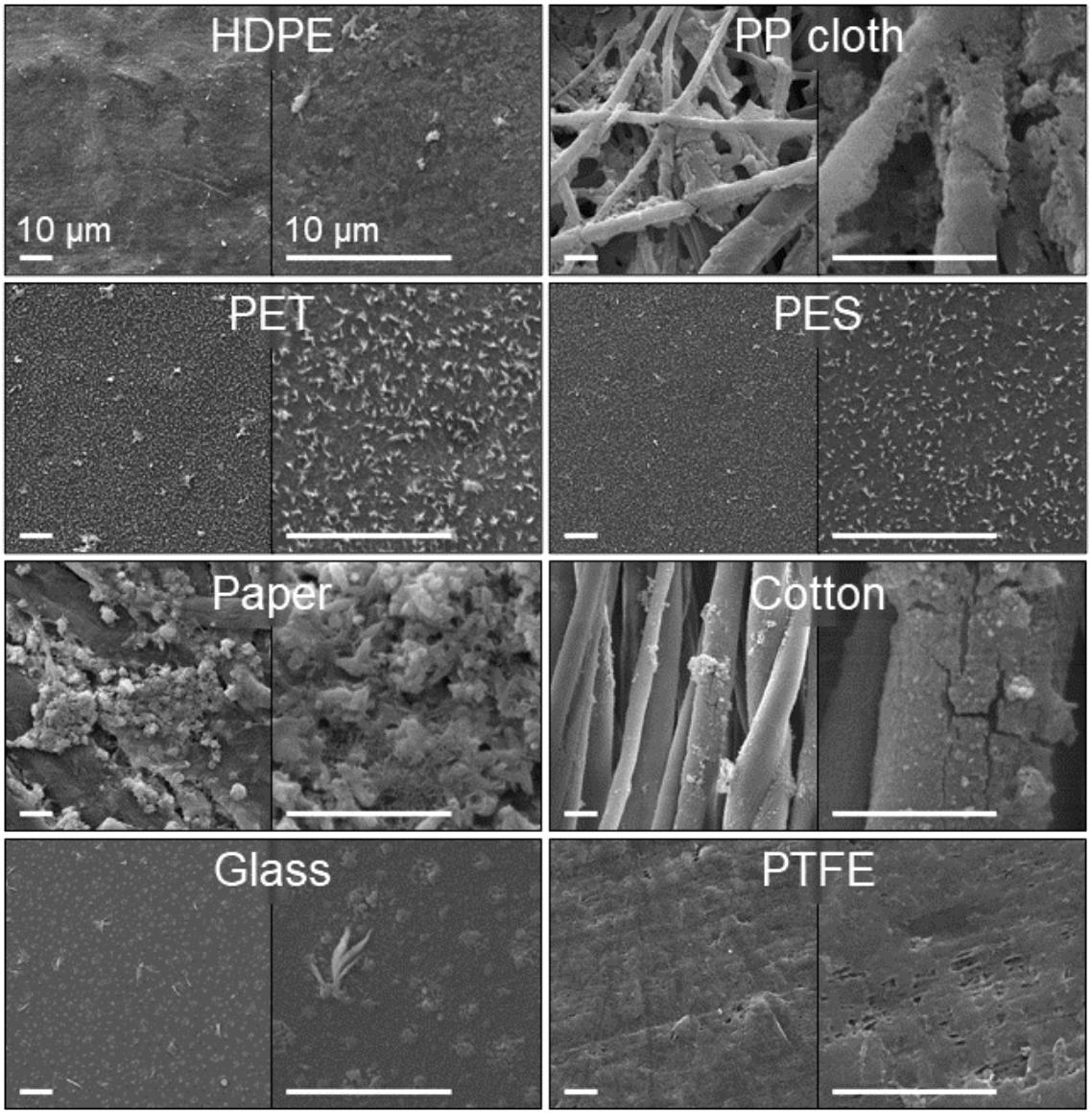

Figure 50: Scanning electron micrographs of 20 layers MOF-508 grown (or attempted to be grown) on different substrates: HDPE, PP cloth, PET, PES, Paper, Cotton, Glass, and PTFE. For each substrate two images at different magnifications are shown, with all scale bars representing 10 µm. Images were captured jointly by PKE & VSB and cropped / evaluated by VSB.

As seen from the infrared spectra (Figure 49), MOF-508 grows significantly more slowly on glass and PTFE than on the other used substrates. On the scanning electron micrographs taken after 20 deposition cycles one can see

sporadic small crystallites on glass that do not seem to form a continuous film. PTFE appears altogether bare of any SURMOF (in contrast to the clip area where MOF-508 did grow, see Figure 64).

On a transparent substrate like PES, the MOF-508 growth can even be seen macroscopically. After 40 deposition cycles, the previously clear polymer sheet appears opaque and white, Figure 51.

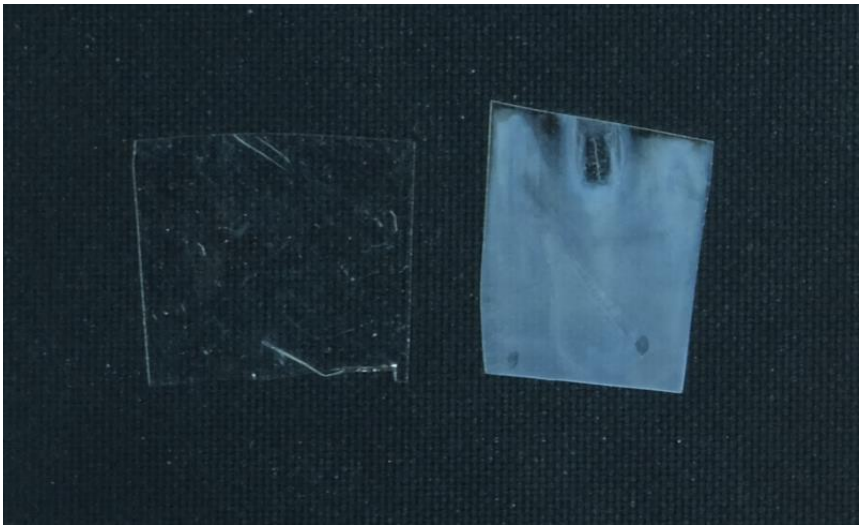

Figure 51: Plain PES (left) and 40-layer MOF-508 on PES (right). Each piece is about 1–1.5 cm wide. The originally clear substrate becomes opaque and white after SURMOF deposition. Near the top of the coated sample, an empty rectangle indicates the clip location. Photo was taken by VSB.

The successful growth of MOF-508 on such a variety of unfunctionalized surfaces raises questions about its nucleation mechanism. In the following sections, three mechanisms are investigated:

1) Substrate swelling due to solvent
2) Adsorption of 4,4'-bipyridine to substrate
3) Adsorption of metal to substrate

Solvent Variation

Tetrahydrofuran is known to cause swelling of polyethylene and polypropylene since it is used to extract additives from these polymers.[381] To investigate whether swelling and subsequent entrapment of reagents nucleates MOF-508 growth, ethanol was used as alternative solvent which is unreactive towards both polyethylene and polypropylene. Ethanol has previously also been used for the epitaxial synthesis of MOF-508, therefore it is known to be a suitable solvent for the reagents but non-solvating towards the MOF crystals.[359]

Comparing the infrared spectra of 20-layer MOF-508 synthesized on polyethylene from THF and ethanol, no major differences were spotted in peak position or intensity of the characteristic absorbance bands, Figure 52.

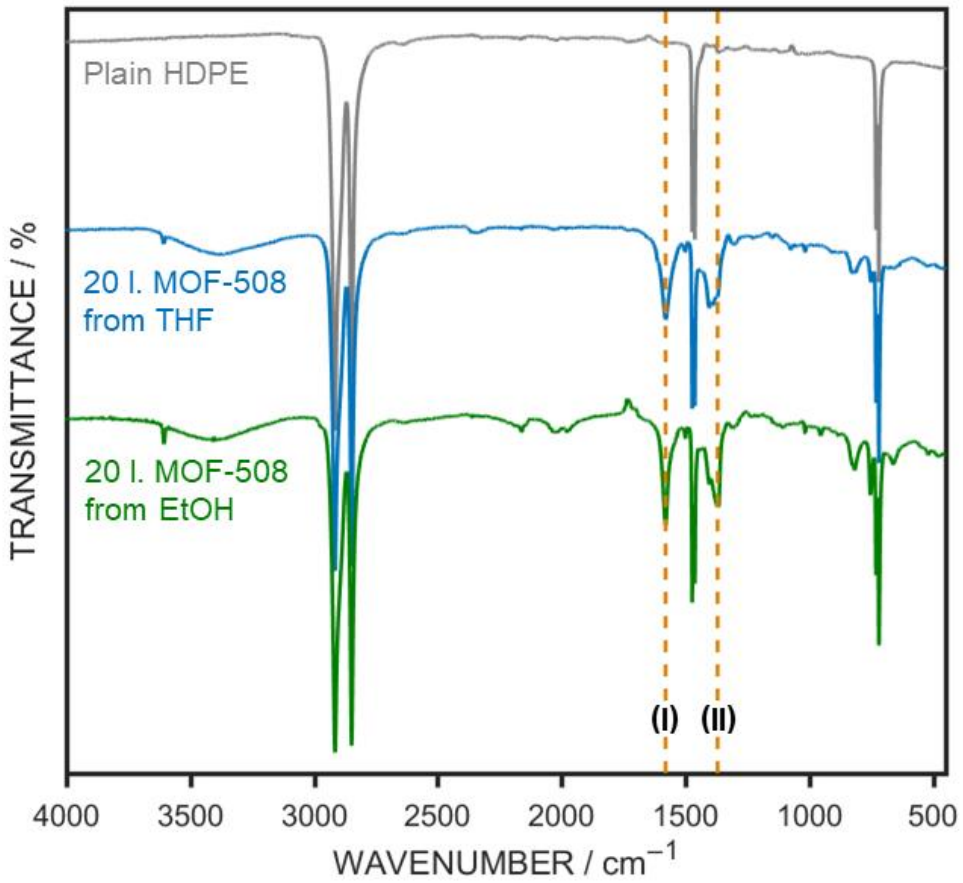

Figure 52: ATR–FTIR spectra of plain high-density polyethylene and 20-layer MOF-508 grown on it from different solvents. The two most intense characteristic MOF508 absorbance peaks are marked with dashed lines. Data was captured by PKE and plotted / evaluated by VSB.

From these infrared spectra, one can conclude that MOF-508 grows just as well from EtOH as from THF and that potential swelling of the substrate has no effect on the nucleation.

MOF-508 vs MOF-5

To test whether MOF-508 growth is nucleated by the adsorption of 4,4'-bipyridine to the substrate, a bipyridine-free MOF was deposited instead. MOF-5 was chosen as it consists of zinc metal centres and terephthalic acid linkers and is therefore nearly identical to MOF-508 save for the replacement of 4,4'-bipyridine pillars with further terephthalic acid, see Figure 53.

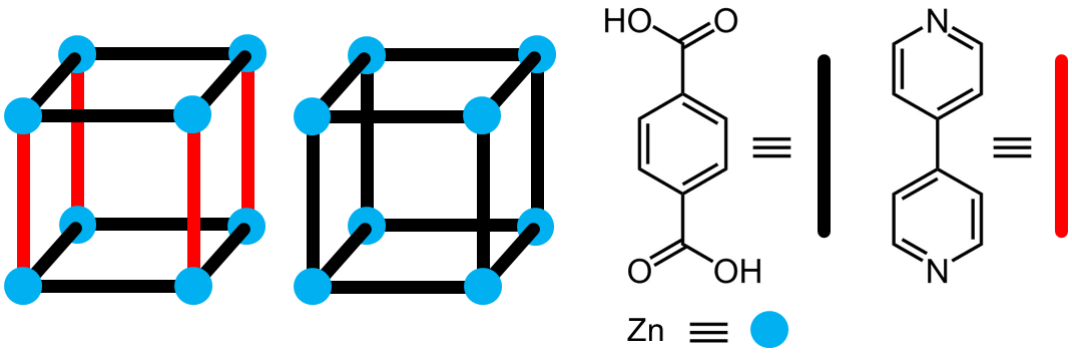

Figure 53: Schematic structures of (from left to right; lengths and angles not to scale) the unit cells of MOF-508 and MOF-5, and the respective organic linkers terephthalic acid (represented by black bars) and 4,4'-bipyridine (represented by red bars). Zinc metal centres of the MOFs are represented with blue spheres. Both MOFs consist of layers formed from zinc and terephthalic acid that are bridged by 4,4'-bipyridine pillars in the case of MOF-508 and by further terephthalic acid in the case of MOF-5.

After deposition of MOF-5 on high-density polyethylene for ten or twenty cycles, the infrared spectra of the substrates appeared very similar to those of MOF-508, Figure 54 a. However, small differences can be found when examining the low wavenumber range in comparison with the linker spectra, Figure 54 b. Near the quadrant stretch absorbance of 4,4'-bipyridine at 1587 cm^{-1} (peak I in Figure 42, marked by dashed line in Figure 54 b), a characteristic peak it does not share with terephthalic acid, one of the main characteristic MOF-508 absorbance peaks is located which contains contributions from the aforementioned quadrant stretch absorbance as well as from asymmetric

stretching of the COO^- groups of deprotonated terephthalic acid. While this peak also appears in the MOF-5 infrared spectrum, it is noticeably narrower, both after ten and twenty deposition cycles. This difference can be explained by the absence of the 1587 cm^{-1} quadrant stretch contribution since MOF-5 does not contain 4,4'-bipyridine.

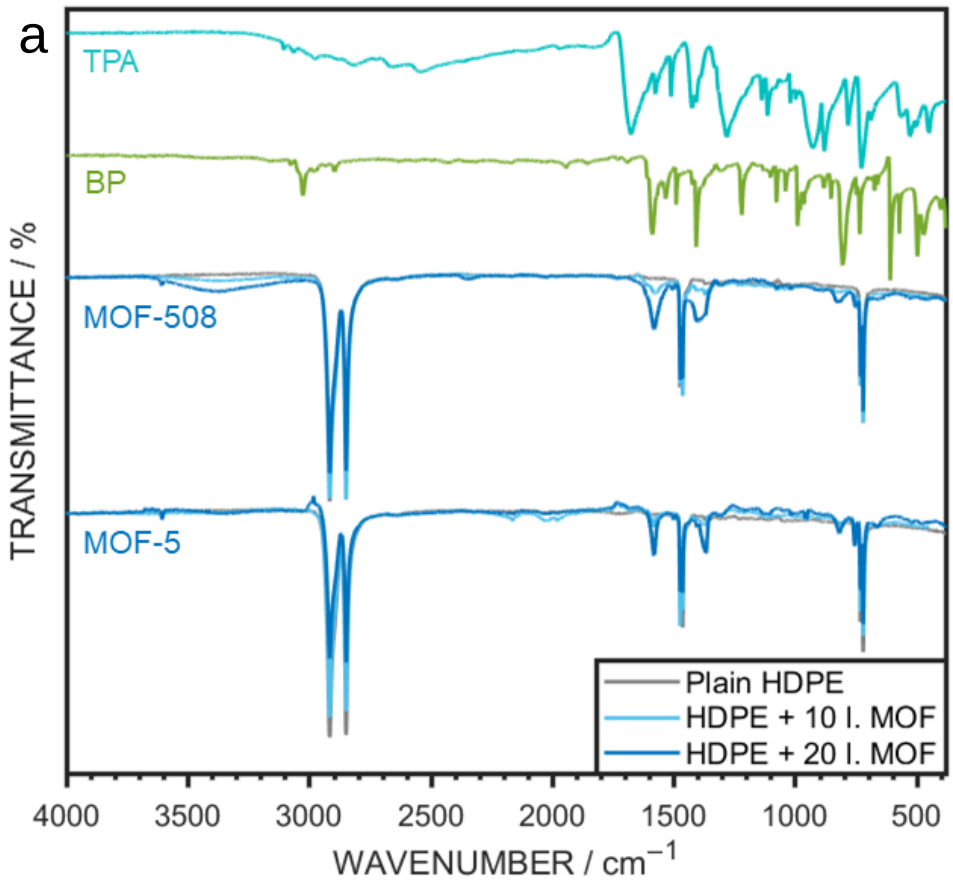

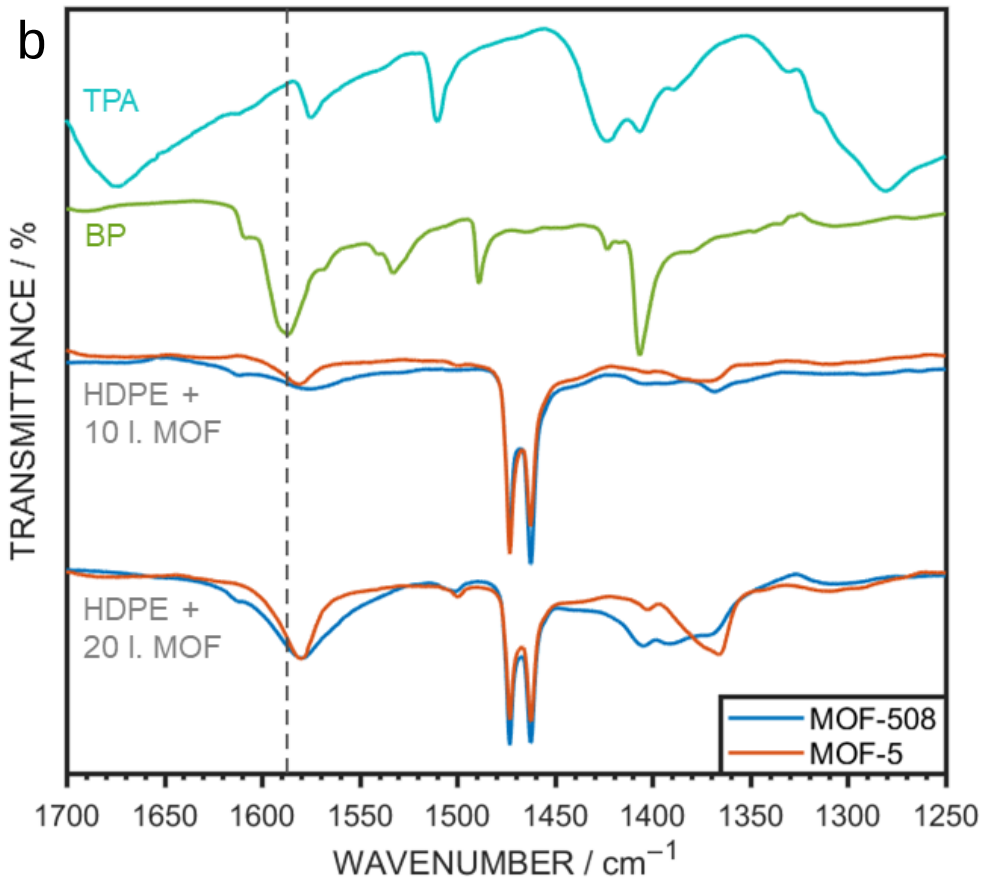

Figure 54: Infrared spectra of 10- and 20-layer MOF-508 and MOF-5 grown on HDPE, as well as infrared spectra of the linkers terephthalic acid (TPA) and 4,4'-bipyridine (BP). Overview a: The spectra of both SURMOFs look very similar with differences caused by the lack of 4,4'-bipyridine in MOF-5 only becoming more evident under closer inspection. Low wavenumber region b: Because MOF-5 does not contain 4,4'-bipyridine linker, the contribution of the quadrant stretch absorbance peak at 1587 cm^{-1} (dashed line) is missing from the MOF-5 infrared spectra, resulting in a narrower peak in the 1565–1600 cm^{-1} region compared to the spectra of MOF-508. Data was captured by PKE and plotted / evaluated by VSB.

Overall, the obtained infrared spectra of MOF-5 appear very similar to those found in the literature[382], indicating its successful growth, which means that 4,4'-bipyridine adsorption to the substrate cannot be the main cause of nucleation.

Component Adsorption

To investigate the MOF-508 nucleation on HDPE in comparison with PTFE, the adsorption of the linkers and of zinc acetate on the substrates after dipping into the respective solutions and subsequent rinsing was analysed via XPS. The theoretical compositions of all involved compounds are listed in Table 10, with the experimentally determined compositions collated in Table 11.

Table 10: Theoretical XPS compositions for HDPE, PTFE, zinc acetate, the MOF linkers 4,4'-bipyridine and terephthalic acid, and the solvent THF.

	Composition / atom %				
Compound	**C**	**F**	**N**	**O**	**Zn**
HDPE	100	–	–	–	–
PTFE	33	67	–	–	–
Bipyridine	83	–	17	–	–
Terephthalic acid	67	–	–	33	–
Zinc acetate	44	–	–	44	11
THF	80	–	–	20	–

Table 11: Experimentally determined XPS compositions for HDPE and PTFE substrates after dipping into linker or zinc acetate solutions and subsequent THF rinsing and drying. Data was captured by HJC and evaluated by VSB.

	Composition / atom %				
Substrate	**C**	**F**	**N**	**O**	**Zn**
HDPE + linker solution	82.9 ± 0.5	0.0	4.1 ± 1.9	13.0 ± 1.4	0.0
PTFE + linker solution	35.4 ± 2.6	63.7 ± 2.9	0.0	0.9 ± 0.4	0.0
HDPE + ZnAc solution	84.5 ± 6.5	0.0	1.8 ± 2.5	12.5 ± 3.5	1.2 ± 0.5
PTFE + ZnAc solution	34.5 ± 2.5	65.5 ± 2.5	0.0	0.0	0.0

XPS analysis of HDPE dipped in linker solution shows the presence of nitrogen and oxygen on the surface, indicating the adsorption of both bipyridine and terephthalic acid to the substrate. In fact, one can calculate from the

composition that the investigated surface consists of about 37% HDPE, 24% 4,4'-bipyridine, and 39% terephthalic acid.

On the other hand, PTFE dipped in linker solution did not carry any nitrogen and only very little oxygen on the surface. Calculations showed that the best approximation is that the surface consists of 95% PTFE and 5% THF solvent. There are reports in the literature that THF can lead to some swelling in PTFE depending on the crystallinity[383], therefore it is possible that in this case a small amount of solvent was absorbed by the polymer and led to the presence of oxygen within the investigated surface.

After dipping in zinc acetate solution, XPS analysis of HDPE showed the presence of both zinc and oxygen on the surface, indicating successful zinc acetate adsorption. Since the oxygen content of the surface is larger than expected from the zinc acetate contribution (based on the zinc content), it is possible that some THF solvent was additionally absorbed into the HDPE, leading to swelling. The small amount of nitrogen that was merely detected in one sample was likely only caused by contamination.

Finally, XPS analysis of PTFE dipped in zinc acetate solution detected no zinc or oxygen on the surface and the elemental composition found was nearly identical to the theoretical composition of pure PTFE, within error margins.

From these analysis results we can conclude that both zinc acetate and the linkers can adsorb to HDPE. Since substrates are first dipped into zinc acetate solution during MOF-508 deposition, it is likely that this step provides the initial nucleation for further SURMOF growth. It has previously been shown that zinc adsorbs equally well to various polymers such as HDPE, PP, and PET,[384] which explains successful MOF synthesis on a wide range of substrates. On the other hand, none of the components adsorbed to PTFE, which matches the IR and SEM observations that indicate very slow and sporadic MOF-508 growth on unfavourable surfaces.

6.2.3 Transfer of MOF Thin Films

Tape transfer

Taking inspiration from the synthesis of atomically thin graphene[385], a thin film of MOF-508 was lifted from the HDPE substrate it was synthesized on by placing adhesive tape onto the MOF-covered HDPE sheet and applying pressure before gently peeling the tape away. Scanning electron micrographs of the original 200-layer SURMOF before and after removal from HDPE are shown in Figure 55.

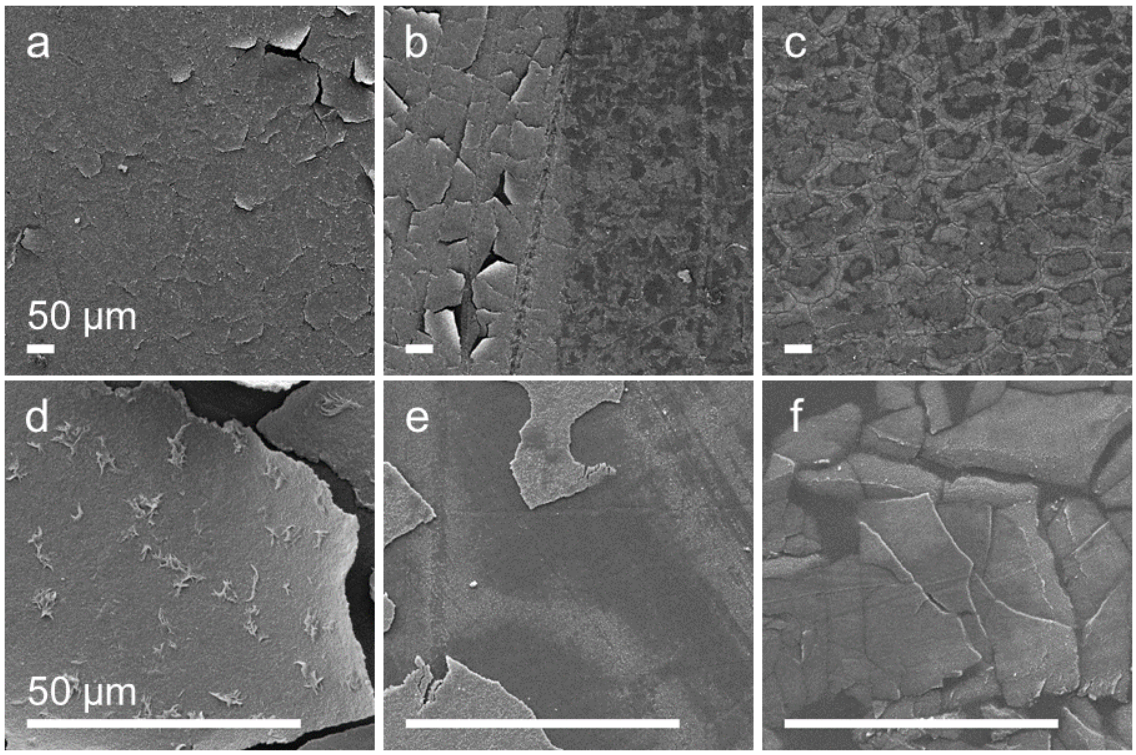

Figure 55: Scanning electron micrographs of 200 layers MOF-508 grown on HDPE and transferred onto tape; a, d: SURMOF on HDPE; b: border region on HDPE with SURMOF on the left and area after SURMOF lift-off via tape on the right; e: HDPE after SURMOF lift-off; c, f: tape carrying MOF-508 removed from HDPE surface. All scale bars represent 50 µm. Images were captured jointly by PKE & VSB and cropped / evaluated by VSB.

When grown on HDPE, MOF-508 formed a continuous layer as found previously, with scattered crystallites atop, Figure 55 a, d. Cracks in the layer are caused by bending of the underlying substrate and help to visually confirm the presence of the SURMOF. At the border of the area where the MOF was removed

from the HDPE substrate via tape (Figure 55 b), the difference between both regions is clear to see with a cracked MOF layer covering the area on the left while the area on the right takes on a patchy appearance. Under closer inspection (Figure 55 e), it becomes apparent that while the SURMOF was completely removed from HDPE in many places, a pattern of islands remains, indicating that the MOF layer was not entirely lifted off. On the tape, the transferred MOF-508 appears even more cracked that on HDPE, which is no surprise given how much easier the tape bends. When looking at the higher magnification image of MOF on tape, Figure 55 f, it is unclear whether a continuous SURMOF layer was lifted from HDPE or whether the floe-like MOF pieces are separated from each other. However, one can clearly see that most of the tape surface is covered with MOF, which shows the success of this lift-off technique.

The infrared spectrum of MOF-508 on tape is compared to the SURMOF spectrum in Figure 56.

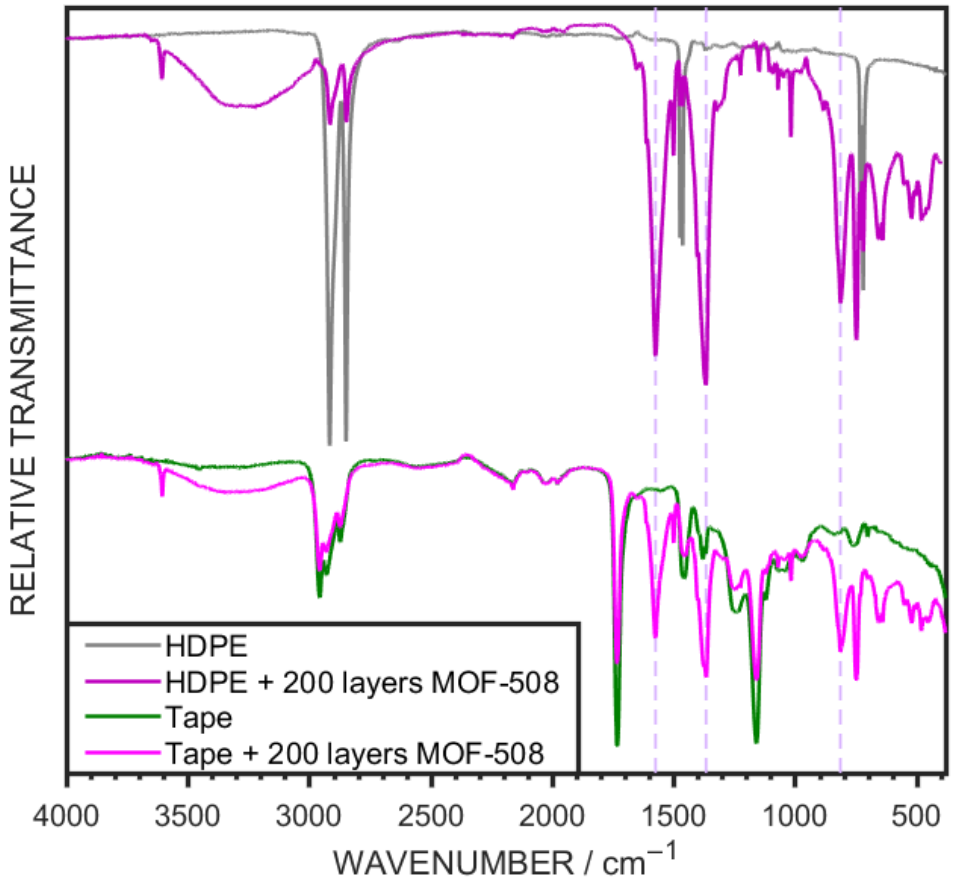

Figure 56: ATR-FTIR spectra of plain HDPE, 200 layers MOF-508 grown on HDPE, Scotch tape, and the same tape after using it to peel the 200 layers MOF-508 off the HDPE. Three of the most characteristic MOF-508 absorbance peaks are marked with

dashed lines, indicating that the MOF was successfully picked up by the tape. Data was captured by PKE and plotted / evaluated by VSB.

Characteristic MOF-508 absorbances as seen in the spectrum of MOF-508 on HDPE appeared at the same positions and with the same intensities relative to each other in the spectrum of MOF-508 on tape, indicating successful transfer. The lower overall intensity of the characteristic MOF-508 absorbance peaks on tape may indicate that the SURMOF was not completely lifted off, although these intensities can depend on the underlying substrate.

Powder-XRD diffractograms of the tape further confirmed the presence of MOF-508 in the same conformation as grown on HDPE, namely mostly well-oriented MOF-508a with some unoriented MOF-508b contributions, Figure 57. As with infrared spectra, the peaks for MOF-508 on tape were less intense than on HDPE.

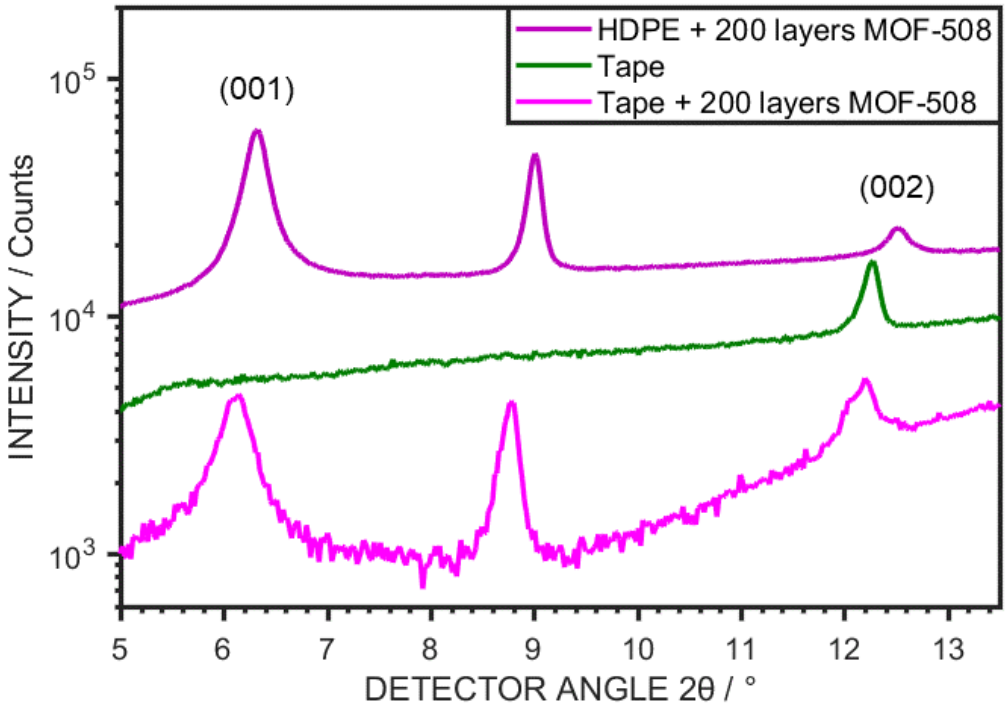

Figure 57: Powder-XRD spectra of 200 layers MOF-508 grown on HDPE, Scotch tape, and the same tape used to peel the MOF off the HDPE. The presence of characteristic MOF (001), non-oriented, and (002) peaks shows the successful transfer of MOF-508 onto the tape. Data was captured by HJC and plotted / evaluated by VSB.

Thermal Release Sheet Transfer

After showing that MOF thin films could be removed from their growth substrate using adhesive tape, the next logical step was to remove the tape from the MOF. This would facilitate the transfer of thin MOF films onto any substrate regardless of whether MOF films can grow on that substrate. Thermal release sheet was used to transfer thin films of MOF-508 from growth substrates such as HDPE onto glass microscopy slides. As with MOF growth on transparent polymers (Figure 51), successful transfer could be verified instantaneously by the appearance of a white coating on the transparent glass, Figure 58.

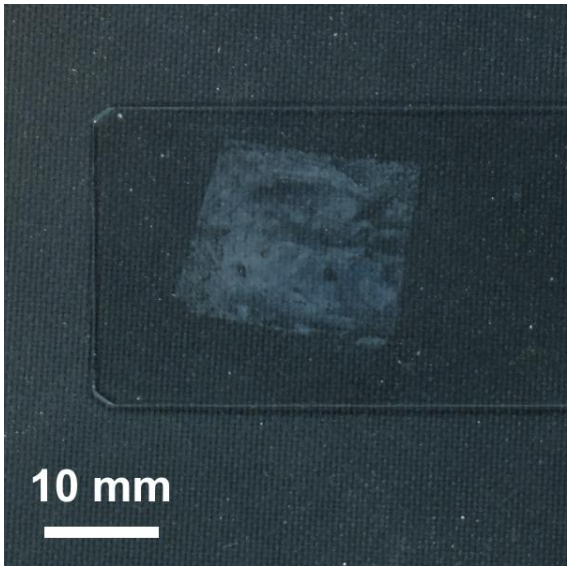

Figure 58: Photograph of 40-layer MOF-508 transferred from HDPE onto a glass microscopy slide via thermal release tape. The appearance of a white coating on the transparent glass indicates successful MOF transfer. Photo was taken by VSB.

The presence of MOF-508 on the glass slide was furthermore confirmed via XRD spectroscopy and scanning electron microscopy. Compared to plain glass, the XRD spectrum of the transferred MOF clearly shows a MOF-508a (001) peak at the same detector angle as observed previously (Figure 44), as well as a small peak for unoriented MOF-508b and a (002) peak of MOF-508a, Figure 59.

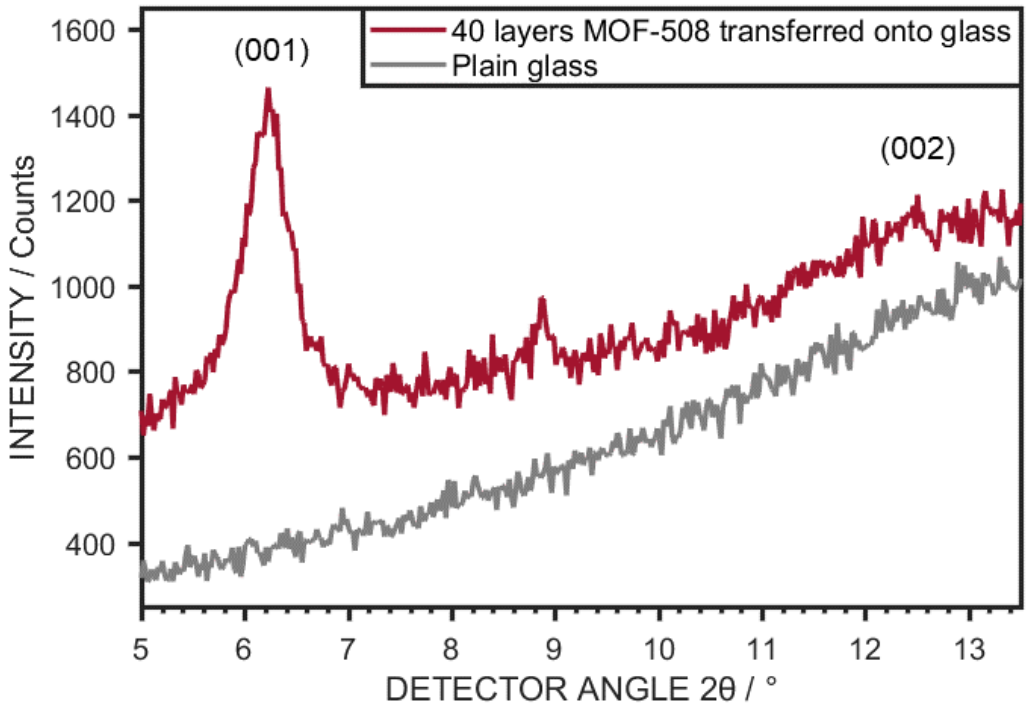

Figure 59: XRD spectra of 40 layers MOF-508 transferred onto plain glass via thermal tape compared to plain glass. Data was captured by HJC and plotted / evaluated by VSB.

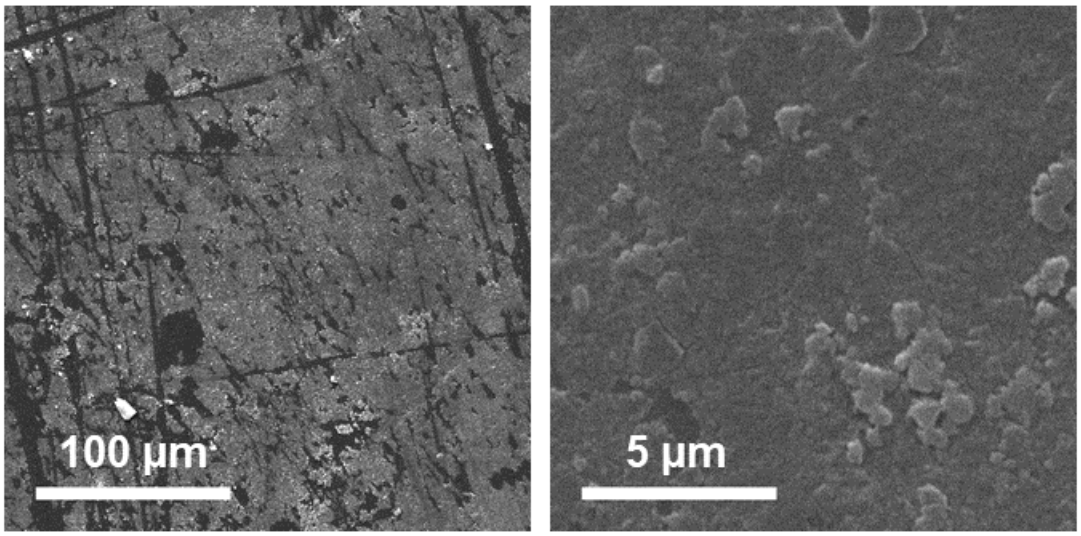

Figure 60: Scanning electron micrographs of 40-layer MOF-508 transferred from HDPE onto a glass microscope slide via thermal release tape. Images were captured jointly by PKE & VSB and cropped / evaluated by VSB.

From the scanning electron micrographs of transferred MOF-508 one can see that while most of the surface is covered in MOF, the layer is interrupted by numerous scratches, Figure 60. These scratches were likely caused by the

tweezers used to apply pressure to the thermal release tape during transfer and could be prevented if a more uniform method of applying pressure was used. The transferred MOF-508 on glass appears less cracked than on regular tape since the thermal release tape is more rigid, which is very promising for achieving complete MOF transfer.

6.3 Discussion

6.3.1 MOF-508 on Linker Layer Free Surfaces

The results evaluated above show that MOF-508 was successfully synthesized on a variety of polymer substrates with no additional linker layer required. The SURMOF was characterized via infrared spectroscopy, X-ray photoelectron spectroscopy, and scanning electron microscopy, and comparisons with MOF-508 grown on poly(1-allylimidazole) coated substrates (both in the literature and in this work) showed that such a linker coating is in fact not necessary for the MOF to grow on polymer substrates like HDPE and PP.

While IR spectroscopy revealed that the two linker components were successfully incorporated in the MOF, XRD spectroscopy further confirmed its crystal structure. Compared to the theoretical peak positions of solvent-inclusive MOF-508a and solvent-free MOF-508b it was clear that the synthesized SURMOF is mostly highly oriented MOF-508a with the layers formed from terephthalate linkers running parallel to the surface, since no (100) or (010) peaks were detected. Furthermore, the height ratio between the intense (001) and weak (002) peaks indicated the formation of an interpenetrated MOF-508a network as in the non-interpenetrated version destructive interference leads to a reversal of the intensity ratio.[359,363] Thus, the MOF-508 grown on linker layer free HDPE was more structurally similar to MOF-508 grown on poly(1-allylimidazole) than MOF-508 grown on 4-pyridyl-terminated self-assembled monolayers.[359,363]

Unlike the cases of surface-mounted MOF-508 described in the literature, here the MOF was for the first time successfully synthesized on a variety of substrates carrying no specific functional groups. The surprising fact that highly oriented MOF-508 can be synthesized on linker layer free surfaces raises many

questions about the nucleation and growth mechanism which will be discussed in the following sections.

6.3.2 MOF-508 Nucleation

In past examples of epitaxial MOF-508 synthesis the supporting substrates were first coated with functional groups that mimicked the functional groups of the bipyridine linker to provide adsorption sites for the zinc and facilitate MOF growth.[359,363] As MOF-508 was now shown to grow on unfunctionalized surfaces, the nucleation mechanism was investigated through a series of experiments, as summarized in Table 12.

Table 12: Summary of experiments conducted to determine the nucleation mechanism of MOF-508 on linker layer free HDPE.

Suspected nucleation mechanism	**Experiment**	**Result**
Substrate swelling by THF	Ethanol solvent instead of THF	✗: Synthesis successful from both solvents
4,4'-bipyridine adsorption	Comparison between MOF-508 and MOF-5	✗: Successful MOF-5 synthesis on HDPE
General component adsorption	XPS analysis of substrates dipped once into solutions	✓: Components found on HDPE, but not on PTFE

Initial SURMOF epitaxial synthesis was performed using THF as solvent, as reported for MOF-508 synthesis on poly(1-allylimidazole).[363] In order to test whether swelling of the polymer substrates by THF and subsequent component entrapment lead to MOF nucleation, the synthesis was instead performed using ethanol as solvent, which has also been reported in epitaxial MOF-508 synthesis. The results (Figure 52) showed no difference between MOF-508 on HDPE grown from THF or ethanol, thus indicating that potential substrate swelling has no influence on MOF nucleation.

Since the synthesized MOF-508 is highly oriented with the layers formed by terephthalic acid running parallel to the substrate, another theory for a possible nucleation mechanism was the adsorption of 4,4'-bipyridine molecules via one of their functional groups, which would lead to their perpendicular orientation to the substrate, like their orientation within the resulting SURMOF. To test MOF growth on linker layer free HDPE in the absence of 4,4'-bipyridine, MOF-5 (a MOF with zinc metal centres that are only connected by terephthalic acid linkers, see Figure 53) was epitaxially synthesized in the same way as MOF-508. However, FTIR spectra indicated that MOF-5 grew just as well on linker layer free HDPE as MOF-508 (see Figure 54), meaning that 4,4'-bipyridine adsorption alone cannot explain MOF nucleation.

Finally, the adsorption of all MOF-508 components to a substrate after one dip into either the metal or linker solution was investigated using XPS. Here, linker layer free HDPE and PTFE were used as substrates since MOF-508 was found to grow well on HDPE but not on PTFE. From the resulting surface compositions, it was found that zinc (acetate) and both linkers adsorb to HDPE but not to PTFE (see section 0, Table 11). Since during fabrication the substrates are first dipped into zinc acetate solution, it is likely that MOF-508 nucleation begins with random adsorption of zinc cations to the substrate through unspecific van der Waals interactions which provides seeding sites for further MOF-508 growth. Zinc adsorption to a variety of polymers including HDPE, PP, and PET has been reported in the literature[384], which helps to explain why MOF-508 was successfully synthesized on many different substrates. Despite the random nucleation, highly ordered MOF-508 can grow on linker layer free substrates, showing that the epitaxial synthesis method is sufficient to lead to oriented growth; a specifically functionalized substrate is not necessary.

6.3.3 Growth Mechanism on the Molecular Scale

When measuring the thickness of MOF-508 grown for 200 cycles through the cross-section of SURMOF flakes via scanning electron microscopy (see 0), an average value of 544 ± 41 nm was found. Based on the MOF-508a cell parameters found in the literature with $c = 14.12$ Å and $\gamma = 78.38°$,[358,378] the theoretical thickness of one MOF-508a layer would be 13.83 Å, meaning that a

thickness of 276.6 nm would be expected for 200 layers. The experimentally determined thickness is however almost exactly twice as large.

Various factors could have led to this result. On one hand, the thickness may have appeared inflated due to measuring errors. It is unclear whether the cross-sectional surface of the flakes, whose height was measured, was in fact perpendicular to the MOF surface—any other angle would lead to the thickness appearing larger than it truly is. However, measuring errors alone cannot account for the large experimentally determined thickness, since even the smallest measured thickness was still 66% larger than expected.

Cases of epitaxially grown SURMOF resulting in larger thicknesses than expected have been reported in the literature though the mechanism is not yet fully understood.[386,387] In the present case, one jar of solvent was used to rinse the substrates after both the metal and linker dipping steps. While the solvent was replaced after every ten growth cycles, it is still possible that a few zinc (acetate) or linker molecules were unintentionally attached to the substrates during rinsing. Such contamination could be avoided by using two separate rinsing solutions. SURMOF growth of more than one layer per cycle could also occur if additional component molecules become trapped within the MOF pores and are thus transported into the other dipping solution.[388] Such a mechanism is however unlikely for intercalated MOF-508 where the pore diameter is barely larger than a methane molecule.[358] Finally, it can also be possible for more linkers than required to adsorb to the surface during the linker solution dipping step.[389] Particularly molecules with carboxylic acid and pyridine functional groups (such as the linkers used for MOF-508) can form adducts held by strong hydrogen bonds in solution.[390,391,392] Figure 61 illustrated schematically how the free ends of 4,4'-bipyridine pillars could form dimers with terephthalic acid molecules, thus holding those additional linker molecules on the substrate. In the following metal solution dipping step, these linker molecules can then be rearranged to lead to the formation of more than one MOF layer, Figure 61 d–f.

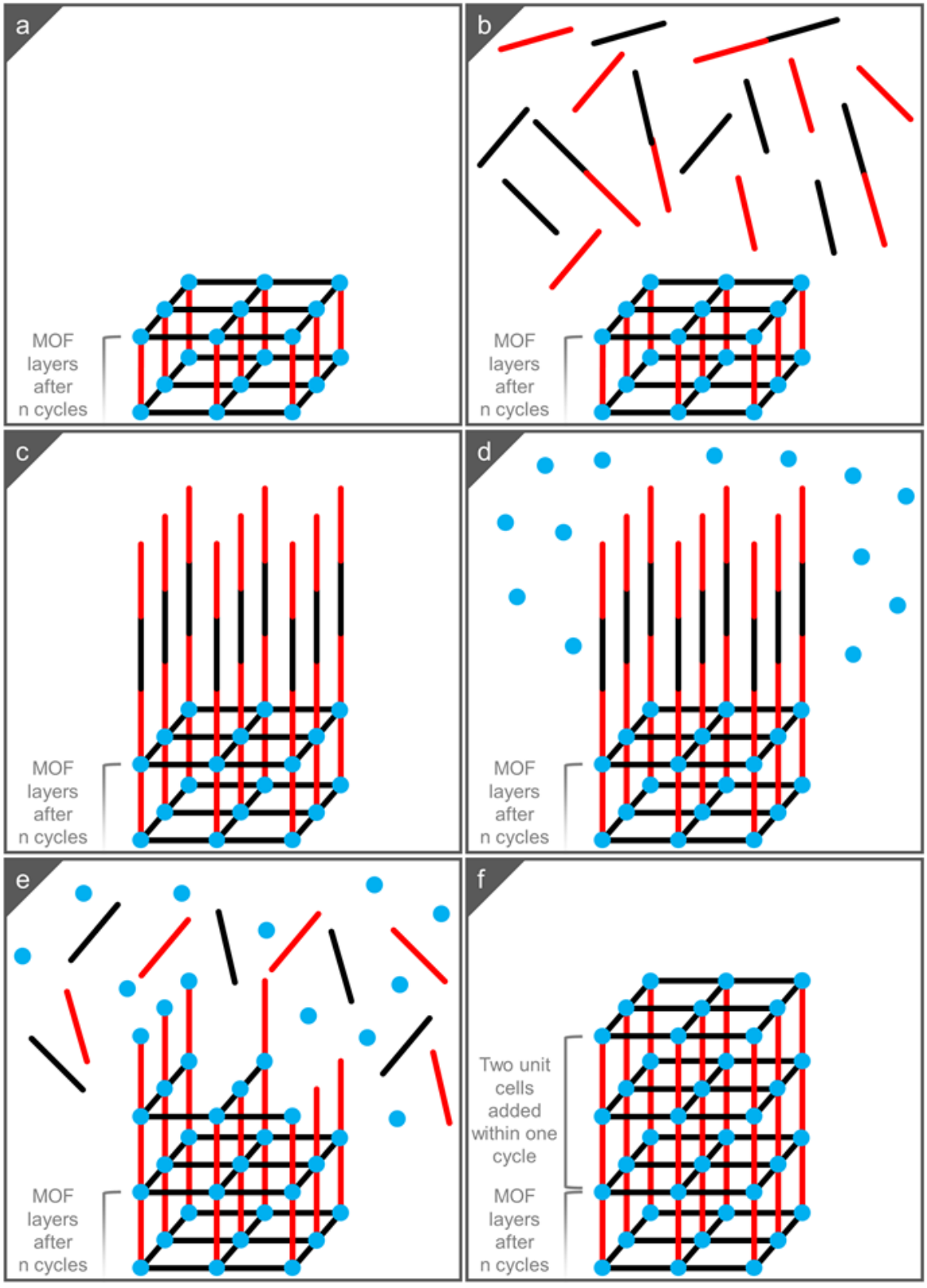

Figure 61: Schematic mechanism through which the growth of more than one unit cell layer per MOF growth cycle is possible; blue dots represent zinc clusters / zinc acetate in solution, black bars terephthalate / terephthalic acid in solution, and red bars 4,4'-bipyridine. Dimensions and angles are not to scale; MOF-508 possesses a triclinic crystal structure with two interpenetrated networks whereas only one is shown here for simplicity. Steps: a) surface-attached MOF-508 after Zn dipping and rinsing steps of previous growth cycle; b) SURMOF dipped into linker solution where linkers can exist as single

molecules or dimers through hydrogen bonding; c) adsorption of 4,4'-bipyridine to zinc centres to form next layer of pillars while further terephthalic acid and 4,4'-bipyridine molecules can be attracted to each other's end groups through hydrogen bonding; d) dipping of SURMOF with additional linker molecules into zinc acetate solution exposes them to each other; e) zinc centres are incorporated into the new SURMOF layer while additional linker molecules can coordinate on top of the newly incorporated zinc centres and offer up even more coordination options; f) completed formation of two MOF-508 unit cell layers within one growth cycle.

6.3.4 Growth Mechanism on the Crystal Scale

On the crystal scale, three main mechanisms of crystal growth have been identified in the literature. Which mechanism the growth of a crystal follows depends on the specific surface energies of the underlying substrate (σ_u) and the crystal (σ_c), as well as their interface energy (σ_i), which together influence the change of surface energy ($\Delta\sigma = \sigma_c + \sigma_i - \sigma_u$) that occurs during the formation of a crystal layer.[393,394]

When $\Delta\sigma > 0$, crystallite islands form independently from each other on the substrate and each grow three-dimensionally.[393,394,395] This mechanism is known as Volmer–Weber growth and has been observed for different surface-attached metal organic frameworks, including MOF-508.[363,396] It leads to the formation of a very rough surface with incomplete crystal coverage, though as the crystallite islands grow, they can also fuse together.

In theory, epitaxially synthesized SURMOFs are usually thought to grow in thin 2D layers whose thickness increases with each deposition cycle; such a morphology has also been observed in numerous cases, once again including MOF-508.[359,362,397,398] This mechanism is known as Frank–van der Merwe growth which usually occurs when $\Delta\sigma \leq 0$ and when the lattice mismatch between crystal and substrate is small.[393,394,399,400] While this layered crystal growth is easy to picture, in reality a perfect Frank–van der Merwe growth is very difficult to accomplish, since $\Delta\sigma \leq 0$ needs to be fulfilled for every layer while the parameters σ_u and σ_i are replaced by the specific surface energy of the previous crystal layer and the interface energy between the previous and the new crystal layers, respectively. Through the influence of the underlying substrate, the specific surface energy of attached crystal layers will initially be similar to that of the substrate but with each layer gradually become more similar to that of the bulk

crystal.[393] It is therefore extremely unlikely for Frank–van der Merwe growth to occur up to extreme thicknesses if a crystal and the substrate it is grown on are not made from the same material.

The intermediate case of crystals that initially form Frank–van der Merwe type layers but switch to a Volmer–Weber type island growth after reaching a critical thickness is called Stranski–Krastanov growth. It occurs when $\Delta\sigma < 0$ and the lattice mismatch between crystal and substrate is large.[393,394,401] While not explicitly named as such, there are SURMOFs in the literature that appear to have grown following a Stranski–Krastanov mechanism.[402,403] All three mechanisms are schematically illustrated in Figure 62.

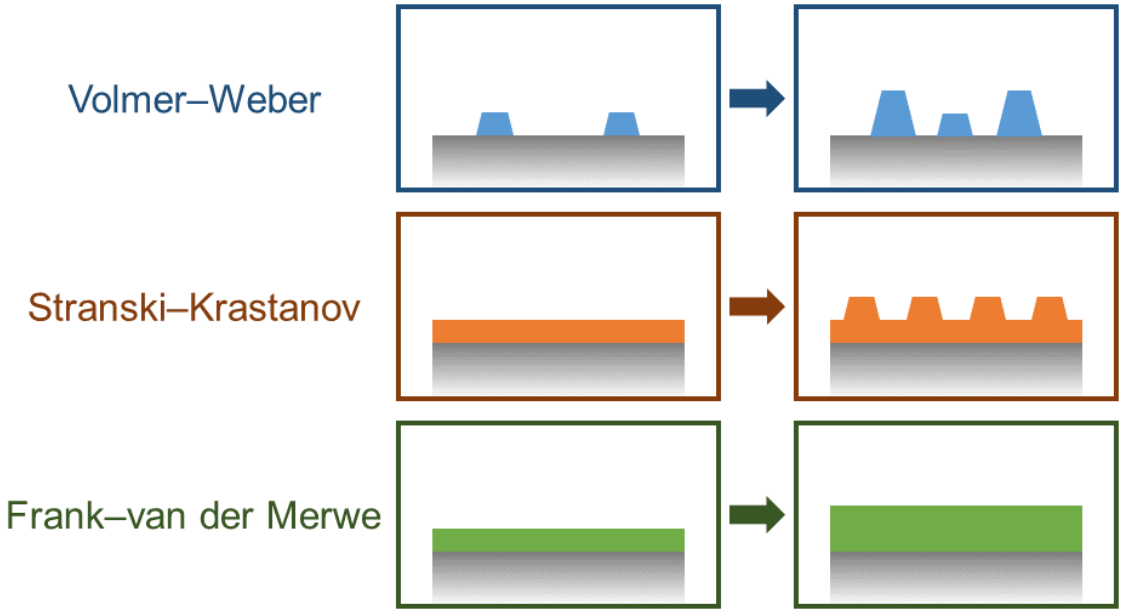

Figure 62: Schematic illustrations of the three main mechanisms of crystal growth. Volmer–Weber: nucleation of crystallite islands that each grow over time. Stranski–Krastanov: initial film growth that switches to island growth at a critical thickness. Frank–van der Merwe: pure film growth. The critical thickness where a Stranski–Krastanov growth switches from being similar to a Frank–van der Merwe growth to becoming like a Volmer–Weber growth depends on the crystal material and surface, meaning that the Stranski–Krastanov mechanism covers all intermediate cases that lie between the Frank–van der Merwe and Volmer–Weber extremes.

The present cases of MOF-508 synthesized on various substrates clearly follow a Stranski–Krastanov growth mechanism as well. On unfunctionalized HDPE, the SURMOF forms a relatively smooth layer after 20 deposition cycles (Figure 50) while after 180 cycles some crystallite islands of different sizes have grown atop the continuous film (Figure 45 c), indicating a passing of the critical

film thickness. These crystallites are even more clearly visible on 200-cycle MOF-508, Figure 55 d.

In comparison, the SURMOF on poly(1-allylimidazole) coated HDPE appears similar as on the uncoated substrate, albeit smoother, which may indicate a slightly larger critical film thickness. Since a poly(1-allylimidazole) coating on HDPE has been shown to greatly reduce the water contact angle of the substrate, the coating has a higher free surface energy than untreated HDPE.[404] An increase in σ_u leads to a decrease in $\Delta\sigma$, meaning that if MOF-508 followed a Stranski–Krastanov growth on HDPE, it needs to follow a Stranski–Krastanov or Frank–van der Merwe growth on poly(1-allylimidazole) as well, which is in line with the experimental results. However, in the literature MOF-508 synthesized on poly(1-allylimidazole) (on Si wafers) has been described to follow a Volmer–Weber island growth.[363] Our considerations of surface energies suggest that it is more likely that the MOF-508 crystals described in the literature in fact also followed a Stranski–Krastanov growth, albeit with a significantly smaller critical film thickness, meaning that they soon switched to an island growth, making it difficult to verify whether a continuous SURMOF film exists underneath. The great difference in MOF morphology on poly(1-allylimidazole) on HDPE and on the same coating on Si wafers shows that substrate chemistry alone does not dictate the morphology of a MOF grown on it. In fact, lattice misfit is an important parameter influencing the critical film thickness at which a crystal following the Stranski–Krastanov mechanism switches from film to island growth. Two cases need to be distinguished here: positive misfit, resulting in a compressed crystal, promotes an island growth with misfits as low as 5%, while negative misfit, resulting in a tensile crystal, leads to a much smaller tendency to switch from film to island growth, even at significantly larger misfits.[394,405] Since poly(1-allylimidazole) carries numerous seeding sites for MOF-508 growth,[363] it is likely that a positive misfit exists between the coated Si wafer and the SURMOF, leading to a low critical film thickness and a quick switch from film growth to island growth. For poly(1-allylimidazole) on HDPE it is possible that the increased roughness of the surface compared to a Si wafer led to a decrease in MOF-508 seeding sites, which would lead to a smaller lattice misfit and a larger critical film thickness.

In addition to the comparison between HDPE and poly(1-allylimidazole), the results of MOF-508 synthesis on different flat substrates further illustrate the influence of surface chemistry on SURMOF morphology. Scanning electron micrographs of MOF-508 grown on PET and PES show numerous crystallite islands appearing after only 20 deposition cycles, unlike the flat SURMOF film on HDPE, Figure 50. Since the surface free energies of PET and PES are significantly higher than of HDPE,[406, 407] $\Delta\sigma$ for both of these substrates is expected to be smaller, meaning that if a Stranski–Krastanov growth occurred on HDPE it should also occur on PET and PES. Indeed, scanning electron micrographs taken where the SURMOF was scratched indicate that a thin continuous MOF layer lies beneath the crystallite islands, Figure 63. The MOF-508 morphology on PET and PES therefore appears similar to the theorized growth mechanism on poly(1-allylimidazole) coated Si wafers, as discussed in the previous paragraph. This small critical film thickness further indicates that the lattice mismatch between PET/PES and MOF-508 is larger than between HDPE and the SURMOF, although it is unclear whether it is a positive or negative mismatch.

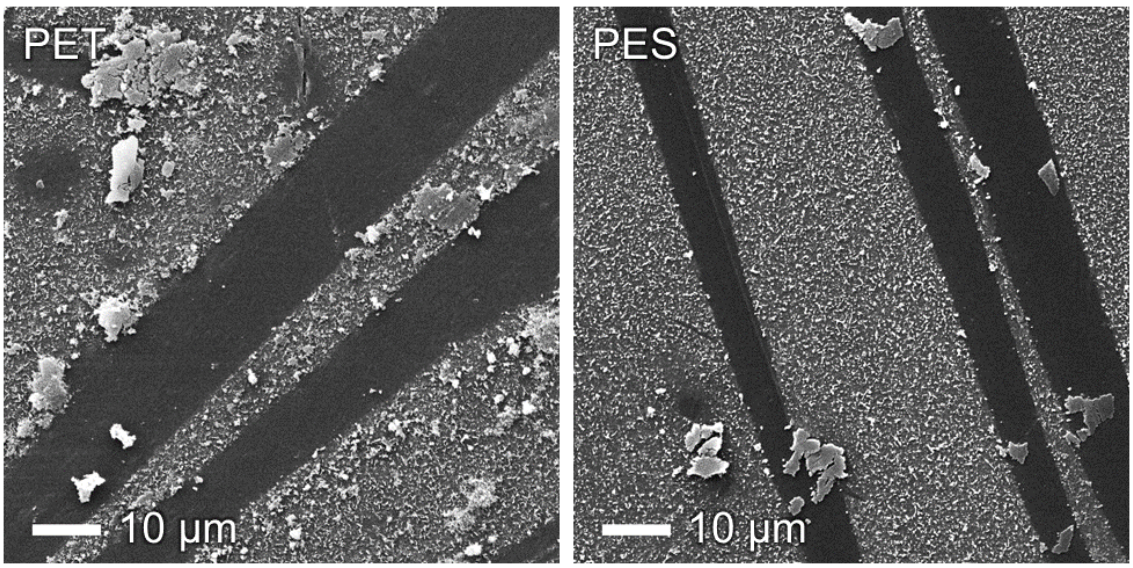

Figure 63: PET and PES substrates functionalized with 20-layer MOF-508 and subsequently scratched to reveal the contrast between uncoated and coated areas. Scale bars represent 10 µm in both images. Flakes that were removed from the scratched areas and settled onto the substrate indicate a complete coverage with a thin SURMOF film carrying small crystallite islands. Images were captured jointly by PKE & VSB and cropped / evaluated by VSB.

PTFE possesses the lowest free surface energy among all flat polymer substrates used in this work.[408] While generally no SURMOF growth was observed on the surface due to the low affinity of zinc and the linkers to adsorb to PTFE (Figure 50), a few crystals could be found near the clip where small amounts of the synthesis solutions may have been trapped, allowing for a longer contact time between the components and the surface, Figure 64. Here, small crystallites were found to be growing independently from each other, indicating a Volmer–Weber growth which is in line with the low free surface energy of PTFE and comparatively large Δσ derived from it.

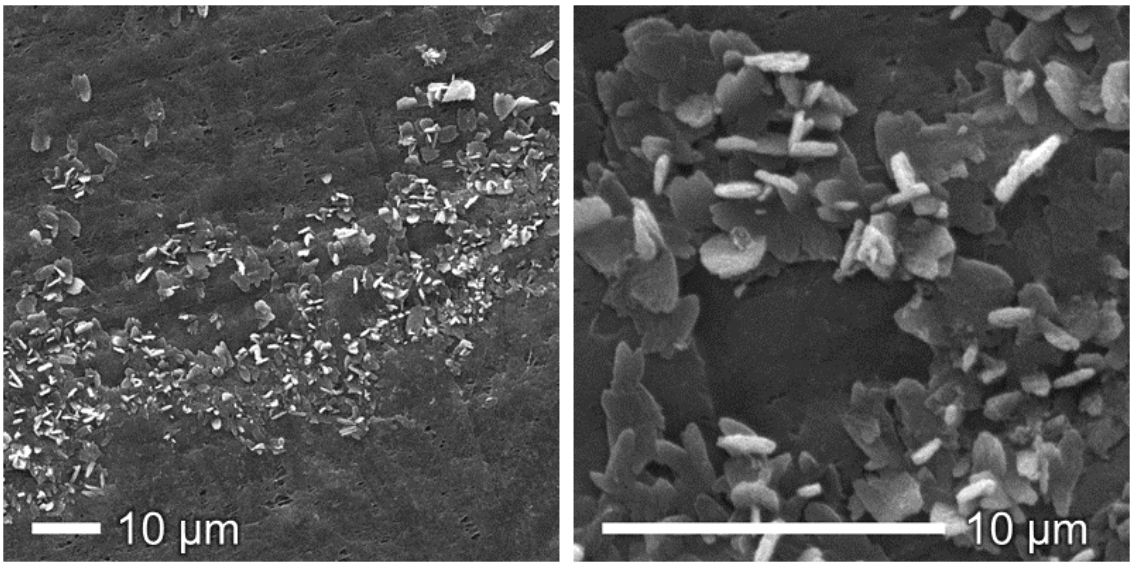

Figure 64: Scanning electron micrographs of a PTFE substrate within the region where it was held by a clip during the attempted synthesis of 20-layer MOF-508 on the surface. While no SURMOF was visible on most of the substrate (Figure 50), some disordered crystals grew in the clipped area, likely because the solutions were trapped by the clip which led to increased contact times. These crystals followed a Volmer–Weber growth, with uncoated substrate visible between them.

Overall, the finding that MOF-508 growth follows a Stranski–Krastanov mechanism on most surfaces is positive for potential applications. Rough Volmer–Weber style growth has been described as “problematic”, likely because such a non-uniform film can contain pin holes, thus reducing its efficiency for applications such as filtration.[409]

6.3.5 MOF transfer

After showing successful epitaxial MOF-508 growth on unfunctionalized substrates, we were interested in testing whether it would be possible to remove the SURMOF from the surface it was grown on and transfer it to another, since it would not be as tightly attached as MOFs grown on surfaces with functional groups that coordinate specifically to the MOF components. In the literature, the removal of epitaxially grown SURMOF from a functional gold substrate has been reported by coating the MOF with PMMA resin and subsequent shaving off the MOF–PMMA composite from the base substrate using a knife.[375] We expected that such strong physical force would not be necessary to remove MOF-508 from unfunctionalized HDPE. Therefore, we took inspiration from the preparation of atomically thin graphene[385] and attempted to remove the SURMOF from the substrate by using tape.

While most of the MOF was successfully transferred onto the tape, as evidenced by FTIR and XRD spectra (Figure 56, Figure 57), SEM micrographs showed that the SURMOF became very cracked in the process, appearing as separate floes on the tape, Figure 55. This damage is not surprising because thin MOF films when independent from a solid substrate are very fragile and difficult to handle.[360] However, it is promising that the adhesiveness of tape is strong enough to lift a MOF-508 thin film from unfunctionalized HDPE.

In the following step we therefore exchanged the tape for thermal release sheet. This sheet consists of a polymer support with a coating that loses its adhesive properties upon heating to 90°C. According to the manufacturer, this sheet is useful in the manufacture of electric components.[410] Similar sheets have been used in the literature to transfer monolayer graphene films from the copper substrate on which they were synthesized to another target substrate, a crucial step for the development of flexible electronics.[411] We used it to transfer epitaxially grown MOF-508 from HDPE to glass, a substrate on whose unfunctionalized surface this MOF does not grow well, as shown in section 6.2.2. Initial results were promising as the transferred MOF could be seen with the naked eye on the transparent glass (Figure 58) and its presence was verified by XRD spectroscopy (Figure 59). However, the process still requires further optimization because the MOF was very scratched due to the application of force

using tweezers during the transfer process, Figure 60. Initial attempts to apply this force by rolling a metal cylinder over the sheet were unsuccessful, because it was difficult to apply pressure and heat simultaneously. It can be expected that a setup where the target substrate and thermal release sheet are passed through heated rolls would probably work better, analogous to roll-to-roll transfer of graphene.[411]

6.4 Conclusions

Expanding on previous studies regarding epitaxial growth of MOF-508, it was discovered that the framework can be synthesized on a variety of polymer substrates without requiring the presence of a linker layer. Simple adsorption of the components is sufficient to seed dense MOF growth, resulting in layers that were even thicker than predicted based on the unit cell dimensions, likely due to the adsorption of a surplus of organic linker molecules.

The observed epitaxial MOF-508 growth followed the Stranski–Krastanov model, where initially a continuous 2D layer was formed atop which 3D crystals developed after a certain critical film thickness was reached. These critical film thicknesses vary depending on the underlying substrates and could be explained well based on the substrate surface energies.

Finally, the epitaxially synthesized MOF-508 was successfully transferred from the polyethylene substrate it was grown on onto tape and transferred twice onto glass. Once this technique is optimized it can open pathways to place MOF layers on any flat surface after being synthesized on a different substrate, which could facilitate the large-scale application of MOFs.

6.5 References

(343) Batten, S.R.; Champness, N.R.; Chen, X.-M.; Garcia-Martinez, J. ; Kitagawa, S.; Öhrström, L.; O'Keeffe, M.; Paik Suh, M.; Reedijk, J. Terminology of metal–organic frameworks and coordination polymers (IUPAC Recommendations 2013). *Pure Appl. Chem.* **2013**, *85* (8), 1715–1724.

(344) Bétard, A.; Fischer, R.A. Metal–Organic Framework Thin Films: From Fundamentals to Applications. *Chem. Ref.* **2012**, *112*, 1055–1083.

(345) Zhou, H.-C.; Long, J.R.; Yaghi, O.M. Introduction to Metal–Organic Frameworks. *Chem. Rev.* **2012**, *112* (2), 673–674.

([346]) Yaghi, O.M.; Li, H. Hydrothermal synthesis of a metal-organic framework containing large rectangular channels. J. Am. Chem. Soc. **1995**, 117, 10401–10402.

(347) Yaghi, O.M.; Li, H. T-Shaped Molecular Building Units in the Porous Structure of Ag(4,4'-bipy)·NO3. *J. Am. Chem. Soc.* **1996**, *118*, 295–296.

([348]) Kondo, M.; Yoshitomi, T.; Seki, K.; Matsuzaka, H.; Kitagawa, S. Three-Dimensional Framework with Channeling Cavities for Small Molecules: {[M2(4,4'-bpy)3(NO3)4]·xH2O}n (M = Co, Ni, Zn). *Angew. Chem. Int. Ed. Engl.* **1997,** *36*, 1727.

([349]) Chui, S.S.-Y.; Lo, S.M.-F.; Charmant, J.P.H.; Orpen, A.G.; Williams, I.D. A Chemically Functionalizable Nanoporous Material [Cu3(TMA)2(H2O)3]n. Science **1999**, *283*, 1148–1150.

([350]) Li, H.; Eddaoudi, M.; O'Keeffe, M.; Yaghi, O.M. Design and Synthesis of an Exceptionally Stable and Highly Porous Metal-Organic Framework. Nature **1999**, *402*, 276–279.

(351) Lee, J.; Farha, O.K.; Roberts, J.; Scheidt, K.A.; Nguyen, S.T.; Hupp, J.T. Metal–Organic Framework Materials as Catalysts. *Chem. Soc. Rev.* **2009**, *38*, 1450–1459.

(352) Kreno, L.E.; Leong, K.; Farha, O.K.; Allendorf, M.; Van Duyne, R.P.; Hupp, J.T. Metal–Organic Framework Materials as Chemical Sensors. *Chem. Rev.* **2012**, *112*, 1105–1125.

(353) Cui, W.-G.; Hu, T.-L.; Bu, X.-H. Metal–Organic Framework Materials for the Separation and Purification of Light Hydrocarbons. *Adv. Mater.* **2020**, *32* (3), 1806445.

(354) Li, H.; Wang, K.; Sun, Y.; Lollar, C.T.; Li, J.; Zhou, H.-C. Recent Advances in Gas Storage and Separation Using Metal–Organic Frameworks. *Materials Today* **2018**, *21* (2), 108–121.

(355) Joseph, L.; Jun, B.-M.; Jang, M.; Park, C.M. ; Munoz-Senmache, J.C.; Hernández-Maldonado, A.J.; Heyden, A.; Yu, M.; Yoon, Y. Removal of Contaminants of Emerging Concern by Metal-Organic Framework Nanoadsorbents: A Review. *Chemical Engineering Journal* **2019**, *369*, 928–946.

(356) Kobielska, P.A.; Howarth, A.J.; Farha, O.K.; Nayak, S. Metal–Organic Frameworks for Heavy Metal Removal from Water. *Coordination Chemistry Reviews* **2018**, *358*, 92–107.

(357) Moosavi, S.M.; Nandy, A.; Jablonka, K.M.; Ongari, D.; Janet, J.P.; Boyd, P.G.; Lee, Y.; Smit, B.; Kulik, H.J. Understanding the Diversity of the Metal-Organic Framework Ecosystem. *Nature Communications* **2020**, *11*, 4068.

([358]) Chen B.; Liang, C.; Yang, J.; Contreras, D.S.; Clancy; Y.L.; Lobkovsky, E.B.; Yaghi, O.M.; Dai, S. A Microporous Metal–Organic Framework for Gas-Chromatographic Separation of Alkanes. *Angew. Chem. Int. Ed.* **2006,** *45*, 1390-1393

(359) Shekhah, O.; Wang, H.; Paradinas, M.; Ocal, C.; Schüpbach, B.; Terfort, A.; Zacher, D.; Fischer, R.A.; Wöll, C. Controlling Interpenetration in Metal–Organic Frameworks by Liquid-Phase Epitaxy. *Nature Materials* **2009**, *8*, 481–484.

(360) Liu, B.; Fischer, R.A. Liquid-Phase Epitaxy of Metal Organic Framework Thin Films. *Sci. China Chem.* **2011**, *54* (12), 1851–1866.

(361) Makiura, R.; Motoyama, S.; Umemura, Y. ; Yamanaka, H.; Sakata, O.; Kitagawa, H. Surface Nano-Architecture of Metal–Organic Framework. *Nature Materials* **2010**, *9*, 565–571.

(362) Shekhah, O.; Wang, H.; Kowarik, S.; Schreiber, F.; Paulus, M.; Tolan, M.; Sternemann, C.; Evers, F.; Zacher, D.; Fischer, R.A.; Wöll, C. Step-by-Step Route for the Synthesis of Metal–Organic Frameworks. *J. Am. Chem. Soc.,* **2007,** *129* (49), 15118–15119.

(363) Wilson, M.; Barrientos-Palomo, S.N.; Stevens, P.C.; Mitchell, N.L.; Oswald, G.; Nagaraja, C.M.; Badyal, J.P.S. Substrate-Independent Epitaxial Growth of the Metal–Organic Framework MOF-508a. *ACS Appl. Mater. Interfaces* **2018**, *10*, 4057–4065.

(364) Zhao, J.; Gong, B.; Nunn, W.T.; Lemaire, P.C.; Stevens, E.C.; Sidi, F.I.; Williams, P.S.; Oldham, C.J.; Walls, H.J.; Shepherd, S.D.; Browe, M.A.; Peterson, G.W.; Losego, M.D.; Parsons, G.N. Conformal and Highly Adsorptive Metal-Organic Framework Thin Films via Layer-by-Layer Growth on ALD-Coated Fiber Mats. *J. Mater. Chem. A* **2015**, *3*, 1458–1464.

(365) Wu, J.; Chen, J.; Wang, C.; Zhou, Y.; Ba, K.; Xu, H.; Bao, W.; Xu, X.; Carlsson, A. ; Lazar, S. ; Meingast, A.; Sun, Z.; Den, H. Metal–Organic Framework for Transparent Electronics. Advanced Science 2020, 7 (8), 1903003.

(366) Pan, L.; Ji, Z.; Yi, X.; Zhu, X.; Chen, X.; Shang, J.; Liu, G.; Li, R.-W. Metal-Organic Framework Nanofilm for Mechanically Flexible Information Storage Applications. Adv. Funct. Mater. 2015, 25, 2677–2685.

(367) Biemmi, E.; Scherb, C.; Bein, T. Oriented Growth of the Metal Organic Framework Cu3(BTC)2(H2O)·*x*H2O Tunable with Functionalized Self-Assembled Monolayers. *J. Am. Chem. Soc.* **2007**, *129* (26), 8054–8055.

(368) Zhuang, J.-L.; Terfort, A.; Wöll, C. Formation of Oriented and Patterned Films of Metal–Organic Frameworks by Liquid Phase Epitaxy: A Review. *Coordination Chemistry Reviews* **2016**, *307*, 391–424.

(369) Rubio-Giménez, V. ; Tatay, S. ; Volatron, F. ; Martínez-Casado, F.J. ; Martí-Gastaldo, C.; Coronado, E. High-Quality Metal–Organic Framework Ultrathin Films for Electronically Active Interfaces. *J. Am. Chem. Soc.* **2016**, *138*, 2576–2584.

(370) Ameloot, R.; Vermoortele, F.; Vanhove, W.; Roeffaers, M.B.J.; Sels, B.F. ; De Vos, D.E. Interfacial Synthesis of Hollow Metal–Organic Framework Capsules Demonstrating Selective Permeability. *Nature Chemistry* **2011**, *3*, 382–387.

(371) Lu, H.; Zhu, S. Interfacial Synthesis of Free-Standing Metal–Organic Framework Membranes. *Eur. J. Inorg. Chem.* **2013**, 1294–1300.

(372) Katayama, Y.; Kalaj, M.; Barcus, K.S.; Cohen, S.M. Self-Assembly of Metal–Organic Framework (MOF) Nanoparticle Monolayers and Free-Standing Multilayers. *J. Am. Chem. Soc.* **2019**, *141* (51), 20000–20003.

(373) Mao, Y.; Shi, L.; Huang, H.; Cao, W.; Li, J.; Sun, L.; Jin, X.; Peng, X. Room Temperature Synthesis of Free-Standing HKUST-1 Membranes from Copper Hydroxide Nanostrands for Gas Separation. Chem. Commun. 2013, 39, 5666.

(374) Zhang, Y.; Gao, Q.; Lin, Z.; Zhang, T.; Xu, J.; Tan, Y.; Tian, W.; Jiang, L. Constructing Free Standing Metal Organic Framework MIL-53 Membrane Based on Anodized Aluminum Oxide Precursor. *Scientific Reports* **2014**, *4*, 4947.

(375) Darbandi, M.; Arslan, H.K.; Shekhah, O.; Bashir, A.; Birkner, A.; Wöll, C. Fabrication of Free-Standing Ultrathin Films of Porous Metal-Organic Frameworks by Liquid-Phase Epitaxy and Subsequent Delamination. *Phys. Status Solidi RRL* **2010**, *4* (8–9), 197–199.

(376) Ben, T.; Lu, C.; Pei, C.; Xu, S.; Qiu, S. Polymer-Supported and Free-Standing Metal–Organic Framework Membrane. *Chem. Eur. J.* **2012**, *18*, 10250–10253.

(377) Lin-Vien, D.; Colthup, N. B.; Fateley, W. G.; Grasselli, J. G. The Handbook of Infrared and Raman Characteristic Frequencies of Organic Molecules; Academic Press, Inc.: San Diego, 1991.

(378) Farzi, N.; Salehi, N.; Mahboubi, A. Molecular Dynamics Simulation of Acetylene Diffusion in MOF-508a and MOF-508b. *Microporous and Mesoporous Materials* **2017**, *248*, 246–255.

(379) Vicente, A.T.; Araújo, A.; Gaspar, D.; Santos, L.; Marques, A.C.; Mendes, M.J.; Pereira, L.; Fortunato, E.; Martins, R. Optoelectronics and Bio Devices on Paper Powered by Solar Cells. In Nanostructured Solar Cells; Das, N.; IntechOpen 2017. Available from: https://www.intechopen.com/chapters/53636.

(380) Jimoh, O.A.; Ariffin, K.S.; Hussin, H.B.; Temitope, A.E. Synthesis of Precipitated Calcium Carbonate: A Review. *Carbonates Evaporites* **2018**, *33*, 331–346.

(381) Ügdüler, S.; Van Geem, K.M.; Roosen, M.; Delbeke, E.I.P.; De Meester, S. Challenges and Opportunities of Solvent-Based Additive Extraction Methods for Plastic Recycling. Waste Management 2020, 104, 148–182.

(382) Bennabi, S.; Belbachir, M. Synthesis and Characterization of a new hybrid material (MOF-5/Mag-H+) based on a Metal-Organic Framework and a Proton Exchanged Montmorillonite Clay (Maghnite-H+) as catalytic support. *J. Mater. Environ. Sci.* **2017**, *8* (12), 4391–4398.

(383) Elaboudi, I.; Mdarhri, A.; Brosseau, C.; Nourdine, A. ; Rzaizi, M. ; Servant, L. Comparing the Sorption Kinetics of Polytetrafluoroethylene Processed either by Extrusion or Spark Plasma Sintering. *Polymer* **2020**, *190*, 122192.

(384) Rochman, C.M.; Hentschel, B.T.; Teh, S.J. Long-Term Sorption of Metals Is Similar among Plastic Types: Implications for Plastic Debris in Aquatic Environments. *PLoS ONE* **2014**, *9* (1), e85433.

(385) Novoselov, K.S.; Geim, A.K.; Morozov, S.V.; Jiang, D.; Zhang, Y.; Dubonos, S.V.; Grigorieva, I.V.; Firsov, A.A. Electric Field Effect in Atomically Thin Carbon Films. *Science* **2004**, *306* (5696), 666–669.

(386) Summerfield, A.; Cebula, I.; Schröder, M.; Beton, P.H. Nucleation and Early Stages of Layer-by-Layer Growth of Metal Organic Frameworks on Surfaces. *J. Phys. Chem. C* **2015**, *119*, 23544–23551.

(387) Arslan, H.K.; Shekhah, O.; Wohlgemuth, J.; Franzreb, M.; Fischer, R.A.; Wöll, C. High-Throughput Fabrication of Uniform and Homogenous MOF Coatings. *Adv. Funct. Mater.* **2011**, *21*, 4228–4231.

(388) Chernikova, V.; Shekhah, O.; Eddaoudi, M. Advanced Fabrication Method for the Preparation of MOF Thin Films: Liquid-Phase Epitaxy Approach Meets Spin Coating Method. *ACS Appl. Mater. Interfaces* **2016**, *8*, 20459–20464.

(389) Stavila, V.; Volponi, J.; Katzenmeyer, A.M.; Dixon, M.C.; Allendorf, M.D. Kinetics and Mechanism of Metal-Organic Framework Thin Film Growth: Systematic Investigation of HKUST-1 Deposition on QCM Electrodes. *Chem. Sci.* **2012**, *3*, 1531–1540.

(390) Hadzki, D. Die Infrarotspektren von Mischungen von Carboxylsäuren mit Pyridin und das Tunnelieren in der Wasserstoffbrücke OH…N. *Berichte der Bunsengesellschaft für physikalische Chemie* **1958**, *62* (10), 1157–1160.

(391) Johnson, S.L.; Rumon, K.A. Infrared Spectra of Solid 1:1 Pyridine–Benzoic Acid Complexes; the Nature of the Hydrogen Bond as a Function of the Acid–Base Levels in the Complex. *The Journal of Physical Chemistry* **1965**, *69* (1), 74–86.

(392) Fernandez-Berridi, M.J.; Iruin, J.J.; Irusta, L.; Mercero, J.M.; Ugalde, J.M. Hydrogen-Bonding Interactions between Formic Acid and Pyridine. *J. Phys. Chem. A* **2002**, *106* (16), 4187–4191.

(393) Bauer, E. Phänomenologische Theorie der Kristallabscheidung an Oberflächen. I. *Zeitschrift für Kristallographie* **1958**, *110*, 372–394.

(394) Prieto, J.E.; Markov, I.; Stranski–Krastanov Mechanism of Growth and the Effect of Misfit Sign on Quantum Dots Nucleation. *Surface Science* **2017**, *664*, 172–184.

(395) Volmer, M.; Weber, A. Keimbildung in übersättigten Gebilden. *Zeitschrift für physikalische Chemie* **1926**, *119* (1), 277–301.

(396) Ohnsorg, M.L.; Beaudoin, C.K.; Anderson, M.E. Fundamentals of MOF Thin Film Growth via Liquid-Phase Epitaxy: Investigating the Initiation of Deposition and the Influence of Temperature. *Langmuir* **2015**, *31*, 6114–6121.

(397) Yao, M.-S.; Tang, W.-X.; Wang, G.-E.; Nath, B.; Xu, G. MOF Thin Film-Coated Metal Oxide Nanowire Array: Significantly Improved Chemiresistor Sensor Performance. *Adv. Mater.* **2016**, *28*, 5229–5234.

(398) Wang, Z.; Liu, J.; Lukose, B.; Gu, Z.; Weidler, P.G.; Gliemann, H.; Heine, T.; Wöll, C. Nanoporous Designer Solids with Huge Lattice Constant Gradients: Multiheteroepitaxy of Metal-Organic Frameworks. *Nano Lett.* **2014**, *14*, 1526–1529.

(399) Frank, F.C.; van der Merwe, J.H. One-dimensional Dislocations. I. Static Theory. Proceedings of the Royal Society of London. Series A. *Mathematical and Physical Sciences* **1949**, *198* (1053), 205–216.

(400) Frank, F.C.; van der Merwe, J.H. One-dimensional Dislocations. II. Misfitting monolayers and oriented overgrowth. Proceedings of the Royal Society of London. Series A. *Mathematical and Physical Sciences* **1949**, *198* (1053), 216–225.

(401) Stranski, I.N.; Krastanov, L. Zur Theorie der orientierten Ausscheidung von Ionenkristallen aufeinander. *Monatshefte für Chemie und verwandte Teile anderer Wissenschaften* **1937**, *71* (1), 351–364.

(402) Wang, Z.; Rodewald, K.; Medishetty, R.; Rieger, B.; Fischer, R.A. Control of Water Content for Enhancing the Quality of Copper Paddle-Wheel-Based Metal-Organic Framework Thin Films frown by Layer-by-Layer Liquid-Phase Epitaxy. *Cryst. Growth Des.* **2018**, *18* (12), 7451–7459.

(403) Hashem, T.; Valadez Sánchez, E.P.; Weidler, P.G.; Gliemann, H.; Alkordi, M.H.; Wöll, C. Liquid-Phase Quasi-Epitaxial Growth of Highly Stable, Monolithic UiO-66-NH2 MOF thin Films on Solid Substrates. *ChemistryOpen* **2020**, *9*, 515–518.

(404) Gürsoy, M.; Harris, M.T.; Downing, J.O.; Barrientos-Palomo, S.N.; Carletto, A.; Yaprak, A.E.; Karaman, M.; Badyal, J.P.S. Bioinspired Fog Capture and Channel Mechanism Based on the Arid Climate Plant Salsola Crassa. *Colloids and Surfaces A* **2017**, *529*, 195–202.

(405) Prieto, J.E.; Markov, I. Thermodynamic Driving Force of Formation of Coherent Three-Dimensional Islands in Stranski–Krastanov Growth. *Physical Review B* **2002**, *66*, 073408.

(406) Lindner, M.; Rodler, N.; Jesdinszki, M.; Schmid, M.; Sängerlaub, S. Surface Energy of Corona Treated PP, PE and PET films, its Alteration as Function of Storage Time and the Effect of Various Corona Dosages on their Bond Strength after Lamination. *J. Appl. Polym. Sci.* **2017**, *135* (11), 45842.

(407) Low, Z.-X.; Ji, J.; Blumenstock, D.; Chew, Y.-M.; Wolverson, D.; Mattia, D. Fouling Resistant 2D Boron Nitride Nanosheet – PES Nanofiltration Membranes. *Journal of Membrane Science* **2018**, *563*, 949–956.

(408) Chen, J.-R.; Wakida, T. Studies on the Surface Free Energy and Surface Structure of PTFE Film Treated with Low Temperature Plasma. *Journal of Applied Polymer Science* **1998**, *63* (13), 1733–1739.

(409) Stassen, D.D.V.; Ameloot, R. Vapor-Phase Deposition and Modification of Metal-Organic Frameworks: State-of-the-Art and Future Directions. *Chem. Eur. J.* **2016**, *22*, 14452–14460.

(410) Thermal Release Sheet for Electronic Component Processing: REVALPHA. Nitto https://www.nitto.com/eu/en/products/e_parts/electronic001/ (accessed on 20 Feb 2022).

(411) Bae, S.; Kim, H.; Lee, Y.; Xu, X.; Park, J.-S.; Zhen, Y.; Balakrishnan, J.; Lei, T.; Kim, H.R.; Song, Y.I.; Kim, Y.-J.; Kim, K.S.; Özyilmaz, B.; Ahn, J.-H.; Hong, B.H.; Iijima, S. Roll-to-Roll Production of 30-Inch Graphene Films for Transparent Electrodes. *Nature Nanotechnology* **2010**, *5*, 574–578.

CHAPTER 7: CONCLUSIONS

7.1 Cr(VI) Capture

Non-woven polypropylene cloth coated with pulsed plasma poly(vinylbenzyl chloride) and functionalized with either a calixarene carrying tertiary amine groups (DMAM-calixarene) or with N-butylimidazole was shown to efficiently capture chromium(VI) oxoanions from water. This filtration was successful at neutral pH and even at low starting concentrations, setting the filter materials apart from most reported in the literature. Furthermore, they successfully removed chromium from real wastewater samples down to safe levels and could be recycled multiple times. The uptake capacities of both functional cloth types were very similar when exposed to 20 mg L^{-1} Cr(VI) solutions: 6.6 ± 0.4 $mg_{Cr(VI)}$ g_{Cloth}^{-1} for DMAM-calixarene and 6.2 ± 0.6 $mg_{Cr(VI)}$ g_{Cloth}^{-1} for butylimidazole. Based on these capacities, one gram of functionalized cloth (about twice the size of the polypropylene cloth used in disposable face masks) would be able to purify 31–33 L of water with a Cr(VI) starting concentration of 200 µg L^{-1}, similar to real-world pollution levels. All these attributes make both cloth types highly promising materials for point-of-use drinking water purification.

The benefit of using DMAM-calixarene lies in its selectivity in the presence of high concentrations of competitive anions. As seen in Chapter 4 Figure 6 and Chapter 5 Figure 4, sulfate and nitrate can particularly impact the capture efficiency of functional cloths for Cr(VI). The capture efficiencies depicted in these figures for filtration solutions containing a 1:100 molar ratio of sulfate or nitrate (relative to Cr(VI)) are listed in Table 13.

Table 13: Comparison of Cr(VI) capture in % between cloths functionalized with DMAM-calixarene, DMAM-phenol, or butylimidazole when using 10 mL filtration solutions containing 2 mg L^{-1} Cr(VI) and sulfate or nitrate anions in a 1:100 molar ratio.

Filtration Solution	**Cr(VI) capture in %; cloths functionalized with:**		
	DMAM-Calix.	***DMAM-Phenol***	***Butylimidazole***
Cr(VI) : Sulfate 1:100	86.7 ± 2.1	71.7 ± 14.1	57.0 ± 8.8
Cr(VI) : Nitrate 1:100	65.1 ± 3.4	29.0 ± 5.1	42.4 ± 0.3

In the presence of large amounts of sulfate, the Cr(VI) capture for DMAM-phenol (the repetition unit of DMAM-calixarene) and butylimidazole functionalized cloths was not as high as for DMAM-calixarene cloth. Notably, a large variation in capture efficiency was found between experiments, further indicating a certain unreliability of the non-calixarene functional cloths. In the presence of large amounts of nitrate, the Cr(VI) capture of both DMAM-phenol and butylimidazole functionalized cloths is even lower. The fact that butylimidazole cloth performed slightly better than DMAM-phenol cloth in this case could be explained by its suitable chemical softness, as discussed in Chapter 5. Once again, however, DMAM-calixarene cloth performed better than the other two cloths, underlining the impact of the calixarene shape on selective pollutant capture.

Nevertheless, butylimidazole functionalized cloth performed just as well as DMAM-calixarene functionalized cloth when it came to purifying real wastewater samples from India. Since N-butylimidazole is a significantly simpler molecule and therefore cheaper in production, it could therefore be suitable for the preparation of filtration materials for many situations, in which the concentration of sulfate or nitrate in the water is not particularly high.

7.2 Point-of-Use Water Purification

As discussed in Chapter 2, there are various toxic heavy metal water pollutants present in different parts of the world, under a variety of circumstances, be it due to natural occurrence (arsenic), plumbing (lead), or industrial pollution (many including chromium and lead). While developed countries are usually able to provide their population with safe tap water, many people in developing countries rely on groundwater and surface water. As stated in the introduction, each year more individuals die from unsafe water than from all forms of violence put together. Many of these deaths can be attributed to illnesses caused by bacteria and viruses, but numerous ways already exist to remove these pollutants at point-of-use, from boiling to filtration through small pores. Removing dissolved contaminants from water is significantly more difficult for the end user. Nevertheless, point-of-use water purification methods that target heavy metal ions are urgently needed, due to the many negative health effects they cause, even at low concentrations, when consumed over an extended period of time.

This thesis contributes to the development of efficient filter materials that selectively capture toxic heavy metal ions from water. While the pandemic prevented me from completing my experiments regarding arsenic and lead filtration, it is my hope that the concepts I developed for chromium capture and my outlined plans for the other two contaminants will inspire others to continue the research in this field. I showed that non-woven polypropylene cloth coated with pulsed plasma poly(vinylbenzyl chloride) is a versatile base to which functional molecules that target specific pollutants can be attached. With this method, I prepared a total of three different filters that efficiently remove Cr(VI) oxoanions from water, even at neutral pH and very low starting concentrations. By changing the functional groups of capture molecules, for example by using slightly different calixarenes, these filters can be expected to be easily adapted to target other ions.

7.3 Outlook

I envision that by continuing this research, a library of functional filters for specific pollutants could be available one day. Depending on the specific needs of a location, the appropriate filters could then be stacked to make water safe to consume. While it is difficult to create filters that selectively target multiple harmful substances—as explained in Chapter 2 there is not even a filter material that can reliably capture both As(III) and As(V)—, functional cloths could be stacked easily, thus creating combined filters. Since they are a continuous material, they would furthermore be safer to handle than powder-like resins, especially when applied by laypeople at point-of-use.

Our experiments with MOF-508 add other potential routes towards the preparation of functional water filters. When a filter is functionalized directly with capture molecules, its maximum uptake is limited by the overall surface area of its fibres. MOFs however have a vast internal surface area and are therefore very attractive for adsorption applications. Our research has shown that MOF-508 can be synthesized on unfunctionalized polymer surfaces and it is likely that this could also work with other MOFs that contain similar metal centres or ligands since in the case of MOF-508 all three (Zn ions and both ligands) adsorbed to the polymer surfaces. One of the substrates used was non-woven polypropylene cloth, indicating that this could offer a straightforward strategy to prepare MOF-based water filters. Another option could be to move a MOF film from a flat substrate it was synthesized on to a porous membrane acting as filter base. Since we showed that MOF-508 grown on unfunctionalized flat HDPE could be transferred onto glass by using a thermal transfer tape, this process could be easily scaled up to industrial production.